VOLUME 75 AUGUST 5, 1971 NUMBER 16

JPCHAx

THE JOURNAL OF PHYSICAL CHEMISTRY

PUBLISHED BIWEEKLY BY THE AMERICAN CHEMICAL SOCIETY

LITERATURE OF CHEMICAL TECHNOLOGY

Advances in Chemistry Series No. 78

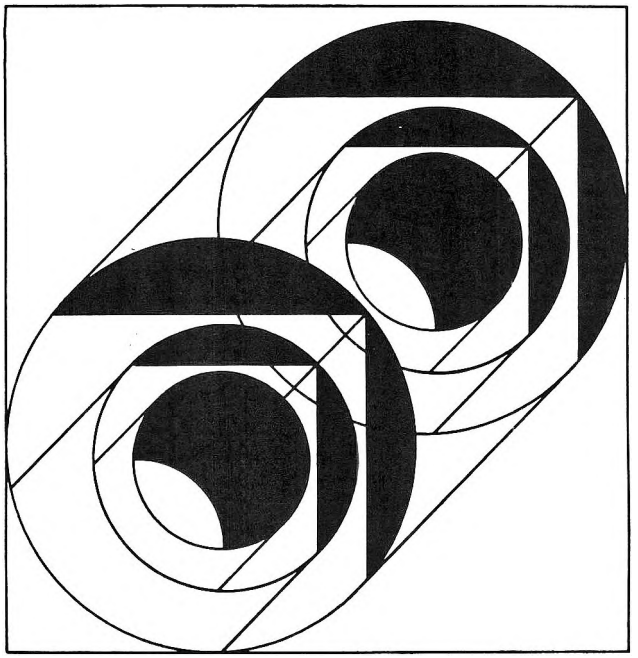

When you need information, knowing where to look is the hard part—right? Not any more. Forty articles in this volume tell you where—

—where the patents are
—where the abstracts and indexes are
—where the background information is
—where the new information is

More than 30 major fields in chemical technology are covered:

- *Chlor-alkali, electrochemistry, industrial gases, noble metals, ceramics, refractories, abrasives, cement, explosives, and rocketry*
- *Pharmaceutical and medicinal, synthetic dyes, photographic chemicals, cosmetics, soaps and detergents, waxes and polishes*
- *Resins and plastics, synthetic rubber, natural rubber, coatings, printing inks, cellulose, pulp and paper, wood naval stores, leather, gelatin, adhesives*
- *Coal, petroleum, carbon black, aerosols, pesticides, food.*

732 pages with index Cloth bound (1968) $17.50
Free set of L. C. cards with library orders upon request.
Other books in the Advances in Chemistry Series of related interest include:

No. 30 Searching the Chemical Literature. Surveys on the use of indexes and abstracts, on name, nomenclature, and language problems, on various types of literature sources, on government sources, on searching techniques, and on the facilities of four leading libraries. 326 pages.
Cloth (1961) $9.00

No. 20 Literature of the Combustion of Petroleum. Twenty-one papers about the chemistry and kinetics of combustion, petroleum products as the fuel for engines, and combustion studies in engines. 295 pages
Paper (1958) $8.00

No. 17 Training of Literature Chemists. Approaches to the training of literature chemists presented by a diversified group of authors from chemical industry, from a consulting laboratory, from a university, from a well known library school, from Chemical Abstracts. 44 pages.
Paper (1956) $5.00

No. 16 A Key to Pharmaceutical and Medicinal Chemistry Literature. Twenty-five illustrative articles range over the several disciplines in the physical and biological sciences which involve the interest of workers in pharmaceutical and medicinal chemistry. 254 pages.
Paper (1956) $7.50

No. 10 Literature Resources for Chemical Process Industries. Information sources on market research (13 papers), resins and plastics (7 papers), textile chemistry (6 papers), food industry (10 papers), petroleum (10 papers), literature searching and language problems (13 papers). 582 pages.
Paper (1954) $12.00

Postpaid in U.S. and Canada; plus 30 cents elsewhere

Order from: Special Issues Sales
American Chemical Society
1155 Sixteenth St., N.W.
Washington, D.C. 20036

THE JOURNAL OF

PHYSICAL CHEMISTRY

 Published biweekly by the American Chemical Society at 20th and Northampton Sts., Easton, Pa. 18042. Second-class postage paid at Easton, Pa.

All manuscripts should be sent to *The Journal of Physical Chemistry,* Department of Chemistry, University of Minnesota, Minneapolis, Minn. 55455.

Additions and Corrections are published once yearly in the final issue. See Volume 74, Number 26 for the proper form.

Extensive or unusual alterations in an article after it has been set in type are made at the author's expense, and it is understood that by requesting such alterations the author agrees to defray the cost thereof.

The American Chemical Society and the Editor of *The Journal of Physical Chemistry* assume no responsibility for the statements and opinions advanced by contributors.

Correspondence regarding accepted copy, proofs, and reprints should be directed to Editorial Production Office, American Chemical Society, 20th and Northampton Sts., Easton, Pa. 18042. Manager: CHARLES R. BERTSCH. Assistant Editor: EDWARD A. BORGER. Editorial Assistant: EVELYN J. UHLER.

Advertising Office: Century Communications Corporation, 142 East Avenue, Norwalk, Conn. 06851.

Business and Subscription Information

Remittances and orders for subscriptions and for single copies, notices of changes of address and new professional connections, and claims for missing numbers should be sent to the Subscription Service Department, American Chemical Society, 1155 Sixteenth St., N.W., Washington, D. C. 20036. Allow 4 weeks for changes of address. Please include an old address label with the notification.

Claims for missing numbers will not be allowed (1) if received more than sixty days from date of issue, (2) if loss was due to failure of notice of change of address to be received before the date specified in the preceding paragraph, or (3) if the reason for the claim is "missing from files."

Subscription rates (1971): members of the American Chemical Society, $20.00 for 1 year; to nonmembers, $40.00 for 1 year. Those interested in becoming members should write to the Admissions Department, American Chemical Society, 1155 Sixteenth St., N.W., Washington, D. C. 20036. Postage to Canada and countries in the Pan-American Union, $4.00; all other countries, $5.00. Single copies for current year: $2.00. Rates for back issues from Volume 56 to date are available from the Special Issues Sales Department, 1155 Sixteenth St., N.W., Washington, D. C. 20036.

This publication and the other ACS periodical publications are now available on microfilm. For information write to: MICROFILM, Special Issues Sales Department, 1155 Sixteenth St., N.W., Washington, D. C. 20036.

Notice to Authors last printed in the issue of June 10, 1971

THE JOURNAL OF

PHYSICAL CHEMISTRY

Volume 75, Number 16 August 5, 1971

COMMUNICATIONS TO THE EDITOR

AUTHOR INDEX

In papers with more than one author the name of the author to whom inquiries about the paper should be addressed is marked with an asterisk in the by-line.

THE JOURNAL OF
PHYSICAL CHEMISTRY

VOLUME 75, NUMBER 16 AUGUST 5, 1971

Hydrogen Displacement in *n*-Butane by Fast T_2 and T_2^+ Collisions[1]

by J. W. Beatty[2] and S. Wexler*

Chemistry Division, Argonne National Laboratory, Argonne, Illinois 60439 *(Received February 22, 1971)*

Publication costs assisted by Argonne National Laboratory

The translational energy dependences of the formation of tritiated *n*-butane resulting from collisions of beams of fast T_2 molecules and of T_2^+ ions with a crossed sheath of *n*-butane molecules have been measured with a "chemical accelerator." For the neutral–neutral collisions the hydrogen displacement reaction possesses a threshold of 6.0 ± 0.6 eV (laboratory system) and the reaction probability rises to a maximum near 30 eV and then remains constant as the kinetic energy of the T_2 molecules is raised to 100 eV. The observed onset energy indicates that the lowest energy observable reaction involves displacement of a hydrogen atom in the butane molecule by a tritium atom from the fast T_2 molecule with concurrent release of the second tritium and the displaced hydrogen as atoms. The reaction probability for T_2^+ impinging on *n*-C_4H_{10} decreases rapidly as the energy of the ion is raised from 5 to 20 eV, remains fairly constant up to 40 eV, and then shows a broad peak centered at about 60 eV. The shape of the yield curve suggests that there are two translational energy dependent mechanisms involved. Below ~20 eV T_2^+ energy, the most likely mode indicated is proton transfer followed by loss of H_2 and hydride transfer. At higher energies, collisional dissociation followed by tritium pickup is suggested.

Introduction

A fundamental problem of chemical kinetics is the determination of the threshold energies and excitation functions of chemical reactions. Knowledge of these important characteristics have, in limited ways, been obtained by nuclear recoil[3] and photochemical[4] techniques, by analysis of the labeled products produced by impingement of fast beams of energy and mass-selected radioactive ions on organic molecules either as a gas at moderately high pressure[5] or as a condensate on a cold surface,[6] by detection of the ions formed by collisions of fast neutral beams with gases,[7] and, for several very low threshold reactions, by crossed-beam studies with velocity-selected thermal beams.[8] Much information on the energy dependences of ion–molecule reactions, in which the ionic product is identified, has also been obtained.[9]

In this paper we describe experiments performed to determine the energy dependences of the probability of chemical reaction between accelerated T_2^+ and *n*-butane and between T_2 and *n*-butane. The product is tritiated *n*-butane in both cases (*i.e.*, the hydrogen displacement reaction is being studied). T_2^+

(1) Work performed under the auspices of the U. S. Atomic Energy Commission.

(2) One of us (J. W. B.) received partial support from the National Science Foundation under NSF Grant No. GY8428.

(3) F. S. Rowland in "Molecular Beams and Reaction Kinetics," Ch. Schlier, Ed., Academic Press, New York, N. Y., 1970, pp 108–116; R. Wolfgang, *Progr. React. Kinet.*, **3**, 99 (1965); R. Wolfgang, *Annu. Rev. Phys. Chem.*, **16**, 15 (1965); A. G. Maddock and R. Wolfgang in "Nuclear Chemistry," L. Yaffe, Ed., Academic Press, New York, N. Y., 1968, pp 186–248.

(4) R. G. Gann and J. Dubrin, *J. Chem. Phys.*, **50**, 535 (1969); *ibid.*, **47**, 1867 (1967); C. C. Chou and F. S. Rowland, *ibid.*, **46**, 812 (1967); A. Kuppermann and J. M. White, *ibid.*, **44**, 4352 (1966); R. M. Martin and J. W. Willard, *ibid.*, **40**, 2999, 3007 (1964); R. J. Carter, W. H. Hamill, and R. R. Williams, *J. Amer. Chem. Soc.*, **77**, 6457 (1955); H. A. Schwartz and R. R. Williams, *ibid.*, **74**, 6007 (1952).

(5) J. M. Paulus and J. P. Adloff, *Radiochim. Acta*, **4**, 146 (1965); J. M. Paulus, *ibid.*, **7**, 141 (1967).

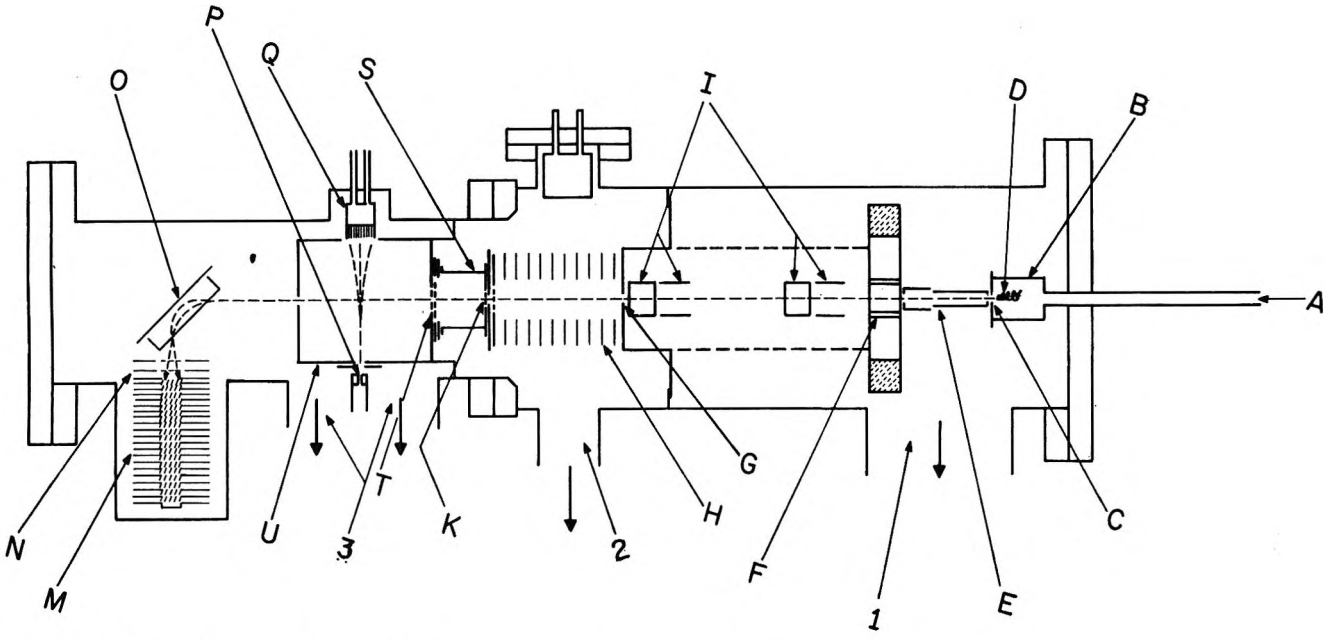

Figure 1. Schematic of the T_2 accelerator. The apparatus is described in the text.

ions are accelerated to well-defined energies (~0.1 eV energy spread) in the range from 5 to 100 eV in a "chemical accelerator" based on the technique of ion acceleration–mass separation–deceleration–neutralization. The energy-selected tritium ions are either made to collide with a crossed beam of the organic molecules or are converted to neutral T_2 of the same translational energy by near resonance-charge exchange prior to collision. The crossed-beam and labeled product molecules are collected on an efficient trap and the yield of the radioactive product determined by a radiogas chromatographic method.

Experimental Section

A schematic drawing of the apparatus appears in Figure 1. Tritium gas (>99% purity) was introduced from an inlet tube A into a miniature isotope separator source B with aperture C and filament D. The source chamber was operated at a potential positive with respect to ground near that of the energy of the species desired, and ions from the low-voltage arc were accelerated first to −500 V and then to −2000 V by a two element lens system E, which also focused the beam on the aperture G. While at this high energy the components of the beam were separated out by a zero deflection mass filter F, so that a pure mass-separated beam of ions entered the region of decelerating lenses H through the aperture G. Sweep plates I served to position the ion beam along the axis of the accelerator. A grid surrounding the region between the mass filter and the aperture to the decelerating section created a field-free path for the ions. The ions were then decelerated to the desired energy in the ring assembly H. The grid (85% open area) at the end of the deceleration system was at ground potential, so that an ion passing through it had an energy near that of the potential of the ion source. In some experiments the ion beam was then partially neutralized by passing it through a gas at low pressure in a neutralization chamber S. The primary ion beam or the neutral species entered the collision chamber U through the grid T of 92% open area. This grid was used to measure the intensity of the ion beam for the T_2^+ experiments, and for the experiments with the neutral beam it was used to prevent ions from entering the collision chamber. In the chamber the fast beam intersected at right angles axially a beam (actually a collimated sheath about 7 cm wide formed by molecules from a row of 48 canals, P) of polyatomic molecules. The sheath of molecules and products of the reactions with the fast tritium beams were condensed on a multivane trap Q, which after 10–30 min of collision time could be moved from the vacuum system through an isolation valve into a transfer chamber. The trap was then rapidly warmed

(6) M. Menzinger and R. Wolfgang, *J. Chem. Phys.*, **50**, 2991 (1969); *J. Amer. Chem. Soc.*, **89**, 5992 (1967); H. M. Pohlit, W. R. Erwin, F. L. Reynolds, R. M. Lemmon, and M. Calvin, *Rev. Sci. Instrum.*, **41**, 1012 (1970); H. M. Pohlit, T. H. Lin, W. Erwin, and R. M. Lemmon, *J. Amer. Chem. Soc.*, **91**, 5421 (1969); H. M. Pohlit, T. H. Lin, and R. M. Lemmon, *ibid.*, **91**, 5425 (1969).

(7) N. G. Utterback, *J. Chem. Phys.*, **44**, 2540 (1966); *Phys. Rev.*, **129**, 219 (1963); 28th Meeting, Propulsion and Energetics Panel, AGARD, NATO, Oslo, Norway, 1966, p 363.

(8) E. F. Greene, A. L. Moursund, and J. Ross, *Advan. Chem. Phys.*, **10**, 135 (1966); J. R. Airey, E. F. Greene, K. Kodera, G. P. Reck, and J. Ross, *J. Chem. Phys.*, **46**, 3287 (1967); J. R. Airey, E. F. Greene, G. P. Reck, and J. Ross, *ibid.*, **46**, 3295 (1967).

(9) J. H. Futrell and F. P. Abramson, *Advan. Chem. Ser.*, **58**, 107 (1966); C. F. Giese, *ibid.*, p 20; A. Henglein, *ibid.*, p 63; M. A. Berta, B. Y. Ellis, and W. S. Koski, *ibid.*, p 80; E. W. McDaniel, V. Cermak, A. Dalgarno, E. E. Ferguson, and L. Friedman, "Ion-Molecule Reactions," Wiley-Interscience, New York, N. Y., 1970, p 296; R. P. Clow and J. H. Futrell, *Int. J. Mass Spectrom. Ion Phys.*, **4**, 165 (1970).

to transfer the condensate to a glass cell with Teflon stopcocks. Absolute yields of the products were determined later by radiogas chromatography. Actually, there were two multivane traps that were operated in sequence, and four cells were attached to each of two manifolds on the apparatus so that eight data points could be obtained per run. Part of the fast ion beam was analyzed before and after each experiment by a parallel plate electrostatic energy analyzer O, then accelerated by grids N, and detected by an electron multiplier M.

The apparatus was pumped by two 6-in. and one 2-in. mercury diffusion pumps with liquid N_2 traps and Freon baffles (1, 2, and 3 in Figure 1). Further cryopumping was done by liquid N_2 baffles and traps (not shown in the sketch). During an experiment with a fast T_2 beam the pressures in the three chambers, as recorded by ion gauges, were typically $\sim 2 \times 10^{-6}$, $\sim 5 \times 10^{-6}$, and 2×10^{-5} Torr, respectively. In order to minimize surface contamination by tritium, the interior materials were highly polished and ultraclean stainless steel, high-fired ceramics and Teflon. Only small amounts of copper and magnetic iron were used where necessary. The entire acceleration–deceleration–neutralization section was supported in cantilever fashion from a large flange which moved on ball bearings along two tracks, a design that greatly facilitated performing repairs and changes on the system. All the electrical leads, current measuring wires, water cooling and gas inlet tubes also entered the vacuum system through this flange. The "gun" was axially aligned by means of a low-power laser beam.

Two different designs of low-voltage arc sources were employed to produce the ion beams. The studies with T_2^+ were conducted with a miniature model of a source for a large isotope separator based on the design of Freeman.[10] A small T-shaped water-cooled molybdenum chamber, with a 1.0-mm diameter ion exit hole, contained a tantalum or tungsten filament extending down the long axis of the chamber. High-fired alumina bushings mounted on the rod insulated the filament from the chamber and sealed the source. Stable arcs were obtained with T_2 gas at 10^{-4} to 10^{-3} Torr of pressure, filament currents of 135 to 200 A depending on the shape and material of the filament, arc currents of 0.2 to 2.0 A, and arc voltages of 90–190 V. In this arrangement the filament was negative in potential relative to the chamber. Under operating conditions the temperature of the source chamber was 800–1000°.

The second source chamber was a commercially available one obtained from the Colutron Corp., Boulder, Colo. It consisted of a boron nitride cylinder, a tantalum anode containing a 0.38-mm diameter aperture, and a conical filament. With this source, stable arcs in pure tritium gas were only possible when the source pressure was 50–100 μ, but lower pressures of tritium could be "burned" in arcs maintained with $\sim 1\ \mu$ of xenon or $\sim 5\ \mu$ of argon. A usual filament current was approximately 18 A, arc current 0.2 to 1.0 A, and arc voltage 90–110 V. The chamber temperature was 600–700° when an arc was struck.

The dimensions of the two-element, cylindrical lens system E were chosen to acclerate and focus an ion beam from the aperture of the source chamber onto a 4-mm aperture, G, which opened into the decelerating system. The ion optics system was designed from compatibility parameters given by Spangenberg.[11] The first electrode of the lens could be moved transverse to the beam axis by controls outside of the vacuum housing.

A low-resolution, zero-deflection mass filter was designed, from equations published by Wahlin,[12] to be compatible with the ion optics of the accelerating system. The permanent magnet was a single piece fabricated from Alnico V. The magnetic field at the center of the gap between the poles was measured to be 362 G, and its uniformity perpendicular to the beam direction and near the beam axis was within 2 G/mm. The voltages on the electrodes providing the opposing electric field were always plus and minus, respectively, relative to the potential along the axis of the beam. The strength of the magnetic field and other parameters were such that with electric field strengths approximately 270, 180, and 125 V/cm, the mass filter passed undeflected pure beams of T^+, T_2^+, and T_3^+ ions, respectively. A resolution of about 10 was determined for the mass filter.

After mass separation, the ions were slowed down to the desired energy by an approximately linear repelling field created by stepwise voltages on ten large-aperture rings spaced 1 cm apart. Actually, the potential on the first ring was 100 V negative relative to the entrance aperture plate so as to prevent secondary electrons formed at the 4-mm hole, G in Figure 1, from entering the ion-deceleration system. The voltage on each ring was adjustable from outside the vacuum chamber, and tests were performed to obtain the conditions for maximum intensity of the ion beam entering the collision chamber. For a few experiments at low energies the voltages on the ten large-aperture rings were controlled to give an einzel decelerating lens system that was operated in the accelerating mode.

After reaching the desired translational energy, the fast ion beam entered a neutralization chamber through a hole 4 mm in diameter, and left through a hole 10 mm in diameter. The chamber was a cylinder whose wall at the beam exit end consisted of an outer guard ring and an inner aperture grid (85% open area) over the 10-mm hole, both of which were electrically isolated from each other and from the cylinder. The D_2 neutralizing gas entered the cell through a side tube.

(10) J. H. Freeman, *Nucl. Instrum. Methods*, **22**, 306 (1963).

(11) K. R. Spangenberg, "Vacuum Tubes," McGraw-Hill, New York, N. Y., 1948, p 379.

(12) L. Wahlin, *Nucl. Instrum. Methods*, **27**, 55 (1964).

The T_2^+ entering this chamber was prevented from hitting it by a guard aperture just before the 4-mm entrance hole. Near resonance-charge exchange between T_2^+ and D_2 partially neutralized the fast T_2^+ beam, producing slow D_2^+ ions that drifted to the walls of chamber, where they were measured by a sensitive electrometer. A potential of 1.5 V on the exit end-guard ring served to make sure that all slow ions were driven to the chamber walls. The intensity of the fast neutralized T_2 molecules entering the collision chamber was taken to be equal to the current of slow D_2^+ ions measured at the chamber corrected for the fractional open areas of the two grids covering, respectively, the exit aperture of the neutralization chamber and the entrance aperture of the collision chamber. Over the range investigated, the current to the cell increased linearly with the pressure of D_2 in the cell. That scattering of the fast T_2^+ beam was not responsible for the current to the chamber was demonstrated by substituting He^4 for D_2 over the same cell-pressure range. No ion current was then recorded to the cell. From comparison of the current to the cell with that hitting the grid over the exit aperture the fraction of the fast T_2^+ beam neutralized by the D_2 could be calculated. The intensity of T_2 did not vary greatly with the energy of T_2^+. This observation is probably due to the decrease in cross section for resonance-charge exchange[13] being balanced by the increase in ion current (Figure 2) as the translational energy is raised. After the intensity of the fast T_2 beam that entered the collision chamber U through a 2.0-cm diameter aperture was determined by the method outlined above, unneutralized fast T_2^+ ions were prevented from entering the chamber by raising the potential of the grid T to a value about 10% higher than the ion beam energy.

Across the waist of the collision chamber at 90° to the fast beam moved a beam of reactant molecules estimated to be approximately 7 cm wide and 0.92 cm thick at the axis of the fast beam. The crossed beam or sheath effused from a close linear array of 48 canals each 1 cm long and 1 mm in diameter, and was further collimated by defining apertures. Constancy of the density of the crossed beam was achieved by maintaining the pressure of the plenum chamber behind the canals fixed by means of an automatic motor-driven needle valve ("Automatic Pressure Controller" (Granville-Phillips Co., Boulder, Colo.)), which was preset and controlled by a calibrated capacitance monometer. The crossed beam was immediately condensed on a movable multivaned cold trap held at liquid nitrogen temperature, the design of the vanes being a variation of that given by Scoles, *et al.*[14] The trap, which when in position straddled a large rectangular opening in the collision chamber opposite the array of canals, could be moved horizontally through a gate valve into a gas-transfer chamber. Actually, there were two such movable traps which came into position from opposite sides

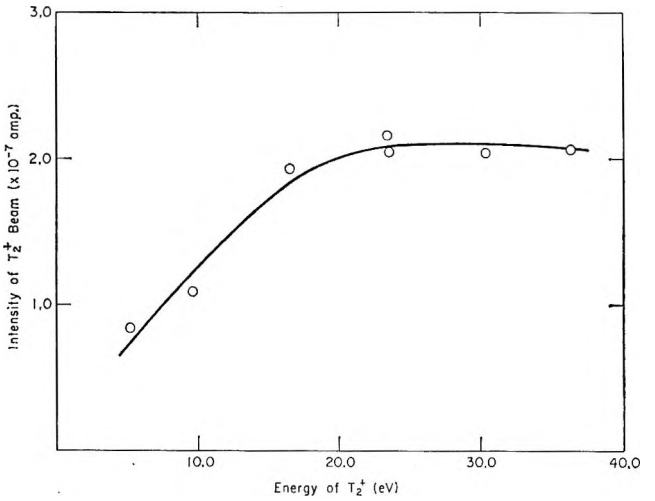

Figure 2. Variation of intensity of T_2^+ ion beam with its energy after deceleration.

of the apparatus and were operated in succession for more efficient performance of the experiments. Tests showed that a minimum of 70–75% of the crossed beam of *n*-butane molecules at room temperature was collected on the multivaned cold trap at liquid nitrogen temperatures. The amounts of crossed-beam gas collected by each of the two traps during 10-min reaction times in an experiment generally agreed to within 5%. For most runs, the average number of molecules/cm^2 in the sheath hit by the fast beam was estimated from the amount of condensate to be 8.9×10^{11}.

A portion of the ion beam was measured for energy distribution by passing it through a parallel plate electrostatic energy analyzer, O. The model constructed was a modified version of one designed by Hutchison.[15] The energy resolution of the analyzer was calculated to be 7.1% to first-order approximation. After passing through the analyzer, the ions were accelerated between grids N and then detected by a 20-stage Cu–Be electron multiplier of the venetian-blind type M. Since the range of energies transmitted by the analyzer is proportional to the mean energy of the range,[16] the true energy distribution of the ion beam was obtained by dividing each ordinate of the observed distribution curve by the corresponding energy.

The condensate on the movable vane-trap (measured to be usually ~3 cc NTP after a 10-min reaction time) was transferred to a glass V-shaped cell. The various products were later separated by a 35-ft column of 20% safrole on firebrick at 0°, at a helium flow rate of 60 cc/min. In the first experiments with a T_2^+ beam crossed with *n*-butane molecules, the *n*-bu-

(13) J. B. Hasted, "Physics of Atomic Collisions," Butterworths, London, 1964, p 416 ff.

(14) G. Scoles, C. J. N. van den Meijdenberg, J. W. Bredewout, and J. J. M. Beenakker, *Physica (Utrecht)*, **31**, 233 (1965).

(15) D. A. Hutchison, *Advan. Mass Spectrom.*, **2**, 527 (1962).

(16) G. D. Yarnold and H. C. Bolton, *J. Sci. Instrum.*, **26**, 38 (1949).

tane fraction was condensed out, its volume was measured, and it was then transferred to a proportional counter. After the counter was filled to 1 atm with methane, the tritium activity was measured absolutely. In later experiments the effluent from the column was mixed with propane, and its activity was measured in a flow proportional counter (100-cc volume). The data were recorded on paper tape by means of a digital integrator (Nuclear-Chicago Corp.) and a Tally tape perforator. Data processing was performed on an IBM-1620 computer.

Characteristics of the Ion Beams

The ion beam could be measured by a number of plates and grids placed at various points along the axis of the ion beam, the monitoring being used to align the beam and to determine the beam composition and intensity. For a source voltage of 30 V, up to 0.7 μA of mass-separated beam was focused through the 4-mm aperture G, reached the grid at the end of the decelerating system, and passed into the collision chamber. The composition of the ion beam extracted from the ion source varied greatly with the type of source and the conditions under which the arc was sustained. For the "miniature Freeman" source, for example, 65% T^+ and 35% T_2^+ were measured when the source pressure was $\sim 6 \times 10^{-3}$ Torr, the arc current 0.23 A, and the arc voltage 150 V. The "Colutron" source, on the other hand, emitted T^+, T_2^+, and T_3^+ in the proportion 0.12:1.0:0.51 under the following conditions: pressure of T_2 50–100 $\times 10^{-3}$ Torr, arc voltage of 78 V, arc current of 0.50 A.

Mixtures of T_2 in argon were also "burned" in the latter arc source. It was found that approximately 1 μ of Xe or 5 μ of argon sustained a stable arc, and tritium could then be added in any proportion to produce ion beams of this gas. The advantages of the latter mode of operation were the avoidance of the excessively high (200–250 μ) pressure of pure T_2 required to strike the arc and the employment of moderately low (2 to 25 μ) pressures of this gas to produce reasonably intense ion beams. Arcs of the pure gas were extinguished when the source pressure was reduced below 50–70 μ. The intensities of light species from T_2–Ar mixtures were usually comparable to those observed from the pure gas. The intensity of an ion beam entering the collision chamber increased roughly linearly with the partial pressure of the lighter gas.

Absolute beam intensities entering the collision chamber tended to change from day to day, but a typical variation with energy of the T_2^+ beam is shown in Figure 2. The data were taken using the miniature "Freeman source." Note that the intensity entering the collision chamber drops off below about 15 eV, but remains fairly constant above this energy. Beam currents measured on the 4-mm aperture plate G and on the grid at the end of the decelerating system, on the other hand, remained invariant with the ion energy.

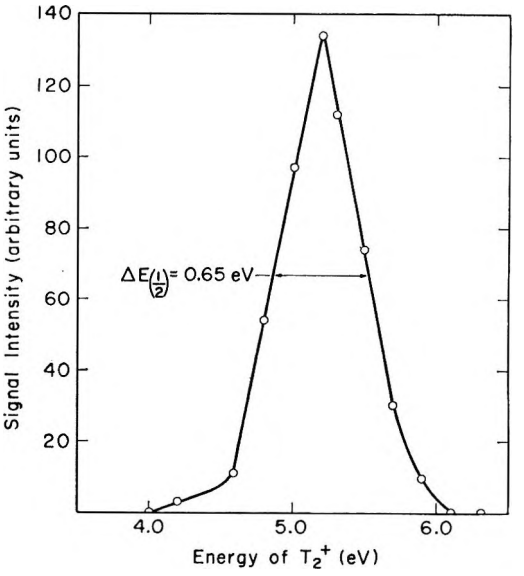

Figure 3. Energy profile of T_2^+ beam at 5.2 eV most probable energy.

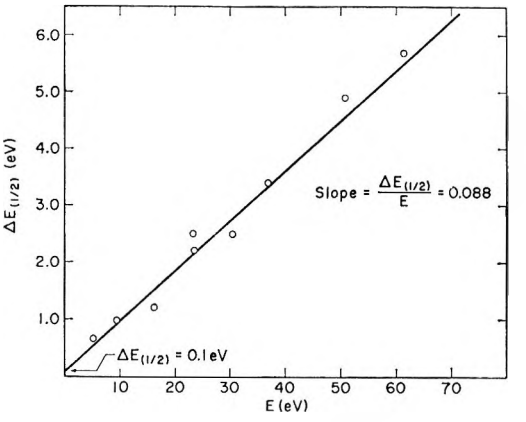

Figure 4. Plot of energy spread of ion beam (full width at half-maximum) as function of most probable energy of decelerated beam.

Of great importance in using these fast beams in meaningful studies of chemical reactions is that the species possess a narrow spread of energies. That such is the case in this apparatus is shown by the data in Figures 3 and 4. The former shows a plot of the energy distribution measured in a 5.2-eV T_2^+ beam. The full width of the curve at half-maximum is 0.65 eV, for an energy spread of 13%. However, this nominal dispersion must be corrected for the resolution of the analyzer. According to the theory of electrostatic energy analyzers,[17] the overall energy resolution R of an ion beam is given by $R = (\Delta E)_{1/2}/E$, where $(\Delta E)_{1/2}$ is the energy spread at half-maximum and E is the most probable energy. ΔE includes the widths of the "win-

(17) G. A. Harrower, *Rev. Sci. Instrum.*, **26**, 850 (1955).

dows" of the analyzer and the natural energy width of the beam. Thus a plot of $(\Delta E)_{1/2}$ *vs.* E should give a straight line whose slope is R. From the data from measurements at several energies shown in Figure 4, R is 8.8%, a value somewhat higher than the nominal resolution of 7.1% calculated for this electrostatic energy analyzer. Extrapolation of the linear function to zero energy gives the natural energy spread of the ions emitted from the ion source. This number is 0.1 eV, which corresponds to 2% of the peak energy at 5.2 eV, and is equivalent to an arc "temperature" of about 1100°K. The resolution obviously improves linearly with increasing ion energy. The data presented in the two figures were taken with the "Freeman source." Similar results were observed for the "Colutron source."

An interesting behavior of the two arc sources at these low energies was their emission of ions with kinetic energies higher than the potential of the source. In general the ion energies were one-half to several volts greater, the difference increasing with the source potential, but it could be as much as 30 V for the "Freeman source" if the arc current was very high (>1.0 A). Apparently, ions may be repelled with appreciable energies by electric fields at the outer sheath of the plasma in the source chamber.[18]

The constancy of the ion current during a 10-min reaction period usually was within 5%. Since the current to the collision chamber grid or to the neutralization chamber (depending on whether T_2^+ or T_2 reactions were being studied) was continuously recorded on a chart, the mean intensity could be determined to 1 to 2%.

Treatment of Data

The measured quantities in a given experiment are the intensity of the tritium beam $I(T_2^+)$ or $I(T_2)$ entering the collision chamber, the amount, η, of tritiated butane and the amount of n-butane, N, collected on the moveable fin-trap in time τ. From these data we may calculate the yield, Y, of the product

$$Y = \frac{\eta}{\int_0^\tau I dt} \tag{1}$$

The intensity of the T_2^+ beam entering the collision chamber is the ion current recorded on the grid over its entrance multipled by the ratio of open to closed area, and converted to number of ions per second. The neutral T_2 intensity, on the other hand, is equal to the slow ion current to the neutralization cell corrected for the limited open areas of the two grids between the cell and the chamber (fractional open areas of 0.80 and 0.92, respectively), and converted to molecular intensity. The amount of tritiated product formed in the experiment is calculated from its integrated activity N^* in the flow proportional counter

$$\eta = \frac{N^* f}{\lambda V} \tag{2}$$

in which f is the total flow rate of helium plus propane (2.2 cc/sec), λ the radioactive decay constant of tritium (1.79×10^{-9} sec $^{-1}$), and V the effective volume of the proportional counter (80 cc). It is assumed that the proportional counter detects the tritium β particle with unit efficiency and that there is only one tritium atom per tagged butane molecule. In the experiments in which T_2^+ and n-C_4H_{10} were the initial beam constituents, and a static counting technique was employed, η was calculated directly from the counting rate and the decay contant. The yield is corrected for extraneous tritiated product formed in properly conducted blank experiments which included beam deflection and alternate introduction of the fast and thermal beams into the collision chamber.

The cross section $\Sigma_\tau(E)$ for reaction is defined by the relation

$$\sum_\tau(E) = \frac{\eta}{\int_0^\tau I dt}(1/\bar{N}) \tag{3}$$

where η is the number of product tritiated molecules formed by intensity I of fast tritium species in a time τ (seconds), and $\bar{N}$ is the average number of molecules per unit target area. This relation is valid because the velocity of the fast beam of tritium far exceeds that of the n-butane target.

The remaining parameter necessary for the calculation of cross sections from eq 3 is the average number of target molecules per unit area $\bar{N}$ hit by the fast beam. A computer calculation of this quantity was performed. The computer program first calculated the relative number $T_b/\bar{v}$, where $\bar{v}$ is the average velocity of n-butane, of target molecules in the volume of the crossed sheath (formed by molecular flow of n-butane from the linear array of 48 canals and collimated by defining aperatures) intersected by the fast T_2 beam. This relative number was then converted to an absolute value by use of the same basic equation to calculate the relative intensity I_t of target molecules on the total area of the condensing fin-trap. I_t was divided into the measured intensity on the trap to remove the proportionality, the latter intensity being obtained from the total amount of n-butane condensed on the trap and the duration of the experiment. The expression relating $\bar{N}$ to N, the number of target molecules on the trap after a time τ, is

$$\bar{N} = \frac{N T_b}{\pi r_b^2 \bar{v} \tau I_t} \tag{4}$$

where r_b is the radius of the fast beam at the intersection with the crossed sheath.

(18) J. R. Reitz and F. J. Milford, "Foundations of Electromagnetic Theory," 2nd ed, Addison-Wesley, Reading, Mass., 1967, p 287.

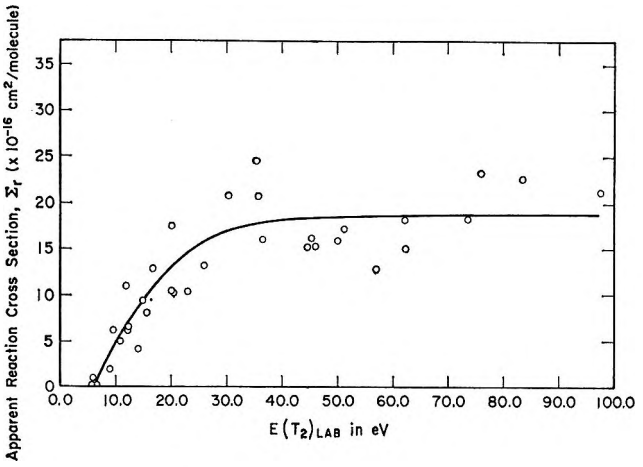

Figure 5. Variation of apparent reaction cross section for formation of tritiated *n*-butane with translational energy of T_2.

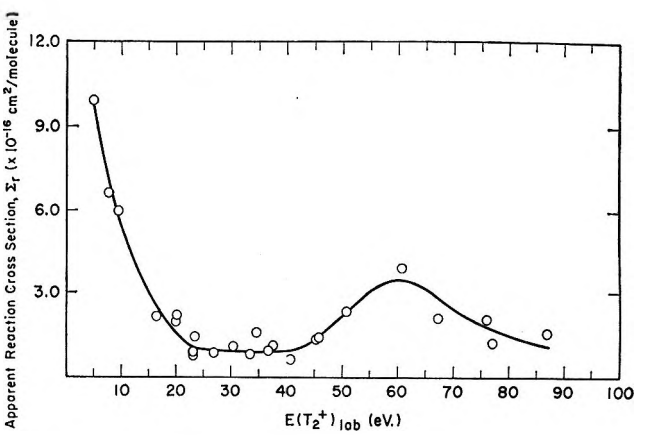

Figure 6. Apparent reaction cross section for formation of tritiated *n*-butane as function of translational energy of T_2^+.

Results and Discussion

In Figure 5 are presented the measured apparent cross sections for formation of tritiated *n*-butane as a function of the translational energy of the neutralized T_2 beam (it is assumed that the translational energy of neutralized species is the same as that of the ion beam). The curve is a least-squares fit to the data (the form is given in eq 17 below). The probability is seen to increase from a threshold value of 6.0 ± 0.6 eV to a maximum at 25 to 30 eV and then remains fairly constant as the translational energy is increased to 95 eV.

In contrast to the behavior of the cross-section dependence on the kinetic energy of fast neutral molecular tritium, that for T_2^+ ions varies in a considerably different manner, as shown in Figure 6. The reaction probability decreases as the translational energy is raised from 5 to 25 eV, remains constant up to 40 eV, and then goes through a broad peak at about 60 eV. Apparently, the lowest threshold energy for reaction of the T_2^+ ion with *n*-butane lies below 5 eV.

The threshold energy observed for the reaction of T_2 with *n*-butane to form tritiated *n*-butane, 6.0 ± 0.6 eV, is only slightly higher than the endothermicity in the laboratory system, 5.0 eV, of the reaction

$$T_2 + n\text{-}C_4H_{10} \longrightarrow n\text{-}C_4H_9T + T + H \qquad (5)$$

However, the onset energy observed is from a few to many electronvolts different from those of all the other chemical reactions leading to formation of tritiated *n*-butane that could conceivably take place in our experiment. The comparison is given in Table I. Consequently, we conclude that the lowest energy displacement reaction is that collision of T_2 and n-C_4H_{10} molecules in which a hydrogen atom is replaced by a tritium atom and the second tritium atom and the displaced hydrogen atom leave as atoms. It is of interest that the threshold energy and deduced mechanism are consistent with recent theoretical trajectory calculations,[19,20] which suggest that a Walden inversion mechanism is involved in the displacement of a H atom in methane or ethane by a fast T atom. The ejection of the light species as atoms rather than as molecular TH in T_2–butane collisions may be due to the H atom leaving from a side of the butane molecule opposite that of the incoming T_2 projectile. Consequently, it would be sterically difficult for the displaced H atom and the second T atom to unite. The hot tritium recoil experiments of Rowland and Chou[21] (with partially deuterated methanes) also lead to the conclusion that substitution is a concerted reaction involving the strong interaction of four or more atoms.

Note that the experimental threshold is considerably higher than the activation energy for deuterium displacement of hydrogen in surface-catalyzed reactions.[22] Further evidence that surface reactions initiated by free-radical formation from collision of the fast beam with a surface were of little importance came from an experiment with mixtures of D_2 and T_2 in the ion source and the T_2 partial pressure near that of a normal T_2 run. D_2^+ was mass selected and converted to D_2 by charge exchange, and the neutralized D_2 collided with a crossed sheath of *n*-butane. No yield of tritiated butane was obtained from these interactions.

The form of the probability curve (Figure 5) suggests that as the translational energy of the T_2 is increased other channels of formation of tritiated butane open. The present experiment can only determine the threshold for the lowest energy process.

The behavior of the curve for tritiated butane production with translational energy of ionic tritium T_2^+ (Figure 6) suggests that there are at least two mechanisms of reaction with butane, a low-energy channel whose threshold is less than 5 eV and a high-energy

(19) D. L. Bunker and M. D. Pattengill, *Chem. Phys. Lett.*, **4**, 315 (1969); *J. Chem. Phys.*, **53**, 3041 (1970).

(20) P. J. Kuntz, E. M. Nemeth, J. C. Polanyi, and W. H. Wong, *ibid.*, **52**, 4654 (1970).

(21) C. C. Chou and F. S. Rowland, unpublished work.

(22) G. C. Bond and P. B. Wells, *Advan. Catal.*, **15**, 92 (1964).

Table I: Possible Mechanisms of Formation of n-C_4H_9T from T_2 and n-C_4H_{10}

	Mechanism	Threshold energy (lab),[a] eV
1.	$T_2 + n\text{-}C_4H_{10} \rightarrow n\text{-}C_4H_9T + T + H$	5.0
2.	$T_2 + n\text{-}C_4H_{10} \rightarrow n\text{-}C_4H_9T + TH$	$\Delta H = 0$, $E_{act} < 2$
3.	$T_2 + n\text{-}C_4H_{10} \rightarrow T + T + n\text{-}C_4H_{10}$ $T + n\text{-}C_4H_{10} \rightarrow n\text{-}C_4H_9T + H$	8.5
4.	$T_2 \xrightarrow{\text{wall}} T + T$ $T + n\text{-}C_4H_{10} \rightarrow n\text{-}C_4H_9T + H$	8.2
5.	$T_2 + n\text{-}C_4H_{10} \rightarrow C_4H_9 + H + T + T$ $C_4H_9 + T_2 \rightarrow C_4H_9T + T$	9.5
6.	$T_2^+ + D_2 \rightarrow T^+ + T + D_2$ (in charge exchange cell) $T + n\text{-}C_4H_{10} \rightarrow n\text{-}C_4H_9T + H$	11.8
7.	$T_2^+ + D_2 \rightarrow TD_2^+ + T$ (in charge exchange cell) $T + n\text{-}C_4H_{10} \rightarrow n\text{-}C_4H_9T + H$	3.7
8.	$T_2 + n\text{-}C_4H_{10} \rightarrow C_4H_9T^+ + H + T + e^-$ $C_4H_9T^+ + n\text{-}C_4H_{10} \rightarrow n\text{-}C_4H_9T + C_4H_9^+$	16.8
9.	$T_2 + n\text{-}C_4H_{10} \xrightarrow[\text{catalysis}]{\text{surface}} n\text{-}C_4H_9T + HT$	0.5

[a] Experimental threshold = 6.0 ± 0.6 eV. The threshold energies have been calculated from the known heats of formation of the species involved and converting from center of mass to laboratory coordinates. In those mechanisms involving two consecutive reactions, the second being the displacement reaction of atomic tritium, the threshold energy of the latter is taken to be 1.7 eV. Furthermore, it is assumed that both tritium atoms in the first reaction must acquire at least 1.7 eV of translational energy each in order that one of them may undergo the subsequent displacement reaction.

mode that peaks at ~60 eV. The most likely mode for the low-energy reaction is a triton transfer reaction

$$T_2^+ + n\text{-}C_4H_{10} \longrightarrow C_4H_{10}T^+ + T \qquad (6)$$

followed by loss of H_2 and H^- pickup at the walls of the collision chamber

$$C_4H_{10}T^+ \longrightarrow C_4H_8T^+ + H_2 \qquad (7)$$

$$C_4H_8T^+ + H^- \text{(wall)} \longrightarrow n\text{-}C_4H_9T \qquad (8)$$

Since the initial ion–molecule reaction is exothermic, its cross section should decrease as the translational energy of T_2^+ is raised.[9] The probability curve observed (Figure 6) is in accordance with this expectation. The higher energy mechanism may involve a collisional dissociation of the butane by the fast T_2^+ followed by reaction of the butyl radical with molecular tritium present in small concentration in the collision chamber or with tritium on the walls.

$$T_2^+ + n\text{-}C_4H_{10} \longrightarrow C_4H_9 + H + T^+ + T \qquad (9)$$

$$C_4H_9 + T_2 \longrightarrow C_4H_9T + T \qquad (10)$$

The endothermicity of the sequence of reactions 9 and 10 is approximately 7 eV. This threshold would therefore not be discernible in the presence of the more probable ion–molecule reactions 6–8.

The translational energy dependences of the reaction probability for tritiated butane formation, presented in Figures 5 and 6, exhibit characteristics that are evidence for certain mechanisms by which the tagged molecules are formed. The curves themselves would be considered "excitation functions" if the ordinates were accurate absolute cross sections for creation of product. Prerequisites for direct determination of the excitation function of a chemical reaction are the control and knowledge of the chemical natures, states of excitation, and the kinetic energies of the two reactants at the moment of their reactive collision. These conditions of course require that the two species collide at most once. Since these requirements are not attainable over the entire energy range under the conditions of the experiment, it was necessary to obtain an excitation function from the data by an indirect method.

The cross sections for formation of tritiated butane from collision of T_2 and n-C_4H_{10}, as calculated from eq 3, are the data points plotted in Figure 5 if the ordinate scale is read in units of 10^{-16} cm^2/molecule. The peak of the curve, ~20×10^{-16} cm^2/molecule, is somewhat lower than that for a gas kinetic collision. However, the observation that the values remain high even at 60–90 eV leads us to the conclusion that at high kinetic energies the fast tritium species and the butane may undergo collisional dissociation. The basis for this conclusion is that our observed probability curve resembles that for dissociative collisions derived by Karplus, Porter, and Sharma[23] from their trajectory calculations on interactions with H_2 and D_2 of fast tritium atoms with energies in the same range as that of the experiment reported here. The dissociation may be into butyl radicals and tritium atoms, the latter displacing hydrogen from other n-butane molecules (mechanisms 3 and 4 of Table I). The reaction of butyl radicals with T_2 (mechanism 5) is apparently ruled out by the absence of tritiated product when fast D_2 molecules were introduced into the chamber.

However, the shape of our curve is also representative of a "thick target" experiment, in which many energy-degrading collisions occur. In our experimental arrangement it is possible that after entering the collision chamber as a reasonably collimated beam, the T_2 molecules pass through the sheath of target molecules and some react. The remainder may reflect off the farthest wall of the collision chamber, being moderated somewhat in kinetic energy in the process. If their initial energy is greater than 8.2 eV, they may dissociate. The atoms and molecules may then pass through the sheath again and will have a second chance to react. The process may continue until the translational energy

(23) M. Karplus, R. N. Porter, and R. D. Sharma, *J. Chem. Phys.*, 45, 3871 (1966).

of the T_2 or the T atoms fall below the threshold energy for the formation of tritiated butane. Since multiple collisions cannot be ruled out, we have further treated our yield data in accordance with the theory of Porter[24] in order to derive an excitation function for the formation of tritiated butane. Assuming numerous energy-degrading encounters of the hot species, this author has given an exact general treatment suitable for transformation of the total yield of product $Y(E)$, defined in eq 1, into the absolute reaction cross section $\Sigma(E)$. His integral equation is

$$Y_i(E) = p_i(E) + \left[1 - \sum_{j=1}^{k} p_j(E)\right] \times \int_0^E \pi(E,E')Y_i(E')\,dE' \quad (11)$$

in which $Y_i(E)$ is the yield of product i when the initial kinetic energy of the tritium is E, $p_i(E)$ is the probability of forming the product i when the collision occurs at the initial energy, $p_j(E)$ the probability of forming another product j at the same kinetic energy, $\pi(E,E')$ the probability that the energy of the fast species is reduced from E to E' in one collision with the target, and $Y_i(E')$ is the product yield at the reduced energy E'. $p_i(E)$ is defined by

$$p_i(E) = \Sigma_i(E)/\Sigma_t(E) \quad (12)$$

$\Sigma_i(E)$ being the cross section for forming i at energy E and Σ_t being the total collision cross section. In order to convert Porter's relation into a tractable form applicable to our results, it is necessary to make approximations as to the behaviors of $\pi(E,E')$, $\sum_{j=1}^{k} p_j(E)$, and $\Sigma_t(E)$ with E. Menzinger and Wolfgang[6] have considered the reasonably valid approximations, eq 13 and 14, respectively

$$\begin{aligned} \pi(E,E') &= [(1-\beta)E]^{-1} && \text{for } \beta E < E' < E \\ &= 0 && \text{for } E < E' < \beta E \end{aligned} \quad (13)$$

where β is the constant energy loss parameter, which may be obtained from kinetic theory analysis of hot T-atom reactions[25]

$$\sum_{j=1}^{k} p_j(E) = A_i p_i(E) \quad (14)$$

which states that both the total reaction probability and the reaction probability of interest have the same functional dependence on E, differing in magnitude by the constant A_i; and

$$\Sigma_t(E) = \Sigma_t(1\text{ eV})E^{-1/6} \quad (15)$$

where $\Sigma_t(E)$ is taken equal to the gas kinetic cross section, whose energy dependence is determined by the inverse power-repulsive wall potential that is controlling in high-energy collisions. $\Sigma_t(1\text{ eV})$ for T_2 on n-C_4H_{10} is taken to be 43×10^{-16} cm^2/molecule.

With these three approximations Menzinger and Wolfgang derived the following relation between product yield and reaction cross section

$$\Sigma_i(E) = \left\{\left[Y_i(E) - \frac{1}{(1-\beta)E}\int_{\beta E}^{E} Y_i(E')dE'\right] \Big/ \left[1 - \frac{A_i}{(1-\beta)E}\int_{\beta E}^{E} Y_i(E')dE'\right]\right\} \times \Sigma_t(1\text{ eV})E^{-1/6} \quad (16)$$

Since grazing collisions in which there is little energy loss are dominant in the interactions of fast light atoms with slow moving molecules in the gas phase, Porter and Kunt[24] have recently concluded that isotropic scattering implicit in the first approximation is not very realistic. However, the classical hard-sphere scattering should be applicable in our case, since the moderation of the energy of the tritium is occurring mainly in collisions with gas molecules adsorbed on the walls of the chamber in this experiment.

We have applied eq 16 to the data in Figure 5, using the third-order polynomial

$$\Sigma_i = -0.39 + 7.278E - 0.16147E^2 + 0.0010981E^3 \quad (17)$$

as the best fit to the experimental results. Equation 16 was solved by computer calculation with several different assumed values of β and A. Representative excitation functions with $A = 1$ are presented in Figure 7. It was found that the curves obtained for a given energy loss parameter β were the same for all values of A from 0.1 to 1.0. However, as seen from the figure, the derived excitation function is strongly dependent on the energy loss parameter. Although the hard-sphere model gives β as the simple function of the masses of the colliding partners

$$\beta = (m_1 - m_2)^2/(m_1 + m_2)^2 \quad (18)$$

which equals 0.66 for T_2 and n-C_4H_{10}, kinetic theory analysis of recoil tritium experiments suggest that inelastic energy losses during energy moderation reduce β to 0.2.[6,26] In Figure 7, we see that the excitation function for $\beta = 0.2$ rises from a threshold at 6 eV (laboratory energy) to a maximum of 4×10^{-18} cm^2/molecule near 20 eV and then drops rapidly as the translational energy is increased to 50 eV. The form of the excitation function derived from our data is thus

(24) R. N. Porter, *J. Chem. Phys.*, **45**, 2284 (1966); R. N. Porter and S. Kunt, *ibid.*, **52**, 3240 (1970).

(25) P. Estrup and R. Wolfgang, *J. Amer. Chem. Soc.*, **82**, 2665 (1960); R. Wolfgang, *J. Chem. Phys.*, **39**, 2983 (1963).

(26) A. H. Rosenberg and R. Wolfgang, *ibid.*, **41**, 2159 (1964); D. Seewald and R. Wolfgang, *ibid.*, **47**, 143 (1967); P. J. Estrup, *ibid.*, **41**, 164 (1964).

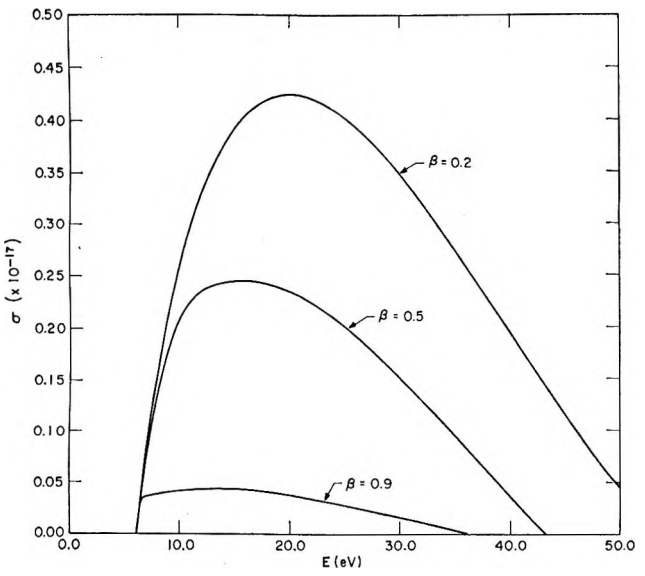

Figure 7. Calculated excitation functions for tritiated n-butane production from reactions of accelerated T_2 and thermal n-butane for various values of the energy loss parameter, β.

similar to those found by Menzinger and Wolfgang for the system T_2^+ + cyclohexane(solid), except that theirs peaks at 10 eV. Of more importance, however, is the great difference in values of the reaction cross sections over the range of energies. We derive cross sections of 0 to 4 × 10^{-18} cm²/molecule for T_2 colliding with gaseous n-C_4H_{10}, whereas their computed values for T_2^+ on condensed c-C_6H_{12} lie in the much higher range of 0 to 5 × 10^{-16} cm²/molecule. A plausible but only partial explanation for the difference may be collisional deexcitation of the tritiated product in the condensed target medium in their experiment, a process much less likely in the very low density crossed sheath in the work reported here. Many labeled products resulting from dissociation of excited parent are thus expected here, and several are indeed observed. They will be the subject of a future publication. The fragmentation of vibrationally and rotationally excited tritiated butane will obviously reduce its yield, and thus decrease the reaction cross section, since the cross sections calculated are almost proportional to the yields of the products. Our measured yields are roughly two orders of magnitude smaller than Menzinger and Wolfgang's. It is of interest to note, however, that the reaction probability curve observed by us is similar in shape to that reported by them for a T_2^+ or T^+ ion beam impinging on a condensed target of cyclohexane.

The measured reaction cross sections for T_2^+ + n-C_4H_{10} (Figure 6) are in agreement with cross sections for ion–molecule reactions.[9] The rise of the curve at low collision energies of the T_2^+ species is in agreement with Paulus' obervations for T^+ reacting with n-C_4H_{10} gaseous target.[5]

Acknowledgments. The aid given by Messrs. T. Cech and L. G. Pobo in performing the experiments is greatly appreciated. Special thanks are due Mr. George Hanz for his expert engineering design of the apparatus and Mr. Anthony Quattrochi for his technical assistance in assembling the machine. Mr. R. Buchal and Mr. F. R. Taraba worked out the computer program for calculating the density of the crossed sheath.

Pyrolysis of 2-Nitropropane

by D. J. Waddington* and M. Ann Warriss

Department of Chemistry, University of York, Heslington, York YO1 5DD, England *(Received February 22, 1971)*

Publication costs borne completely by The Journal of Physical Chemistry

A study of pyrolysis of 2-nitropropane at 323 and 350° is compared with recent data obtained for the decomposition of nitromethane and nitromethane-d_3. Additional experiments with added oxides of nitrogen and with oxygen show that 2-nitropropane decomposes almost exclusively by an intramolecular mechanism to propylene. Minor products such as acetone and methyl cyanide, previously discussed in terms of a chain mechanism involving the nitroalkane, are probably formed by secondary oxidation of propylene. Independent experiments involving the oxidation of propylene and nitrogen dioxide are described.

Introduction

Nitromethane decomposes *via* fission of the C–N bond to yield methyl radicals which, in turn, react with the nitroalkane by a short-chain radical mechanism.[1,2] It has been suggested that the higher nitroalkanes[1a,c,3–6] decompose by intramolecular rearrangement to eliminate an alkene. However, some of the reaction products from the pyrolysis of these nitro compounds suggest a radical mechanism,[5] and the present work is concerned with elucidating the importance of radical reactions in the pyrolysis of 2-nitropropane.

Experimental Section

Materials. 2-Nitropropane (BDH) was purified by fractional distillation using a spinning-band column (Buchi). Methyl cyanide (Fisons Ltd.) and isopropyl nitrite (Koch-Light Laboratories Ltd.) were also purified by fractional distillation, while the gases were commercially available at over 99.5% purity, impurities not being detectable by gas chromatography.

Apparatus. The apparatus was similar to that already described,[2] pressure measurements being made with a transducer (Consolidated Electrodynamics) connected to a recorder (Goertz RE 511).

Analysis. The reactant and most of its pyrolysis products were determined by gas chromatography,[2] the chromatograph being linked to a mass spectrometer (AEI MS 12) in order to identify the peaks. Columns of silica gel (100–150 mesh) (for hydrocarbons), Celite (acid-washed, 100–120 mesh)–10% Carbowax 1500 (for nitromethane, acrolein, 2-nitropropane, acetone, methyl cyanide, 1,2-epoxypropane, and isopropyl nitrite), and Porapak Q (100–120 mesh) (for hydrogen, nitrogen, and nitric oxide)[7] were used.

The total concentration of nitric oxide and nitrogen dioxide was determined by an adaptation of a method for nitrogen dioxide, using azulene and *p*-nitroaniline,[8] and the concentration of nitrogen dioxide was found by subtraction.

Results and Discussion

At the start of reaction, the yield of propylene from 2-nitropropane is quantitative (Figure 1). The principal nitrogen-containing products are nitric oxide and nitrogen dioxide, the yield of nitrogen at the end of reaction being less than 3%. Small amounts of acetone, acrolein, 1,2-epoxypropane, methyl cyanide, and nitromethane were also detected, their presence being confirmed by mass spectral analyses (Table I).

Propylene may be formed from 2-nitropropane by intramolecular elimination of HNO_2

or by fission of the C–N bond, followed by radical reactions

$$\underset{\text{(I)}}{CH_3{-}\overset{NO_2}{\overset{|}{C}}H{-}CH_3} \longrightarrow \underset{\text{(II)}}{CH_3{-}\dot{C}H{-}CH_3} + NO_2 \quad (2)$$

$$\text{(I)} + \text{(II)} \longrightarrow C_3H_8 + \left(CH_3{-}\overset{NO_2}{\overset{|}{C}}{-}CH_3 \text{ or } CH_3{-}\overset{NO_2}{\overset{|}{C}}H{-}\dot{C}H_2\right) \quad (3)$$

(III)

The activation energy has been determined in several previous studies. In a static system a value of

(1) (a) C. Frejacques, *C. R. Acad. Sci.*, **231**, 1061 (1950); (b) T. L. Cottrell, T. E. Graham, and T. J. Reid, *Trans. Faraday Soc.*, **47**, 584 (1951); (c) P. Gray, A. D. Yoffe, and L. C. Roselaar, *ibid.*, **51**, 1489 (1955).

(2) C. G. Crawforth and D. J. Waddington, *ibid.*, **65**, 1334 (1969).

(3) T. L. Cottrell, T. E. Graham, and T. J. Reid, *ibid.*, **47**, 1089 (1951).

(4) T. E. Smith and J. G. Calvert, *J. Phys. Chem.*, **63**, 1305 (1959).

(5) K. A. Wilde, *Ind. Eng. Chem.*, **48**, 769 (1956).

(6) G. N. Spokes and S. W. Benson, *J. Amer. Chem. Soc.*, **89**, 6030 (1967).

(7) C. G. Crawforth and D. J. Waddington, *J. Gas Chromatogr.*, **6**, 103 (1968).

(8) E. E. Garcia, *Anal. Chem.*, **39**, 1605 (1967).

Table I: Formation of Some Products (mm) at 350° from (a) the Pyrolysis of 2-Nitropropane, (b) the Reaction of 2-Nitropropane and Oxygen, (c) the Reaction of 2-Nitropropane and Nitrogen Dioxide, and (d) the Reaction of Propylene and Nitrogen Dioxide

	Product					
Reaction	Acetone	Acrolein	1,2-Epoxy-propane	Methyl cyanide	Nitro-methane	2-Nitro-propane
(a) 2-Nitropropane, 20 mm	0.15	0.3	0.2	1.1	0.5	0.0
(b) 2-Nitropropane, 20 mm; oxygen, 40 mm	0.6	0.04	0.1	1.0	1.6	0.0
(c) 2-Nitropropane, 20 mm; nitrogen dioxide, 20 mm	0.4	0.3	0.2	1.4	1.2	0.0
(d) Propylene, 50 mm; nitrogen dioxide, 50 mm	0.8	0.4	0.3	0.8	0.4	2.6

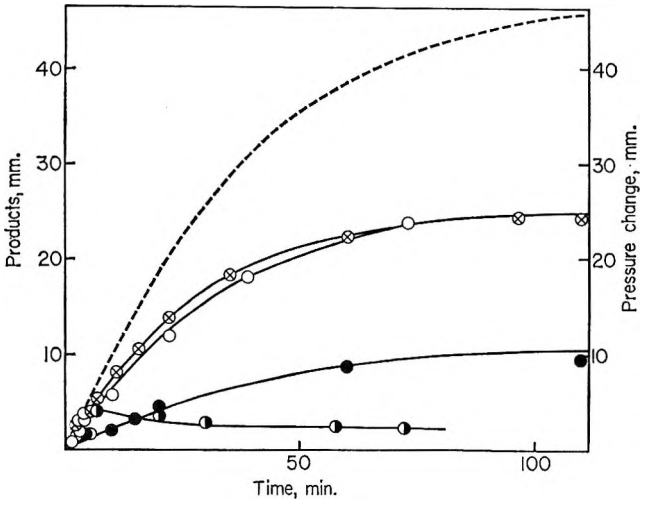

Figure 1. Pyrolysis of 2-nitropropane. Formation of products at 323°: Initial pressure, 30 mm; ●, hydrogen (×10); ◑, nitrogen dioxide; ○, nitric oxide; ⊗, propylene; - - -, pressure change.

164.4 kJ mol^{-1} was found (between 250 and 337°),[4] while, in flow systems, values of 163.1 (between 367 and 397°)[5] and 167.3 ± 2.1 kJ mol^{-1} (between 500 and 705°)[6] have been reported. Computation for the enthalpies of reactions 1 and 2 may be compared with these experimental activation energies. Standard enthalpies of formation of 2-nitropropane, propylene, isopropyl, nitrogen dioxide, and HNO_2 of −143.9, 20.1, 73.6, 33.0, and −77.9 kJ mol^{-1} were used.[9] On considering reaction 1 first, and attempting to estimate Arrhenius parameters, one may apply the generalization that the activation energy of such an endothermic reaction is at least (ΔH + 34) kJ mol^{-1}.[10] As both the NH group and the oxygen atom appear to be sterically equivalent to the methylene group and, in general, the same strain conditions will prevail in heterocyclic compounds as in carbocyclic systems,[11] one may allow for a strain energy of approximately 44 kJ mol^{-1},[12] giving a lower limit for the activation energy of 164 kJ mol^{-1}, compared with an endothermicity of 251 kJ mol^{-1} for reaction 2. Moreover, significant amounts of propane are not found during the reaction, and the addition of oxygen does not markedly alter the yield of propylene in the early stages of reaction (Table II), although the yield of propylene is reduced towards the end of reaction and the yield of acetone increases (Table I). Under these conditions, oxygen would have reacted with the precursor, as occurs on its addition to decomposing nitromethane, the yield of methane being reduced from 30% to zero.[2]

Table II: The Pyrolysis of 2-Nitropropane and the Formation of Propylene at 323°

	Propylene, mm		
Time, min	2-Nitropropane, 20 mm	2-Nitropropane, 20 mm; oxygen, 40 mm	2-Nitropropane, 20 mm; nitrogen dioxide, 20 mm
1.0	0.8	0.8	
2.0	1.2	1.4	1.2
2.5	1.3		
4.0	3.0		1.3, 1.4
5.0		3.4	1.5, 2.0
6.0	3.2		2.7
7.0		4.0	2.8
8.0			2.8
9.0	4.2		3.3
9.5	4.0		
10.0		4.4	4.1, 4.5
11.0	5.6		
12.0	7.0		

To test further whether radicals are formed during the pyrolysis of 2-nitropropane, nitric oxide was added. The rate of pressure increase was not altered (Table III), but this is not, in itself, a diagnostic test for the absence of radicals in the system. For example, addi-

(9) S. W. Benson, F. R. Cruickshank, D. M. Golden, G. R. Haugen, H. E. O'Neal, A. S. Rodgers, R. Shaw, and R. Walsh, *Chem. Rev.*, 69, 279 (1969).

(10) S. W. Benson, *J. Amer. Chem. Soc.*, 87, 972 (1965).

(11) For example, M. Hanack, "Conformational Theory," Academic Press, New York, N. Y., 1965, p 20.

(12) For example, E. L. Eliel, N. L. Allinger, S. J. Angyal, and G. A. Morrison, "Conformational Analysis," Interscience, New York, N. Y., 1965, p 200.

tion of nitric oxide does not affect the rate of decomposition of nitromethane, yet the pattern of reaction products is changed.[13] Methyl radicals react with excess nitric oxide to form nitrogen, the radicals being regenerated. The overall reaction can be represented as

$$4NO \xrightarrow{\dot{C}H_3} N_2 + 2NO_2 \qquad (4)$$

Similar reactions have been reported involving ethyl[14] and *tert*-butyl[15] radicals. Thus, if radicals are taking part in the pyrolysis of 2-nitropropane, one would expect the yield of nitrogen to increase in the presence of excess of nitric oxide, but this does not occur.

Experiments with nitrogen dioxide confirm that radical reactions do not contribute extensively to the pyrolysis of 2-nitropropane. On addition of nitrogen dioxide, the rates of pyrolysis of nitromethane and nitromethane-d_3 are *decreased*, showing that radicals are being stabilized and the chain reaction retarded[16]

$$\dot{C}H_3 + NO_2(+M) \longrightarrow CH_3NO_2(+M) \qquad (5)$$

Likewise, the action of nitrogen dioxide on the pyrolysis of 2-nitropropane gives important information about the mechanism. The rate of consumption of nitroalkane is unaltered (Table IV), showing the absence of radicals. Isopropyl nitrite is not observed, even in presence of excess nitrogen dioxide although one would expect it to be formed if the nitroalkane decomposes *via* an alkyl radical.

It has been suggested that acetone and methyl cyanide are formed from radical III

$$III \longrightarrow (CH_3—CO—CH_3 + NO)$$

$$\text{or } (C_3H_6 + NO_2) \qquad (6)$$

$$III \longrightarrow HCHO + CH_3\dot{C}HNO \longrightarrow$$

$$CH_3\dot{C}NOH \xrightarrow{NO} CH_3CN \qquad (7)$$

However, III is not formed *via* reactions 2 and 3, but it has been suggested that it is formed by interaction of hydroxyl with 2-nitropropane. The most likely source of hydroxyl might be considered to be from HNO_2 but it is believed that this species decomposes by a bimolecular reaction to yield nitric oxide and nitrogen dioxide.[6] Furthermore, on addition of nitrogen dioxide the yields of acetone and methyl cyanide, together with those of acrolein, 1,2-epoxypropane, and nitromethane are increased (Table IV) without altering the rate of deeomposition of 2-nitropropane.

The formation of acrolein and 1,2-epoxypropane indicate that it is the alkene that is the principal source of minor products. Independent experiments with propylene and nitrogen dioxide were necessary as the only report on this reaction does not give analytical data.[17] The reaction is rapid under these conditions (Table V) and acetone, acrolein, 1,2-epoxypropane, methyl cyanide, nitromethane, and 2-nitropropane are among the products (Table I). Moreover, propylene reacts faster than 2-nitropropane with nitrogen dioxide (Tables IV and V), showing that the minor products are largely formed from the alkene. It is not in order to discuss a detailed mechanism for the oxidation of the alkene, but acetone and 1,2-epoxypropane are no doubt formed by attack at the double bond and acrolein by attack at the methyl group, in much the same way as the oxidation of

Table III: The Pyrolysis of 2-Nitropropane; the Addition of Nitric Oxide at 323°

Pressure of nitric oxide added, mm	Time (min) for change of pressure 5 mm	10 mm	15 mm	20 mm	25 mm	Final pressure (mm) of nitrogen formed
	2-Nitropropane, 30 mm					
0.0	5.0	10.0	15.0	21.0	28.0	<1
20.0	4.5	9.0	14.0	19.0		<1
20.0	4.5	9.0				<1
20.0	4.0	9.0	14.0			<1
20.0	4.0	7.5	12.0	17.0		<1
57.0	5.0	11.0	14.0	20.0	30.0	<1
100.0	5.0	9.0	14.0			<1

Table IV: The Rate of Consumption of 2-Nitropropane and Formation of Some Products (mm) at 350°

	2-Nitropropane, 20 mm							2-Nitropropane, 20 mm; nitrogen dioxide, 20 mm						
Time, min	Acetone	Acrolein	1,2-Epoxypropane	Methyl cyanide	2-Nitropropane	Nitromethane	Propylene	Acetone	Acrolein	1,2-Epoxypropane	Methyl cyanide	2-Nitropropane	Nitromethane	Propylene
10	0.08	0.03	0.05	<0.02	12.5	1.35	8.9	0.27	0.09	0.10	0.20	12.0	1.85	8.0
22	0.12	0.08	0.10	0.20	7.1	0.6	11.0	0.58	0.17	0.22	0.62	6.4	0.52	8.6
30	0.17	0.15	0.13	0.35	5.8	0.8	12.3	0.59	0.23	0.26	0.85	5.4	1.26	10.1
44	0.15	0.17	0.16	0.42	3.5	0.7	14.3	0.58	0.25	0.27	0.85	3.5	1.0	11.0
110	0.15	0.30	0.18	[illegible]05	0.0	0.5	16.8	0.35	0.26	0.20	1.35	0.0	1.2	11.8

(13) C. G. Crawforth, Ph.D. Thesis, University of York, 1968.

(14) G. L. Pratt, *J. Chem. Soc. A*, 1757 (1966).

(15) B. G. Gowenlock and M. J. Healey, *J. Chem. Soc. B*, 1014 (1968).

(16) C. G. Crawforth and D. J. Waddington, *J. Phys. Chem.*, **74**, 2793 (1970).

(17) T. L. Cottrell and T. E. Graham, *J. Chem. Soc.*, 3644 (1954).

Table V: The Reaction of Propylene with Oxygen and Nitrogen Dioxide at 323°

Time, min	Propylene, mm: Propylene, 30 mm; oxygen, 30 mm	Propylene, mm: Propylene, 30 mm; nitrogen dioxide, 30 mm
0	30.0	30.0
5	30.0	24.0, 24.6
10		24.0
11	23.2	
15	22.1	24.0

propylene[18] and higher alkenes[19] occurs in presence of molecular oxygen.

Experiments with oxygen and with the oxides of nitrogen indicate that intramolecular decomposition of 2-nitropropane is the most important process, but products such as acetone, 1,2-epoxypropane, methyl cyanide, and nitromethane are formed by subsequent oxidation of propylene by nitrogen dioxide.

Acknowledgments. Thanks are due to Shell Research Ltd. for financial assistance for apparatus and to Dr. C. B. Thomas for mass spectrometric analyses.

(18) S. Oba and W. Sakai, *Bull. Chem. Soc. Jap.*, **40**, 681 (1967).

(19) D. J. M. Ray and D. J. Waddington, *J. Amer. Chem. Soc.*, **90**, 7176 (1968).

The Radiation Chemistry of Octamethyltrisiloxane

by G. B. Tanny and L. E. St. Pierre*

Department of Chemistry, McGill University, Montreal, Canada *(Received January 27, 1971)*

Publication costs assisted by the National Research Council of Canada

The irradiation chemistry of octamethyltrisiloxane was studied in an attempt to define the nature of the scissioning reaction in polydimethylsiloxane. Three linear products, hexamethyldisiloxane, decamethyltetrasiloxane, and dodecamethylheptasiloxane were produced in high yields. The cyclic product, octamethylcyclotetrasiloxane, was also present in appreciable quantities. On the basis of the dimer yields, the G cross-linking was found to be 2.85.

Introduction

The behavior of silicones exposed to ionizing radiations such as ^{60}Co γ rays has been of considerable interest for the past decade. Several low molecular weight species, both cyclic and linear,[1-4] as well as linear polymers and elastomers[5-8] have been studied. Although numerous investigators[1,7,9,10] characterized quite thoroughly the cross-linking phenomena at an early date, the extent and mechanism of any backbone scission and rearrangement remained obscure for some time. This was due largely to the fact that in most techniques used the results of scissioning and cross-linking were observed simultaneously, yielding thereby a net cross-linking or scissioning but neither phenomena could be observed alone. On this basis, the rather small yields which were obtained from the first attempted radiation polymerizations of cyclic monomers,[11,12] the early viscosity data of Charlesby[13] and the results of Kilb's light scattering measurements[14] all led to the conclusion that backbone scissioning was either nonexistent or negligible with respect to cross-linking.[15]

The first evidence that the extent of scissioning was underestimated came from a study of hexamethyldisiloxane[3] in which the ratio of products assignable to scissioning to those of cross-linking was 1:2.5. Later, working with polydimethylsiloxane, PDMS, Charlesby[16]

(1) S. W. Kantor, Abstracts, 140th National Meeting of the American Chemical Society, Atlantic City, N. J., Sept 1956, ORGN 94.

(2) E. L. Warrick, *Ind. Eng. Chem.*, **47**, 2388 (1955).

(3) H. A. Dewhurst and L. E. St. Pierre, *J. Phys. Chem.*, **64**, 1063 (1960).

(4) L. E. St. Pierre, H. A. Dewhurst, and A. M. Bueche, *J. Polym. Sci.*, **36**, 105 (1959).

(5) A. A. Miller, *J. Amer. Chem. Soc.*, **82**, 3519 (1960).

(6) A. A. Miller, *ibid.*, **83**, 31 (1961).

(7) A. M. Bueche, *J. Polym. Sci.*, **19**, 297 (1956).

(8) R. K. Jenkins, *J. Polym. Sci. Part B*, **2**, 999 (1964).

(9) S. Okamura, T. Manabe, S. Futami, T. Iwasaki, A. Nakajima, K. Odan, H. Inagaki, and I. Sakurada, *Proc. Int. Conf. Peaceful Uses At. Energy, 3rd*, **29**, 176 (1958).

(10) M. Koike, *J. Phys. Soc. Jap.*, **18**, 387 (1963).

(11) C. J. Wolf and A. C. Stewart, *J. Phys. Chem.*, **66**, 1119 (1962).

(12) E. J. Lawton, W. T. Grubb, and J. S. Balwit, *J. Polym. Sci.*, **19**, 455 (1956).

(13) A. Charlesby, *Proc. Roy. Soc., Ser. A*, **230**, 120 (1955).

(14) R. W. Kilb, *J. Phys. Chem.*, **63**, 1838 (1959).

(15) A. Chapiro, "Radiation Chemistry of Polymeric Systems," Interscience, New York, N. Y., 1962, Chapter IX, Section 8.

(16) M. G. Ormerod and A. Charlesby, *Polymer*, **4**, 459 (1963).

found that his own earlier solubility fraction data and that of Miller,[5] replotted according to the method of Charlesby and Pinner,[17] yielded ratios of 1:6 and 1:4, respectively. Finally, a recent study of scissioning in pure PDMS networks by *in situ* stress relaxation[18] revealed that G(scission) was not only substantial but was also dose rate dependent.

In order to resolve the apparent conflict in the results, a study of octamethyltrisiloxane was undertaken in the hope that some insight into the mechanism of backbone cleavage and rearrangement could be gained from the nature of the radiolysis products. Octamethyltrisiloxane was chosen because (a) it contains all the elements of a linear polydimethylsiloxane, (b) its radiation products could be expected to be of sufficiently low molecular weight to permit analysis by gas chromatography, (c) its fragmentation pattern could be studied in the mass spectrometer, and (d) Si–O recombination products can be discriminated from those resulting from fragment exchange between molecules.

Experimental Section

1. Preparation of Octamethyltrisiloxane. Octamethyltrisiloxane (MDM) obtained from the General Electric Co. was purified on a Varian Aerograph preparative gas chromatograph using a 20 ft $^3/_8$ in. silicone SE-30 column, 30% on Chromosorb W, and nitrogen carrier gas.

2. Preparation of Samples. The bulk liquid was placed in a flask, A, equipped with a break-seal side arm, and was degassed by repeating a cycle of freezing, pumping at high vacuum (1 μ) for 15 min, and thawing at least 14 times. With the liquid frozen the flask was then sealed. Silica gel contained in an adjoining tube was activated by wrapping a heating tape about it and pumping for 24 hr at high vacuum and at a temperature of approximately 200°. The system was then sealed and the break-seal to flask A was opened, allowing the siloxane to pass through the silica gel prior to being condensed in a third flask, B, the latter being immersed in liquid nitrogen. After all the MDM had passed through the column, flask B was sealed. Flask B was then attached to a row of ampoules. The ampoules were dried by playing a bunsen flame over them for 0.5 hr and then left at 200° overnight under high vacuum. The entire section was subsequently closed to vacuum, the break-seal opened and individual ampoules containing ~2 ml of MDM were sealed off. The samples to be irradiated contained an impurity content of less than three parts per thousand.

3. Dosimetry. The samples were irradiated in an Atomic Energy of Canada Ltd. Gammacell 220, 3500 Ci cobalt-60 γ-ray source. The dose at a given irradiation position was determined by Fricke[19] dosimetry using a $G(Fe^{2+} \rightarrow Fe^{3+}) = 15.5$. All doses were corrected for the difference between the electron density of the sample and that of the dosimeter solution. The dose rate was 2.51 ± 0.08 times 10^{19} eV g^{-1} hr^{-1} and the samples were given a maximum dose of 3.11×10^{21} eV/g.

4. Analyses of Samples. Immediately after they were opened, the irradiated solutions were analyzed on a Varian 90-B chromatograph equipped with a thermal conductivity detector. The same column mentioned in section 1, with helium as the carrier gas, was used to separate the components of the irradiated mixture for both analytical and preparative purposes. This technique had three advantages: (a) sufficiently large injections (0.5 ml) could be made to allow for collection and identification of peaks by mass spectrometry and ir, (b) the amount injectable for analytical purposes could be increased so that peaks due to radiolysis products could be observed at recorder attenuations which were free of noise and possessed a stable base line, and (c) the length of the column gave excellent resolution of almost all the peaks. A Beckman 10-in. recorder was equipped with a disk integrator so that areas of peaks were obtained directly.

Identification of products by gas chromatography was based on retention time studies of standard compounds on two different length silicone columns (3 and 20 ft) and at different temperatures. Mass spectra and ir analyses were performed on samples obtained by collection of the peak immediately after it left the detector.

Once the products were identified, *n*-octane was selected as an internal standard and calibration solutions of *n*-octane and known compounds were prepared. With a constant bridge current of 200 mA and detector temperature of 300°, the response factor, R_x for each compound relative to *n*-octane, was obtained according to eq 1

$$R_x = \frac{\text{wt \% (x)}}{\text{area (x)}} \times \frac{\text{area (}n\text{-octane)}}{\text{wt \% (}n\text{-octane)}} \qquad (1)$$

The values for the linear siloxanes were plotted *vs.* molecular weight (Figure 1) so that response factors could be extrapolated for cross-link products which were unavailable as calibration standards.

The weight per cent of any product of radiolysis was determined by chromatographing a mixture of *n*-octane added to a weighed amount of irradiated liquid. The weight per cent was obtained by the application of eq 1, and this was then corrected to its value in the irradiated liquid alone by eq. 2

$$\text{true wt \% of irrad product} = \text{wt \% (x)}\left(1 + \frac{\text{wt } n\text{-octane}}{\text{wt MDM}}\right) \qquad (2)$$

(17) S. Pinner and A. Charlesby, *Proc. Roy. Soc., Ser. A*, **249**, 367 (1959).

(18) G. B. Tanny and L. E. St. Pierre, unpublished work.

(19) N. Miller and J. Wilkinson, *Trans. Faraday Soc.*, **50**, 690 (1954).

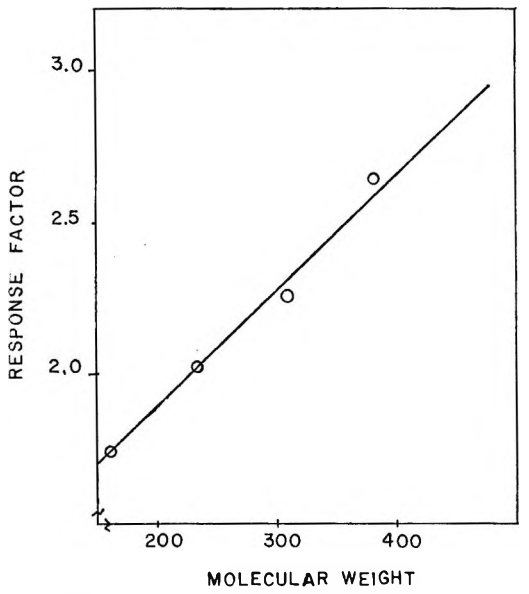

Figure 1. Calibration curve of response factors of known linear siloxane standards *vs.* molecular weight. Chromatograph, Varian 90-B; detector temperature 300°; detector current 200 mA.

where wt *n*-octane = weight added to *n*-octane and wt MDM = weight of irradiated MDM.

All mass spectrometry was performed on an AEC MS902 mass spectrometer.

Results and Discussion

1. Radiolysis Products. A typical chromatogram of the liquid products obtained on the 20-ft silicone column is shown in Figure 2. Peak no. 1, 3, and 4 were identified from their retention times and mass spectra as the linear siloxanes, hexamethyldisiloxane (MM), decamethyltetrasiloxane (MD_2M), and dodecamethylheptasiloxane (MD_3M), respectively. Their yield *vs.* dose curves (Figure 3) are nearly linear at low doses, but exhibit a positive deviation from linearity at higher values, *i.e.*, higher total conversion. This suggests that irradiation of products or reaction of reactive species with them is beginning to occur. This observation is not surprising since in the region of curvature the overall conversion has reached 6–8%.

Peak no. 2, in Figure 2, had a retention time identical with that of octamethylcyclotetrasiloxane (D_4). However, since to our knowledge this would represent the first time that a cyclic product has been reported to arise from a linear siloxane as a result of irradiation, the possibility that the peak might be some other product was checked by infrared and mass spectroscopy.

Although the mass spectrum (see Table III) tended to support the assignment of D_4 as the product, infrared spectra were necessary, as nonamethyltetrasiloxane has the same highest mass (281) in the low-resolution mass spectrum and might have a retention time coincidental with D_4. Since the infrared spectrum (see Table III) did not reveal any peak in the 2100–2300-cm^{-1} region in which Se–H is observed,[20] the product was concluded to be D_4.

The yield *vs.* dose curve for D_4 is shown in Figure 4. Once again a positive deviation from linearity is apparent at higher doses.

It is noteworthy in the present work that the SiH functionality, reported by earlier authors,[4,5,7] is not present. It was first thought that the careful exclusion of moisture might have been the reason that none was found. However, ir measurements on bulk MDM which had been irradiated in the presence of moisture also failed to reveal any Si–H absorption.

Peaks no. 5–10, in Figure 2, were identified both from their position on the chromatogram and from the highest mass peaks of their low-resolution mass spectra, as the cross-linked dimer products (Table I). The cross-linked products proposed are functionally the same as those determined by Dewhurst and St. Pierre[3] for hexamethyldisiloxane. These were the disilane, the sil-methylene, and the sil-ethylene bridged dimers. Since there are two equivalent and one nonequivalent silicon atoms in MDM, there are three possible structural isomers for each type of product.

Table I

Peak no.	Highest ionization peak,[a] *m/e*	Designation	*G*(molecules/100 eV)
1	147	MM	0.95
2	281	D_4	0.40
3	295	MD_2M	1.26
4	369	MD_3M	0.40
5, 6, 7	427	Si–Si dimers	0.38
8, 9	441	Si–CH_2–Si dimers	1.82
10	455	Si–CH_2–CH_2–Si dimers	0.65

[a] To obtain molecular mass add 15 because of CH_3 loss.

Although three disilane peaks (which could be removed upon addition of Br_2) were found, only two sil-methylene and one sil-ethylene appeared in the chromatogram. It would thus seem that under the column conditions used, isomer resolution is lost as the mass of the dimer increases. The *G* values for ≡Si–Si≡, ≡Si–CH_2–Si≡, and ≡Si–CH_2–CH_2–Si≡, 0.38, 1.82, and 0.65, respectively, are larger than those found in the previous model compound investigation, but are in good agreement with average *G*(gas) results obtained from two linear silicone oligomers by others working in this laboratory.[21] Their values were $G(CH_4) = 2.15$, $G(H_2) = 0.61$ and $G(C_2H_6) = 0.36$. The value of *G*(total cross-links) = 2.85 is also in excellent agreement with other

(20) L. J. Bellamy, "Infra-red Spectra of Complex Molecules," Wiley, New York, N. Y., 1954, Chapter 20, Section 4.

(21) K. S. Maeng and L. E. St. Pierre, unpublished work.

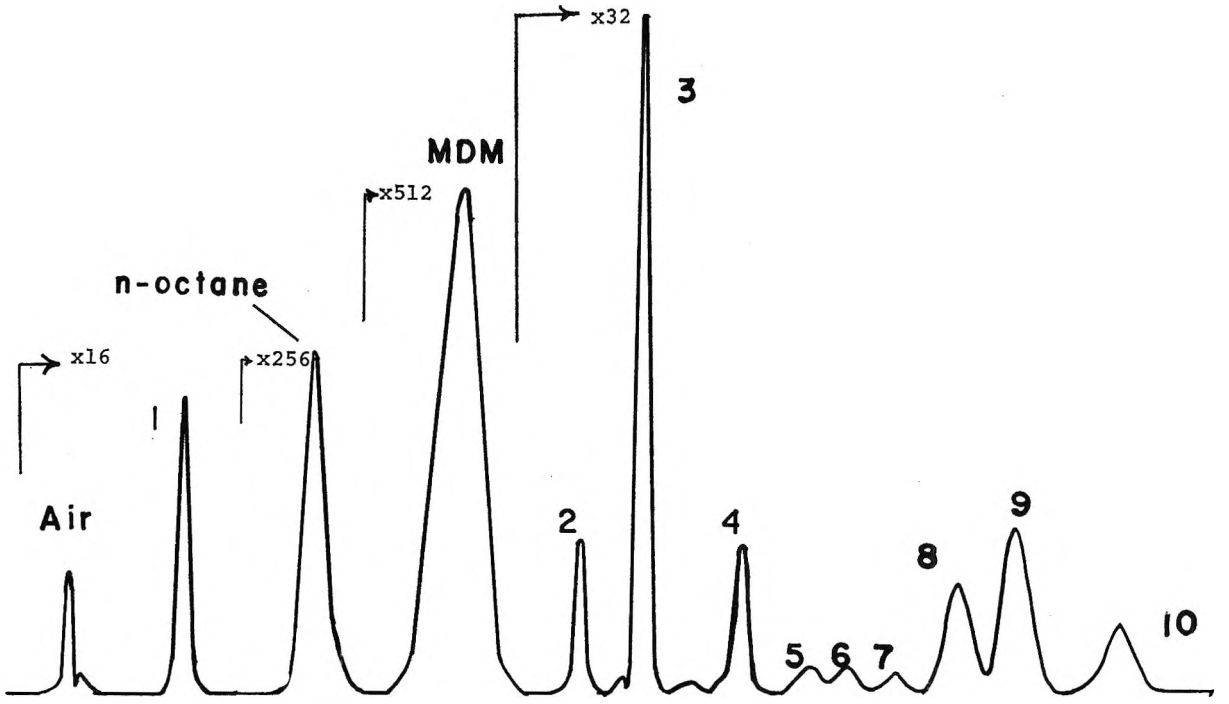

Figure 2. Typical chromatogram of product analysis, SE-30 column. Column temperature 130° until MDM peak (× 512) reached; temperature then raised to 220° at 10°/min and maintained at this temperature for duration.

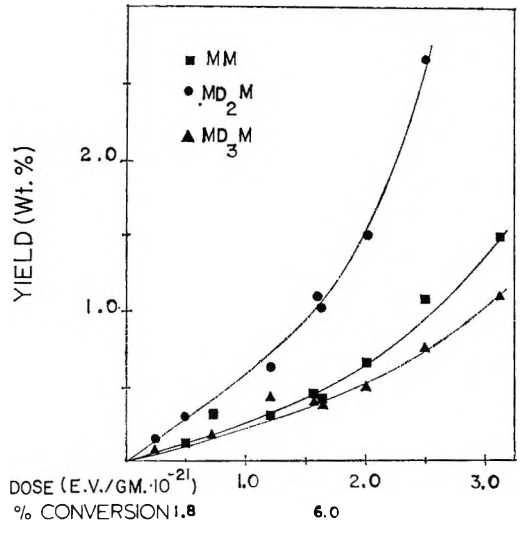

Figure 3. Linear product formation from the radiolysis of octamethyltrisiloxane.

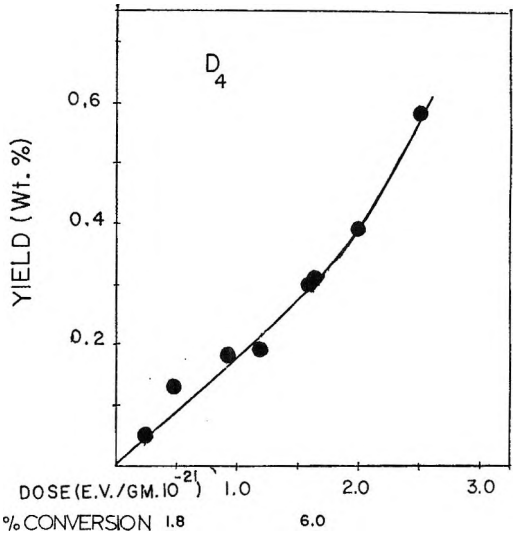

Figure 4. Cyclic product formation from the radiolysis of octamethyltrisiloxane.

Table II

Author	G(cross-links)
Warrick[2]	2.8
St. Pierre, *et al.*[3]	2.5
Miller[5]	3.0
Charlesby[13]	3.1
Okamura[9]	2.8
This publication	2.8

published results, a short resumé of which is shown in Table II.

The yield *vs.* dose curves (Figure 5) for the cross-linked products also begin to exhibit a deviation from linearity at the same value of total yield as the other conversion products.

2. Mechanism of Product Formation. (A) D_4 and MD_3M. The presence of D_4 as a radiation product of MDM cannot be explained *a priori* without resorting to assumptions involving more than one radiation event per molecule, a path which is statistically highly unlikely. In an attempt to establish a more probable alternative, reference was made to the behavior of MDM in the mass spectrometer, since mass spectrometric studies

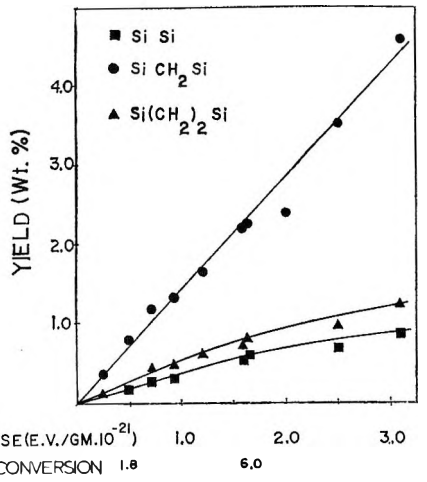

Figure 5. Dimer product formation from the radiolysis of octamethyltrisiloxane.

have been helpful in explaining the radiolysis behavior of some hydrocarbons.[22]

Orlov[23] has published results of a thorough examination of the mass spectra of a number of siloxanes, both cyclic and linear. We have been able to reproduce his results for MDM and have also performed exact mass measurements on the more important ions. Of particular interest is the process by which the MDM ion which has lost a CH_3, termed $MDM^+(-CH_3)$, is transformed to the species $-\overset{|}{\underset{|}{Si}}{}^+$ with the concurrent ejection of a neutral molecule $(C_2H_6SiO)_2$. This is shown schematically as

$$\underset{(CH_3)_8Si_3O_2}{MDM} \xrightarrow{-e} \underset{(CH_3)_8Si_3O_2^+}{MDM^+} \xrightarrow{-CH_3} \underset{(0.02)}{}$$

$$\underset{(CH_3)_7Si_3O_2^+}{MDM^+(-CH_3)} \longrightarrow \underset{(100)}{-\overset{|}{\underset{|}{Si}}{}^+} + \underset{(70)}{(C_2H_6SiO)_2}$$

where ( ) = relative abundance compared with largest peak taken at 100; $\dashrightarrow$ = postulated process; $\longrightarrow$ = based on metastable ion.

The general mechanism of decomposition of the linear siloxanes under electron impact may be summarized from Orlov's work as (1) very fast loss of a methyl group ($\tau < 10^{-6}$ sec),[23] (2) a slower ($\tau < 10^{-6}$ sec) rearrangement which often leads to ejection of a cyclic neutral molecule. Thus the most logical structure for the neutral molecule shown above is D_2, perhaps present as the metastable cyclic

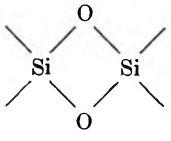

Even if the reaction does not proceed in exactly the same manner in the liquid state radiolysis, the existence in the liquid of such a highly strained ring species would provide a plausible path both for the formation of D_4 and MD_3M. For instance

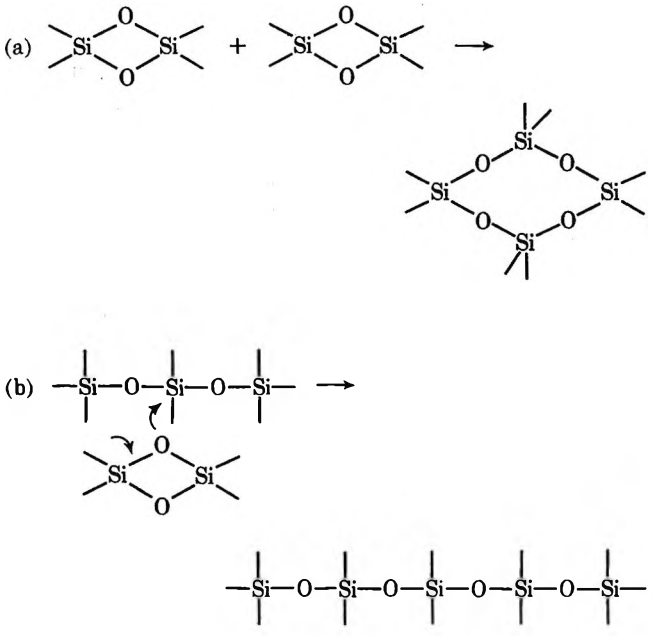

At first glance there may not seem to be a very large probability in favor of the reaction $D_2 + D_2 \rightarrow D_4$ since the metastable species can be present in only very low concentrations. One must bear in mind, however, as Chapiro[24] has pointed out, that radiation processes occur in "tracks" and "spurs" in which the effective concentration of active species is very high. Thus it is only after the species have had an opportunity to diffuse away from one another that their concentration is decreased. On this basis the proposed second-order reaction does not seem unlikely.

(*B*) *MM and* MD_2M. Dewhurst and St. Pierre suggested that all the products obtained from the radiolysis of MM could be qualitatively explained by a simplified free radical combination scheme, but that quantitative analysis revealed discrepancies which required additional mechanisms such as ion–molecule rearrangements. By reference to those radiolysis products of MM labeled by Dewhurst and St. Pierre as "intermediate products," one would predict numerous non-dimer products with small G values to result from the irradiation of MDM, if free radical combination is the mechanism. On the other hand, if only a few such products with substantial G values are found, then the predominant mechanism is probably an ion rearrangement, as such reactions are by their nature highly specific.

(22) A. Chapiro, "Radiation Chemistry of Polymeric Systems," Interscience, New York, N. Y., 1962, Chapter III.

(23) V. Yu Orlov, *Zh. Obsch. Khim.*, **37**, 2300 (1967).

(24) A. Chapiro, "Radiation Chemistry of Polymeric Systems," Interscience, New York, N. Y., 1962, Chapter II, Section 5.

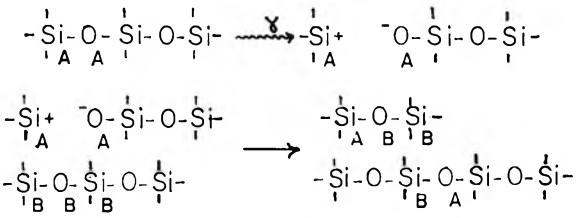

Figure 6. Proposed mechanism for SiO bond exchange due to γ-ray scission. CH_3 groups omitted.

Since observed yields followed the latter pattern, the ionic mechanism appears to be operative. On this basis the mechanism shown in Figure 6 was chosen in order to explain the high yields of MM and MD_2M. This mechanism is in effect a "radiation-induced SiO bond equilibration" and is attractive because it is consistent with the chemically catalyzed siloxane chemistry postulated by Hurd[25] to explain the catalyzed stress relaxation behavior of polydimethylsiloxane networks. Such a mechanism would predict that MM and MD_2M should be formed from MDM with equal G values. As can be seen from Table I, this is very nearly the case.

The small excess of MD_2M can be explained on the grounds that, just as there is a route for the formation of MDM from the radiolysis of MM, a similar subordinate mechanism probably exists for the production of MD_2M from MDM.

Thus, on the basis of the mechanism proposed in Figure 6, the apparent conflict can be resolved between those physical measurements which showed no evidence of scission and the large values of G(scission) obtained from *in situ* stress relaxation experiments. For example, St. Pierre, *et al.*,[4] obtained a value for G(cross-links) from a study of $\bar{M}_n$ for MD_3M as a function of dose. The interpretation of the data required the assumption that G(scission) = 0, yet the value they obtained for G(cross-links) was identical with that found from the present model study. The present data suggest that there was indeed scission of MD_3M, but that it took place mostly as SiO bond equilibration, leaving the number of molecules constant. Thus $\bar{M}_n$ was only influenced by the cross-linking events. Other experiments which failed to show evidence of scission can also be explained in a similar manner.

Table III

Mass spectra	Highest ionization peak, m	Other strong peaks	Peak height ratio $(m+1)/(m+2)$ Standard	Found
(1) MM	147	73, 66		
(2) D_4[a,b]	281	221, 147, 73	1.62	1.53
(3) MD_2M	295	207	1.63	1.63
		metastable 147		
(4) MD_3M	369	281, 147	1.55	1.53
		213, 234 metastables		
5, 6, 7	427[c]			
8, 9	441	221, 147, 73		1.60
10	455	221, 147, 73		1.58

[a] It was impossible to collect D_4 free of starting material MDM. For this reason the spectrum of D_4 contains some quite strong peaks, *e.g.*, 221, 147 which are *not* found in pure D_4. [b] The infrared of D_4 contained the following absorptions: ~2940, ~1260, ~1080, 1040, 840, 820, and 800 cm^{-1}. Those at 1040, 840, and 800 cm^{-1} were assigned to the SiO stretching and CH_3–Si stretching, respectively, of MDM. [c] The yield of products 5, 6, and 7 were insufficient to allow reliable mass spectrometric analyses over the complete mass range. However, the highest mass peaks, 427 in all cases, were clearly assignable.

Acknowledgment. The authors wish to acknowledge financial aid from the National Research Council of Canada and the award of a studentship to one of us (G. B. T.).

(25) R. C. Ostoff, A. M. Bueche, and W. T. Grubb, *J. Amer. Chem. Soc.*, **76**, 4659 (1954).

Dose Rate Effects in the Steady and Pulse Radiolysis of Liquid Chloroform[1,2]

by Ned E. Bibler

Savannah River Laboratory, E. I. du Pont de Nemours and Company, Aiken, South Carolina 29801
(Received April 23, 1971)

Publication costs assisted by the U. S. Atomic Energy Commission

The effect of dose rate on the 100-eV yields of organic products in the radiolysis of chloroform was studied at intensities of 1.6×10^{16} and 17×10^{16} eV/g-sec using a ^{60}Co γ-ray source and at maximum instantaneous dose rates of 2.5×10^{24} and 6.4×10^{24} eV/g-sec using a pulse X-ray generator. The radiolysis products were CH_2Cl_2, C_2Cl_4, CCl_4, sym-$C_2H_2Cl_4$, C_2HCl_5, and C_2Cl_6. As the dose rate increased, $G(CH_2Cl_2)$ and $G(C_2Cl_6)$ decreased, $G(C_2H_2Cl_4)$ and $G(C_2HCl_5)$ increased, and $G(C_2Cl_4)$ and $G(CCl_4)$ remained unchanged. These results are consistent with a free-radical mechanism involving the reaction of Cl and $CHCl_2$ radicals with $CHCl_3$ to produce CCl_3 radicals. The dose rate effects result from a competition between $CHCl_3$ molecules and radicals for the $CHCl_2$ radicals, with higher dose rates favoring the radical–radical reactions. The observed 100-eV yields in both the steady and pulse radiolysis experiments agreed with those calculated by the application of the previously proposed independent action model. A value of 1.3 ± 0.2 M^{-1} sec^{-1} was determined for the rate constant for the reaction of $CHCl_2$ radicals with $CHCl_3$ at 25° from the steady radiolysis experiments, and the magnitude of this value was confirmed by the results of the pulse radiolysis experiments. The results of the pulse radiolysis experiments suggest that the rate constant of Cl atom attack on $CHCl_3$ is lower in the liquid than in the vapor phase. Evidence is also presented that indicates that Cl atoms and $CHCl_2$ radicals are not radiolytically formed with equal 100-eV yields.

Introduction

In the radiolysis of liquid chloroform, evidence has been cited[3-5] for the effects of dose rate variations on the 100-eV yields of the organic products (CH_2Cl_2, C_2Cl_4, CCl_4, sym-$C_2H_2Cl_4$,C_2HCl_5, and C_2Cl_6). At constant temperature, as the dose rate increases, $G(CH_2Cl_2)$ and $G(C_2Cl_6)$ decrease, $G(C_2H_2Cl_4)$ and $G(C_2HCl_5)$ increase, and $G(C_2Cl_4)$ and $G(CCl_4)$ remain unchanged.[5] These results are consistent with a free-radical mechanism involving the reaction of Cl and $CHCl_2$ radicals with $CHCl_3$ to produce CCl_3 radicals. The competition between the $CHCl_3$ molecules and radicals for the $CHCl_2$ radicals accounts for the dose rate effects. Abramson and Firestone[5] have calculated this dose rate effect in $CHCl_3$ by the application of an independent action model. In this model two radiolytic mechanisms are proposed to occur simultaneously but independently. One mechanism (the spur mechanism) involves reactions that occur in the tracks and is not affected by the presence of the radical scavenger Br_2[6] or changes in the dose rate.[5] The other (the homogeneous mechanism) involves reactions of $CHCl_2$ and CCl_3 radicals distributed homogeneously throughout the solution. The rates of these reactions are dose rate dependent.[5] By solving for the steady-state concentrations of the radicals in the homogeneous mechanism, Abramson and Firestone calculated values for $G(CH_2Cl_2)$, $G(C_2H_2Cl_4)$, $G(C_2HCl_5)$, and $G(C_2Cl_6)$ that were in agreement with their experimental results at dose rates in the range of 1.3×10^{15} to 13×10^{15} eV/g-sec and temperatures of 0 to 63°. Further, their calculations predicted that at very high dose rates, $G(CH_2Cl_2)$ should approach zero, and the values for $G(C_2H_2Cl_4)$, $G(C_2HCl_5)$, and $G(C_2Cl_6)$ should be 1.5, 2.0, and 1.2, respectively.

We have tested these predictions using an intense ^{60}Co γ-ray source for steady radiolysis experiments at dose rates slightly greater than 10^{17} eV/g-sec and an X-ray generator for pulse radiolysis experiments at dose rates approaching 10^{25} eV/g-sec.

Experimental Section

Chloroform from several commercial sources was purified by treating with Br_2 to remove unsaturates, then washed once with aqueous Na_2SO_3 solution and several times with pure water. It was then triply distilled in an inert atmosphere. The only detectable impurity in the final distillate was 1,1-$C_2H_4Cl_2$ ($\sim 5 \times 10^{-5}$ M). The oxygen-induced decomposition of the purified $CHCl_3$ could be prevented by storing it under distilled water.

Samples were prepared by vacuum distilling $CHCl_3$ (previously dried by passage through a 5-Å molecular sieve attached to the vacuum line) into Pyrex[7] irradia-

(1) The information contained in this article was developed during the course of work under Contract AT(07-2)-1 with the U. S. Atomic Energy Commission. This work is being sponsored by the Division of Peaceful Nuclear Explosives of the USAEC.

(2) Presented in part at the 153rd National Meeting of the American Chemical Society, Miami Beach, Fla., Apr 9–14, 1967.

(3) G. M. Meaburn, Ph.D. Dissertation, The University of Leeds, England, 1959.

(4) J. B. Gardner and B. G. Harper, Paper No. 53, 8th Annual Meeting of the Radiation Research Society, San Francisco, Calif., May 9–11, 1960. The results of this study are published in ref 5.

(5) F. P. Abramson and R. F. Firestone, *J. Phys. Chem.*, **70**, 3596 (1966).

(6) H. R. Werner and R. F. Firestone, *ibid.*, **69**, 840 (1965).

(7) Trademark of Corning Glass Works, Corning, N. Y.

tion cells, where it was carefully degassed by at least six freeze–pump–thaw cycles. The cells were then sealed with the sample at liquid nitrogen temperatures under vacuum. For irradiations with the ^{60}Co sources, the cells were 15-mm o.d. tubes. For the pulsed irradiations, the cells were 1.7 cm square by 2 cm high.

Irradiated solutions were analyzed with an F & M Model 400 gas chromatograph employing flame ionization detection. Three different columns were used isothermally. For CH_2Cl_2, a 16-ft, $^1/_4$-in. column (30% silicone 200 on Celite[8]) were used; for C_2Cl_4, $C_2H_2Cl_4$, C_2HCl_5, and C_2Cl_6, a 50-ft, $^1/_8$-in. column (2% SE-30 on diatomaceous earth); and for CCl_4, a 6-ft, $^1/_4$-in. polar column (10% Triton[9] x-305 on 60–80 mesh Chromosorb P) followed by a 6-ft, $^1/_4$-in. nonpolar column (20% SE-30 on Gas Chrom X[10]). On the polar column, CCl_4 had a shorter retention time than $CHCl_3$. The nonpolar portion resolved CCl_4 from the 1,1-$C_2H_4Cl_2$ impurity. The gas chromatograph was calibrated using standards prepared from carefully purified solutes each time samples were analyzed. The solute peaks were very narrow; consequently, the concentrations of products were determined by comparing their peak heights with those of the standards.

Steady irradiations were performed using ^{60}Co γ-ray sources containing either ~240,000 or 22,800 Ci of radioactivity. The more intense source was calibrated with both LiF and the air-saturated cupric–ferrous dosimeter [$G(Fe^{3+}) = 0.66$].[11] The agreement between the results of the two dosimeters was good and the dose rate in $CHCl_3$, after correcting for differences in electron densities, was 1.7×10^{17} eV/g-sec. The other source was a Gammacell 220 (Atomic Energy of Canada), which was calibrated using the Fricke dosimeter. The dose rate in $CHCl_3$ was 1.6×10^{16} eV/g-sec. In both sources, the temperature of the samples was maintained at 25 ± 1°, and the samples were irradiated to doses no larger than 2.40×10^{19} eV/g.

Pulsed irradiations were performed at ambient temperature (~25°) using a Febetron[12] Model 705 pulsed electron accelerator. This electron pulse (maximum energy = 2.0 MeV) was impinged on a 20-mil tungsten target, creating an intense X-ray pulse. This pulse was passed through a 5-mil tantalum foil and then through the samples. The total time length of the pulse was ~40 nsec with 80% of the total dose delivered within 20 nsec.[13] The effective time width (total dose/maximum instantaneous intensity) of the pulse was 19 nsec.[13] Samples were positioned behind the tantalum foil so that they were completely within the X-ray beam and irradiated with up to 63 pulses with at least a 2-min recycle time between pulses.

The dose/pulse absorbed by the samples were determined using manganese-activated LiF. Samples of this material were irradiated in the cells in positions identical with those of the $CHCl_3$ samples. Earlier studies have shown that the response of LiF is independent of dose rates less than 2×10^{11} rads/sec[14] and that LiF serves as a good secondary standard for measuring doses from pulsed X-rays.[15] (The dose rate in this article was somewhat less than that cited above.) The response of the LiF was calibrated against the Fricke dosimeter using 0.84[16] as the ratio of the dose in LiF to that in the Fricke dosimeter. To determine the dose/pulse received by the $CHCl_3$, the dose/pulse in the LiF was multiplied by the ratio of the effective mass energy absorption coefficients for each compound. These two coefficients were calculated by graphical integration of the monoenergetic absorption coefficients for each compound[17] over the energy spectrum of the photons in the beam. Since the electrons impinging on the target are not monoenergetic, it is difficult to determine the exact energy spectrum of the emitted photons. This spectrum has been approximated by Charbonnier[18] to be closely equivalent to the bremsstrahlung spectrum measured by Tochilin and Goldstein[19] when 2.0-MeV electrons were impinged on a comparable tungsten transmission target. Recently, more elaborate calculations[18] correlating the measured electron energy spectrum of the Febetron 705 with the measured photon spectrum from constant-voltage electron accelerators[14,19] substantiated this approximation. In our experiments, the purpose of the tantalum foil was to "harden" the X-ray spectrum by removing a major portion of the X-rays of energies lower than 70 keV. Based on the calculations of Charbonnier[18] the energy spectrum of the X-rays irradiating our samples has a peak at 200 keV, with >91% of the photons having energies larger than this. Using this spectrum, the ratio of the effective mass energy absorption coefficients for $CHCl_3$ to LiF was 1.13. This is only slightly larger than 1.05, the ratio for the coefficients calculated for energies when energy absorption is predominantly by the Compton process.

The reproducibility of the dose/pulse for the samples was determined from three or more independent LiF dosimeters. The variance was 8% or less. Small dosimeters placed along the length of a cell indicated

(8) Trademark of Johns–Manville Sales Corp.

(9) Trademark of Rohm and Haas Co.

(10) Trademark of Applied Science Laboratories.

(11) E. Bjergbakke and K. Sebested, *Advan. Chem. Ser.*, **81**, 579 (1968).

(12) Field Emission Corp., McMinnville, Ore.

(13) Field Emission Corp., Technical Bulletin, Vol. 4, No. 1 (1965).

(14) N. Goldstein and E. Tochilin, *Health Phys.*, **12**, 1705 (1966).

(15) E. M. Fielden and E. J. Hart, *Advan. Chem. Ser.*, **81**, 585 (1968).

(16) A. Brnjolfsson, *ibid.*, **81**, 550 (1968).

(17) E. Storm and H. I. Israel, "Photon Cross Sections from 0.001 to 100 MeV for Elements 1 through 100," La-3753 (1967).

(18) F. M. Charbonnier, Field Emission Corp., McMinnville, Ore., private communication.

(19) E. Tochilin and N. Goldstein, USNDRL-TR-939 (1965).

that the intensity of the radiation varied from the front to the back of a sample by a factor of 2.5 or less. In view of the reproducibility (8%) of the dose/pulse, uncertainties in the dose/pulse for each sample are probably no greater than 15%. The maximum instantaneous dose rate for the samples was calculated by dividing the dose/pulse by the effective time width of the pulse (19 nsec[13]).

Results

The 100-eV yields of all the organic products at the three dose rates are summarized in Table I.[20] At the two lower dose rates, the dose dependence of the yields was always linear up to the maximum dose of 2.40 $\times$ 10^{19} eV/g. Also, the maximum relative difference in the 100-eV yields determined in independent experiments varied by less than 8%. The results at 1.6 $\times$ 10^{16} eV/g-sec agree with those of Abramson and Firestone determined at 1.3 $\times$ 10^{16} eV/g-sec and 26°.[5]

Table I: Dose Rate Dependence of the 100-eV Yields in the Radiolysis of Chloroform at ~25°

	100-eV yields		
Product	1.6 $\times$ 10^{16} eV/g-sec[a]	1.7 $\times$ 10^{17} eV/g-sec[a]	2.5–6.4 $\times$ 10^{24} eV/g-sec[b]
CH_2Cl_2	1.9	1.2	0.2 ± 0.1
CCl_4	0.89	0.86	0.94 ± 0.06
C_2Cl_4	0.085	0.084	0.078 ± 0.08
$C_2H_2Cl_4$	0.73	1.0	1.5 ± 0.1
C_2HCl_5	1.6	1.9	1.8 ± 0.1
C_2Cl_6	2.0	1.4	0.85 ± 0.06

[a] Irradiated at 25 ± 1°. Uncertainties are estimated at <±5%. [b] Range of maximum instantaneous dose rates from the pulse radiolysis experiments. Irradiated at room temperature (~25°). Uncertainties calculated by a least-squares treatment of yield–dose curves. For $G(CH_2Cl_2)$, the uncertainty is the average deviation from the mean of determinations in seven samples.

The dose dependence of the yields of C_2Cl_6, $C_2H_2Cl_4$, and C_2HCl_5 determined in the pulse radiolysis experiments is shown in Figure 1. For each product the line is drawn with a slope and intercept determined by the method of least squares. The similarities of the sets of data about each line indicate that the major source of error in these experiments is the determination of the dose received by each sample. This error is primarily due to slight differences in the positions of the samples and the dosimeters in the X-ray beam. Since the data are linear, there was no effect of dose on the 100-eV yields up to the maximum dose of 1.2 $\times$ 10^{19} eV/g. Also, the closeness of the intercepts to zero indicates that the degassings had sufficiently removed O_2 from the samples.[21] Plots similar to those in Figure 1 were obtained for the yields of C_2Cl_4 and CCl_4, and a least-squares analysis was performed. Because of the small 100-eV yield of CH_2Cl_2 in these experiments, and the

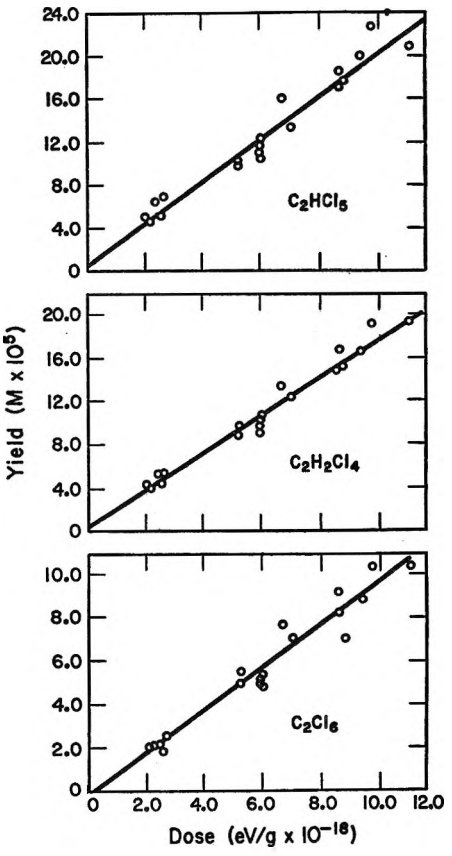

Figure 1. Dose dependence of the yields of C_2Cl_6, $C_2H_2Cl_4$, and C_2HCl_5 in the pulse radiolysis of chloroform at ~25°. Dose rate = 2.5–6.4 $\times$ 10^{24} eV/g-sec.

relatively low sensitivity of the analytical method for this compound, its yield could only be determined in those samples irradiated to doses larger than 6 $\times$ 10^{18} eV/g. Also, because the amount of CH_2Cl_2 being measured was close to the analytical sensitivity, the data for the dose dependence of its production were scattered. Therefore at least-squares analysis of the data was not performed, and the 100-eV yield of CH_2Cl_2 was calculated by averaging the results of several independent experiments. The largest dose/pulse irradiating the sample was 1.9 $\times$ 10^{16} eV/g, and the smallest, 6.9 $\times$ 10^{15} eV/g.

The dose rate dependence of $G(CH_2Cl_2)$, $G(C_2H_2Cl_4)$, $G(C_2HCl_5)$, and $G(C_2Cl_6)$ in Table I is similar to the results of other workers.[4,5] Also, the invariance of $G(C_2Cl_4)$ and $G(CCl_4)$ at low dose rates is in agreement with other results of the γ radiolysis of $CHCl_3$.[5]

(20) The results at the highest dose rate are different from those cited in the original abstract of this paper (Abstract R-51) submitted at the 153rd National Meeting of the American Chemical Society, Miami Beach, Fla., Apr 1967. This difference is due to the presence of trace amounts of *cis*-$C_2H_2Cl_2$ in the earlier samples. Consequently, the interpretation in that abstract does not apply to pure $CHCl_3$.

(21) Experiments performed in this laboratory have demonstrated that traces of O_2 completely inhibit the formation of C_2Cl_6 at low dose.

Discussion

The following mechanism has been proposed[5,6] to explain the effects of temperature,[5,6] dose rate,[5] and the presence of various solutes[6] on the product yields. Reactions involving neutral species can account for all the organic products except CCl_4. The predominant neutral intermediates found as a result of ionization, neutral excitation, and charge neutralization processes in $CHCl_3$ are Cl atoms, $CHCl_2$ radicals, and small yields of dichloromethylene (CCl_2). By reaction with $CHCl_3$, both Cl and $CHCl_2$ radicals produce CCl_3 radicals.

$$Cl + CHCl_3 \longrightarrow HCl + CCl_3 \quad (1)$$

$$CHCl_2 + CHCl_3 \longrightarrow CH_2Cl + CCl_3 \quad (2)$$

$$2CHCl_2 \longrightarrow C_2H_2Cl_4 \quad (3)$$

$$CCl_3 + CHCl_2 \longrightarrow C_2HCl_5 \quad (4)$$

$$2CCl_3 \longrightarrow C_2Cl_6 \quad (5)$$

$$CCl_2 + CHCl_3 \longrightarrow C_2HCl_5^* \quad (6)$$

$$C_2HCl_5^* \longrightarrow HCl + C_2Cl_4 \quad (7)$$

$$C_2HCl_5^* \xrightarrow{M} C_2HCl_5 \quad (8)$$

Recent experiments[22] using NH_3 or n-C_4H_9OH as positive ion scavengers have established that CCl_4, the remaining organic product, is formed by a charge neutralization process. As will be shown, the results of the present experiments lend further support to the above overall mechanism.

Values for the 100-eV yields of C_2Cl_4 and CCl_4 are independent of dose rate from[6] 7.8×10^{14} to 6.4×10^{24} eV/g-sec (Table I). The failure of the highest intensity to change these 100-eV yields implies that these products are formed by efficient radical–solvent reactions or reactions involving ions or excited species.[23] Reaction 6, leading to the production of C_2Cl_4, represents an efficient reaction involving the solvent. Strong evidence for reactions 6–8 has been furnished by the pyrolysis of $CHCl_3$ vapor at 500°, where HCl and C_2Cl_4 are the principal products.[24] In addition to being independent of dose rate, $G(C_2Cl_4)$ is unaffected by the presence of the radical scavengers Br_2[6] or I_2[25] and also exhibits a small positive temperature coefficient.[5,6] All these facts support the occurrence of reactions such as 6 and 7 in the radiolysis of liquid $CHCl_3$. For CCl_4, the lack of a dose rate effect supports the finding that this product is formed by a charge neutralization reaction.[22] Such reactions are expected to be dose rate independent.

The 100-eV yields of $CHCl_2$ and CCl_3 radicals appearing as products from the free radical mechanism (reactions 1–5) are summarized in Table II. As the dose rate increases, $G(CHCl_2)$ remains unchanged while $G(CCl_3)$ decreases. The decrease is consistent with a decline in the rate of the radical–solvent reaction 2. At the higher dose rates a larger fraction of $CHCl_2$ radicals undergo radical–radical reactions rather than reacting with $CHCl_3$. Such a competition does not occur for Cl atoms (the other precursor of CCl_3 radicals) at low dose rates, since at these intensities reaction 1 is 100% efficient.[6] The efficiency of this reaction is supported by the recent observation[25] that $G(ICl) = 0$ in the radiolysis of $CHCl_3$ containing $\sim 10^{-2}$ M I_2. In these experiments, $G(CH_2Cl_2)$ was equal to zero, as it is in the radiolysis of similar solutions containing Br_2,[6] indicating that reaction 2 is completely inhibited.

Table II: Dose Rate Dependence of the 100-eV Yields of $CHCl_2$ and CCl_3 Radicals Appearing as $C_2H_2Cl_4$, C_2HCl_5, and C_2Cl_6

Dose rate, eV/g-sec	$G(CHCl_2)^a$	$G(CCl_3)^b$
1.6×10^{16}	5.0	5.6
1.7×10^{17}	5.1	4.7
$2.5\text{–}6.4 \times 10^{24}$ [c]	5.0	3.5

[a] $G(CHCl_2) = G(CH_2Cl_2) + 2G(CH_2Cl_4) + G(C_2HCl_5)$. [b] $G(CCl_3) = G(C_2HCl_5) + 2G(C_2Cl_6)$. [c] Maximum instantaneous dose rates from the pulse radiolysis experiments.

As mentioned earlier, Abramson and Firestone[5] have quantitatively calculated the effect of dose rate variations on the product yields at intensities lower than those in this study by employing an independent action model. In the model, two mechanisms occur simultaneously but independently of each other. In one mechanism, the products are formed by fast reactions occurring in the spurs or tracks; this mechanism is termed the spur mechanism. In the other mechanism, product formation results from the reactions of free radicals at thermal energies distributed homogeneously through the solution. The 100-eV yields of products from the spur mechanism have been measured[6] in the presence of Br_2, which scavenges the homogeneous mechanism. These spur yields are $G(C_2H_2Cl_4)_{spur} = 0.34$, $G(C_2HCl_5)_{spur} = 0.18$, $G(CH_2Cl_2)_{spur} = 0.00$, and $G(C_2Cl_6)_{spur} = 0.02$. Also, the entire yield of CCl_4 can be attributed to a fast reaction ($G = 0.89$),[22] that is independent of dose rates and radical scavengers.

The 100-eV yields of $CHCl_2$ and CCl_3 radicals in the homogeneous mechanism have not been measured by radical-scavenging techniques. However, these yields can be estimated by subtracting from the observed yield for the radicals, the contribution to each from the above spur mechanism. The results of this calculation for the experiments at both the low and high

(22) J. N. Baxter and N. E. Bibler, *J. Chem. Phys.*, **53**, 3444 (1970).

(23) W. G. Burns and R. Barker, *Progr. React. Kinet.*, **3**, 303 (1965).

(24) G. P. Semeluk and R. B. Bernstein, *J. Amer. Chem. Soc.*, **79**, 46 (1957); A. I. Shilov and R. D. Sabirova, *Russ. J. Phys. Chem.*, **34**, 408 (1960).

(25) N. E. Bibler, unpublished results.

dose rates appear in Table III. The 100-eV yield of homogenously distributed $CHCl_2$ radicals [$G(CHCl_2)'$] appears independent of dose rate over the whole range of dose rates studied. Further, these values are in good agreement with the value calculated by Abramson and Firestone.[5] Values for the 100-eV yield of CCl_3 radicals distributed homogenously [$G(CCl_3)'$] determined in the steady radiolysis experiments are equal within experimental error. Also, these values are close to 3.8 radicals/100-eV calculated for $G(CCl_3)'$ from Abramson and Firestone's[5,26a] data. The decrease in $G(CCl_3)'$ in going from the steady to the pulse radiolysis experiments appears real in light of the good precision calculated for $G(C_2Cl_6)$ and $G(C_2HCl_5)$ in the pulse radiolysis experiments (6–7%) and the rather large number (19) of samples irradiated. Also, samples irradiated in the steady radiolysis experiment and those irradiated in the pulse radiolysis experiments were analyzed on the gas chromatograph after the instrument was calibrated using the same set of standards. This eliminates any systematic error in determining the relative values for the product and, thus, the calculated radical yields.

Table III: Dose Rate Dependence of the 100-eV Yields of $CHCl_2$ and CCl_3 Radicals in the Homogeneous Free Radical Mechanism

Dose rate, eV/g-sec	$G(CHCl_2)'$[a]	$G(CCl_3)'$[b]
1.6×10^{16}	4.1	3.5
1.7×10^{17}	4.2	3.3
$2.5\text{–}6.4 \times 10^{24}$ [c]	4.1	3.1

[a] $G(CHCl_2)' = G(CH_2Cl_2) + 2G(C_2H_2Cl_4) - 2G(C_2H_2Cl_4)_{spur} + G(C_2HCl_5) - G(C_2HCl_5)_{spur}$. [b] $G(CCl_3)' = G(C_2HCl_5) - G(C_2HCl_5)_{spur} + 2G(C_2Cl_6) - G(CH_2Cl_2)$. [c] Maximum instantaneous dose rates of the pulse radiolysis experiments.

Failure of $G(CHCl_2)'$ to equal $G(CCl_3)'$ in the steady radiolysis experiments where all the Clatons react with $CHCl_3$ molecules[4,5] suggests that $CHCl_2$ radicals and Cl atoms are not produced with equal 100-eV yields. The dissociation of neutral excited $CHCl_3$ molecules probably leads to $CHCl_2$ radicals and Cl atoms in equal yields. Also, an ionic mechanism involving $CHCl_3^+$ as the cation and Cl^- (formed from $CHCl_3$ by dissociative electron attachment[26b]) as the anion probably produces $CHCl_2$ and CCl_3 radicals in equal yields (reactions 9 and 10). Consequently, these reactions cannot account for the difference between $G(CHCl_2)'$ and $G(CCl_3)'$. Mechanisms involving cations such as $CHCl_2^+$ and anions such as $CHCl_3^-$ can account for the difference, but the lack of sufficient data renders these mechanisms speculative. However, the difference between the two 100-eV yields is closely equal to $G(CCl_4)$, and this suggests that the mechanism may involve the precursor for CCl_4. The collisionally stabilized anion $CHCl_3^-$ has been suggested as a precursor for CCl_4.[22]

$$CHCl_3 + e^- \longrightarrow CHCl_2 + Cl^- \quad (9)$$

$$Cl + CHCl_3^+ \longrightarrow HCl + CCl_3 \quad (10)$$

The dose rate dependence of the product yields in the homogeneous mechanism for the steady radiolysis experiments can be calculated from the steady-state concentrations of $CHCl_2$ and CCl_3 radicals determined by solving (11) and (12), where I is the dose rate.

$$d(CHCl_2)'/dt = G(CHCl_2)'I/100 - k_2(CHCl_2)(CHCl_3) - 2k_3(CHCl_2)^2 - k_4(CHCl_2)(CCl_3) \quad (11)$$

$$d(CCl_3)'/dt = G(CCl_3)'I/100 + k_2(CHCl_2)(CHCl_3) - 2k_5(CCl_3)^2 - k_4(CHCl_2)(CCl_2) \quad (12)$$

Using $5.0 \times 10^7\ M^{-1}\ sec^{-1}$ for k_5,[27] Abramson and Firestone found agreement with their experimental results at 26° when the ratio $k_3:k_4:k_5$ was equal to 1.0:1.5:11.0 and k_2 was equal to $1.1\ M^{-1}\ sec^{-1}$. The results of similar calculations on the data in the present article for the the ^{60}Co sources appear in Table IV. The agreement between the calculated and observed results is good except for the values of $G(CH_2Cl_2)$ and $G(C_2H_2Cl_4)$ at the higher dose rate. As indicated in Table IV, better overall agreement was attained by raising k_2 by 25% to $1.3\ M^{-1}\ sec^{-1}$. In addition to varying k_2 in our calculations, the ratio $k_3:k_4:k_5$ was also varied. Satisfactory agreement between the observed and calculated results was attained only when the ratio was equal to 1.0:1.5:1.0. As in the calculations of Abramson and Firestone, the value determined for k_2 depends upon the value chosen for k_5. Published values[28,29] for this constant range all lie within the range 3.5×10^7 to $8.0 \times 10^7\ M^{-1}\ sec^{-1}$ at 24°. With these two different values, best agreement with the experimental results was attained when k_2 was 1.1 or $1.5\ M^{-1}\ sec^{-1}$, respectively.

For calculating the product yields resulting from the pulse radiolysis experiments, the steady-state hypothesis is no longer applicable. The differential equations describing the rates of radical formation and reaction and also those for product formation must be integrated numerically. A digital computer was used and the

(26) (a) The equation used by Abramson and Firestone[5] for calculating $G(CCl_3)'$ differs slightly from that used in this study (see footnote b, Table III). In their equation, a term for CCl_4 formation in the homogeneous mechanism was included. In light of recent data,[22] all the CCl_4 can be attributed to the spur mechanism, and this term should not be included in the calculation. (b) W. E. Wentworth, R. S. Becker, and R. Tung, *J. Phys. Chem.*, 71, 1652 (1967).

(27) H. W. Melville, J. C. Robb, and R. C. Tutton, *Discuss. Faraday Soc.*, 14, 150 (1953).

(28) D. J. Carlsson, J. A. Howard, and K. U. Ingold, *J. Amer. Chem. Soc.*, 88, 4726 (1966).

(29) W. I. Bengough and R. A. M. Thomson, *Trans. Faraday Soc.*, 57, 1928 (1961).

Table IV: Observed and Calculated 100-eV Yields in the Homogeneous Mechanism for the Steady Radiolysis of $CHCl_3$ at 25°

	100-eV yields					
	1.6×10^{16} eV/g-sec			1.7×10^{17} eV/g-sec		
	Observed	Calculated		Observed	Calculated	
Products	*a*	*b*	*c*	*a*	*b*	*c*
CH_2Cl_2	1.9	1.9	2.1	1.2	0.84	1.0
$C_2H_2Cl_4$	0.39	0.42	0.34	0.66	0.85	0.77
C_2HCl_5	1.4	1.4	1.3	1.7	1.6	1.6
C_2Cl_6	2.0	1.9	2.1	1.4	1.3	1.4

[a] Determined by subtracting the spur yield for each product from the observed yield. [b] Calculated using published[5] rate constants. [c] Calculated using $k_2 = 1.3\ M^{-1}\ \text{sec}^{-1}$.

equations were integrated by a fourth-order Runge Kutta technique.[30] Since the intensity of the radiation pulse was not constant, the computer program also contained a subroutine that simulated the time dependence of this intensity. When eq 11 and 12 were integrated (this assumes that all the Cl atoms react with $CHCl_3$ in the pulse radiolysis experiments) along with the equations describing the rates of product formation, the results (see column 3, Table V) were in good agreement with all the observed product yields except $G(C_2Cl_6)$, where the relative difference was ~20%. This difference results primarily from using a value for $G(CCl_3)$ in the calculations that is higher than that determined in the high-intensity experiments.

Table V: Observed and Calculated 100-eV Yields in the Homogeneous Mechanism for the Pulse Radiolysis of $CHCl_3$ at ~25°

	100-eV yields		
		Calculated[b]	
Products	Observed[a]	Mechanism I[c]	Mechanism II[d]
CH_2Cl_2	0.2	0.1–0.2	0.1–0.3
$C_2H_2Cl_4$	1.2	1.2–1.1	1.2–1.1
C_2HCl_5	1.6	1.6–1.5	1.5–1.5
C_2Cl_6	0.85	1.0–1.1	0.83–0.95

[a] Determined by subtracting the open yield for each product from the actual observed yield. [b] Calculated for doses per pulse of 4.8×10^{16} and 12×10^{16} eV/g, respectively, for each mechanism. [c] Mechanism where all the Cl atoms are assumed to react with $CHCl_3$. [d] Mechanism including radical recombination reactions for Cl atoms.

The lower value for $G(CCl_3)$ estimated from the pulse radiolysis experiments suggests that some process is interfering with reaction 1 at these high intensities. The extent of the interference is only ~10% at this intensity. Spur overlap, leading to an increased probability of the recombination of $CHCl_2$ and Cl radicals or their precursors, does not appear to be the interfering process, since excellent agreement is obtained among the different values for $G(CHCl_2)$ calculated from both the steady and pulse radiolysis experiments. Also, the value for $G(CCl_4)$ in the pulse radiolysis experiments is within 6% of the value determined in the steady radiolysis experiments, further suggesting that spur overlap is not a significant factor.

To test whether it is reasonable that back reactions of Cl atoms in the homogeneous mechanism might compete at this high intensity with reaction 1, and thus lower $G(CCl_3)'$, terms for the rates of these back reactions were included in the rate equations. Reactions 13–15 were considered. Rate constants for these were

$$Cl + CHCl_2 \longrightarrow CHCl_3 \quad (13)$$

$$Cl + CCl_3 \longrightarrow CCl_4 \quad (14)$$

$$2Cl \longrightarrow Cl_2 \quad (15)$$

estimated from the modified Debye equation,[31] after assuming that the reactions were diffusion controlled. The values for the rate constants were $k_{13} = 2.0 \times 10^{10}$, $k_{14} = 2.0 \times 10^{10}$, and $k_{15} = 1.3 \times 10^{10}$. Also, in the expanded rate equations a term for the rate of reaction 1 was included. In this equation, $G(Cl)'$ (the 100-eV yield of Cl atoms in the homogeneous mechanism) was set equal to 3.4 atoms/100-eV, and $G(CCl_3)'$ was replaced by $k_1(Cl)(CHCl_3)$. Product yields were then calculated as a function of k_1. Best agreement for all the yields was obtained (see column 4, Table V) when k_1 was equal to $6 \times 10^4\ M^{-1}\ \text{sec}^{-1}$. With this value, $G(13)$ was equal to 0.1, $G(14)$ to 0.07, and $G(15)$ to 0.05. The sum $G(13) + 2G(14) + 2G(15)$ is equal to the difference between the values calculated for $G(CCl_3)'$ from the pulse and steady radiolysis experiments. The value for k_1 that allows the best agreement between the observed and calculated results depends, of course, upon the values assigned to k_{13}, k_{14}, and k_{15}. Since these values are, at best, only order of magnitude estimates, any value for k_1 derived from the above calculation is also a rough estimate.

The value for k_1 has not been independently determined in the liquid phase. Its magnitude has been estimated[32] to be $\sim 10^7\ M^{-1}$ from the results of competitive photochloronation studies,[33] after assuming that Cl atoms react with identical rates in liquid and vapor c-C_5H_{10}[33] and using the absolute value for the rate constant for the reaction of Cl atoms with c-C_5H_{10} vapor.[34] There are data,[35] however, that imply that the assump-

(30) S. Gill, *Proc. Cambridge Phil. Soc.*, **47**, 96 (1951).

(31) H. L. J. Bäckström and K. Sandros, *Acta Chem. Scand.*, **14**, 48 (1960).

(32) G. A. Russell, A. Ito, and D. G. Hendry, *J. Amer. Chem. Soc.*, **85**, 2976 (1963).

(33) G. A. Russell, *ibid.*, **80**, 4997 (1958).

(34) J. H. Knox and A. F. Trotman-Dickenson, "Reactions of Free Radicals in the Gas Phase," Special Publication No. 9, The Chemical Society, London, 1957, p 35.

(35) I. Galiba, J. M. Tedder, and J. C. Walton, *J. Chem. Soc. B*, 604 (1966); H. Singh and J. M. Tedder, *ibid.*, 605 (1966).

tion of equal rates of reaction for Cl atoms in the vapor and liquid phase is erroneous. The value of 10^7 M^{-1} sec^{-1} for k_1 is nearly equal to the value determined in chloroform vapor.[36] Although both these values are roughly 160 times the value determined in the present study, it is tentatively concluded, in light of possible entropy or solvation effects on the rates of Cl atom reactions in liquids,[35] that the model fits the results. However, further data at different temperatures or higher intensities are necessary to confirm that the observed effect does result from a competition between reaction 1 and reactions 13–15 for Cl atoms. Based on this model, it appears that k_1 is clearly one to two orders of magnitude smaller in the liquid than in the vapor phase. Recently, it was determined that k_2 is an order of magnitude smaller in liquid chloroform than in the vapor, due primarily to an entropy effect.[37]

As in the calculations for the steady radiolysis experiments, the value for k_2 that gave best agreement with the observed results was dependent on the values assigned to k_4, k_5, and k_6. With the range presented earlier for k_5, agreement with the experimental results was attained when k_2 was equal to 1.3 ± 0.2 M^{-1} sec^{-1}. This value was independent of the rate constants for reaction 1 and also reactions 13–15, as shown by the results of the calculations (mechanism I, Table V), when these latter reactions were ignored and the first reaction was assumed to be 100% efficient for all the Cl atoms. Consequently, these results can be interpreted as strong support for the published value of k_2.[5]

In the calculations for the pulse radiolysis condition, the G values were dependent upon the dose rather than the time width of the pulse. For example, when the dose/pulse was increased by a factor of 5, the calculated value for $G(CH_2Cl_2)$ decreased to 0.03. However, increasing the time width of the pulse by this same factor did not affect $G(CH_2Cl_2)$. This results from the fact that only a small fraction ($<10^{-4}$% of the $CHCl_2$ radicals and 6% of the Cl atoms) of the radicals react during the pulse. Consequently, the final relative yields of the products depend upon the relative concentrations of Cl, $CHCl_2$, and CCl_3 radicals at the end of the pulse.

When the maximum instantaneous dose rates associated with the pulse radiolysis experiments were used in the calculations for the steady radiolysis experiments, the calculated values for $G(CH_2Cl_2)$ were in the range $\sim 3 \times 10^{-4}$ molecules/100 eV. The larger values (0.1–0.3) that were calculated using the equations for the pulse situation resulted from a relatively low concentration of $CHCl_2$ radicals. For example, at $\sim 10^{24}$ eV/g-sec and the steady radiolysis conditions, the calculated steady-state concentration of $CHCl_2$ radicals is $\sim 7 \times 10^{-4}$ M and the calculated fraction of these radicals that reacts with chloroform is only 0.02%. Using the equations for pulse radiolysis, the maximum instantaneous concentration of $CHCl_2$ radicals is roughly 2×10^{-5} M. At this concentration 1.4% of the $CHCl_2$ radicals react with chloroform. As the radical concentration decreases, however, this fraction increases. When 90% of the $CHCl_2$ radicals have reacted, this fraction is 7%. The observed distribution of $CHCl_2$ radicals in the products indicates that 5% of the $CHCl_2$ radicals reacted with the chloroform. At the intensities of the ^{60}Co γ-ray sources used in this study, 1.6×10^{16} and 1.7×10^{17} eV/g-sec, the calculated steady-state concentrations of $CHCl_2$ radicals were 5.2×10^{-8} and 2.5×10^{-7} M, respectively. At these concentrations the fractions of $CHCl_2$ radicals reacting with the solvent are 0.55 and 0.30, in agreement with those calculated from the observed products.

Acknowledgments. The author wishes to thank Robert C. Kuckuck and his staff at the Lawrence Radiation Laboratory, Livermore, Calif., for performing the pulsed irradiations. Also, the assistance of F. M. Charbonnier of the Field Emission Corp. is greatly acknowledged for his calculation of the X-ray spectrum.

(36) P. G. Ashmore and M. S. Spencer, *Trans. Faraday Soc.*, **60**, 1608 (1964); J. H. Knox, *ibid.*, **58**, 275 (1962).

(37) L. C. Dickey and R. F. Firestone, *J. Phys. Chem.*, **74**, 4310 (1970).

Thermal Decay Effects on Spatial Distributions of Radicals in γ-Irradiated Poly(methyl methacrylate)

by Walter Kaul

Physikalisch-Technische Bundesanstalt, Braunschweig, Germany

and Larry Kevan*

Department of Chemistry Wayne State University, Detroit, Michigan 48202 *(Received November 12, 1970)*

Publication costs assisted by the U. S. Atomic Energy Commission and the Air Force Office of Scientific Research

Spin–spin, T_2, and spin–lattice, T_1, relaxation times were measured for the radicals in γ-irradiated PMMA at room temperature *vs.* radiation dose and *vs.* thermal decay time after irradiation. T_2 is related to the local spin concentration around a radical. The local spin concentrations are larger than the average spin concentrations over the entire sample up to doses of about 5 Mrads. This indicates that the radicals are trapped in regions of high local spin concentration called spurs. At doses above 7 Mrads the local and average spin concentrations are comparable. During thermal decay at doses less than 5 Mrads the local spin concentration decreases fractionally faster than the average spin concentration which indicates intraspur decay. During thermal decay at doses greater than 7 Mrads the local and average spin concentrations decrease at similar fractional rates.

Introduction

Nonuniform spatial distributions of trapped paramagnetic species are often produced by γ irradiation and by photolysis of solids. The most obvious type of nonuniformity is the production of radical pairs by radiolytic or photolytic bond scission.[1] A more general type of nonuniformity, characteristic of γ radiolysis, is the production of clusters of radicals called spurs. This is simply a reflection of the inhomogeneous deposition of radiation energy in condensed systems.

In the past several years electron paramagnetic resonance methods have proved powerful for studying nonuniform distributions of trapped radicals.[2] We have used paramagnetic relaxation to measure T_2, the spin–spin relaxation time, which is inversely proportional to the local spin concentration.[3,4] Although the absolute value of T_2 may be subject to significant experimental error, relative values of T_2 give an accurate picture of how the local spin concentration changes with an experimental parameter. It has been found that electrons trapped in polar solids[3-8] and some polymer radicals[9-12] are trapped in spurs in which the local spin concentration exceeds the average spin concentration over the whole sample. As the radiation dose or the total radical concentration increases, the local spin concentration remains essentially constant until the spurs begin to overlap significantly.

In this study we explore how the local radical concentration decreases with respect to the average radical concentration during the process of thermal decay. By this, some insight is achieved into the relative importance of intraspur and interspur radical decay. The radicals formed in γ-irradiated poly(methyl methacrylate) (PMMA) form a suitable system since they are produced in spurs at low radiation doses,[9] they undergo slow thermal decay at room temperature, and it is possible to measure their relaxation times by microwave saturation methods at room temperature.

Experimental Section

The PMMA samples were prepared by thermal polymerization from methyl methacrylate monomer supplied by Rohm and Haas. The monomer was quoted to be 99.95% pure and contained no inhibitors. The monomer was degassed in glass tubes and then polymerized by heating for 45 min at 90° and 24 hr at 56°. The transparent PMMA samples were broken out of the 0.4-cm i.d. glass tubes and cut to cylinders 2 cm long.

(1) For example, see A. V. Zubkov, A. T. Koritsky, and Ya. S. Lebedev, *Dokl. Akad. Nauk SSSR*, **180**, 1150 (1968); D. A. Wiersma and J. Kommandeur, *Mol. Phys.*, **13**, 241 (1967).

(2) B. G. Ershov, *Actions Chim. Biol. Radiat.*, **14**, 191 (1970).

(3) J. Zimbrick and L. Kevan, *J. Chem. Phys.*, **47**, 2364 (1967).

(4) B. L. Bales and L. Kevan, *ibid.*, **52**, 4644 (1970).

(5) L. Kevan and D. H. Chen, *ibid.*, **49**, 1970 (1968); D. H. Chen and L. Kevan in "Organic Solid State Chemistry," G. Adler, Ed., Gordon and Breach, London, 1969, p 183.

(6) H. Hase and L. Kevan, *J. Chem. Phys.*, **52**, 3183 (1970).

(7) D. Smith and J. J. Pieroni, *Can. J. Chem.*, **43**, 876 (1965).

(8) B. G. Ershov, G. P. Chernova, O. Ya. Grinberg, and Ya. S. Lebedev, *Izv. Akad. Nauk SSSR, Ser. Khim.*, 2439 (1968).

(9) (a) A. T. Bullock, W. E. Griffiths, and L. H. Sutcliffe, *Trans. Faraday Soc.*, **63**, 1846 (1967); (b) A. T. Bullock and L. H. Sutcliffe, *ibid.*, **60**, 2112 (1964).

(10) H. Yoshida, K. Hayashi, and S. Okamura, *Ark. Kemi*, **23**, 177 (1965).

(11) J. Zimbrick, F. Hoecker, and L. Kevan, *J. Phys. Chem.*, **72**, 3277 (1968).

(12) O. M. Taranukha, V. A. Vonsyansky, and Ya. S. Lebedev, *Khim. Vys. Energ.*, **2**, 476 (1968).

These samples contained some residual radicals from the polymerization which were removed by heating at 90° for 24 hr. Irradiations were carried out at 31° in a ^{60}Co γ-source at a dose rate of 0.42 Mrad/hr in the dark.

Measurements were made with a Varian 4502 epr system which included a dual cavity with a quartz dewar insert. The microwave bridge was operated in the low-power mode and the automatic frequency control was locked to the sample cavity. The microwave power was variable over a 50-db range. The microwave power, P, was measured with a thermistor and power meter and the microwave magnetic field, H_1, is given by $H_1 = 2.22P^{1/2}$ G with P in watts for our spectrometer.[4]

Slow passage progressive saturation measurements were made at room temperature in a quartz dewar as previously described.[4] A magnetic field modulation frequency of 40 Hz and a modulation amplitude of 0.3 G satisfied slow passage conditions. A DPPH sample, which does not saturate within the power range used, was also measured in the dual cavity. Since the DPPH signal intensity should be linear with H_1, deviations were interpreted to be due to attenuator calibration errors and the experimental saturation curves were corrected accordingly.

The radical spin concentrations were determined by comparing the doubly integrated first-derivative PMMA spectra at 300°K with the uncorrected trapped-electron spectrum in γ-irradiated 10 M NaOH at 77°K. Correction was made for the temperature difference. The uncorrected trapped-electron sample contains 1.3×10^{18} spins g^{-1} $Mrad^{-1}$. This corresponds to 2.1 electrons per 100 eV of radiation energy absorbed (G value).[13]

Results

The normal nine-line epr spectrum associated with irradiated PMMA at room temperature[14] was observed in all samples. Although there has been some controversy about whether this spectrum is due to one or two radicals, it now seems clearly established that it is due to a single radical of the type $RCH_2C(CH_3)COOCH_3$ with slightly different conformational angles of the two C–H_β bonds to the p orbital containing the unpaired electron.[15]

The signal intensity (height times width squared of the first derivative curve) of the central line of the spectrum was measured *vs.* the microwave magnetic field, H_1, to give a power saturation curve. Figures 1 and 2 show typical power saturation curves at 4.9 Mrads for two different decay times. The shape of a saturation curve is related to the spin–lattice, T_1, and spin–spin, T_2, relaxation times of the radical. The relevant theory for obtaining relaxation times from saturation curves under slow-passage conditions has been summarized in a previous paper.[3] The PMMA radical saturation curves were analyzed in terms of nonideal inhomogeneous saturation by Castner's treatment.[16] In this analysis, groups of spins are considered to form noninteracting lorentzian spin packets which are superimposed to form an observed gaussian line. The parameter $a = 1.47\ \Delta H_{ms}{}^{L}/\Delta H_{ms}{}^{G}$, where $\Delta H_{ms}{}^{L}$ and $\Delta H_{ms}{}^{G}$ are the spin packet and observed line widths at maximum slope, is determined from the saturation curves. Then T_2 is given by eq 1

$$T_2 = 1.70/a(\gamma \Delta H_{ms}{}^{G}) \quad (1)$$

where γ equals 1.76×10^7 G^{-1} sec^{-1}. The value of a depends on the ratio of two H_1 values from the satura-

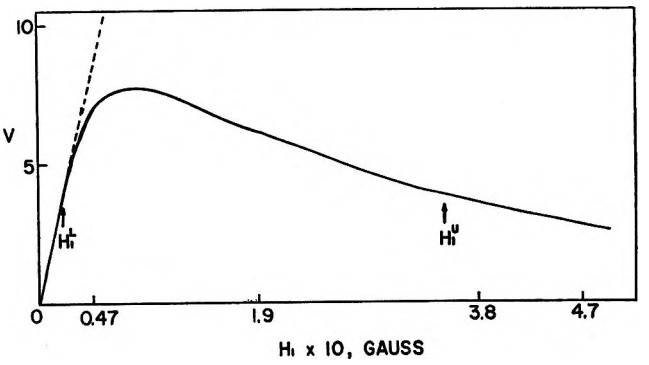

Figure 1. Power saturation curve for the central line in the epr spectrum of the radical in γ-irradiated PMMA at room temperature. The radiation dose was 4.9 Mrads and the data were taken after 3 hr of thermal decay following irradiation. The relative signal intensity, V, is the height times the width squared of the first derivative epr signal and H_1 is the microwave magnetic field. The symbols $H^{L}{}_1$ and $H^{u}{}_1$ refer to parameters used in the analysis of the saturation curve according to ref 16.

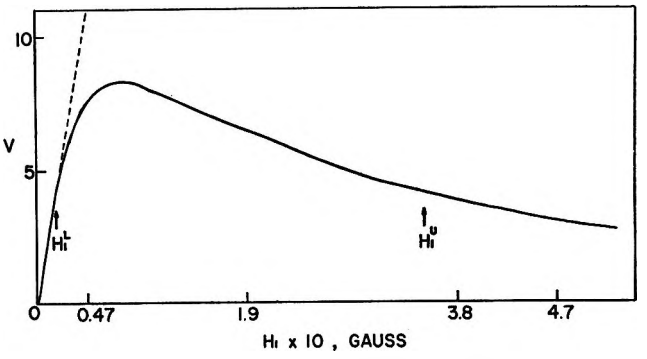

Figure 2. Power saturation curve for the central line in the epr spectrum of the radical in γ-irradiated PMMA at room temperature. The radiation dose was 4.9 Mrads and the data were taken after 54 hr of thermal decay following irradiation. The symbols are defined as in the caption to Figure 1.

(13) L. Kevan in "Radiation Chemistry of Aqueous Systems," G. Stein, Ed., Wiley-Interscience, New York, N. Y., 1968, pp 21–72.

(14) E. E. Schneider, M. J. Day, and G. Stein, *Nature*, **168**, 645 (1951).

(15) M. Iwasaki and Y. Sakai, *J. Polym. Sci. Part A-1*, **7**, 1537 (1969).

(16) T. G. Castner, *Phys. Rev.*, **115**, 1506 (1959).

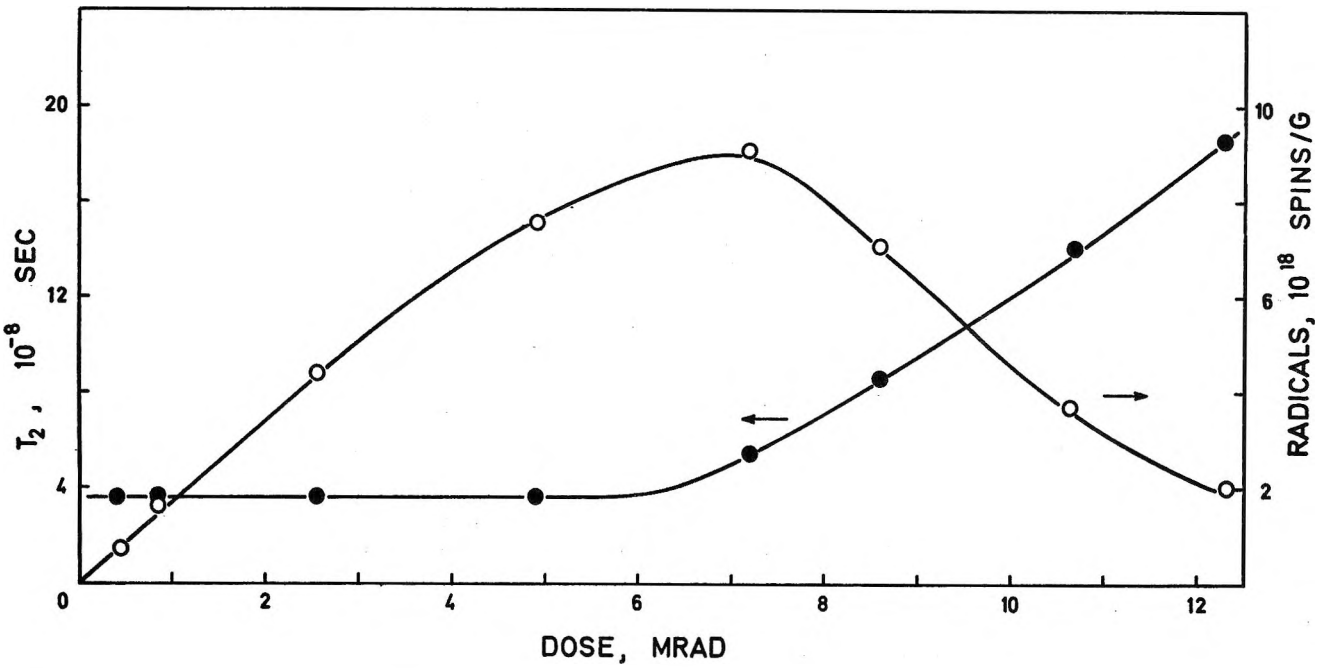

Figure 3. Variation of PMMA radical concentration (O) and spin–spin relaxation time, T_2 (●) *vs.* γ-radiation dose at room temperature.

tion curve and is therefore independent of the absolute value of H_1. T_1T_2 is given by eq 2 where $H_{1/2,\,cor}$ is obtained from the saturation curve and does depend on the H_1 calibration.

$$T_1T_2 = 1/\gamma^2 H_{1/2,\,cor} \qquad (2)$$

It should be noted that the absolute values of T_2 and T_1 derived from the above analysis depend on the assumption of noninteracting spin packets (*i.e.*, no spin diffusion within the observed gaussian line). This assumption is probably not completely correct, but only the relative values of T_2 are of principal interpretive significance.

Figure 3 shows the PMMA radical yield in spins per gram and T_2 *vs.* radiation dose at room temperature. Most of the decrease in radical yield above 7 Mrads is apparently due to slow thermal decay of the radicals during irradiation. Data on this decay are given in Figures 2–6. The observed decay rates in Figures 2–6 do not seem fast enough to account for more than 10–20% of the observed decrease in initial radical yield above 7 Mrads. However, the decay rates seem to decrease with the time elapsed after irradiation and are presumably faster at earlier times during irradiation. We note that the maximum in the radical yield *vs.* dose is phenomenologically analogous to maxima observed for electron yields *vs.* dose in organic glasses at 77°K,[17] but we do not have a quantitative understanding of this effect at present. The T_1 values were constant at about 1.8×10^{-5} sec from 0.4 to 5 Mrads and then decreased slowly to about 0.4×10^{-5} sec at 10.7 Mrads.

The line width at maximum slope of the central line of the PMMA spectrum is 5.4 G and is independent of

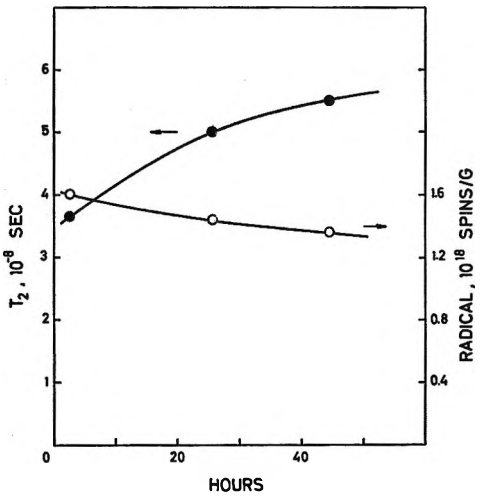

Figure 4. Variation of PMMA radical concentration (O) and spin–spin relaxation time, T_2 (●) *vs.* time after 0.85-Mrad γ irradiation at room temperature.

dose. At the greatest saturation achieved the line broadened to about 8 G. The line shape parameter defined by Pake and Purcell[18] averages 2.3 independent of dose. Since the theoretical value for a pure gaussian line is 2.2, the line shape is closely gaussian as expected for inhomogeneous broadening.

Figures 4–8 show the effect of thermal decay at room temperature on the radical yields and on T_2 at five doses. For each dose the value of T_1 was constant over the time of decay. During the thermal decay periods

(17) M. Shirom and J. E. Willard, *J. Amer. Chem. Soc.*, **90**, 2184 (1968).

(18) G. E. Pake and E. M. Purcell, *Phys. Rev.*, **74**, 1184 (1948).

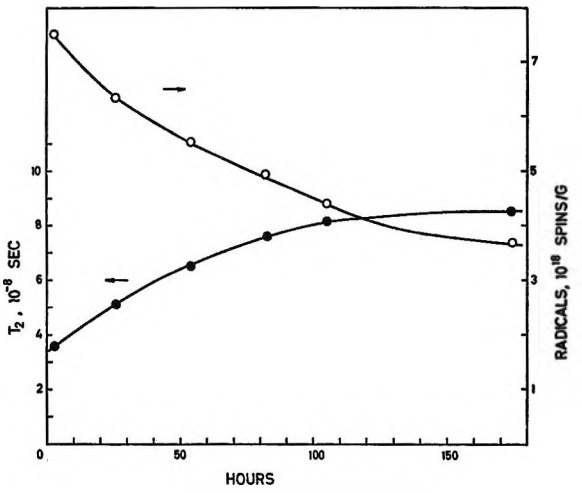

Figure 5. Variation of PMMA radical concentration (O) and spin–spin relaxation time, T_2 (●) *vs.* time after 4.9-Mrad γ irradition at room temperature.

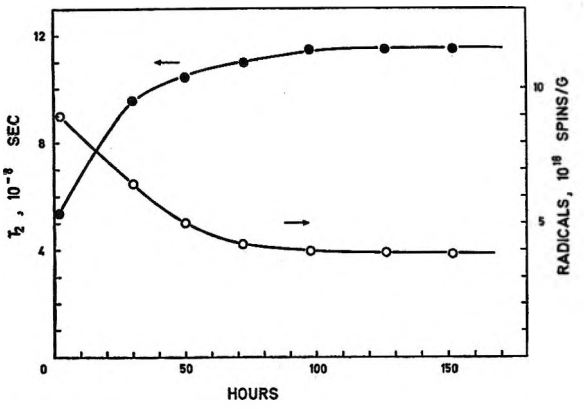

Figure 6. Variation of PMMA radical concentration (O) and spin–spin relaxation time, T_2 (●) *vs.* time after 7.2-Mrad γ irradiation at room temperature.

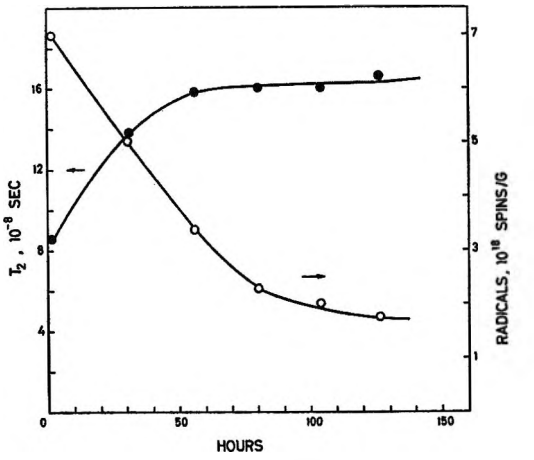

Figure 7. Variation of PMMA radical concentration (O) and spin–spin relaxation time, T_2 (●) *vs.* time after 8.6-Mrad γ irradiation at room temperature.

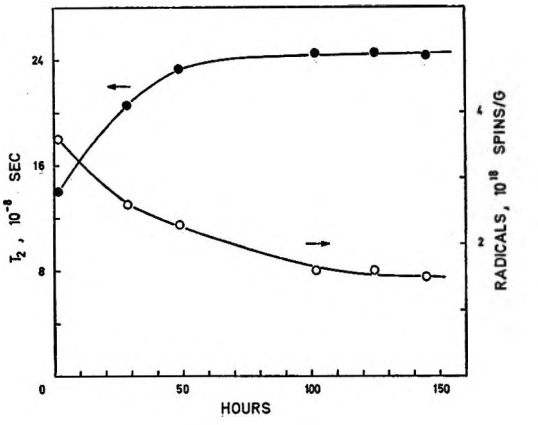

Figure 8. Variation of PMMA radical concentration (O) and spin–spin relaxation time, T_2 (●) *vs.* time after 10.7-Mrad γ irradiation at room temperature.

the samples were stored in the dark. Similar results were obtained for doses at 2.5 and 12.7 Mrads but are not plotted.

Discussion

Since T_2 is related to the local spin concentration in the region of the trapped radicals, the thermal decay data in Figures 2–6 allow us to compare quantitatively how the local and average spin concentrations change. Kittel and Abrahams[19] calculated the frequency moments for spin–spin dipolar broadening from spins randomly distributed on a cubic lattice with the external magnetic field along the 100 axis. For a polycrystalline sample where the crystallites are oriented randomly with respect to the magnetic field this dipolar width is reduced by the factor 0.71.[20] The width is further reduced by g anisotropy[20] which we do not consider here. When the fractional spin population is less than 0.01, as it is for radiation-produced magnetic species, the dipolar line is lorentzian and is identified with the spin-packet of the saturation analysis. The relation between T_2 in seconds and the local spin concentration N_{loc} in spins/cm^3 is then given by eq 3.

$$N_{loc} = (1.23 \times 10^{-12} T_2)^{-1} \quad (3)$$

The local spin concentrations at each dose immediately after irradiation and after 50 hr of thermal decay are collected in Table I. These are compared with the average spin concentrations, N_{av}, in the same samples. N_{av} is converted to spins/cm^3 with a density of 1.18 for PMMA. Note that $N_{loc} > N_{av}$ when only two radicals per cluster are separated by $r_{loc} < r_{av}$.

At low doses the ratio N_{loc}/N_{av} equals 25 at 0.42 Mrads and 12 at 0.85 Mrad. The N_{loc} corresponds to an average distance between radicals of 44 Å if spherical volumes around each radical are assumed. Even though our absolute value of T_2, on which this ratio

(19) C. Kittel and E. Abrahams, *Phys. Rev.*, **90**, 238 (1953); in the expression for A on the second page of this paper, g should be squared.
(20) S. J. Wyard, *Proc. Phys. Soc., Ser. A*, **86**, 587 (1965).

Table I: Local and Average Spin Concentrations (spins/cm³) of Radicals in γ-Irradiated PMMA at Room Temperature

Dose	0.85 Mrad	2.5 Mrads	4.9 Mrads	7.2 Mrads	8.6 Mrads	10.7 Mrads	12.7 Mrads
N_{loc} initial	2.3×10^{19}	2.3×10^{19}	2.3×10^{19}	1.5×10^{19}	9.5×10^{18}	5.8×10^{18}	4.4×10^{18}
N_{loc} after 50 hr	1.4×10^{19}	1.4×10^{19}	1.3×10^{19}	7.8×10^{18}	5.3×10^{18}	3.5×10^{18}	2.3×10^{18}
Decrease	39%	39%	43%	48%	44%	40%	48%
N_{av} initial	1.9×10^{18}	5.2×10^{18}	8.9×10^{18}	10.6×10^{18}	8.3×10^{18}	4.2×10^{18}	2.4×10^{18}
N_{av} after 50 hr	1.6×10^{18}	4.3×10^{18}	6.6×10^{18}	5.9×10^{18}	4.4×10^{18}	2.7×10^{18}	1.2×10^{18}
Decrease	16%	17%	26%	44%	47%	36%	50%
N_{loc}/N_{av} initial	12	4.6	2.6	1.4	1.1	1.4	1.8
N_{loc}/N_{av} after 50 hr	8.8	3.3	2.0	1.3	1.2	1.3	1.9

depends, may be in error by a factor of 2 or 3, N_{loc}/N_{av} is clearly greater than 1 at doses less than 5 Mrads. This means that the radicals are formed in localized regions of higher than average radical concentration. Such regions are called spurs in radiation chemistry and reflect the nonhomogeneous deposition of radiation energy. At high doses we expect the average and local spin concentrations to become comparable. This is observed at doses above 7 Mrads where N_{loc}/N_{av} is of the order of unity.

Bullock, *et al.*,[9] have made similar measurements on PMMA radicals up to about 1.5 Mrads. They do not quote radiation doses but we deduce them from their ref 2. Thus they observed only the isolated spur region in which $N_{loc}/N_{av} > 1$. Their average local spin concentration was 1.80×10^{19} spins/cm³. However, they assumed that the *g* factor of the radical was anisotropic (see ref 20) so their value should be decreased to 1.2×10^{19} for comparison with ours at low dose. Still, the agreement is reasonable. Our average spin concentrations are about 3 times as large as theirs at comparable doses. The initial linear portion of our yield–dose curve in Figure 3 corresponds to a 100-eV yield (*G* value) of 2.7 which is a typical value for radicals in nonaromatic organic solids.

Bullock and Sutcliffe[9b] also reported that for radicals in γ-irradiated PMMA T_2 increased by about a factor of 2 when the temperature was lowered from 299 to 77°K. This suggests that the local concentration decreases when the temperature is lowered. Similar results have been observed in an analogous polymeric system.[11] This temperature effect could possibly be caused by contraction of adjacent polymer chains so as to increase the distance between nearby radicals when the temperature is lowered. Our results were all taken at room temperature and do not bear on this question; however, they do indicate that T_2 changes can be reasonably related to changes in local radical concentration.

One objective of this work was to compare how local and average spin concentrations change during thermal decay of the radicals. Figures 4–8 show that the radical decay rates decrease with time at room temperature at all doses studied. Table I shows the fractional decay rates, based on both local and average spin concentrations, as the per cent decrease for 50 hr of decay.

At doses less than 5 Mrads the fractional decrease in local spin concentration is about 2.5 times as great as the fractional decrease in the average spin concentration. This is consistent with intraspur decay. Since the spurs are isolated and the radical concentration is highest within the spurs this result is not unexpected. However, the experimental approach used here provides a more direct observation of intraspur decay than does thermal decay kinetics alone.

A consequence of intraspur decay is that the kinetics should *not* be second order with respect to the total (average) spin concentration, even if the decay mechanism is simple radical combination. This is best substantiated by looking at the effect of total spin concentration on the fractional decay rate. At 0.85 and 2.5 Mrads the fractional decay rates based on the total spin concentration are the same even though the spin concentrations differ by a factor of 3. Similar results are obtained for limited data at 0.4 Mrad. On the other hand, if random radical combination occurred within the spur the kinetics would be second order with respect to the *local* concentration. Our data do not convincingly fit either first- or second-order plots based on local concentrations below 5-Mrad dose, so we are unable to deduce unique intraspur kinetics. However, the data can be fitted to two or more concurrent first-order decays of different rates. Below 5 Mrads the initial local concentration is constant, so the dose independence of the fractional decay rate with respect to local concentration cannot be used as a criterion for concurrent first-order decays. However, the fractional decay rates based on local concentrations are roughly independent of the local spin concentrations if the high dose data are also included. This is consistent with concurrent first-order decays within the spur. Simple radical combination within the spur is consistent with such kinetics if the combination is not random.

At doses above 7 Mrads the local and average spin concentrations are comparable and show comparable fractional decay rates. In this dose range we make no distinction between intraspur and interspur decay. Again the radical decay kinetics do not fit simple first

or second order, but seem best represented by concurrent first-order decays.

We have observed intraspur decay for radiation-produced organic radicals by spin–spin relaxation measurement of local radical concentrations. We suggest that intraspur decay is a common situation in irradiated organic solids and that it complicates the interpretation of radical decay based on total spin concentrations. Conversely, if pure second-order decay, substantiated at several initial radical concentrations, is observed in irradiated solids these radicals cannot be trapped in spurs containing other radicals. An example of this latter situation has been observed for 3-methylpentyl radicals in irradiated 3-methylpentane at 77 and 87°K.[21]

Acknowledgment. This research was supported by the Air Force Office of Scientific Research under Grant No. AFOSR-70-1852 and by the Atomic Energy Commission under Contracts AT(11-1)-1852 and AT-(11-1)-2086. The experimental work was initiated at the University of Kansas. L. K. wishes to thank the John Simon Guggenheim Foundation for a fellowship and the Danish AEC Research Establishment Risö for their hospitality and services.

(21) W. G. French and J. E. Willard, *J. Phys. Chem.*, **72**, 4606 (1968).

Electron Spin Resonance of Free Radicals Prepared by the Reactions of Methylene. Deuteriomethyl and Formaldiminoxy Radicals

by J. B. Farmer, C. L. Gardner, M. C. L. Gerry, C. A. McDowell,* and P. Raghunathan

Department of Chemistry, The University of British Columbia, Vancouver 8, British Columbia, Canada
(Received February 22, 1971)

Publication costs assisted by the National Research Council of Canada

The electron spin resonance spectra of the deuteriomethyl (CH_2D and CHD_2) and the formaldiminoxy (CH_2NO) radicals have been obtained by photolyzing diazomethane in the presence of D_2O and NO, respectively, in an argon matrix at 4.2°K. Hyperfine coupling constants and g factors have been evaluated for each radical. The assignment of the structure of the formaldiminoxy radical and the correctness of the interpretation of its esr spectrum has been confirmed by experiments performed using ^{15}NO. This work shows that nitric oxide may be used as a spin trap for triplet state radicals. Furthermore, it confirms the existence of the CH_2NO radical which had previously been postulated as an intermediate in certain gas phase reactions.

Introduction

One of the primary products of the photolysis of both diazomethane and ketene is the methylene radical (CH_2). Its electronic spectrum, giving evidence of both singlet and triplet states, has been observed in the gas phase,[1] and the electron paramagnetic resonance spectrum of radicals trapped in a xenon matrix at 4.2°K has confirmed that the ground state is a triplet.[2] We have photolyzed both diazomethane and ketene in argon matrices at 4.2°K and have observed in many experiments the characteristic four-line spectrum of the methyl (CH_3) radical superimposed on a further broad signal. Methyl radicals cannot be formed in the primary photolytic step of either diazomethane or ketene. There is considerable evidence, however, that methylene radicals produced in this step can abstract hydrogen atoms[3] to produce methyl radicals, and this would seem to be a reasonable method of generating the latter.

In an attempt to obtain further evidence for the abstraction reaction, we photolyzed diazomethane in the presence of heavy water (D_2O) in an argon matrix at 4.2°K. Should abstraction be occurring, the spectrum anticipated was that of the CH_2D radical. This was indeed found, and the details of the results are given in a later section. The success of these experiments suggested that the photolysis of diazomethane in the

(1) G. Herzberg, *Proc. Roy. Soc., Ser. A*, **262**, 291 (1961).

(2) R. A. Bernheim, H. W. Bernard, P. S. Wang, L. S. Wood, and P. S. Skell, *J. Chem. Phys.*, **53**, 1280 (1970); E. Wasserman, W. A. Yager, and V. J. Kuck, *Chem. Phys. Lett.*, **7**, 409 (1970); E. Wasserman, V. J. Kuck, R. S. Hutton, and W. A. Yager, *J. Amer. Chem. Soc.*, **92**, 7491 (1970).

(3) See, for example, G. B. Kistiakowsky and T. A. Walters, *J. Phys. Chem.*, **72**, 3952 (1968); D. F. Ring and B. S. Rabinovitch, *Can. J. Chem.*, **46**, 2435 (1968).

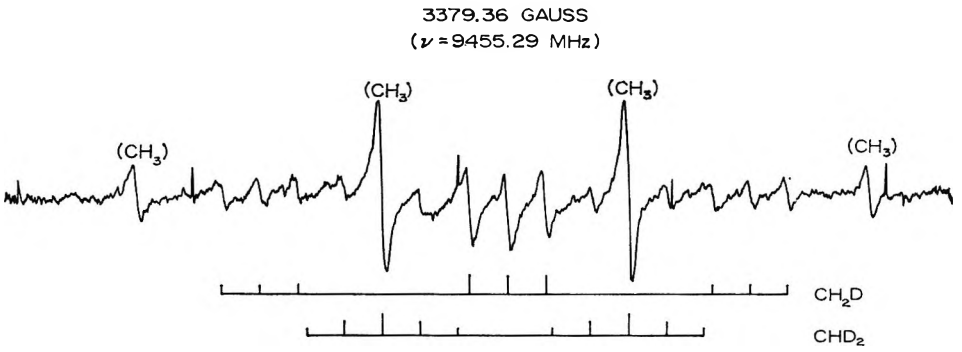

Figure 1. Esr spectrum obtained from the photolysis of the CH_2N_2–D_2O–Ar system. The stick diagram shows the assignment of the hyperfine splittings.

presence of other substances which might be subject to addition or abstraction reactions with methylene radicals would be a useful and interesting method of preparation of free radicals for esr study. In the final section we report the spectrum of the first of these, the formaldiminoxy radical (CH_2NO), obtained by photolysis of diazomethane in the presence of nitric oxide in an argon matrix; this nitric oxide thus acts as a spin trap for the triplet state methylene radical.

Experimental Section

Diazomethane, CH_2N_2, was prepared by the alkaline hydrolysis of reagent grade *N*-methyl-*N*-nitroso-*p*-toluene sulfonamide (Eastman Organic Chemicals) in ethylene glycol. Light and also contact with a variety of impurities cause explosive decomposition of diazomethane, and after considerable experimentation it was found best to use a clean polyethylene-coated high-vacuum system. "Kel-F" grease was used for all vacuum joints and the diazomethane was prepared and handled in the dark.

Heavy water of 99.75% minimum isotopic purity was obtained from Merck Sharp and Dohme of Canada. Gaseous ^{14}NO (Matheson of Canada) was purified according to the steps outlined by Guillory and Johnston.[4] ^{15}NO, specified to be 99.3 atom % pure in ^{15}N, was obtained from Isomet Corp. All the above chemicals were further purified by a trap-to-trap distillation *in vacuo* prior to use. Research grade argon purchased from Matheson of Canada (less than 5 ppm N_2) was used as the matrix material. In a typical experimental run, 5 Torr of gaseous CH_2N_2 and 5 Torr of NO were mixed in a darkened sample bulb and diluted with enough argon so that the mixture had a ratio of 1:1:1000 (CH_2N_2–NO–Ar). A similar volume ratio was used for the CH_2N_2–D_2O–Ar mixture.

The superheterodyne X-band spectrometer and the associated cryogenic assembly for matrix isolation experiments have been described previously.[5] Saturation of the detected signal was avoided by choosing low enough microwave power levels—typically 30 dB below the 200 mW klystron output. The magnetic field was calibrated using a proton magnetic resonance probe. Samples were deposited onto a target surface held at 4.2°K inside the esr cavity. Photolysis was achieved with light from a GE AH6 high-pressure mercury arc, the radiation from which was filtered through a column of water and focused on the sample through a quartz collimating system.

Results and Discussion

I. Deuterated Methyl Radicals. The esr spectrum obtained after 20 min irradiation of the CH_2N_2–D_2O–Ar system is shown in Figure 1. Transitions assigned to the CH_3, CH_2D, and CHD_2 radicals are indicated. All three spectra can be interpreted in terms of an isotropic hyperfine coupling; the *g* values and hyperfine splitting constants derived from the spectra are given in Table I. The latter are in good agreement with those published previously.[6] Spectra calculated from the appropriate spin Hamiltonian using the derived values are given in the lower portion of Figure 1; it is evident that there is excellent agreement between these and the observed spectra.

These results support the hypothesis that methylene radicals have been formed in the photolytic decomposition of diazomethane and are capable of abstracting hydrogen atoms to form methyl radicals. The CH_2D radicals were probably formed simply by abstraction of deuterium atoms from heavy water by methylene radicals. To account for the CHD_2 radicals observed, however, it seems reasonable to assume that some exchange of hydrogen and deuterium between diazomethane and heavy water occurred in the gas phase before deposition, so that photolysis of diazomethane produced CHD radicals which in turn abstracted deuterium atoms from the heavy water. These results spurred the subsequent search for formaldiminoxy radicals, it being assumed that nitric oxide would serve as an appropriate spin trap for the triplet state methylene radical.

(4) W. A. Guillory and H. S. Johnston, *J. Chem. Phys.*, **42**, 2457 (1965).

(5) C. A. McDowell, H. Nakajima, and P. Raghunathan, *Can. J. Chem.*, **48**, 805 (1970).

(6) R. W. Fessenden, *J. Phys. Chem.*, **71**, 74 (1967); see also R. W. Fessenden and R. H. Schuler, *J. Chem. Phys.*, **39**, 2147 (1963).

Table I: g Values and Hyperfine Splittings (in G) for the CH_2D and CHD_2 Radicals

Species	g Values		Isotropic hyperfine splittings	
	This work	Fessenden[a]	This work	Fessenden[a,b]
CH_2D	2.0020 ± 0.0002	Not reported[c]	a_H = 22.97 ± 0.25 a_D = 3.52 ± 0.25	a_H = 23.1 ± 0.01 a_D = 3.531 ± 0.01
CHD_2	2.0020 ± 0.0002	Not reported[c]	a_H = 23.12 ± 0.25 a_D = 3.50 ± 0.25	a_H = 23.21 ± 0.01 a_D = 3.552 ± 0.01

[a] Reference 6. [b] Observed in a krypton matrix at 85°K. [c] The g factors of the CH_3 and CD_3 radicals have previously been reported by Fessenden and Schuler (ref 6) to be 2.0026. The small difference between this value and our results probably arises from temperature and/or matrix effects.

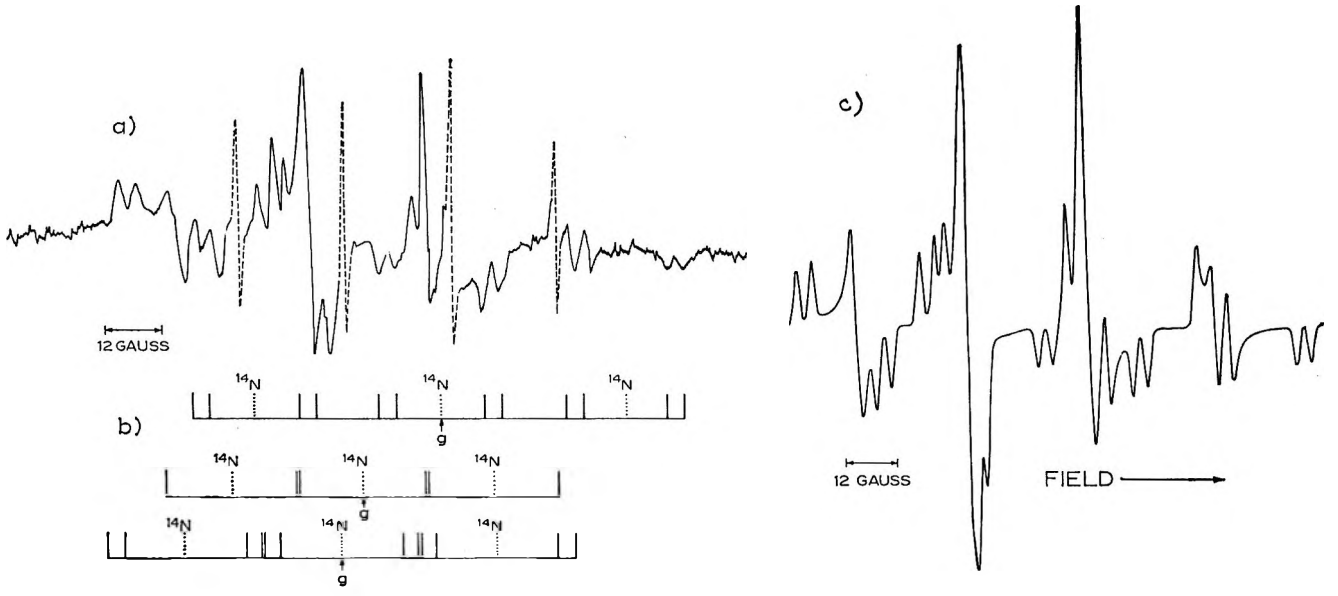

Figure 2. Esr spectrum obtained from the photolysis of the CH_2N_2–^{14}NO–Ar system: (a) experimental spectrum; the dotted lines show the methyl radical spectrum, the rest of the spectrum being ascribed to R; (b) analysis of the hyperfine pattern of R; (c) computer-simulated esr spectrum of radical R.

II. Evidence for the Formation of the Formaldiminoxy Radical. After 20 min irradiation of the CH_2N_2–NO–Ar system the spectrum shown in Figure 2a was obtained. It is seen to be a superposition of (i) the four lines of the methyl radical spectrum and (ii) a complicated line shape due to a second paramagnetic species, R. From the overall pattern of this spectrum, it is immediately clear that this center possesses anisotropic Zeeman (**g**) and hyperfine (**A**) tensors. The methyl radical spectrum could be suppressed, and that of the species R enhanced, by doubling the amount of NO in the irradiated gaseous mixture. The spectrum of the new species is interpretable in terms of an $S = {}^1/_2$ center interacting with a nitrogen nucleus and two inequivalent hydrogens. Our assignment of the various components of the spectrum of R is represented by the stick diagram shown in Figure 2b.

Although the measurements of the g values could be performed accurate to ±0.0002, the widths of the component lines of the polycrystalline spectrum, and the somewhat poor overall resolution, tended to limit the accuracy of our measurements of the hyperfine splittings. In particular, the smaller proton couplings are of the same order of magnitude as the line width.

A more complete parametrization of the spectral components was therefore attempted by a computer simulation of the polycrystalline spectrum of R. The computer program used here has been previously described elsewhere.[7] A spin Hamiltonian of the form

$$\mathcal{H} = \beta H \cdot \mathbf{q} \cdot S + I \cdot \mathbf{A} \cdot S$$

where the principal axes of the Zeeman and hyperfine tensors were assumed to be collinear, was used to interpret the spectrum. The resonance field positions calculated were fitted with a gaussian line shape function, and the resulting simulation is shown in Figure 2c. The parameters that led to the "best fit" of the experimental spectrum are set forth in Table II. From the principal values of the nitrogen hyperfine tensor, the scalar or isotropic nitrogen splitting is calculated to be |33.3| G. Similarly, the experimentally observed proton splittings yield |26.2| G and |2.8| G, respectively, for the large and small isotropic proton couplings of R.

(7) R. Lefebvre and J. Maruani, *J. Chem. Phys.*, **42**, 1480 (1965).

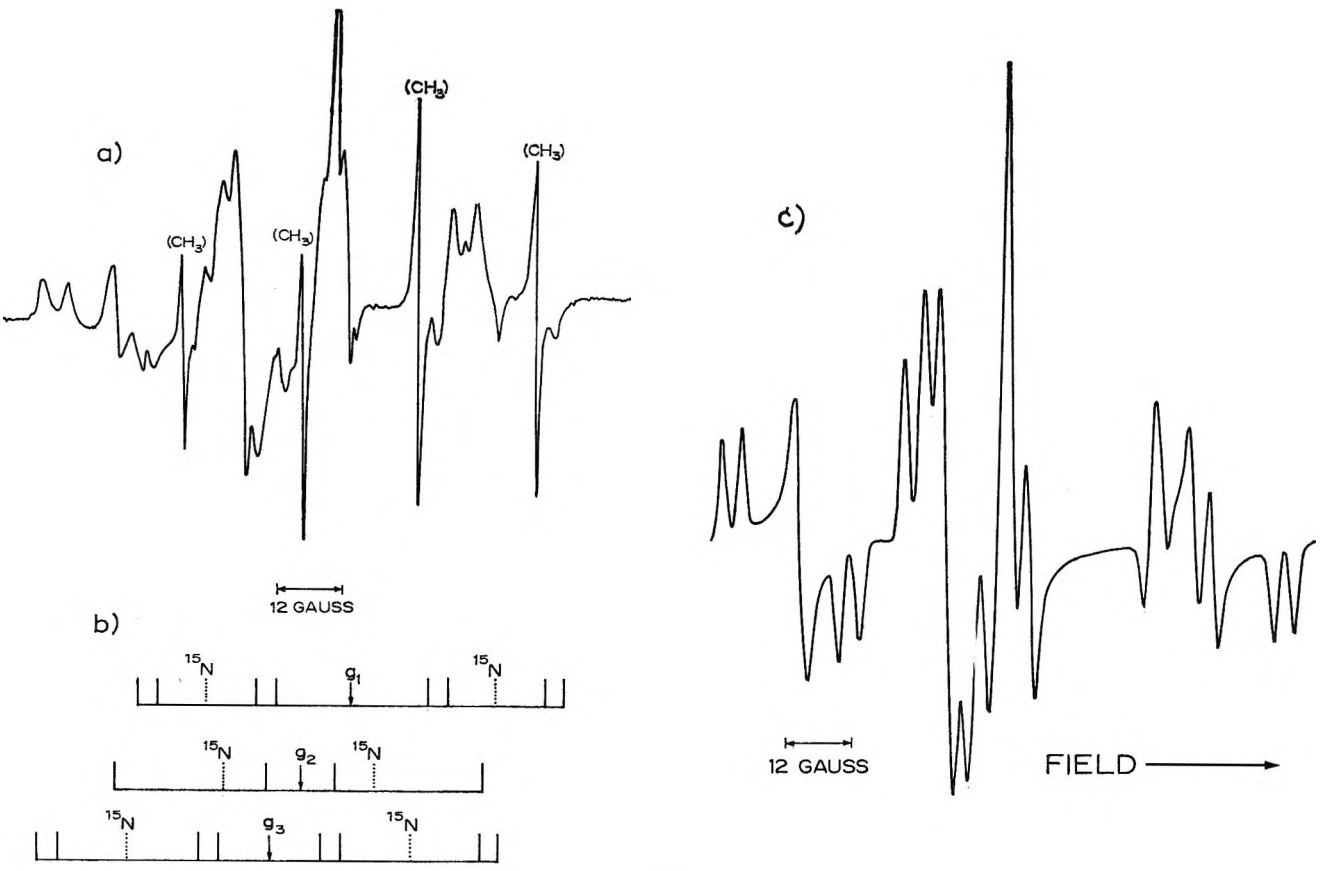

Figure 3. Esr spectrum obtained from the photolysis of CH_2N_2–^{15}NO–Ar system: (a) experimental spectrum; (b) analysis of the hyperfine pattern; (c) computer simulation of the esr spectrum of $CH_2{}^{15}NO$.

Table II: Computer-Fitted Parameters of the g Factor and Hyperfine Splittings (in G) of the Radical R[a]

$g_1 = 1.9930$	$g_2 = 2.0021$	$g_3 = 2.0042$
$A_1(^{14}N) = 38.5$	$A_2(^{14}N) = 27.0$	$A_3(^{14}N) = 35.5$
A_1(H large) = 22.5	A_2(H large) = 27.0	A_3(H large) = 29.0
A_1(H small) = 3.6	A_2(H small) = 1.2	A_3(H small) = 3.6

[a] Component line shape: gaussian; component line width: 1.3 G.

We were successful in checking the above assignment by a further experiment using ^{15}NO in place of ^{14}NO in the photolysis mixture. The somewhat simpler 20-line spectrum that resulted is shown in Figure 3a, and it can be seen that the triplet splitting of ^{14}N has been replaced by a doublet pattern from the ^{15}N, and the spacing of the nitrogen hyperfine components has been increased by the ratio expected for the nuclear g factors $g(^{15}N)/g(^{14}N)$ of 1.41. The complete assignment of the hyperfine coupling pattern of this spectrum is shown in Figure 3b, and the simulated line shape appears in Figure 3c. To compute this line shape, values of $A_1(^{15}N) = 55.0$ G, $A_2(^{15}N) = 38.0$ G, and $A_3(^{15}N) = 51.0$ G were used, the rest of the parameters remaining the same as in Table II.

Structure of the Radical R. The foregoing experimental data indicate that we have to propose a structure for R whose hyperfine splitting pattern is caused by (i) a large nitrogen splitting and (ii) two inequivalent proton splittings, one of which is an order of magnitude larger than the other. The large nitrogen hyperfine interaction at once indicates that a substantial part of the odd electron spin density is located in a totally symmetric MO of nitrogen, presumably an A_1-type antibonding orbital — a situation reminiscent of the planar σ electron structures NO_2[8] and CO_2^-.[9] The inequivalent protons may then be located cis and trans to the odd electron orbital of nitrogen in a planar structure (nonplanar structures are expected to be energetically unfavorable).[10]

The above results could very well be accommodated by a planar structure of the type

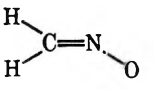

and at least two recent theoretical studies[11,12] have predicted isotropic hyperfine splittings for such a radical,

(8) T. J. Schaafsma, G. A. van der Velde, and J. Kommandeur, *Mol. Phys.*, **14**, 501 (1968).

(9) D. W. Ovenall and D. H. Whiffen, *ibid.*, **4**, 135 (1961).

(10) P. R. Andrews, *J. Mol. Struct.*, **6**, 85 (1970).

(11) G. Berthier, H. Lemaire, A. Rassat, and A. Veillard, *Theor. Chim. Acta*, **3**, 213 (1965).

(12) T. Yonezawa, T. Kawamura, and H. Kato, *Bull. Chem. Soc. Jap.*, **43**, 74 (1970).

Table III: Isotropic Coupling Constants (in G) of the Formaldiminoxy Radical

Nucleus	Calculated values, Ref 12	Calculated values, Ref 11	Experimental values found for radical R, this work
^{14}N	+37.5	≃+30	|33.3|
H(trans)	+61.6[a]	≃+27	|26.2|
H(cis)	+10.2[a]	≃+6	| 2.8|

[a] These and other hydrogen coupling constants tabulated for several σ-electron radicals in ref 12 are probably overestimated since they compare very poorly with well established experimental values. From Table I of ref 12 it is apparent that a "contracted" Slater-type 1s hydrogen orbital has been used for these calculations.

viz., the "formaldiminoxy" radical. In Table III, the values of the nitrogen and the larger hydrogen isotropic coupling constants calculated using self-consistent field theory[11] are seen to show excellent agreement with the values obtained by us; the somewhat greater discrepancy for the smaller hydrogen coupling constant is due, at least in part, to experimental inaccuracy. The CH_2NO, which we conclude is in fact our trapped radical R, may be considered to be the prototype of a wide variety of aldiminoxy radicals for which solution esr spectra have been reported in recent years.[13-15] In all of these, the mechanism of the hyperfine coupling to the protons on the carbon moiety of the structure is believed to operate through long-range transmission of the σ-spin density. The isotropic g value of 1.9998 which may be calculated from our results strongly accords with a σ-electronic structure for this radical.

Indeed, the radical species CH_2NO has been invoked from time to time[16,17] as an intermediate in the gas phase reactions of CH_2 and NO, and we believe that our work provides the first clear-cut experimental evidence for this radical in the isolated state.

Acknowledgment. We wish to thank the National Research Council of Canada for generous grants in support of this work.

(13) J. R. Thomas, *J. Amer. Chem. Soc.*, **86**, 1446 (1964).

(14) B. C. Gilbert and R. O. C. Norman, *J. Chem. Soc. B*, 722 (1966).

(15) R. O. C. Norman and B. C. Gilbert, *J. Phys. Chem.*, **71**, 14 (1967).

(16) M. Burton, T. W. Davis, A. Gordon, and H. A. Taylor, *J. Amer. Chem. Soc.*, **63**, 1956 (1941).

(17) R. D. Cadle and F. E. Grahek in "International Conference on Photochemistry," Max Planck Institute Publ., Munich, 1967, Part 1, p 113.

Nuclear Spin Relaxation in Nematic Liquid Crystals[1a]

by Charles L. Watkins and Charles S. Johnson, Jr.*[1b]

Department of Chemistry, University of North Carolina, Chapel Hill, North Carolina 27514 *(Received February 16, 1971)*

Publication costs assisted by UNC Materials Research Center

Studies of proton spin-lattice relaxation as a function of temperature are reported for the following liquid crystals: *p*-azoxyanisole (I), butyl *p*-(*p*-ethoxyphenoxycarbonyl)phenyl carbonate (II), *p*-(*p*-ethoxyphenylazo)phenyl hexanoate (III), *p*-(*p*-ethoxyphenylazo)phenyl undecylenate (IV), and *p*-[*N*-(*p*-methoxybenzylidene)amino]-*n*-butylbenzene (V). Compound V has also been studied with an electric field of strength ~5 kV/cm perpendicular to the applied magnetic field. Order parameters (S) and second moments obtained from wide line spectra are displayed for compounds II–V. It is found that T_1 increases with increasing temperature immediately above the melting point for compounds I–V and that T_1 does not depend on the alignment of the major molecular axis with respect to the magnetic field for compound V. These results suggest that spin relaxation in the nematic phase is determined by translational diffusion. The frequency dependence of T_1 probably does not distinguish between rotational and translational contributions to spin relaxation.

Introduction

Liquid crystals are of considerable practical and theoretical interest at present because of their unusual physical properties.[2] Nematic liquid crystals, which are investigated in this paper, exhibit a mesophase in which one-dimensional molecular order is maintained; *i.e.*, the long (major) molecular axes tend to be parallel. A particularly interesting manifestation of this long-range order is the molecular alignment which these sys-

(1) (a) Supported in part by grants from the National Science Foundation and the UNC Materials Research Center (Contract SD-100 with the Advanced Research Projects Agency): (b) Alfred P. Sloan Research Fellow, 1966–1972.

(2) G. W. Gray, "Molecular Structure and the Properties of Liquid Crystals," Academic Press, New York, N. Y., 1962.

tems show in modest magnetic and electric fields.[3] In spite of the high degree of molecular ordering the molecules are still quite free to rotate about their long axes and to undergo translational diffusion. However, physical properties such as viscosity and self-diffusion rates show large changes on going from the nematic to the isotropic phase for nemalogens such as *p*-azoxyanisole (PAA).

Early investigations of the nematic mesophase of *p*-azoxy ethers by proton magnetic resonance spectroscopy revealed spectra with total widths similar to those found for the solid phases and two orders of magnitude larger than for the corresponding high-temperature isotropic phases.[4-7] The structure in these spectra was quite logically attributed to direct magnetic dipole–dipole interactions which are not completely averaged out since the molecular tumbling is anisotropic. Further information relating to the molecular motion in these compounds has been derived from studies of the second moments of the nmr absorption lines as functions of temperature.[8,9]

Only in the last few years have the dynamics of the nematic state been studied by means of nuclear spin-lattice relaxation measurements.[10-14] The first attempt to relate orientational fluctuations to spin relaxation in the nematic mesophase was presented by Pincus, who considered only the intramolecular dipole interaction between a pair of protons.[15] This work, which was based on collective modes of fluctuations in molecular order, resulted in

$$\frac{1}{T_1} = \omega_D^2\left(\frac{kT}{K}\right)[\omega(D + K/\eta)]^{-1/2} \qquad (1)$$

where ω_D is the dipole frequency, K is a Frank elastic constant, D is the diffusion constant, η is the viscosity, and ω is the Larmor frequency for the proton. Similar calculations by Blinc, *et al.*, agree with this result except in magnetic fields sufficiently high to affect the thermal fluctuations.[11] Experimental studies of proton relaxation rates have for the most part confirmed the frequency dependence predicted by eq 1, but the observed temperature dependence is completely counter to this equation.[10]

Doane and Johnson have recently attempted to refine the theory by adopting a more realistic model in which high-frequency fluctuations about the local preferred orientation are superimposed on the collective long-range fluctuations.[16] The resulting equation for $1/T_1$ is similar to eq 1 except that a factor of S^2 is included where $S = -1/2\langle 1 - 3\cos^2\theta\rangle$ is the order parameter and θ is the angle between the long axis of the molecule and the applied magnetic field. Lubensky has independently obtained the same result using a quite different method.[17] When the experimental temperature dependence of $T/(K/\eta + D)^{1/2}$ is considered, it turns out that the modified equation predicts little temperature dependence for $1/T_1$ in somewhat better agreement with experiment. There is still, however, the unknown contribution of intermolecular dipole–dipole interactions.

I. p-Azoxyanisole

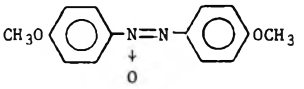

II. Butyl p(p-ethoxyphenoxycarbonyl)phenyl Carbonate

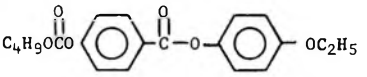

III. p-(p-Ethoxyphenylazo)phenyl Hexanoate

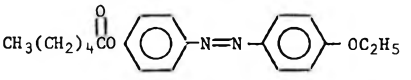

IV. p-(p-Ethoxyphenylazo)phenyl Undecylenate

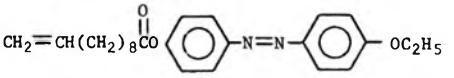

V. p-[N-(p-Methoxybenzylidene)amino]-n-butylbenzene

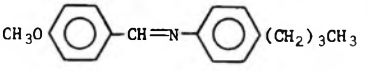

Figure 1. The structures for compounds I–V.

In this paper we report studies of proton spin-lattice relaxation for the five nematogens listed in Figure 1 in their solid, nematic, and isotropic phases. The temperature dependence of T_1 in the nematic phase was of primary interest as a test of the theory for these varied structures where the temperature widths of the nematic mesophases range from 17° (I) to 45° (III, IV). Wide line spectra were also obtained for these systems in order to follow the order parameters S and the second moments of the absorption lines as functions of temperature and to provide an independent determination

(3) E. F. Carr, *Advan. Chem. Ser.*, **No. 63** (1967).

(4) R. D. Spence, H. A. Moses, and P. L. Jain, *J. Chem. Phys.*, **21**, 380 (1953).

(5) R. D. Spence, H. S. Gutowsky, and C. H. Holm, *ibid.*, **21**, 1891 (1953).

(6) P. L. Jain, J. C. Lee, and R. D. Spence, *ibid.*, **23**, 878 (1955).

(7) P. L. Jain, H. A. Moses, J. C. Lee, and R. D. Spence, *Phys. Rev.*, **92**, 844 (1953).

(8) H. Lippmann, *Ann. Physik*, (7) **2**, 287 (1958).

(9) H. Lippmann and K. H. Weber, *ibid.*, (6) **20**, 265 (1957).

(10) M. Weger and P. Cabane, "Colloque Sur Les Cristaux Liquides," Montpellier, France, 1969.

(11) R. Blinc, D. L. Hogenboom, D. E. O'Reilly, and E. M. Peterson, *Phys. Rev. Lett.*, **23**, 969 (1969).

(12) J. W. Doane and J. J. Visintainer, *ibid.*, **23**, 1421 (1969).

(13) R. Blinc, D. E. O'Reilly, and E. M. Peterson, *Solid State Commun.*, **6**, 839 (1968).

(14) R. Y. Dong and C. F. Schwerdtfeger, *ibid.*, **8**, 707 (1970).

(15) P. Pincus, *ibid.*, **7**, 415 (1969).

(16) J. W. Doane and D. L. Johnson, *Chem. Phys. Lett.*, **6**, 291 (1970).

(17) T. C. Lubensky, *Phys. Rev. A*, **2**, 2497 (1970).

of the transition temperatures. Compound V, which has a room temperature nematic phase, was studied in an electric field to determine the dependence of T_1 on the direction of the molecular alignment with respect to the applied field, H_0. The results of these studies, which are discussed in the Results section, reveal a more or less linear increase in T_1 with temperature in all three phases except near phase transitions, and the electric field experiment shows no measurable change of T_1 with change in the alignment angle. On the basis of these results we argue in the Discussion and Conclusions section that proton relaxation is not dominated by the dipole–dipole interactions between adjacent protons on the rings and that a translational diffusion mechanism is consistent with the data. The relevance of current theories of spin relaxation in liquid crystals appears to be in considerable doubt.

Experimental Section

Compounds I–IV were obtained from Eastman Kodak and Aldrich Chemical Co. and were purified by several recrystallizations with hot methanol and ethanol. The melting points and isotropic points for compounds I–IV are: I, mp 118°, ip 135°; II, mp 58°, ip 90°; III, mp 78°, ip 123°; IV, mp 68°, ip 113°. Compound V was synthesized in this laboratory by a standard condensation reaction and purified by vacuum distillation.[18] This compound shows a hysteresis effect so that on heating the mp is 21° and the ip is 41° while on cooling the mp is 12°. All samples were degassed by repeated freezing and thawing under vacuum to remove molecular oxygen.

The T_1 measurements were made at 30 MHz using a Magnion Spin-Echo nmr spectrometer with the high-power modification and a Magnion 12-in. electromagnet. Typical 90° pulse times were less than 2 μsec and the receiver deadtime was about 10 μsec. The data were obtained using repeated 180°–τ–90° pulse sequences. Instead of measuring the null point, which is subject to instrumental and systematic errors, the height of the free induction decay M following the 90° pulse was measured as a function of τ. A plot of $\ln[(M_0 - M)/M_0]$ *vs.* τ yields a slope of $1/T_1$, where M_0 is the height of the free induction decay at very long τ or after a 90° pulse applied at thermal equilibrium.

To control the temperature up to 200°, the following system was devised. A large dewar was constructed to hold the probe assembly in the 2-in. gap of the electromagnet. A furnace machined from a cylinder of lava was mounted in a vertical manner on the probe assembly so that it contained the sample coil. Grooves were cut in the furnace and nichrome wire was wound onto the furnace to provide a resistance of about 30 ohms. The temperature was then controlled to ±1° by resistance heating using a Leeds and Northrup CAT 60 control unit and a Kepco CK36 regulated power supply as the current source. The "DC" magnetic amplifier supplied with the Leeds and Northrup system turned out to be completely unsatisfactory for this experiment since it generated current pulses.

The second moment calculations were based on line shapes obtained on a wide-line nmr spectrometer constructed in this laboratory. The spectrometer consists of a crystal controlled oscillator of the Robinson type,[19] a PAR Model 120 lock-in amplifier, a Varian V3900 12-in. magnet with Fieldial, a Hewlett-Packard No. 7005B recorder, and the necessary power supplies. The x axis of the recorder was driven by the Fieldial.

The detected signal was digitized using a Digital Specialities A/D converter and an ASR-33 Teletype. The information was then processed using the Chemistry Department's Raytheon 706-SCC computer facility. Standard second-moment calculations were made, and the modulation correction of Andrew was applied.[20] Typically, 300 points were used for each second-moment calculation.

The electric field dependence of the spin-lattice relaxation time was investigated by applying 2600 V across a rectangular glass cell with copper electrodes, having a separation of 0.55 cm. The cell was rotated manually inside a room temperature probe assembly supplied by Magnion.

Results

A. Spin-Lattice Relaxation Measurements. Plots of the temperature dependence of the proton spin-lattice relaxation time as a function of reciprocal temperature are shown in Figures 2–6 for compounds I–V, respectively. There are discontinuities in each plot corresponding to the melting and isotropic points. The solid phase behavior for each of the nematogens is quite similar. A linear increase in T_1 with increasing temperature occurs up to a few degrees below the melting point indicating a simple motional process, probably methyl rotation. A maximum is reached a few degrees below the melting point for each compound, and a further increase in temperature leads to a decrease in T_1 until the melting point is reached. This decrease in T_1 is attributed to premelting, *i.e.*, to the presence of regions having high molecular mobility.

At the solid–nematic transition there is a large decrease in T_1, indicating fast rotational or translational diffusion. The appearance of structure in the wide-line spectra of the compounds indicates that these fast diffusional processes partially average out the secular part of the intermolecular dipole–dipole interactions. The nonsecular part of these interactions may, of course, still contribute to T_1.

In the nematic mesophase T_1 increases with increasing temperature until a few degrees below the isotropic point. Further increase in temperature leads to a de-

(18) D. Jones, *Appl. Phys. Lett.*, **16**, 61 (1970).
(19) R. Blume, private communication.
(20) E. R. Andrew, *Phys. Rev.*, **91**, 425 (1953).

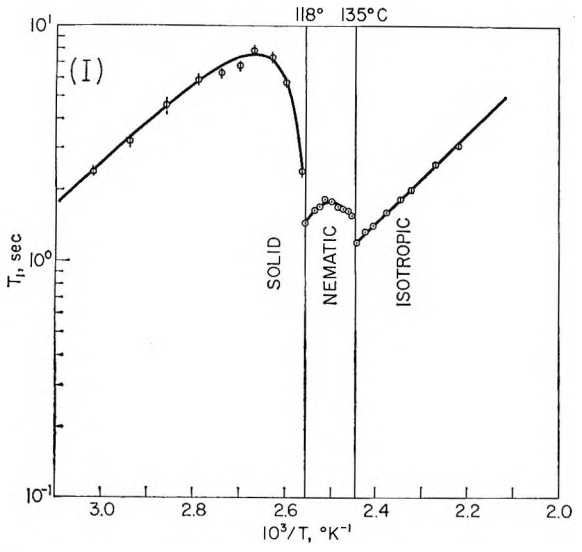

Figure 2. Proton spin-lattice relaxation time T_1 *vs.* $10^3/T$ for compound I.

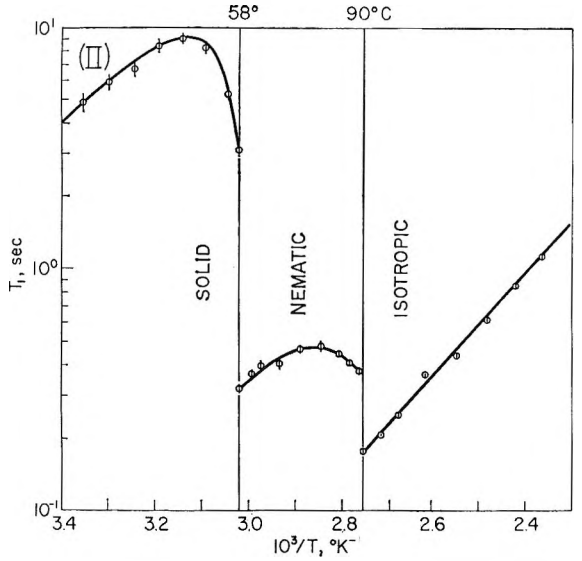

Figure 3. Proton spin-lattice relaxation time T_1 *vs.* $10^3/T$ for compound II.

crease in T_1 which may be attributed to the presence of liquid-like regions in which the self-diffusion coefficient is similar to that found in the isotropic liquid. For the compounds with large nematic temperature ranges, there is a linear relationship of log T_1 with inverse temperature which is consistent with a simple motional process such as translational diffusion. Such a temperature dependence is in direct conflict with the existing theories. At the nematic–isotropic transition point, there is a decrease in T_1 indicating a significant change in the rate of molecular motion.

In the isotropic region, the dependence of log T_1 on reciprocal temperature is sufficiently linear to be described by an activation energy. The resulting energies of activation for compounds I–V are 8.5, 9.3, 8.7,

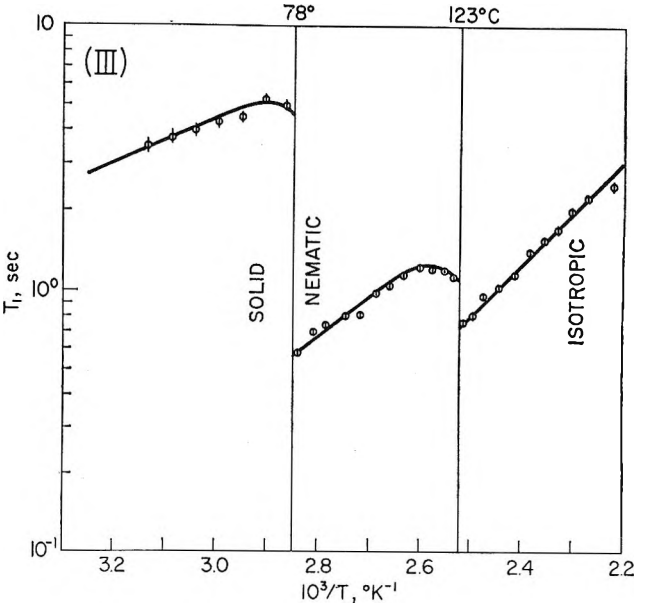

Figure 4. Proton spin-lattice relaxation time T_1 *vs.* $10^3/T$ for compound III.

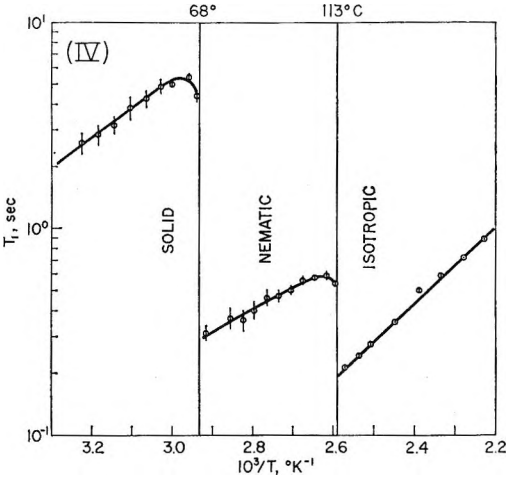

Figure 5. Proton spin-lattice relaxation time T_1 *vs.* $10^3/T$ for compound IV.

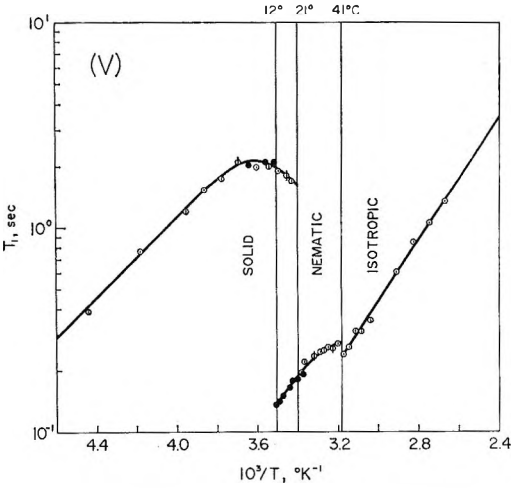

Figure 6. Proton spin-lattice relaxation time T_1 *vs.* $10^3/T$ for compound V.

8.4, and 7.0 kcal/mol, respectively. These values were calculated using a standard least-squares program.

An electric field of 5 kV/cm was applied to compound V at 25° as a means of orienting the long axes of the molecules away from the direction of the magnetic field. The relaxation theories, which are based on intramolecular dipole interactions, make use of a fluctuating Hamiltonian whose magnitude depends on the angle of alignment of the internuclear axes. Accordingly, these theories predict that T_1 should depend on the angle of alignment of the long axis of a molecule with respect to the applied field if the dipole interaction between adjacent ring protons makes a dominant contribution to relaxation. In our experiment T_1 was measured with the normal to the electrodes oriented at various angles up to 90° away from the direction of the magnetic field. In each case no differences could be detected between measurements made with the electric field on and off; *i.e.*, no orientational dependence of T_1 was found at 25°.

B. Line Shapes and Second Moments. Typical nmr spectra of compounds II–V in the nematic mesophase are shown in Figure 7. The doublet splitting is assigned to the interaction of the adjacent hydrogens on the benzene rings. The central peaks, which are prominent for compounds I and V, are assigned to the relatively isolated methyl groups.

In the solid phase each compound exhibits a broad featureless spectrum with a line width of about 10 G. Upon melting, the intermolecular contributions to the line widths decrease dramatically, and the spectra reveal structure. The total widths of the spectra continue to decrease as the temperature is increased throughout the nematic mesophase. At the isotropic point the spectral width decreases to the limit of resolution of our spectrometer. The transition temperatures determined by inspection of the wide line spectra agree with those determined by the spin-lattice relaxation studies.

The second-moment calculations for compounds II–V are shown in Figures 8–11, respectively. The second moment in each case decreases with increasing temperature as the intramolecular dipole interactions are more completely averaged. Breaks in the plots of second moment *vs.* temperature occur at the melting and isotropic points.

The doublet splitting δH arising from the dipole–dipole interaction of the adjacent ring protons was used to calculate the order parameter S by means of the equation[21]

$$\delta H = 4\alpha(^3/_2 \cos^2 \Phi - {}^1/_2)S \qquad (2)$$

where α is $^3/_2 \mu_H r^{-3}_{HH}$ and Φ is the angle between the para axis of a ring and the major molecular axis. In these calculations we assumed that $r_{HH} = 2.45$ Å and Φ = zero so that $\delta H = 5.73S$ (in gauss). The results are shown in Figures 8–11 as a function of temperature for each compound. As expected, S falls in the range from 0.3 to 0.8.[22] The angle Φ is, of course, not accurately known and may be as large as 10°. If 10° is adopted for Φ, all of our S values must be multiplied by 1.048.

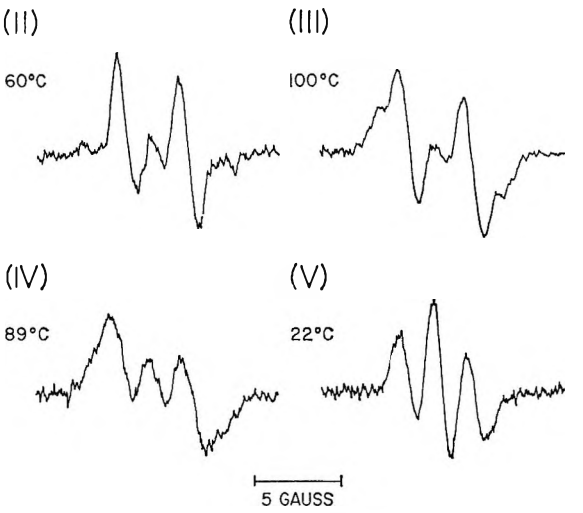

Figure 7. Representative wide line spectra (first derivatives) for compounds II–V.

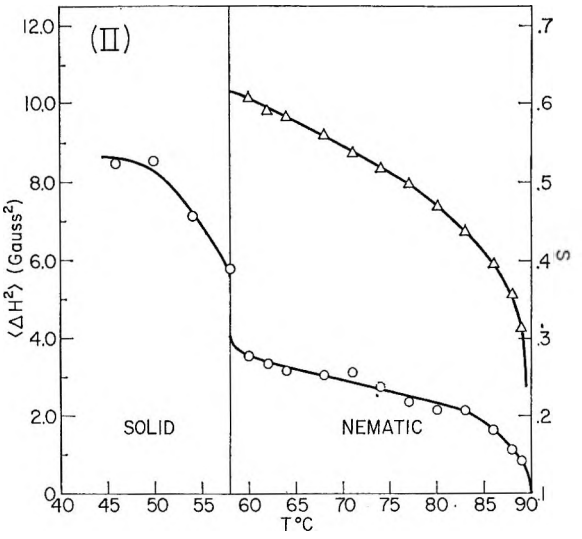

Figure 8. The second-moment $\langle \Delta H^2 \rangle$ and the order parameter S *vs.* temperature for compound II.

Discussion and Conclusions

The relaxation theories discussed in the Introduction predict the dependence of T_1 on temperature and frequency. A dependence on molecular alignment is also implied since the fluctuation of an intramolecular dipole–dipole interaction is treated. All three of these predictions are subject to experimental tests.

(21) J. C. Rowell, W. D. Phillips, L. R. Melby, and M. Panar, *J. Chem. Phys.*, **43**, 3442 (1965).

(22) A. Saupe, *Angew. Chem., Int. Ed. Engl.*, **7**, 97 (1968).

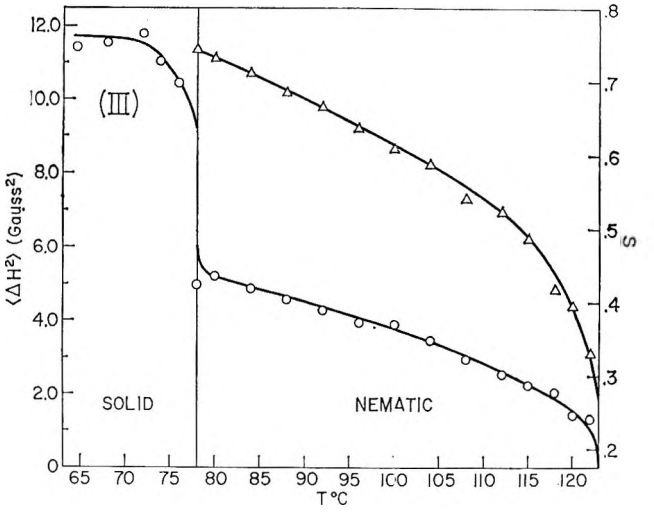

Figure 9. The second-moment $\langle \Delta H^2 \rangle$ and the order parameter S *vs.* temperature for compound III.

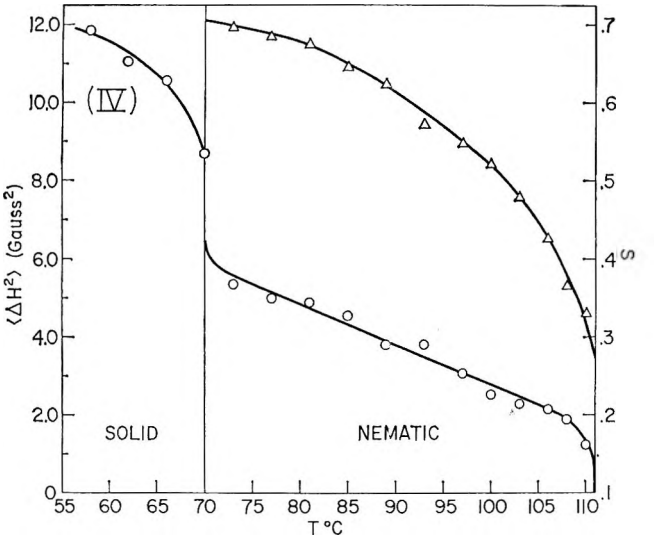

Figure 10. The second-moment $\langle \Delta H^2 \rangle$ and the order parameter S *vs.* temperature for compound IV.

First, we consider the question of molecular alignment. Doane and Visintainer were able to control the alignment of 4,4′-bis(heptyloxy) azobenzene (HAB) by working with the smetic phase where a planar structure is maintained and the preferred direction is "frozen" in.[12] Relaxation measurements for the various orientations could then be made by manually rotating the sample in the magnetic field. In their experiment T_1 was found not to vary outside the experimental uncertainty.

An alignment experiment has also been reported by Dong and Schwerdtfeger for the nematogen, 4-methoxybenzylidene-4-amino-α-methylcinnamic acid *n*-propyl ester.[14] In their work an electric field of strength ~2 kV/cm was applied perpendicular to H_0, and T_1 was found to have a slightly lower value than with the electric field off. The difference was about 5%. Our

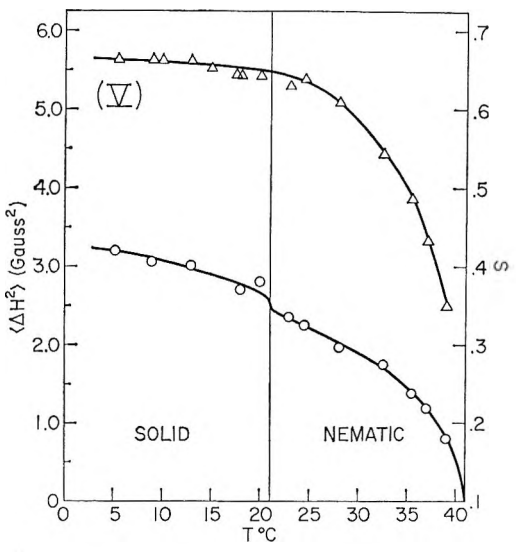

Figure 11. The second-moment $\langle \Delta H^2 \rangle$ and the order parameter S *vs.* temperature for compound V.

experiment with compound V was quite similar except that a 5-kV/cm field was used and no change in T_1 was detected.

In summary the experiments indicate that T_1 has little or no dependence on the alignment of the major axes of the molecules with respect to the applied magnetic field. Therefore, these experiments cast doubt on the importance of rotational contributions to spin-lattice relaxation for the nematic phase. Of course, it must be kept in mind that some of the molecules in question have extensive side chains in which the inter-proton directions bear little relation to the direction of the major molecular axis. Relaxation induced by the "wagging" of the side chains or the internal rotation of the methyl and methylene groups may lead to different relaxation times for the protons on the side chains and the ring protons. It should be kept in mind that our T_1 experiments have low resolution and cannot distinguish the relaxation times for the different kinds of protons. The ring protons may, in fact, have relaxation rates in closer agreement with theory than is the apparent relaxation rate of all of the protons.

The temperature dependence of T_1 in the nematic phase has also been reported by several groups.[11-14] Without exception T_1 is found to increase with temperature immediately above the melting point. Doane and Visintainer have discussed the failure of eq 1,[12] and as previously mentioned this equation has been "improved" to essentially remove the predicted temperature dependence of $1/T_1$.[16,17] In contrast to this prediction, our results for compounds which exhibit wide nematic ranges (III–IV) clearly show a significant temperature dependence and, in fact, reveal Arrhenius-type behavior. These data are not sufficient to establish the relaxation mechanism, but we point out that they are consistent with an intermolecular relaxation mechanism controlled by translational diffusion.

Finally, we come to the frequency dependence of T_1. The unambiguous prediction of eq 1 is that T_1 is proportional to $\omega^{1/2}$. Experiments on compound I (PAA) reveal that [10-12]

$$T_1 \simeq A + B\omega^{1/2} \quad (3)$$

and appear to provide support for the theory. However, the theory of spin relaxation by translational diffusion is not without a frequency dependence.[23] In fact, Harmon and Muller have demonstrated that[24,25]

$$\frac{1}{T_1} \propto \tau[1 - a(\omega\tau)^{1/2}] \quad (4)$$

where τ is the mean time between diffusion jumps and a is of order unity. For $\omega\tau \ll 1$ eq 4 is clearly of the same form as eq 3 and a comparison with the experimental data ($A \simeq 0.72$, $B \simeq 0.66$) shows that τ is of order 10^{-9} sec.[12] The magnitude of τ appears to be reasonable, and we believe that this provides additional support for a relaxation mechanism which depends on translational diffusion. Spin relaxation by translational diffusion is also consistent with the marked decrease in T_1 which occurs on passing from the nematic to the isotropic phase since the diffusion constant is known to drop by a factor of about 3.[26]

In conclusion, we find that the dependence of T_1 on molecular alignment and on temperature does not support a rotational mechanism for spin relaxation and that the frequency dependence of T_1 does not distinguish between the rotational and translational mechanisms. An experiment is called for, perhaps making use of totally deuterated liquid crystals, to separate the inter- and intramolecular contributions to spin relaxation.[27]

Acknowledgments. We would like to thank Dr. H. M. McIntyre for assistance in the wide line experiments and in the computer analysis of data. Also, we thank Dr. M. K. Wilson for preliminary T_1 measurements.

(23) H. C. Torrey, *Phys. Rev.*, 92, 962 (1953).

(24) J. F. Harmon and B. H. Muller, *ibid.*, 182, 400 (1969).

(25) J. F. Harmon, *Chem. Phys. Lett.*, 7, 207 (1970).

(26) M. Weger and B. Caban, preprint.

(27) Note Added in Proof. Wide line nmr studies of compound V by Dr. C. Wade using electric fields aboqe 5 kV/cm do not confirm that the molecules are being aligned by the field. The dependence of T_1 on orientation in the magnetic field, therefore, remains unknown for this compound.

Application of the Method of the Steepest Descent to the Calculation of the Translational Energy of Fragments of Ion Decomposition[1a]

by K. H. Lau and S. H. Lin*[1b]

Department of Chemistry, Arizona State University, Tempe, Arizona 85281 *(Received March 8, 1971)*

Publication costs assisted by the National Science Foundation

It is shown that the total number of states $W(E)$ and the average translational energy $\bar{\epsilon}_t$ of the products of unimolecular dissociation from the election impact are related to the inverse Laplace transform of the functions $Q(\beta)/\beta$ and $Q(\beta)/\beta^2$, respectively, where $Q(\beta)$ is the partition function. The first-order steepest-descent method is applied to carry out the integration involved in the inverse Laplace transformation. The numerical results of total number of states and average translational energies are in good agreement with those obtained from direct counting.

Introduction

The major assumption of the quasiequilibrium theory of unimolecular reactions developed by Rosenstock, *et al.*,[2a] is that the transfer of energy among the oscillators in the activated state is much faster than the dissociation into products, so that the oscillators reach energy equilibrium. According to the quasiequilibrium theory, the translational energy of the activated complex in the reaction coordinate becomes part of the translational energy of the dissociated products.[2b] If the excess energy $E^{\ddagger}$ of the activated complex is divided into the vibrational energy ϵ_v and the translational energy ϵ_t in the reaction coordinate, then the calculation

(1) (a) Supported by the National Science Foundation, the Petroleum Research Fund, and A. P. Sloan Foundation; (b) John Simon Guggenheim Fellow.

(2) (a) H. M. Rosenstock, M. B. Wallenstein, A. L. Wahrhaftig, and H. Eyring, *Proc. Nat. Acad. Sci. U. S.*, 38, 667 (1952); (b) C. E. Klots, *J. Chem. Phys.*, 41, 117 (1964).

of the average translational energy is essentially the problem of calculating the distribution of vibrational energy among a collection of oscillators whose total energy is $E^{\pm}$. The average vibrational energy of the activated complex is given by the integral[2]

$$\bar{\epsilon}_v = \int_0^{E^{\pm}} \epsilon_v P(E^{\pm}, \epsilon_v)\, d\epsilon_v \quad (1)$$

where $P(E^{\pm}, \epsilon_v)\, d\epsilon_v$ is the probability that a system with total energy $E^{\pm}$ will have vibration energy ϵ_v and $P(E^{\pm}, \epsilon_v)$ can be expressed as[2]

$$P(E^{\pm}, \epsilon_v) = \frac{\rho(\epsilon_v)}{W(E^{\pm})} \quad (2)$$

$W(E^{\pm})$ is the total number of states with energy $E^{\pm}$. $\rho(\epsilon_v)$ is the density of states and can be expressed by $dW(\epsilon_v)/d\epsilon_v$ when the totality of states is a continuous function of energy. If the average translational energy $\bar{\epsilon}_t$ is taken to be the difference in the excess energy and the average vibrational energy, then by substituting eq 2 into eq 1, we obtain

$$\bar{\epsilon}_t = E^{\pm} - \frac{1}{W(E^{\pm})} \int_0^{E^{\pm}} \epsilon_v \frac{dW(\epsilon_v)}{d\epsilon_v} d\epsilon_v \quad (3)$$

Integrating by part of eq 3 yields

$$\bar{\epsilon}_t = \frac{1}{W(E^{\pm})} \int_0^{E^{\pm}} W(\epsilon_v) d\epsilon_v \quad (4)$$

A comparison of calculation of the average translational energy using various methods of enumerating the total number of states has been carried out by Klots[2b] and Franklin.[3,4] The method of direct counting of states gives good agreement with experimental values and the approximate calculation of $\bar{\epsilon}_t$ based on the method proposed by Vestal, *et al.*,[5] and its modification by Tou and Wahrhaftig[6] shows good agreement with that from the direct counting of states only in the medium and high energy range. It is clear that the complexity of the computation of $\bar{\epsilon}_t$ increases with the number of degrees of freedom of the system. So in order to carry out the integration in eq 4, a good continuous approximation to $W(E)$ is required. In the present paper, we shall discuss the application of the method of steepest descent[7-11] to the computation of $\bar{\epsilon}_t$.

Derivation

As we can see from eq 4, in order to evaluate $\bar{\epsilon}_t$ we have to find $W(E)$, the total number of states. For a system (or part of the system) with the partition function represented by

$$Q(\beta) = \sum_i e^{-\beta\epsilon_i} \quad (5)$$

it can be shown (Appendix) that $W(E)$ can be expressed by the inverse Laplace transform of the function $Q(\beta)/\beta$,[7,8] *i.e.*

$$W(E) = \frac{1}{2\pi i} \int_{\gamma-i\infty}^{\gamma+i\infty} \frac{Q(\beta)}{\beta} e^{\beta E} d\beta = L^{-1}\left[\frac{Q(\beta)}{\beta}\right] \quad (6)$$

$Q(\beta)$ defined by eq 5 is a regular analytic function of the variable $\beta = \beta_1 + i\beta_2$ defined in the half-plane $\beta_1 > 0$. The path of integration in eq 6 can be an arbitrary line parallel to the imaginary axis in the half-plane $\beta_1 > 0$, and hence we can write eq 6 as a real integral[7,8]

$$W(E) = \frac{1}{2\pi} \int_{-\infty}^{\infty} e^{f(\beta)} d\beta_2 \quad (7)$$

where

$$f(\beta) = \log Q(\beta) - \log \beta + \beta E \quad (8)$$

In this problem, it can be seen that $f(\beta)$ has one minimum ($f''(\beta) > 0$) along the real axis and this minimum is very steep. The position of minimum is denoted by the point $\beta = (\beta^{\pm}, 0)$. As the integrand is analytic the minimum cannot be absolute, but a saddle point. The values of the integrand fall off sharply as we leave the real axis at $(\beta^{\pm},0)$. If we expand $f(\beta)$ about the point $\beta = (\beta^{\pm},0)$ in the imaginary direction at which the function has a minimum, we obtain

$$f(\beta) = \log Q(\beta^{\pm}) - \log \beta^{\pm} + \beta^{\pm}E - \frac{1}{2}\left[\left(\frac{\partial^2 \log Q(\beta)}{\partial\beta^2}\right)_{\beta^{\pm}} + \frac{1}{(\beta^{\pm})^2}\right]\beta_2^2 + \ldots \quad (9)$$

where the point $(\beta^{\pm},0)$ is the root of $\partial f(\beta)/\partial\beta = 0$ or

$$\left(\frac{\partial \log Q(\beta)}{\partial\beta}\right)_{\beta=\beta^{\pm}} - \frac{1}{\beta^{\pm}} + E = 0 \quad (10)$$

For a more detailed discussion of the method of steepest descent, other references should be consulted.[7,8] Combining eq 8 and 9 with eq 7, we obtain the expression for $W(E)$ as

$$W(E) = (2\pi)^{-1/2}(\beta^{\pm})^{-1} e^{\beta^{\pm}E} Q(\beta^{\pm}) \times \left[\left(\frac{\partial^2 \log Q(\beta)}{\partial\beta^2}\right)_{\beta=\beta^{\pm}} + \frac{1}{(\beta^{\pm})^2}\right]^{-1/2} \quad (11)$$

$W(E)$ in eq 11, is the result of the first-order approximation of the method of steepest descent. The high-order approximations for $W(E)$ can be obtained easily.

(3) M. A. Haney and J. L. Franklin, *J. Chem. Phys.*, **48**, 4093 (1968).
(4) E. L. Spatz, W. A. Seitz, and J. L. Franklin, *ibid.*, **51**, 5142 (1969).
(5) M. Vestal, A. L. Wahrhaftig, and W. J. Johnson, *ibid.*, **37**, 1276 (1962).
(6) J. C. Tou and A. L. Wahrhaftig, *J. Phys. Chem.*, **72**, 3034 (1968).
(7) (a) C. Kittel, "Elementary Statistical Physics," Wiley, New York, N. Y., 1958; (b) P. M. Morse and H. Feshbach, "Methods of Theoretical Physics," Vol. 1, McGraw-Hill, New York, N. Y., 1953.
(8) (a) M. R. Hoare and Th. W. Ruijgrok, *J. Chem. Phys.*, **52**, 113 (1970); M. R. Hoare, *ibid.*, **52**, 5695 (1970); (b) W. Forst, Z. Prášil, and P. St. Laurent, *ibid.*, **46**, 3736 (1967).
(9) S. H. Lin and H. Eyring, *ibid.*, **39**, 1577 (1963); **43**, 2153 (1965).
(10) J. C. Tou and S. H. Lin, *ibid.*, **49**, 4187 (1968).
(11) K. H. Lau and S. H. Lin, *J. Phys. Chem.*, **75**, 981 (1971).

For a system with a given energy E, $\beta^{\pm}(E)$ can be found by solving eq 10, and then the total number of states $W(E)$ can be calculated by using eq 11.

If we take the Laplace transform of eq 4, we obtain

$$L[\bar{\epsilon}_t(E^{\pm})W(E^{\pm})] = \int_0^{\infty}\left[\int_0^{E^{\pm}} W(\epsilon_v)\,d\epsilon_v\right]e^{-\beta E^{\pm}}dE^{\pm} \quad (12A)$$

Integrating by parts, we find

$$L[\bar{\epsilon}_t(E^{\pm})W(E^{\pm})] = \frac{1}{\beta}\int_0^{\infty} W(E^{\pm})e^{-\beta E^{\pm}}dE^{\pm} = \frac{1}{\beta}L[W(E^{\pm})] \quad (12B)$$

Because of eq 6, it follows that

$$L[\bar{\epsilon}_t(E^{\pm})W(E^{\pm})] = \frac{Q(\beta)}{\beta^2} \quad (13)$$

Therefore, the function $\bar{\epsilon}_t(E^{\pm})W(E^{\pm})$ can be evaluated by taking the inverse Laplace transform of $[Q(\beta)]/(\beta^2)$. Repeating the same processes as given above, we write this inverse transform integral as

$$\bar{\epsilon}_t(E)W(E) = \frac{1}{2\pi}\int_{-\infty}^{\infty} e^{g(\beta)}d\beta_2 \quad (14)$$

where

$$g(\beta) = \log Q(\beta) - 2\log\beta + \beta E \quad (15)$$

Applying the steepest-descent method, we obtain, to the first-order approximation of the method of steepest descent, the following result

$$\bar{\epsilon}_t = \frac{(2\pi)^{-1/2}}{W(E^{\pm})}(\beta^{\pm})^{-2}e^{\beta^{\pm}E^{\pm}} \times \left[\left(\frac{\partial^2 \log Q(\beta)}{\partial\beta^2}\right)_{\beta=\beta^{\pm}} + \frac{2}{(\beta^{\pm})^2}\right]^{-1/2}Q(\beta^{\pm}) \quad (16)$$

where $\beta^{\pm}$ is to be determined by

$$\left(\frac{\partial \log Q(\beta)}{\partial\beta}\right)_{\beta=\beta^{\pm}} - \frac{2}{\beta^{\pm}} + E^{\pm} = 0 \quad (17)$$

Thus from eq 16, one can calculate $\bar{\epsilon}_t$, the average translation energy of dissociated fragments.

An approximation can be introduced here to simplify the calculation of $\bar{\epsilon}_t$. Suppose the factor $1/\beta$ in eq 12 is replaced by the first-order value $1/\beta^{\pm}$ in which $\beta^{\pm}$ is defined in eq 10; in this approximation the average translational energy $\bar{\epsilon}_t$ can be calculated by taking the inverse Laplace transform of both sides of eq 12. We find

$$\bar{\epsilon}_t = \frac{1}{\beta^{\pm}} \quad (18)$$

This expression should be compared with the result of a pressure-maintained thermal distribution, $\bar{\epsilon}_t = kT$.

Next let us apply the result of the derivation to a system of N harmonic oscillators of frequencies ν_1, ν_2, ..., ν_n with energies $\epsilon_i = (n_i + 1/2)\hbar\nu_i$; $i = 1, 2, \ldots, N$. The partition function of this system is given by

$$Q(\beta) = \prod_{i=1}^{N}\frac{e^{1/2\beta\hbar\nu_i}}{1 - e^{-\beta\hbar\nu_i}} \quad (19)$$

Substitution of eq 19 into eq 11 gives

$$W(E) = (2\pi)^{-1/2}(\beta^{\pm})^{-1}e^{\beta^{\pm}(E-E_0)} \times \prod_{i=1}^{N}\frac{1}{1 - e^{-\beta^{\pm}\hbar\nu_i}} \times \left[\sum_{i=1}^{N}\frac{(\hbar\nu_i)^2e^{-\beta^{\pm}\hbar\nu_i}}{(1 - e^{-\beta^{\pm}\hbar\nu_i})^2} + \frac{1}{(\beta^{\pm})^2}\right]^{-1/2} \quad (20)$$

which is slightly different from that derived by Hoare and Ruijgrok,[8] who replaced the factor $1/\beta$ in the integrand of eq 6 by the first-order value $1/\beta^{\pm}$ of the function of the density of states at the saddle point. That is, $W(E) = (1/\beta^{\pm})L^{-1}[Q(\beta)] = [\rho(E)]/(\beta^{\pm})$, since $\rho(E) = (dW/dE) = L^{-1}[Q(\beta)]$ from eq 6. Equation 20 for $W(E)$, on the other hand, is obtained directly from eq 6 by using the first-order approximation of the method of steepest descent. In other words, in the method of Ruijgrok and Hoare, to evaluate $W(E)$ one has to evaluate the corresponding $\rho(E)$ first and then $W(E) = \rho(E)/\beta^{\pm}$. $\beta^{\pm}$ in eq 20 is to be determined by

$$E - E_0 = \sum_{i}^{N}\frac{\hbar\nu_i}{e^{\beta^{\pm}\hbar\nu_i} - 1} + \frac{1}{\beta^{\pm}} \quad (21)$$

Similarly, substituting eq 19 into eq 16 yields

$$\bar{\epsilon}_t(E) = \frac{(2\pi)^{-1/2}}{W(E^{\pm})}(\beta^{\pm})^{-2}e^{\beta^{\pm}(E^{\pm}-E_0')} \times \prod_{i=1}^{N'}\frac{1}{1 - e^{-\beta^{\pm}\hbar\nu_i'}} \times \left[\sum_{i=1}^{N'}\frac{(\hbar\nu_i')^2e^{-\beta^{\pm}\hbar\nu_i'}}{(1 - e^{-\beta^{\pm}\hbar\nu_i'})^2} + \frac{2}{(\beta^{\pm})^2}\right]^{-1/2} \quad (22)$$

with $\beta^{\pm}$ determined by

$$E^{\pm} - E_0' = \sum_{i=1}^{N'}\frac{\hbar\nu_i'}{e^{\beta^{\pm}\hbar\nu_i'} - 1} + \frac{2}{\beta^{\pm}} \quad (23)$$

E_0 (and E_0') represents the zero-point energy of the system of harmonic oscillators. $N' = N - 1$ for a bound activated complex, and $N' = N - 3$ for a loose complex.[3,4]

When the system has an extreme high energy, β approaches zero. In this limiting case, the partition function becomes the classical

$$Q(\beta) = \frac{e^{-\beta E_0}}{\beta^N\prod_{i=1}^{N}\hbar\nu_i} \quad (24)$$

By using eq 24, $\beta^{\pm}$ in eq 10 and $(\partial^2 \log Q(\beta)/(\partial\beta^2))_{\beta=\beta^{\pm}}$ can be evaluated as $N/(E - E_0)$ and $(E - E_0)^2/N$, respectively. $W(E)$ in this case becomes

Table I: Comparison of the Calculated and Exact Values of $W(E)$ for Selected Molecules

$(E - E_0)$, kcal/mol	$W_{ex}(E)$	$W(E)^a$	$W(E)^b$	$W(E)^c$
		Cyclopropane[d]		
16	8.02×10^2	7.43×10^2	7.23×10^2	7.49×10^2
20	7.75×10^4	7.68×10^4	7.56×10^4	7.75×10^4
30	2.69×10^6	2.68×10^6	2.64×10^6	2.69×10^6
40	4.97×10^7	4.99×10^7	4.95×10^7	5.03×10^7
50	6.12×10^8	6.16×10^7	6.12×10^7	6.22×10^8
100	5.84×10^{12}	5.82×10^{12}	5.80×10^{12}	5.88×10^{12}
150	3.00×10^{15}	2.98×10^{15}	2.97×10^{15}	3.01×10^{12}
		Water[e]		
10	3	3.72	3.54	3.24
20	11	11.39	11.22	10.77
30	23	25.63	25.49	24.83
40	46	48.42	48.38	47.44
50	78	81.79	81.91	80.63
100	466	476.27	478.78	474.52
150	1405	1433.33	1442.21	1432.46
		Acetylene[f]		
2.31	5	3.84	3.58	4.34
4.61	15	14.91	14.19	16.77
9.23	94	99.26	96.07	108.86
13.84	390	401.30	392.39	433.26
18.45	1.198×10^3	1.243×10^3	1.223×10^3	1.33×10^3
23.06	3.163×10^3	3.237×10^3	3.198×10^3	3.43×10^3
27.68	7.333×10^3	7.447×10^3	7.380×10^3	7.84×10^3
36.90	2.969×10^4	3.035×10^4	3.018×10^4	3.17×10^4

[a] Results of eq 20. [b] Results of eq 3.2 in ref 8. [c] References 10 and 11. [d] Using the following rounded frequencies: 3221 (6), 1478 (3), 1118 (7), 879 (3), 750 (2), cm^{-1}. [e] ν_i = 3652, 1595, 3756 cm^{-1}. [f] ν_i = 612 (2), 729 (2), 1974 (1), 3287 (1), 3374 (1).

$$W(E) = [(2\pi)^{1/2}e^{-(N+1)}(N+1)^{N+1/2}]^{-1} \times \left[\prod_{i=1}^{N} \hbar\nu_i\right]^{-1}(E - E_0)^N \quad (25)$$

which differs from the exact result in the use of the Stirling approximation for the Γ function.

Substitution of eq 25 into eq 4 gives the classical result of $\bar{\epsilon}_t$, $\bar{\epsilon}_t = (E - E_0)/N$, where $N = N' + 1$ and N' has the same meaning as mentioned before. It should be noticed that this classical result of $\bar{\epsilon}_t$ can be obtained directly from eq 18, where $\beta^{\mp}$ is to be determined by eq 21 for a system of N' harmonic oscillators.

Results and Discussion

In order to test the reliability of the equations derived in the previous section for calculating $\bar{\epsilon}_t$, we have to make sure that the approximation methods used in calculating $W(E)$ are accurate enough. For this purpose, cyclopropane, water, and acetylene are chosen as test cases. A comparison of $W(E)$ for these molecules calculated by using the exact counting, the methods of Lin and Eyring,[9] those of Hoare and Ruijgrok,[8] and eq 20 is shown in Table I. We can see that the results from the three approximation methods are in good agreement with those from the exact counting. This is not surprising, because it has been shown by Lau and Lin[11] that as far as the calculation the density of states is concerned, the methods by Lin and Eyring and by Hoare and Ruijgrok are equivalent, though the approximation introduced in the calculation of $W(E)$ is different for the two methods. It is to be noted that for a quantized system, $W(E)$ is well defined while $\rho(E)$ is defined only when $W(E)$ is a continuous function of E.

For the calculation of the average translational energy of the fragments, we consider two possible intermediates for the activated complex, a bound ion with $N - 1$ oscillators and a loose one with $N - 3$ oscillators. We compute $\bar{\epsilon}_t$ using eq 18 and eq 22 for $N - 1$ and $N - 3$ models and the calculated results are given in Tables II and III. The results, calculated by using eq 18 and eq 22 are in excellent agreement with those obtained from the direct counting for the whole energy range. Roots of eq 21 and eq 23 can be solved easily by the use of a false-position numerical method.[12] The computations are carried out by using a GE 425 computer.

(12) S. S. Kuo, "Numerical Methods and Computers," Addison-Wesley, Reading, Mass., 1965.

Table II: Comparison of Average Translational Energy Calculated Using Different Methods of Enumerating the States for $N - 1$ Complex (in kcal/mol)

	$E^{\ddagger}$[a]	Observed[a]	Direct[b]	Eq 22	Eq 18	VWJ[b]	TW[b]
$C_2N_2^+ \rightarrow CN^+ + CN$	19	4.8	3.7	3.69	3.66	3.7	3.6
$C_2H_2^+ \rightarrow CH^+ + CH$	19	6.4	4.2	4.15	4.09	4.2	4.0
$c\text{-}C_3H_6^+ \rightarrow C_2H_2^+ + CH_4$	15	1.6	2.0	2.07	2.03	3.8	4.0
$c\text{-}C_3H_6^+ \rightarrow C_2H_3^+ + CH_3$	21	2.8	2.5	2.47	2.43	3.2	4.4
$c\text{-}C_3H_6^+ \rightarrow CH_2^+ + C_2H_4$	113	12.1	7.4	7.36	7.34	7.4	7.4

[a] Reference 3. [b] Reference 4.

Table III: Average Translational Energy Calculated from Eq 18 and Eq 22 from Various Sets of Excluded Modes (in kcal/mol)

Reaction	$E^{\ddagger}$[a]	$\bar{\epsilon}_{exp}$[a]	$\bar{\epsilon}_{ex}$[b]	$\bar{\epsilon}_t$ (eq 22)	$\bar{\epsilon}_t$ (eq 18)	Modes and fundamentals excluded, cm^{-1}		
$c\text{-}C_3H_6^+ \rightarrow C_2H_2^+ + CH_4$	15	1.6	2.0	2.07	2.03	a	Ring deformation	868
			2.1	2.16	2.12	b	Ring deformation	868
							CH stretch	3024
$c\text{-}C_3H_6^+ \rightarrow C_2H_3^+ + CH_3$	21	2.8	2.5	2.47	2.43	a	Ring deformation	868
			2.5	2.59	2.55	b	Ring deformation	868
							CH stretch	3024
$C_2N_2^+ \rightarrow CN^+ + CN$	19	4.8	3.7	3.69	3.66	a	CC stretch	848
			5.2	5.13	5.09	b	CC stretch	848
							(2) CCN bend	226
$CH_2Cl_2^+ \rightarrow CH_2^+ + Cl_2$	36	8.3	5.7	5.68	5.65	a	CCl_2 stretch	283
			7.1	7.08	7.04	b	CCl_2 stretch	283
							CCl stretch	702
							CH_2 rock	899
$C_2H_2^+ \rightarrow CH^+ + CH$	19	6.4	4.2	4.15	4.09	a	C≡C stretch	870
			5.5	5.67	5.58	b	C≡C stretch	870
							(2) CH bend	1312
$CH_3CN^+ \rightarrow CH_2^+ + HCN$	17	2.8	3.0	2.95	2.89	a	CC stretch	918
			3.2	3.35	3.29	b	CC stretch	918
							CH stretch	2942
							C CN bend	380

[a] Reference 3. [b] Reference 4.

Franklin[4] has attributed the discrepancies between the calculated results and experimental values to uncertainties in the heats of formation and the experimental data as well as to a lack of knowledge of the vibrational modes existing in the ion. The effect of the exclusion of disallowed states from $\rho(E)$ and $W(E)$ on unimolecular reactions has been investigated by Forst and Prášil.[13,14] It will be of interest to study this effect on the average translational energy of the fragments.

In concluding the discussion, it should be noted that the methods given in this paper for calculting $W(E)$ and $\bar{\epsilon}_t(E)$ are easy to use, no matter how complicated the systems are, and though only the results of the first-order approximation of the method of steepest descent are given and seem to be sufficient in most cases, the high-order approximations for $W(E)$, $\rho(E)$,[8] and $\bar{\epsilon}_t$ can be derived easily.

Appendix

From the definition of the Heaviside function $H(x)$ [$H(x) = 1, x > 0$; $H(x) = 0, x < 0$], we can express $W(E)$ as

$$W(E) = \sum_i H(E - \epsilon_i) \qquad \text{(A-1)}$$

Introducing the integral representation of $H(x)$

$$H(E - \epsilon_i) = \frac{1}{2\pi_i}\int_{\gamma-i\infty}^{\gamma+i\infty} \frac{e^{\beta(E-\epsilon_i)}}{\beta}\,d\beta \qquad \text{(A-2)}$$

eq A-1 becomes

$$W(E) = \sum_i \frac{1}{2\pi_i}\int_{\gamma-i\infty}^{\gamma+i\infty} \frac{e^{\beta(E-\epsilon_i)}}{\beta}\,d\beta = \frac{1}{2\pi_i}\int_{\gamma-i\infty}^{\gamma+i\infty} \frac{e^{\beta E}}{\beta}Q(\beta)d\beta \qquad \text{(A-3)}$$

(13) W. Forst and Z. Prášil, *J. Chem. Phys.*, **48**, 1431 (1968); **51**, 3006 (1969).

(14) W. Forst and Z. Prášil, *ibid.*, **53**, 3065 (1970).

Evaluation of Photoluminescence Lifetimes

by J. N. Demas[1] and A. W. Adamson*

Department of Chemistry, University of Southern California, Los Angeles, California 90007 *(Received January 19, 1971)*

Publication costs borne completely by The Journal of Physical Chemistry

A new method is described for calculating emission lifetimes for flash decay data. The technique, based on a linear phase-plane plot, handles the case where the emission lifetime is comparable to the observed flash duration, and its accuracy compares favorably with that of other procedures. It requires only a desk calculator, is rapid, and provides an internal check as to whether or not a single decay time is being observed.

Introduction

Perhaps the most popular and direct method for measuring photoluminescence lifetimes employs a flash procedure. The sample luminescence is excited by a flash lamp or laser pulse, and the emission, monitored by a photomultiplier, is displayed on an oscilloscope.[2] For the most commonly encountered special case where the sample decays by only first-order or pseudo-first-order paths (the decay can thus be characterized by a mean lifetime τ), flash techniques can be especially appealing. If the flash duration and time scale of instrumental distortion are short compared with τ, the transient observed on the oscilloscope is exponential with a lifetime τ; τ may readily be evaluated from a semilogarithmic plot of emission intensity *vs.* time. Unfortunately, when the time scale of instrumental distortion, the flash duration, and τ are comparable, this simple procedure fails; however, in spite of the fact that the observed sample decay now reflects, in a complex fashion, the detailed nature of the flash, the distortions, and τ, various mathematical techniques allow one to extract τ from the flash and sample decay data.[3-5]

For the case where the semilogarithmic plot fails to yield accurate lifetime estimates, we shall present a new method for evaluating τ from the flash and the sample decay data as well as experimental verification of the procedure. The approach is related to, but avoids certain disadvantages of existing procedures and these last will be described briefly so as to provide a proper context.

Three time-dependent functions must first be defined. $F(t)$ is the oscilloscope response to the flash stimulation in the absence of the sample. $D(t)$ is the oscilloscope response when the system views the sample luminescence; $D(t)$ is assumed to contain no direct contribution from the flash. Both $F(t)$ and $D(t)$, however, will contain instrumental distortions such as phototube rise time, RC time constant effects, and amplifier bandwidth limitations. We shall subsequently assume that all distortions are linear and are the same in type and degree in the measurement of both $F(t)$ and $D(t)$. The "true" dependence of the sample decay, $d(t)$, is defined as that sample decay signal that would be observed if the excitation flash were infinitely short, an impulse, and the optical detector and electronics introduced no signal distortion.

Lifetimes may, for example, be evaluated from the statistical moments of $D(t)$ and $F(t)$;[3-5] computation of a lifetime can be relatively rapid (0.5–2 hr) on a desk calculator. The principal disadvantage of the moments methods is that since only a calculated τ is obtained, no warning is given of multiple decay kinetics.[6,7] Also, since the moments are defined as integrals to infinite time, there is a practical problem associated with taking experimental data to large enough times to ensure that reasonably good convergence is obtained.

Alternatively, the theory of Fourier transformations allows one, in principle, to construct from $F(t)$ and $D(t)$ the true decay curve, $d(t)$.[8] The τ value may then be computed from $d(t)$. For the case where $d(t)$ is not an exponential or a sum of exponentials, this method is the only available one for computing $d(t)$. Implementation of this technique appears to be relatively difficult, however. Munro and Ramsay[8] have mentioned the use of the scarce "optical Fourier transform" computers to carry out the calculations, but to our knowledge the only attempt to employ a digital computer for such evaluations was unsuccessful, presumably due to the difficult programming and ill-conditioned convergence.[9] Digital computer evaluation of the transforms should

(1) National Science Foundation Postdoctoral Fellow.

(2) (a) C. A. Parker, "Photoluminescence of Solutions," Elsevier, New York, N. Y., 1968; (b) J. G. Calvert and J. N. Pitts, Jr., "Photochemistry," Wiley, New York, N. Y., 1966.

(3) D. H. Cooper, *Rev. Sci. Instrum.*, **37**, 1407 (1966).

(4) J. N. Demas and G. A. Crosby, *Anal. Chem.*, **42**, 1010 (1970).

(5) S. S. Brody, *Rev. Sci. Instrum.*, **28**, 1021 (1957).

(6) An ingenious extension of the moments methods has been described by Isenberg and Dyson.[7] Their method allows one to fit $d(t)$ to a sum of exponentials rather than a single decay. The method requires, however, large numbers of data points of rather high accuracy to obtain meaningful results, thus preventing the use of oscilloscope data collection methods. A digital computer is required to carry out the data reduction.

(7) I. Isenberg and R. D. Dyson, *Biophys. J.*, **9**, 1337 (1969).

(8) I. H. Munro and I. A. Ramsay, *J. Sci. Instrum.*, **1**, 147 (1968).

eventually be possible since the approach has been successful for similar problems.[10]

Perhaps the most widely used method for evaluating τ under adverse conditions is that of curve simulation, CS.[3,4,11] If $d(t)$ is a simple exponential, then

$$D(t) = Ke^{-t/\tau} \int_0^t F(x)e^{x/\tau}dx \qquad (1)$$

The procedure is to calculate a sample decay curve, $D_{calcd}(t)$, for an assumed value of τ, and to compare this $D_{calcd}(t)$ with the observed function, $D(t)$. The proportionality constant, K, which takes into account the various instrumental, geometric, and sample properties is adjusted to give the best fit between $D_{calcd}(t)$ and $D(t)$. The calculation is repeated for successive τ values until an acceptable fit to the observed $D(t)$ is obtained. Efficient procedures for obtaining a best τ value have been discussed.[4]

The CS method has the advantage that $D_{calcd}(t)$ can be compared with the observed $D(t)$, a procedure which gives insight into how well an exponential describes the emission kinetics. Inability to obtain a satisfactory fit constitutes strong evidence for a more complex decay function and, conversely, a good fit implies simple exponential decay of the emission. The disadvantage is that a large number of calculations is required; thus, the method is usually practical only if a digital computer is available.[12,13] Also, both $D(t)$ and $F(t)$ must be taken to the same zero reference time, which precludes the use of the normal internal triggering mode on the oscilloscope in obtaining the data. The readout must be externally triggered by another pulse of fixed time relation to the initiation of the flash, usually by a signal from a second photomultiplier which views the flash directly.

In summary, there is no available technique which allows *both* the rapid evaluation of a decay constant by means of a desk calculator *and* also a check that $d(t)$ is indeed a simple exponential. The method described below has both attributes.

The Phase-Plane Method. The phase-plane, PP, method is based on the fact that while eq 1 is not linear, it may be converted to a linear form (see Appendix A). This form is

$$Z(t) = -\tau W(t) + K\tau \qquad (2)$$

where

$$Z(t) = \frac{\int_0^t D(y)dy}{\int_0^t F(y)dy}$$

and

$$W(t) = \frac{D(t)}{\int_0^t F(y)dy}$$

The integrals are readily evaluated from the experimental $D(t)$ and $F(t)$, and a plot of $Z(t)$ *vs* $W(t)$ will then yield a straight line of slope $-\tau$ and intercept $K\tau$.

We have found it convenient to calculate the integrals numerically using the trapezoidal rule and a programmable desk calculator (see Appendix B). With this procedure computation of the PP plot is about as rapid as a moments calculation (20 min for 40 data points using the programmable calculator and about 2 hr otherwise). Further, if the PP plot is not linear, then $d(t)$ is presumably complex in nature; one thus has an internal check on the correctness of the assumption that $d(t)$ is a single exponential decay. In practice, however, $W(t)$ and $Z(t)$ are not accurately defined at short times because of experimental error, and the plot will usually be nonlinear at small $Z(t)$. In a least-squares or visual fitting of a straight line to the PP plot, these early points should be given reduced weight. The entire procedure can, of course, be carried out be means of a digital computer.

Since the PP method is based on eq 1, it shares some of the attributes of the CS method. Thus both $D(t)$ and $F(t)$ must be taken to a common zero time. As with the latter method, linear instrumental distortion (*e.g.*, transit time spread and delay and RC distortion) do not invalidate the results so long as $D(t)$ and $F(t)$ are obtained under identical conditions of distortion. We feel, however, that the PP method allows easier detection of any nonsimple $d(t)$ although, of course, no direct readout of two or more τ values is possible. Also, we suggest that even if the CS method is used, the calculations should be routinely checked by our procedure. Occasionally the integral of eq 1 is evaluated erroneously in the CS method because of convergence problems—the presence of the exponential factor may give the plot of $F(t)\exp(t/\tau)$ *vs.* t, an irregular shape, and an apparently acceptable simulation can be obtained with an incorrect τ value.[14]

Experimental Test of the Phase-Plane Method. Demas and Crosby[4] tabulated luminescence decay data for tris(2,2′-bipyridine)ruthenium(II) chloride, $[Ru(bipy)_3]Cl_2$, at 77°K, and the corresponding plots of $F(t)$ and $D(t)$ are shown in Figure 1. The flash duration was about 20 μsec, while τ was about 5 μsec.

(9) J. A. McIntosch, "A Pulsed Excitation Method for Determining Nanosecond Fluorescent Lifetimes," National Bureau of Standards Clearing House for Federal Scientific and Technical Information, AD-651-799.

(10) J. B. Bassingthwaghte, *Science*, **167**, 1347 (1970).

(11) O. J. Steingraber and I. B. Berlman, *Rev. Sci. Instrum.*, **34**, 524 (1963).

(12) An exception is the TRW lifetime computer. This device is an on-line analog computer; visual matching of the synthetic decay curve and the actual curve is carried out on an oscilloscope.[13]

(13) TRW Systems, El Segundo, California, TRW Instruments, Application Note 6, 1967.

(14) Convergence difficulties can be minimized by assuming a functional form for the flash curve between data points and then carrying out the integrations of eq 1 exactly rather than by approximate numerical methods.[4]

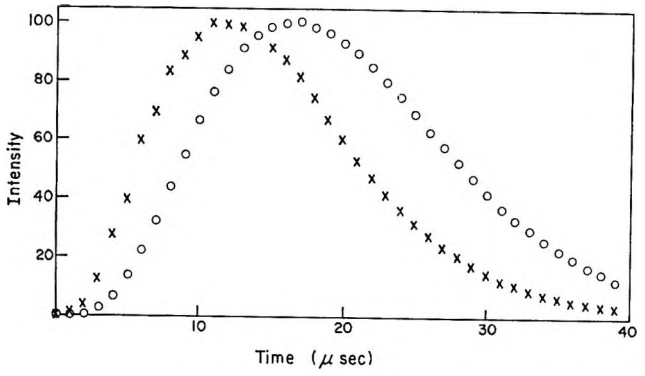

Figure 1. Observed flash and sample decay for $[Ru(bipy)_3]Cl_2$ at 77°K (from ref 4). Curve F (×) is the observed flash. Curve D (○) is the observed sample decay. The true sample lifetime is ~4.92 μsec.

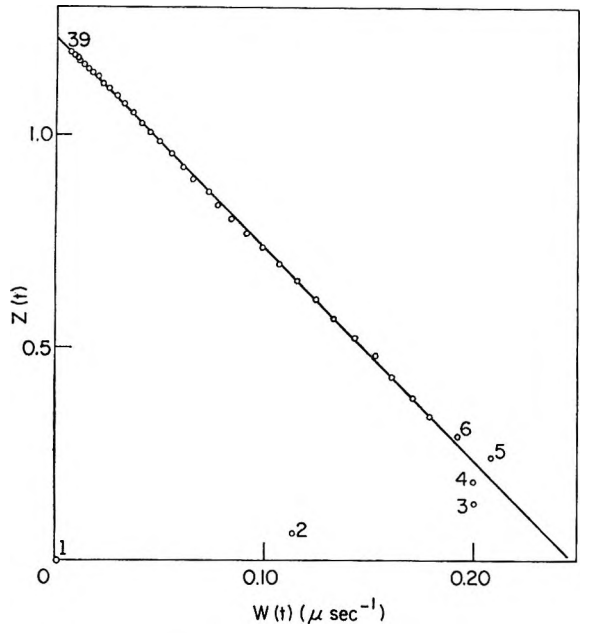

Figure 2. Phase-plane plot for the data of Figure 1. The times (in microseconds) at which the points were evaluated are given by the numbers (those between 7 and 38 being omitted).

These parameters are such, of course, as to preclude a direct evaluation of τ from a semilogarithmic plot of $D(t)$ *vs.* time. The corresponding PP plot is essentially linear, however, as shown in Figure 2. An unweighted linear least-squares fit through points 3 to 39 gives a line from whose slope τ is 5.00 μsec, with a standard deviation of ±0.06 μsec. The intercept, $K\tau$, is 1.229 ± 0.006. The first two points for very low $Z(t)$ values are clearly unreliable.

The "true" lifetime (from a short flash experiment[4]) is 4.92 ± 0.05 μsec for this system, while other evaluation methods[4] applied to the data of Figure 1 give 4.91 μsec (moments method 1), 4.79 μsec (moments method 2), and 5.15 μsec (CS method). The CS result presumably could have been made more accurate by using a larger number of trial τ values. The PP method clearly gives accuracy comparable to that of the established techniques.

Conclusion

We feel that the PP plot method is so simple and rapid that it can routinely be applied whenever there is a discernible difference between an observed sample luminescence and the excitation pulse. Then, as long as $F(t)$ and $D(t)$ are not too similar, one obtains an estimate of τ and a good indication of whether or not the decay kinetics are simple. For nearly identical $F(t)$ and $D(t)$, of course, a rough estimate of τ is the only information present.

Acknowledgment. This investigation has been supported in part by the National Science Foundation and by Contract DA-ARO-D-31-124-G1010 with the Army Research Office (Durham).

Appendices

A. Derivation of Equation 2. We first integrate both sides of eq 1 between the limits 0 and t

$$\int_0^t D(y)\mathrm{d}y = K\int_0^t e^{-y/\tau}\left[\int_0^y e^{x/\tau}F(x)\mathrm{d}x\right]\mathrm{d}y \qquad (3)$$

Integration of the right-hand side of eq 3 by parts yields

$$\int_0^t D(y)\mathrm{d}y = -K\tau e^{-t/\tau}\int_0^t e^{x/\tau}F(x)\mathrm{d}x + K\tau\int_0^t F(y)\mathrm{d}y \qquad (4)$$

Equation 4 simplifies since the first term on the right-hand side is just $-\tau D(t)$ (by eq 1), so

$$\int_0^t D(y)\mathrm{d}x = -\tau D(t) + K\tau\int_0^t F(y)\mathrm{d}y \qquad (5)$$

which rearranges to eq 2.[15-18]

B. Calculational Procedure. Our procedure for generating the data points of Figure 2 requires that the flash and emission intensities be measured (that is, read off the curves of Figure 1) at the same equal time intervals. The times are then $t_0, t_1 \ldots t_j \ldots t_n$, each with a corresponding value of $F(t)$ and $D(t)$. The data are taken so that $F(t_0) = D(t_0) = 0$.

(15) Equation 5 is a generalization of the phase-plane method used by Huen.[16,17] Huen's technique applies only when $F(t)$ is a delta function or an impulse so that $\int_0^t F(y)\mathrm{d}y$ is a constant. Under this condition eq 2 simplifies and a plot of $\int_0^t D(y)\mathrm{d}y$ *vs.* $D(t)$ gives a straight line with a slope of $-\tau$, Huen's original form.

(16) T. Huen, *Rev. Sci. Instrum.*, **40**, 1067 (1969).

(17) A. Bernalte and J. Le Page, *ibid.*, **40**, 41 (1969).

(18) Dividing both sides of eq 5 by $D(t)$ also yields a linear form; τ is obtained from an intercept rather than a slope. Since the intercept is extrapolated from the data, this alternative form does not appear to be as accurate for evaluating τ as eq 2.

The integrals are then estimated by the trapezoidal rule, which gives

$$\int_0^{t_j} D(y)\mathrm{d}y \simeq \frac{(t_1 - t_0)}{2} R_j \tag{6}$$

where

$$R_j = [D(t_j) + D(t_{j-1})] + R_{j-1}; \qquad j \geq 1 \text{ and } R_0 = 0$$

and

$$\int_0^{t_j} F(y)\mathrm{d}y \simeq \frac{(t_1 - t_0)}{2} Q_j \tag{7}$$

with

$$Q_j = [F(t_j) + F(t_{j-1})] + Q_{j-1}; \qquad j \geq 1 \text{ and } Q_0 = 0$$

Insertion of the above relationships into the definitions of $Z(t)$ and $W(t)$ then gives

$$W(t_j) = \frac{2D(t_j)}{(t_1 - t_0)Q_j} \tag{8}$$

and

$$Z(t_j) = R_j/Q_j \tag{9}$$

Our calculator was a Wang 360 machine equipped with a CP-1 card programmer. The card program for the calculation is available upon request.

The Optical Activity of Alkyl-Substituted Cyclopentanones. INDO Molecular Orbital Model[1]

by F. S. Richardson,* D. D. Shillady, and J. E. Bloor

Department of Chemistry, University of Virginia, Charlottesville, Virginia 22903 *(Received January 25, 1971)*

Publication costs assisted by the Petroleum Research Fund

An INDO molecular orbital model is used to compute the oscillator strengths, rotatory strengths, and anisotropy factors for several of the lowest-lying singlet → singlet transitions in seven chiral cyclopentanone systems. The computational model provides for limited configuration interaction and calculates all electric transition moments in the dipole velocity formalism. The structures studied were: (1) unsubstituted cyclopentanone with the five-membered carbocyclic ring twisted into a half-chair conformation (belonging to the C_2 point group); (2) three conformational isomers of (+)-3-methylcyclopentanone—two in which the ring is twisted into a C_2 geometry (the methyl group equatorial to the ring in one and the methyl group axial to the ring in the other), and one in which the ring is planar; (3) two conformational isomers of 2-methylcyclopentanone—one in which the ring is twisted and one in which it is planar; (4) one conformational isomer of 2,3-dimethylcyclopentanone in which the ring is twisted, the 2-methyl group is axial to the ring, and the 3-methyl group is equatorial. The rotatory strengths calculated for the n → π^* transition are in good agreement with the experimentally determined values for several twisted cyclopentanone systems. The computed results indicate that in the β-substituted systems the inherent chirality of the twisted carbocyclic ring is the primary source of optical activity, whereas in the α-substituted systems the substituents exert the dominant influence. The rotatory strengths calculated for higher energy singlet → singlet transitions appear not to be in good agreement with the experimental data, although in these cases the analysis is ambiguous and inconclusive.

I. Introduction

The molecule 3-methylcyclopentanone is of particular interest in theoretical studies concerned with the optical rotatory properties of carbonyl electronic transitions. This saturated, cyclic ketone was selected as the model system for the first detailed one-electron calculation of the rotatory strength associated with the carbonyl n → π^* transition[2] and was also adopted as a test system in several subsequent theoretical studies on the optical activity of carbonyl compounds.[3-5] In each of these studies, the cyclopentanone ring was assumed to be in a rigid, planar conformation and only the

(1) This work was supported in part by a National Science Foundation grant (CASS Institutional, 3760-2195) administered through the Center for Advanced Studies, University of Virginia.

(2) W. J. Kauzmann, J. Walter, and H. Eyring, *Chem. Rev.*, **26**, 339 (1940).

(3) T. Watanabe and H. Eyring, *J. Chem. Phys.*, **40**, 3411 (1964).

(4) M. V. Volkenshtein and M. P. Kruchek, *Opt. Spectrosk.*, **9**, 243 (1960).

(5) D. Caldwell and H. Eyring, *Ann. Rev. Phys. Chem.*, **15**, 281 (1964).

optical rotatory properties of the n → π* transition were treated. Furthermore, in each case the optical activity was computed on a model in which the molecule was first partitioned into separate groups (of atoms and bonds) whose electronic charge distributions were assumed to be nonoverlapping, and then interactions between the carbonyl chromophoric group and the remaining groups were treated by perturbation techniques. Our treatment of 3-methylcyclopentanone differs from the previous studies in three ways. First, we consider several conformational isomers of the molecule and the possible influence of conformational mobility and pseudorotational motion in the ring. Second, we calculate the optical rotatory properties of the five lowest lying singlet–singlet electronic transitions. Third, we construct approximate electronic wave functions by use of a semiempirical molecular orbital method (the INDO variant) in which the molecule is treated as a whole. That is, the wave functions are approximations to the total molecular electronic wave functions rather than to carbonyl group wave functions.

Two of the reasons commonly given for using 3-methylcyclopentanone as a model system are its rigidity and the presumably symmetric (C_{2v} point group) structure of the five-membered ring.[6] If these two conditions exist, then the only sources of dissymmetry in the molecule are the hydrogen atom and methyl group substituted on C-3. However, there now exists considerable experimental evidence that the ring in cyclopentanone and in alkyl-substituted cyclopentanones is not planar and does not possess C_{2v} symmetry (on the average).[7-11] Furthermore, it would appear that the ring is not rigid and that a restricted, internal pseudorotational motion occurs.[10,11] This experimental evidence corroborates the findings obtained in a conformational analysis reported for a series of substituted cyclopentanones.[12] The predictions of the one-electron theory of optical rotation are in error with respect to both the sign and the magnitude of the n → π* rotatory strength in 3-methylcyclopentanone with a planar ring. The calculated rotatory strength is several orders of magnitude too small[4] and the predicted sign, based on the octant rule,[13] is wrong. In applying the octant rule to the planar ring system, only the influences of the C-3 substituent atoms are considered. By considering nonplanar ring conformations, Ouannes and Jacques[12] predict rotations of the correct sign for a series of substituted cyclopentanones.

The temperature-dependence CD studies made by Djerassi and coworkers[14,15] on cyclopentanone derivatives emphasize the possible significance of conformational mobility in these compounds. They observed that optically active cyclopentanones show a marked augmentation in rotatory strength upon lowering of the temperature, possibly indicative of a conformational equilibrium at room temperature. For (+)-3-methylcyclopentanone the reduced rotatory strengths were found to be: $R(25°) = +6.02$, $R(-192°) = +9.88$.

According to the one-electron theory, the magnitude of the n → π* rotatory strength should exhibit an approximate R^{-4} dependence on the radial distance R between the carbonyl chromophore and the perturber group (ring substituent). Furthermore, the number of substituents which can exert a direct vicinal effect should significantly influence the magnitude of the rotatory strength. The experimental ORD[12] and CD[15] data for various substituted cyclopentanones do show that the rotatory strength depends upon the number and the size (*i.e.*, number of atoms) of the substituent groups and upon the distances of the substituent groups from the carbonyl chromophore. However, the observed relationship between the experimental rotatory strength and the number of substituents, substituent size, and substituent positions cannot be directly accounted for on the basis of the one-electron model if a planar ring is assumed. Furthermore, the CD data reported in ref 15 exhibit a significant temperature dependence. It appears that the substituents exert both a direct "vicinal-like" influence on the carbonyl chromophore and an indirect influence which depends upon the substituent group's ability to give a permanent chiral distortion to the ring.

We included the planar and twisted conformations of both 2-methylcyclopentanone and 3-methylcyclopentanone in our study in order to assess the possible influence of substituent proximity to the carbonyl group on the rotatory strength. The rotatory strength of 2,3-dimethylcyclopentanone was also computed in order to estimate the extent to which substituent contributions can be considered to be additive. The rotatory strength of twisted, unsubstituted cyclopentanone was also computed.

There are two main reasons why previous studies on the optical activity of cyclopentanone systems (and of most other carbonyl compounds) have been restricted to the n → π* carbonyl transition. First, this is the only carbonyl electronic transition which is observed in

(6) D. Urry, *Ann. Rev. Phys. Chem.*, **19**, 477 (1968).

(7) G. Erlandsson, *J. Chem. Phys.*, **22**, 563 (1964).

(8) C. G. LeFevre, R. J. W. LeFevre, and B. Rao, *J. Chem. Soc.*, 2340 (1959).

(9) C. G. LeFevre and R. J. W. LeFevre, *ibid.*, 3549 (1956); 3458 (1957).

(10) H. Kim and W. D. Gwinn, *J. Chem. Phys.*, **51**, 1815 (1969).

(11) W. D. Chandler and L. Goodman, *J. Mol. Spectrosc.*, **35**, 232 (1970).

(12) C. Ouannes and J. Jacques, *Bull. Soc. Chim. Fr.*, 3611 (1965).

(13) W. Moffitt, R. Woodward, A. Moscowitz, W. Klyne, and C. Djerassi, *J. Amer. Chem. Soc.*, **83**, 4013 (1961).

(14) K. Wellman, E. Bunnenberg, and C. Djerassi, *ibid.*, **85**, 1870 (1963).

(15) C. Djerassi, R. Records, C. Ouannes, and J. Jacques, *Bull. Soc. Chim. Fr.*, 2378 (1966).

a spectral region accessible to commercially available ORD and CD instrumentation. Second, this is the only carbonyl transition which has been fully characterized with respect to its absorption spectrum and for which there exists a reliable (if not accurate and complete) quantum mechanical description. Recent advances in CD instrumentation, however, have made it possible to extend experimental observation down to ≈165 nm on vapor-phase samples,[16,17] and both vapor-phase and polarized single-crystal absorption spectra have recently been made available for identifying and characterizing the higher-energy transitions in carbonyl compounds.[18,19]

Simple aldehydes and ketones exhibit four absorption bands in the 150–300-nm spectral region: a very intense band at 150 nm, two moderately intense bands at 175 and 195 nm, and a weak band at around 300 nm. It is generally agreed that the 150-nm band arises from the $\pi \rightarrow \pi^*$ transition and that the 300-nm band is due to the $n \rightarrow \pi^*$ transition. The correct assignments for the 175 and 190-nm bands, however, are less certain. El Sayed and Udvarhazi[18] examined the gas-phase spectra of cyclobutanone, cyclopentanone, and cyclohexanone in the 167–270-nm spectral region in an attempt to determine the correct transition assignments for the 195 and 175-nm bands. They concluded that the band at 195 nm is probably due to the $n \rightarrow \sigma^*_{c-o}$ carbonyl transition or to a $\sigma_{c-c} \rightarrow \pi^*$ transition, and that the 175-nm band can be assigned to either an $n \rightarrow \sigma^*_{c-c}$ transition or to a $\sigma_{c-o} \rightarrow \pi^*$ transition.

There have been four previously reported studies in which semiempirical molecular orbital models were used to calculate the rotatory strengths of carbonyl compounds. Pao and Santry[20] calculated the $n \rightarrow \pi^*$ rotatory strengths for a series of rigid, substituted cyclohexanone derivatives on a CNDO/2 molecular orbital model, and Gould and Hoffmann[21] calculated the $n \rightarrow \pi^*$ rotatory strengths for a similar series of compounds using an extended-Hückel molecular orbital model. In an attempt to correlate the changes in rotatory strength of the $n \rightarrow \pi^*$ band of 2-substituted cyclohexanones with familiar properties of the substituents, Lynden-Bell and Saunders[22] employed an extended-Hückel model to calculate rotatory strengths. Very recently, Hug and Wagniere[23] reported molecular orbital calculations (using both extended-Hückel and CNDO methods) of the rotatory strengths associated with the two lowest energy transitions in skewed diketones.

Two additional studies have been reported in which semiempirical molecular orbital methods were used to calculate the electronic rotatory strengths of transitions in noncarbonyl chromophores. Linderberg and Michl[24] applied CNDO techniques to the twisted H_2S_2 system, and Yaris, Moscowitz, and Berry[25] treated twisted olefin chromophores in a similar way. Although these semiempirical molecular orbital models are not expected to yield highly accurate representations of molecular excited states, they will faithfully represent the nodal structure of the molecular electronic states and should provide valuable insight into the structural origins of the molecular optical rotatory properties. They should be especially useful for assessing the failures, successes, and limits of applicability of the simpler one-electron theory.

In the present study we use the INDO[26] variant of semiempirical molecular orbital theory. This method is not expected to be significantly more accurate than CNDO methods (except with respect to singlet–triplet splittings), but our use of limited configuration interaction should provide some improvement in the excited state descriptions (compared to those of Pao and Santry,[20] for example). Our computed transition energies are consistently higher than the experimental values. This fault lies mainly in the standard parameters used. No attempt was made to find new parameters which would improve the transition energies, since there would be little assurance that the new wave functions would provide a better basis for calculating dipole strengths or rotatory strengths.

II. Methods of Calculation

A. Approximate Molecular Orbital Method (INDO-CI). The SCF computations carried out in this study were performed on a Burroughs B-5500 computer using a modified form of the ALGOL program CNDO2X written by Dr. B. R. Gilson.[27] Essentially the program used the CNDO/2 approximations set forth by Pople, *et al.*,[28,29] for closed-shell molecules and provided several options including allowance for nonstandard CNDO/2 parameters and configuration interaction between singly excited determinantal wave functions for both singlets and triplets. For the present study, the program was modified to include the one-center exchange integrals developed by Pople, *et al.*,[26] in their

(16) S. Feinleib and F. A. Bovey, *Chem. Commun.*, 978 (1968).
(17) O. Schnepp, E. Pearson, and E. Sharman, *ibid.*, 545 (1970).
(18) M. A. El Sayed and A. Udvarhazi, *J. Chem. Phys.*, **42**, 3335 (1965).
(19) W. C. Johnson, Jr., and W. T. Simpson, *ibid.*, **48**, 2168 (1968).
(20) V. Pao and D. P. Santry, *J. Amer. Chem. Soc.*, **88**, 4157 (1966).
(21) R. Gould and R. Hoffmann, *ibid.*, **92**, 1813 (1970).
(22) R. M. Lynden-Bell and V. R. Saunders, *J. Chem. Soc. A*, 2061 (1967).
(23) W. Hug and G. Wagniere, *Theor. Chim. Acta*, **18**, 57 (1970).
(24) J. Linderberg and J. Michl, *J. Amer. Chem. Soc.*, **92**, 2619 (1970).
(25) M. Yaris, A. Moscowitz, and S. Berry, *J. Chem. Phys.*, **49**, 3150 (1968).
(26) J. A. Pople, D. L. Beveridge, and P. Dobosh, *ibid.*, **47**, 2026 (1967).
(27) B. R. Gilson, Ph.D. Thesis, University of Virginia, 1969.
(28) J. A. Pople, D. P. Santry, and G. A. Segal, *J. Chem. Phys.*, **43**, S129, S136 (1965).
(29) J. A. Pople and G. A. Segal, *ibid.*, **44**, 3289 (1966).

INDO calculations. The exchange integrals were included both in the SCF interative calculations and in the configuration interaction (CI) matrix. The program was also modified for punch card output in the proper format for later use in another program (ANGMOMT)[30] for the computation of either natural or magnetically-induced rotatory strengths. The modified program was tested by performing a calculation on the electronic structure of formaldehyde and then comparing these results with those obtained from a standard INDO calculation on the same molecule. The agreement between these two calculations was excellent. We will refer to the modified program henceforth as INDO-CI.

The methods used in INDO-CI represent straightforward application of well known concepts so that we will only outline them briefly here. The ground state of the molecule is approximated by assuming perfect screening for the core electrons and by representing the N valence electrons as a single determinantal wave function formed from linear combinations of a minimum basis set of STO's $\{\chi_i\}$.

$$\Psi_0 = \left(\frac{1}{N!}\right)^{1/2} \begin{vmatrix} \psi_1(1)\alpha(1) & \psi_1(1)\beta(1) & \cdots & \psi_{N/2}(1)\beta(1) \\ \psi_1(2)\alpha(2) & \psi_1(2)\beta(2) & \cdots & \vdots \\ \vdots & \vdots & & \psi_{N/2}(N)\beta(N) \end{vmatrix}$$

$$= |\psi_1\bar{\psi}_1 \cdots \psi_{N/2}\bar{\psi}_{N/2}| \quad (1)$$

The functions $\{\psi_i\}$ are molecular orbitals determined iteratively by minimizing the electronic energy of the N valence electrons, subject to the SCF contraints. We have

$$\psi_i = \sum_\mu C_{i\mu}\chi_\mu \quad (2)$$

where $C_{i\mu}$ is the coefficient of the μth atomic orbital in the ith molecular orbital. For the various atomic orbitals, the standard parameters and exponents used in the INDO approximation of Pople, *et al.*,[26] were adopted.

For the excited singlet and triplet states, it was assumed that an adequate description can be obtained by using a small number of singly excited states formed by the replacement of one occupied orbital in the ground-state determinant with a virtual orbital.[31,32]

$${}^1\Psi_p = \sum_\nu C_{p\nu}[i(\nu), j(\nu)](1/2)^{1/2} \times \{|\psi_1\bar{\psi}_1\psi_2\bar{\psi}_2 \ldots \psi_i\bar{\psi}_j \ldots \bar{\psi}_{N/2}| - |\psi_1\bar{\psi}_1\psi_2\bar{\psi}_2 \ldots \psi_j\bar{\psi}_i \ldots \bar{\psi}_{N/2}|\} \quad (3)$$

$${}^3\Psi_q = \sum_\nu C_{q\nu}[i(\nu), j(\nu)](1/2)^{1/2} \times \{|\psi_1\bar{\psi}_1\psi_2\bar{\psi}_2 \ldots \psi_i\bar{\psi}_j \ldots \bar{\psi}_{N/2}| + |\psi_1\bar{\psi}_1\psi_2\bar{\psi}_2 \ldots \psi_j\bar{\psi}_i \ldots \bar{\psi}_{N/2}|\} \quad (4)$$

An interaction matrix is then set up for the singlet and the triplet cases, once the set of specifiers $\{i(\nu),j(\nu)\}$ is defined, by using eq 5 and 6

$${}^1M_{rs} = F_{ss} - F_{rr} + J_{rs} + K_{rs} \quad (5)$$

$${}^3M_{rs} = F_{ss} - F_{rr} + J_{rs} - K_{rs} \quad (6)$$

The respective matrices are then diagonalized to determine the coefficients $C_{p\nu}[i(\nu),j(\nu)]$ and $C_{q\nu}[i(\nu),j(\nu)]$ in eq 3 and 4.

The molecular coulomb and exchange integrals are represented by J and K, respectively, and the F_{ss} and F_{rr} are the eigenvalues of the ground-state semiempirical Fock matrix. The eigenvalues of ${}^1\mathbf{M}$ and ${}^3\mathbf{M}$ are excited-state energies above the ground-state energy, which is arbitrarily taken to be the zero reference level. Thus a limited configuration interaction calculation was carried out in which the correct $(1/r_{ij})$ interaction operator was used along with semiempirical values of J and K. This procedure should lead to somewhat better descriptions of the electronic excited states (at least with respect to energy) than can be achieved by direct use of the virtual orbitals alone as was done by Pao and Santry.[20] Furthermore, the use of INDO K values leads to finite singlet–triplet splittings, thus mimicking reality more closely than the CNDO/2 CI procedure used by Del Benet and Jaffe[33] in which all exchange integrals are neglected.

B. Oscillator and Rotatory Strengths. The optical activity associated with a single electronic transition, say $0 \rightarrow k$, in a molecule can be conveniently expressed in terms of the reduced rotatory strength for the transition. The reduced rotatory strength is defined by[34]

$$[R_{0k}] = (100/\beta D)\mathrm{Im}[\langle\Psi_0|\vec{\mu}|\Psi_k\rangle\cdot\langle\Psi_k|\vec{\mathbf{m}}|\Psi_0\rangle] = (100/\beta D)R_{0k} \approx 1.08 \times 10^{40}R_{0k} \quad (7)$$

where β is the Bohr magneton, D is the Debye unit, $\vec{\mu}$ is the magnetic dipole operator, and $\vec{\mathbf{m}}$ is the electric dipole operator. The wave functions Ψ_0 and Ψ_k are, in general, linear combinations of determinants after configuration interaction, but we have restricted the ground state Ψ_0 to the INDO determinant and the excited states Ψ_k to linear combinations of singly excited (with respect to the INDO ground-state determinant) determinants only. The operators in eq 7 are defined by

$$\mathrm{Im}(a + ib) = b \quad (8)$$

$$\vec{\mathbf{m}} = e\sum \vec{r} \quad (9)$$

$$\vec{\mu} = \frac{e\hbar}{2mci}\sum_j (\vec{r}_j \times \vec{\nabla}_j) = \frac{e}{2mc}\sum_j \vec{L}_j \quad (10)$$

where j labels electrons.

Usually the electric transition moment is expressed

(30) D. D. Shillady, Ph.D. Thesis, University of Virginia, 1969.

(31) J. A. Pople, *Proc. Phys. Soc. London, Sect. A*, **68**, 81 (1955).

(32) R. Pariser, *J. Chem. Phys.*, **24**, 250 (1956).

(33) J. Del Benet and H. Jaffe, *ibid.*, **48**, 1807, 4050 (1968); **49**, 1221 (1968); **50**, 1126 (1969).

(34) A. Moscowitz, *Advan. Chem. Phys.*, **4**, 67 (1962).

in terms of the dipole length formula, but Moscowitz[35] has stressed the fact that nonsymmetry-adapted wave functions lead to origin dependent results unless the dipole velocity formula is used. Ehrenson and Phillipson[36] have also shown that the dipole velocity formula emphasizes the portion of the molecular orbitals which have been optimized by energy dependence using the variational theorem, in contrast to the dipole length formula which depends more on the outer tails of the wave functions which are usually given poorly (especially in minimum basis sets). A third reason for preferring the dipole velocity form given in eq 11 is that

$$\langle\Psi_i|\vec{r}|\Psi_j\rangle = \left(\frac{\hbar^2}{m}\right)\langle\Psi_i|\vec{\nabla}|\Psi_j\rangle/(E_j - E_i) \qquad (11)$$

the usual derivation of electric transition probabilities starts out by assuming a perturbation involving $\vec{\nabla}$ and then at the end invokes the restriction given in eq 12

$$\left(\frac{\hbar}{i}\right)\vec{\nabla} = \mathbf{H}\vec{r} - \vec{r}\mathbf{H} = [\mathbf{H}, \vec{r}] \qquad (12)$$

where $\mathbf{H}$ is the total Hamiltonian of the system. Since eq 12 is approximate even for *ab initio* minimum basis set calculations, we favor using the dipole velocity directly, especially for semiempirical wave functions.

An additional benefit to be gained by using the dipole velocity operator is that the two-center magnetic moment integrals can be reduced to combinations of overlap and dipole velocity integrals. Consider L_x^0 in cartesian coordinates with respect to (0, 0, 0). Then consider a second point (x^b, y^b, z^b). The matrix element of angular momentum (L_x) between an atomic orbital $|a>$ at (0, 0, 0) and $|b>$ at (x^b, y^b, z^b) is given by eq 13. Now define new coordinates as given in

$$\langle a|L_x^0|b\rangle = \left\langle a\left|\left(\frac{\hbar}{i}\right)\left[y^0\left(\frac{\partial}{\partial z^0}\right) - z^0\left(\frac{\partial}{\partial y^0}\right)\right]\right|b\right\rangle \qquad (13)$$

eq 14. Expanding, we obtain eq 15 where the primed

$$q' = q^0 - q^b; \quad (\partial/\partial q^0) = (\partial/\partial q') \quad (q = x, y, z) \qquad (14)$$

coordinates are with respect to (x^b, y^b, z^b). Equations 16 and 17 are similarly obtained.

$$\begin{aligned}\langle a|L_x^0|b\rangle &= \left\langle a\left|\left(\frac{\hbar}{i}\right)\left[(y' + y^b)\left(\frac{\partial}{\partial z'}\right) - (z' + z^b)\left(\frac{\partial}{\partial y'}\right)\right]\right|b\right\rangle \\ &= \left\langle a\left|\left(\frac{\hbar}{i}\right)\left[y'\left(\frac{\partial}{\partial z'}\right) - z'\left(\frac{\partial}{\partial y'}\right)\right]\right|b\right\rangle + y^b\left(\frac{\hbar}{i}\right)\left\langle a\left|\frac{\partial}{\partial z'}\right|b\right\rangle - z^b\left(\frac{\hbar}{i}\right)\left\langle a\left|\frac{\partial}{\partial y'}\right|b\right\rangle \\ &= \langle a|L_x'|b\rangle + y^b\left(\frac{\hbar}{i}\right)\left\langle a\left|\frac{\partial}{\partial z'}\right|b\right\rangle - z^b\left(\frac{\hbar}{i}\right)\left\langle a\left|\frac{\partial}{\partial y'}\right|b\right\rangle \qquad (15)\end{aligned}$$

$$\langle a|L_y^0|b\rangle = \langle a|L_y'|b\rangle + z^b\left(\frac{\hbar}{i}\right)\left\langle a\left|\frac{\partial}{\partial x'}\right|b\right\rangle - x^b\left(\frac{\hbar}{i}\right)\left\langle a\left|\frac{\partial}{\partial z'}\right|b\right\rangle \qquad (16)$$

$$\langle a|L_z^0|b\rangle = \langle a|L_z'|b\rangle + x^b\left(\frac{\hbar}{i}\right)\left\langle a\left|\frac{\partial}{\partial y'}\right|b\right\rangle - y^b\left(\frac{\hbar}{i}\right)\left\langle a\left|\frac{\partial}{\partial x'}\right|b\right\rangle \qquad (17)$$

Note that since L_q' are centered on (x^b, y^b, z^b), their effect on any spherical harmonic function such as $|b\rangle$ in an STO basis is reduced to products of ladder operator constants,[37] $\hbar$, and overlap integrals which we calculate using the algorithm of Lofthus.[38]

The dipole velocity algorithm of Fraga[39] was programmed for the B-5500 after some enlightening correspondence with Professor Fraga, and the values were checked against Shull's[40] values for the H_2 molecules. The Lofthus overlap has been checked previously in this laboratory and has been used in the past for up to and including 6p STOs.[30] Thus we used the formulas of eq 15–17 to generate the antisymmetric angular momentum matrices in a real STO basis.

The resulting program (ANGMOMT) will accept atomic orbital basis sets (STO), molecular orbital coefficients, and CI coefficients from either *ab initio* or semiempirical source programs provided all two-center terms are included in the overlap. We deorthogonalized the INDO molecular orbitals as described by Pullman,[41] but we used the CI coefficients unchanged since deorthogonalization is a unitary transformation and applying it to a linear combination of determinants would leave each determinant unchanged in value; hence the coefficients would also be unchanged. This is rigorously true only if the INDO Fock matrix is related to the corresponding *ab initio* calculation in the same basis by a unitary transformation. However, some recent work has shown that generally deorthogonalization tends to improve the charge description in CNDO2 and we have assumed that the same trend holds in our INDO study. In any event, this seems to be the most acceptable way of introducing two-center bond contributions into the rotatory strength calculations, rather than delete them as did Pao and Santry.[20]

Our program also provides for a limited treatment of spin–orbit coupling and for calculating singlet–triplet transition probabilities. To first order in the spin–

(35) A. Moscowitz, "Modern Quantum Chemistry," Vol. 3, O. Sinanoglu, Ed., Academic Press, New York, N. Y., 1965, p 31.

(36) S. Ehrenson and P. E. Phillipson, *J. Chem. Phys.*, **34**, 1224 (1961).

(37) R. H. Dicke and J. P. Witke, "Introduction to Quantum Mechanics," Addison-Wesley, Reading, Mass., 1960, Chapter 12.

(38) A. Lofthus, *Mol. Phys.*, **5**, 105 (1962).

(39) S. Fraga, *Can. J. Chem.*, **42**, 2509 (1964).

(40) H. Shull, *J. Chem. Phys.*, **20**, 18 (1952).

(41) C. G. Prettre and A. Pullman, *Theor. Chim. Acta*, **11**, 159 (1968).

orbit coupling operator H_{so}, the singlet–triplet transition integrals can be expressed as[42]

$$\langle {}^3\Psi_{n,\tau}|\hat{O}|{}^1\Psi_k\rangle = \langle {}^3\phi_{n,\tau}|\hat{O}|{}^1\phi_k\rangle + \sum_l \frac{\langle {}^1\phi_l|H_{so}|{}^3\phi_{n,\tau}\rangle^*}{({}^3E_n - {}^1E_l)}\cdot\langle {}^1\phi_l|\hat{O}|{}^1\phi_k\rangle + \sum_m \sum_\tau \frac{\langle {}^3\phi_{m,\tau}|H_{so}|{}^1\phi_k\rangle}{({}^1E_k - {}^3E_m)}\langle {}^3\phi_{n,\tau}|\hat{O}|{}^3\phi_{m,\tau}\rangle \quad (18)$$

where τ denotes the spin components of the triplet state ($\tau = 0, \pm 1$), the functions $|\phi\rangle$ are the unperturbed CI states, and $\hat{O}$ is either the electric dipole or magnetic dipole moment operator. We approximate the spin–orbit perturbation operator as

$$H_{so} = \sum_K^{\text{atoms}} \zeta_K \vec{L}\cdot\vec{S} \quad (19)$$

where $\vec{L}$ is the orbital angular momentum operator, $\vec{S}$ is the total spin angular momentum operator, and ζ_K is an empirically determined spin–orbit coupling constant for the Kth atom. The justification for using this very approximate form of H_{so} will not be detailed here. Ginsberg and Goodman[42] have shown (at least for carbonyl electronic states) that application of the central field approximation and the neglect of two-electron spin–orbit couplings do not lead to significant errors in the calculation of spin–orbit interactions. Furthermore, all two-center spin–orbit matrix elements have been neglected in the present study Because of the strong inverse dependence of H_{so} on r (it goes as r^{-3}, where r is the electron radial coordinate), these two-center terms are expected to be of negligible magnitude. The values of ζ_K used in this study for oxygen and carbon were[43] $\zeta_o = 152\ \text{cm}^{-1}$; $\zeta_c = 28\ \text{cm}^{-1}$. Test calculations on formaldehyde indicated that the INDO-CI energies were reasonable with respect to magnitude and splittings, and that the computed n $\rightarrow$ $^3\pi^*$ transition probability was of the approximately correct order of magnitude[44] (computed oscillator strength was 10^{-7}).

The matrix elements of the electric and magnetic dipole operators between determinants were computed from an extension of formulas used by Koutecky, *et al.*[45] They are expressed in eq 20 for an arbitrary one-electron operator $\hat{O}$ between singly excited determinants. The symbols

$$\langle \Psi_{ij}|\hat{O}|\Psi_{kl}\rangle = \langle j|\hat{O}|l\rangle\delta_{ik}(1-\delta_{ij})(1-\delta_{kl}) - \langle i|\hat{O}|k\rangle\delta_{jl}(1-\delta_{kl})(1-\delta_{ij}) + \left[2\sum_p^{\text{OCC}}\langle p|\hat{O}|p\rangle\right]\delta_{ik}\delta_{jl} + (2)^{1/2}\langle k|\hat{O}|l\rangle\delta_{ij}(1-\delta_{kl}) + (2)^{1/2}\langle i|\hat{O}|j\rangle\delta_{kl}(1-\delta_{ij}) \quad (20)$$

where i, j, k, l, and p all refer to molecular orbitals using eq 21, where

$$\langle i|\hat{O}|j| = \sum_\mu^{\text{AO}}\sum_\nu^{\text{AO}} C_{i\mu}C_{j\nu}\langle\chi_\mu|\hat{O}|\chi_\nu\rangle \quad (21)$$

$|\chi_\mu\rangle$ and $|\chi_\nu\rangle$ are atomic orbitals in the basis set. The formula is more general than is actually needed here since the angular momentum and dipole velocity operators are both antisymmetric, which means that all diagonal $\langle p|O|p\rangle$ matrix elements are zero. These zero terms were left in the program, however, so that we may use the same program to compute rotatory strengths using the dipole length formula. In that case, the diagonal elements would be quite important.[46] By convention the closed shell ground state is treated as $|\Psi_{N/2}{}^{N/2}\rangle$ for N electrons.

In the calculation of the singlet–triplet transition moments the procedure recommended by Hameka and Goodman[46] was followed in that eq 18 was used directly for the perturbed dipole velocity matrix elements with eq 22 being used for each of the matrix elements involving zero-order eigenfunctions of the unperturbed Hamiltonian. In this way, the error due to the use of

$$\langle \Psi_p|\vec{r}|\Psi_q\rangle = \frac{(557.8123047)}{[E_p(\text{kK}) - E_q(\text{kK})]}\langle \Psi_p|\vec{\nabla}|\Psi_q\rangle \quad (22)$$

an incomplete set of states is much less than if the dipole length diagonal elements were included in the perturbation. In other words, since the dipole velocity has zero diagonal elements, widely differing dipole moments of excited states are not encountered. Of course, in the limit of completeness of the set $\{|\Psi_p\rangle\}$, the operators are rigorously interchangeable.

The constant in eq 22 reflects the fact that all energies were in kilokaysers (kK), the dipole velocity and dipole length were in atomic units, and in the discussion to follow the angular momentum integrals are in units of $\hbar$. Thus we obtain the reduced rotatory strength in eq 23 where the units are that of a pure number and eq 22 has been used.

$$[R_{pq}] = (166.5631616)\times \sum_i^{d_p}\sum_j^{d_p}\sum_k^{d_q}\sum_l^{d_q}[\langle i|\vec{r}|l\rangle\cdot\langle j|\vec{L}|k\rangle] \quad (23)$$

Note that since states p and/or q may be triplets, we have summed over the respective degeneracies of the unperturbed states d_p and d_q. It is debatable whether the summation should be twofold or fourfold. We have used the fourfold summation because neither operator is diagonal in the molecular orbital basis. However, since this is the first discussion of rotatory strengths between degenerate states of which we are aware, our convention may be the subject of further

(42) J. L. Ginsberg and L. Goodman, *Mol. Phys.*, **15**, 441 (1968).
(43) D. G. Carroll, L. Vanquickenborne, and S. P. McGlynn, *J. Chem. Phys.*, **45**, 2777 (1966).
(44) J. W. Sidman, *ibid.*, **29**, 644 (1958).
(45) J. Koutecky, P. Hockman, and J. Michl, *ibid.*, **40**, 2439 (1964).
(46) H. F. Hameka and L. Goodman, *ibid.*, **42**, 2305 (1965).

consideration. Equation 23 obviously reduces to the conventional formula given in eq 7 in the singlet–singlet case, so that there is no controversy when $d_p = d_q = 1$.

C. Anisotropy Factor. Another spectroscopic quantity of interest which was included in our computational procedure is the anisotropy factor

$$g_{pq} = 4R_{pq}/D_{pq} \tag{24}$$

where R_{pq} is the rotatory strength and D_{pq} is the dipole strength associated with the $p \rightarrow q$ transition. Condon[47] first defined the factor as proportional to the ratio of the integrated CD and absorption intensities. Moffitt and Moscowitz[48] and, more recently, Robinson and Weigang[49] have given detailed consideration to the relationships between g, frequency distributions in CD and absorption bands, and vibronic coupling. In earlier studies of the g factor, Kuhn[50] proposed that g should remain constant throughout the band of a single electronic transition and that any variation in g in a particular spectral region could be used as evidence for multiple, overlapping electronic transitions. In making this proposal, Kuhn had to assume that the anisotropy factors for all vibronic components of a particular electronic transition are the same. Moffitt and Moscowitz's results demonstrate that in general this is not the case, and Weigang's[51] studies on vibronic effects in the CD spectra of electric-dipole forbidden transitions suggest that Kuhn's approach can lead to erroneous conclusions.

Experimentally the g factor is determined by integrating over the entire CD band and the entire absorption band. We have

$$g_{pq} = 4R_{pq}/D_{pq} = 4 \times 0.24 \times 10^{-38} \times \int \frac{\Delta\epsilon(\lambda)}{\lambda} d\lambda / 0.96 \times 10^{-38} \int \frac{\epsilon(\lambda)}{\lambda} d\lambda \tag{25}$$

where $\Delta\epsilon(\lambda) = \epsilon_L(\lambda) - \epsilon_R(\lambda)$, $\epsilon(\lambda) = [\epsilon_L(\lambda) + \epsilon_R(\lambda)]/2$, $\epsilon_L(\lambda)$ and $\epsilon_R(\lambda)$ are the decadic extinction coefficients for the left and right circularly polarized light, and the constants are expressed in cgs units. The experimental g factor includes, therefore, all vibronic contributions to both $\Delta\epsilon$ and ϵ. Vibronic effects are completely neglected in our INDO-CI computational model, so that the computed g factors include only the nonvibronic contributions to R_{pq} and D_{pq}.

We define dipole strength by

$$D_{pq} = e^2\langle p|\vec{r}|q\rangle \cdot \langle q|\vec{r}|p\rangle = \left(\frac{\hbar^4 e^2}{m^2}\right)\langle p|\vec{\nabla}|q\rangle \cdot \langle q|\vec{\nabla}|p\rangle/(E_p - E_q)^2 \tag{26}$$

III. Conformations of Cyclopentanone and Alkyl-Substituted Cyclopentanones

As was discussed in the Introduction 3-methylcyclopentanone has been a favorite model system for testing theories of molecular optical activity. According to Urry,[6] the reason for this choice is that in this molecule all the structural features desirable in a model system are present. The model system should be small, planar, rigid, and cyclic with a single asymmetric center. From the recent microwave results of Kim and Gwinn[10] and the polarized photoexcitation spectra reported by Chandler and Goodman,[11] it is rather certain that the most stable ground-state conformation of cyclopentanone is one in which the ring is twisted into a half-chair form with only C_2 symmetry. In cyclopentanone, two such conformations exist and they are isoenergetic. However, in 3-methylcyclopentanone these conformations are not equivalent and are probably not isoenergetic. In this case, even when the barrier between the two ring conformational isomers is sufficiently low that pseudorotational ring motion occurs at room temperature, it is not correct to say that the ring is "planar" on-the-average.

One of the objectives of the present study was to determine how sensitive the optical rotatory properties are to ring puckering and to ascertain the conformer or conformer-mixture responsible for the observed CD at various temperatures. It was also of some interest to find out how ring chirality *vs.* direct, substituent vicinal effects influence the optical rotatory properties of the higher excited states of the carbonyl chromophore (*i.e.*, excited states other than $n\pi^*$). Only the $n \rightarrow \pi^*$ transition had been treated previously.

INDO-CI ANGMOMT calculations were carried out on seven different molecular systems. These systems were: (1) (L)-cyclopentanone (I); unsubstituted cyclopentanone with a twisted ring ($L \equiv$ left-handed twist in ring), Figure 1a; (2) 3-methylcyclopentanone (II), planar ring, Figure 1b; (3) 3(e)-methyl-(*L*)-cyclopentanone (III), twisted ring with equatorial methyl substituent, Figure 1c; (4) 3(a)-methyl-(*R*)-cyclopentanone (IV), twisted ring ($R \equiv$ right-handed twist in ring) with axial methyl substituent, Figure 1d; (5) 2-methylcyclopentanone (V), planar ring, Figure 1e; (6) 2(a)-methyl-(*L*)-cyclopentanone (VI), twisted ring with axial methyl substituent, Figure 1; (7) 2,3(a,e)-dimethyl-(*L*)-cyclopentanone (VII), twisted ring with axial methyl substituent at position 2 and equatorial methyl substituent at position 3, Figure 1g. We used the data of Kim and Gwinn[10] directly for the structure of cyclopentanone. The dihedral twist angle was reported to be 23.6°. For each of the substituted derivatives of cyclopentanone, the C(methyl)–C(ring) bond was assumed to be 1.54 Å and tetrahedral HCH angles were used with a C–H bond length of 1.091 Å. The hydrogen atoms on the methyl substituent were taken to be staggered with respect to

(47) E. U. Condon, *Rev. Mod. Phys.*, **9**, 432 (1937).
(48) W. Moffitt and A. Moscowitz, *J. Chem. Phys.*, **30**, 648 (1959).
(49) G. Robinson and O. Weigang, *J. Amer. Chem. Soc.*, **91**, 3709 (1969).
(50) W. Kuhn, *Annu. Rev. Phys. Chem.*, **9**, 417 (1958).
(51) O. E. Weigang, *J. Chem. Phys.*, **43**, 3609 (1965).

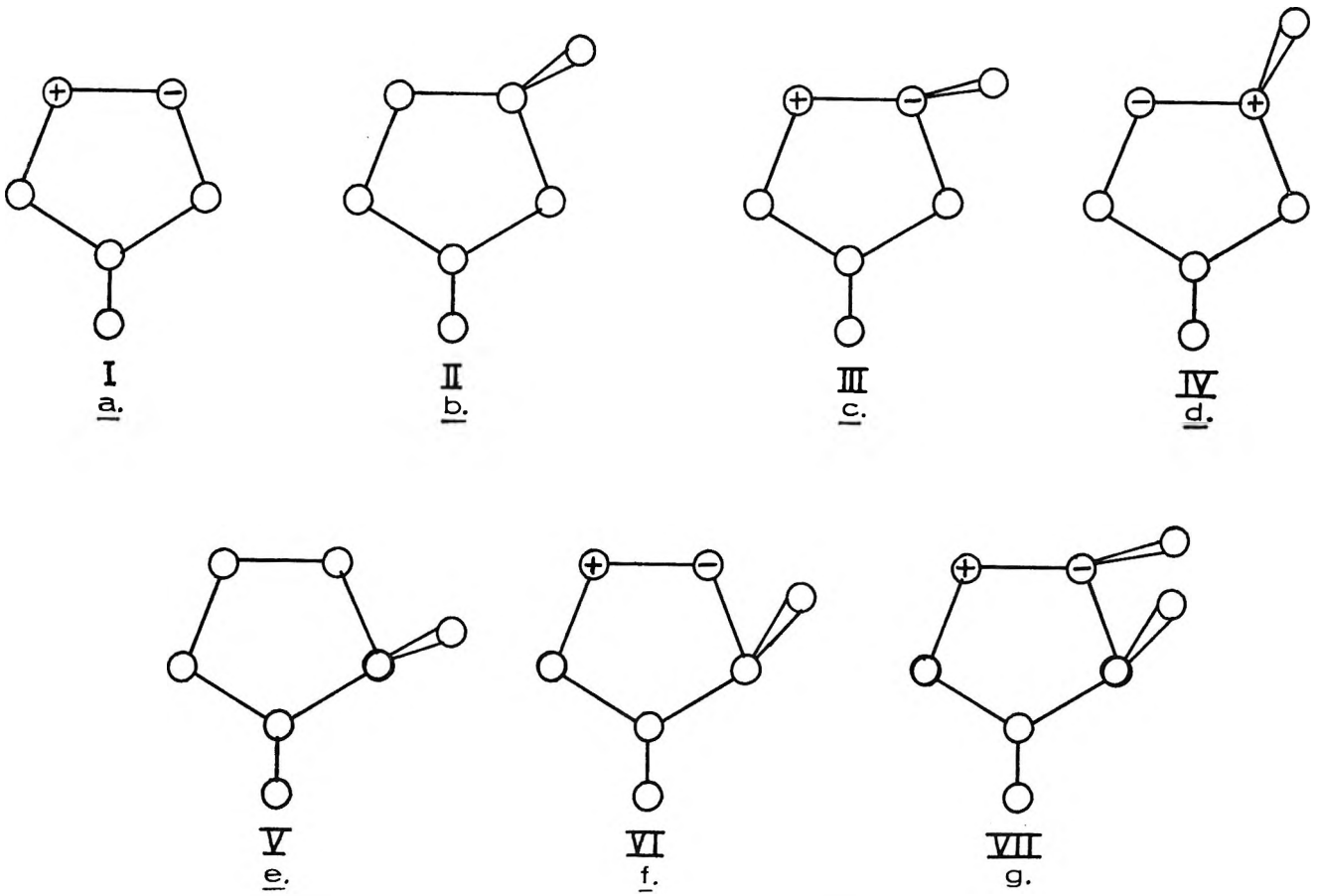

Figure 1. Cyclopentanone (I), 3-methylcyclopentanone (II, III, IV), 2-methylcyclopentanone (V, VI), and 2,3-dimethylcyclopentanone (VII). Structures: ⊕ = ring carbon atom above plane of figure; ⊖ = ring carbon atom below plane of figure.

the other hydrogen atom attached to the same ring carbon atom. For the axial and equatorial isomers of 3-methylcyclopentanone, the cyclopentanone skeleton parameters were used and the angles and distances were checked and found to be within the tolerances given by Kim and Gwinn. For the planar case we could not use all of the same parameters, so we arbitrarily kept the constraint of $r(C_2-C_3) = r(C_3-C_4) = 1.557$ Å, and we relaxed the interior angles $C_1C_2C_3$ and $C_2C_3C_4$ to 107° as required for planarity, keeping angle $C_5C_1C_2$ at 110.5°. The numbering system for the atoms is given in Figure 2.

The structural parameters for planar and twisted 2-methylcyclopentanone and for 2,3-dimethylcyclopentanone were obtained using the same considerations and assumptions described above for the 3-methylcyclopentanone structures. Note that for the single 2,3-dimethylcyclopentanone isomer which we considered (VII), the ring is twisted, the 2-methyl group is axial to the ring, and the 3-methyl group is equatorial to the ring.

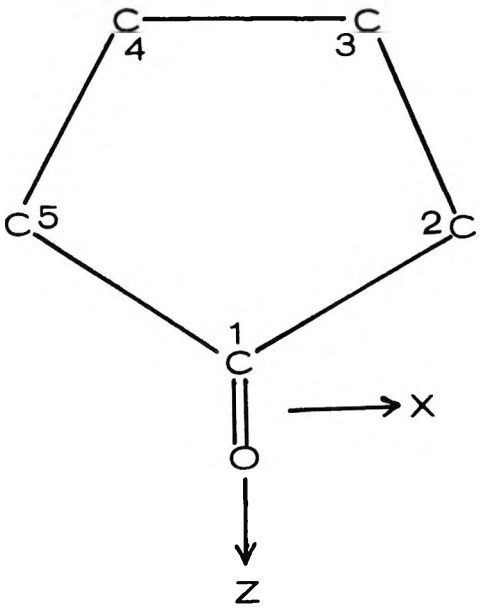

Figure 2. Numbering system for cyclopentanone ring atoms.

IV. Conformational Energies. 3-Methylcyclopentanone

After the electronic valence shell energy of the ground state was computed for each of the three 3-methylcyclopentanone isomers (II, III, and IV), the total valence shell energy was estimated by assuming com-

plete screening of the inner core electrons on carbon and oxygen and adding the repulsion energy of the remaining core charges to the electronic (negative) energy. In this way we could estimate the relative energies of the three conformational isomers. In Table I the computed energies are given and we see that the axial conformation is favored. This result is perhaps somewhat surprising since one might expect that CH_3-----H repulsive interactions across the ring would be much larger in the axial conformer than in the equatorial conformer. The results given in Table I do indeed show that the nuclear repulsion energy of the axial conformer is significantly larger than that of the planar and equatorial conformers. However, the total electronic energy of the axial conformer is somewhat lower than that of the other two conformers and this is the source of its relatively greater stability. Due to the rather serious approximations inherent in in INDO molecular orbital model, these results must be accepted with some reservation. However, the results achieved by Pople, Beveridge, and Dobosh[26] for bond angles and molecular geometries using the INDO method are in rather good agreement with experiment.

Table I: INDO Computed Valence Shell Energies of 3-Methylcyclopentanone

Conformation	Electronic energy, eV	Nuclear repulsion, eV	Total, eV
Axial (IV)	−6400.82419	+4591.67773	−1809.14646
Planar (II)	−6343.39774	+4534.31320	−1809.08454
Equatorial (III)	−6342.99716	+4533.91142	−1809.08574

In summary, according to our calculations the equatorial and axial conformations are more stable than the planar conformation which was assumed in the previous treatments of optical rotation in 3-methylcyclopentanone. Also, while the equatorial conformation is only slightly more stable than the planar form, our computed values indicate that the axial conformation is more stable by about 1.4 kcal/mol. Since nuclear repulsions are highest, as expected, for the axial conformation, the only rationale we can offer is that evidently some weak bonding is set up between the methyl group hydrogens and the carbonyl group in this conformation which is negligible in the other two.

V. Results and Discussion

A. $n \rightarrow \pi^*$ (Singlet) Transition. The CI eigenvectors calculated for the first excited singlet states of the structures I–VII indicate that an orbital description of these states can be given entirely in terms of a single promotion of an electron from the highest lying occupied ground-state molecular orbital to the lowest lying unoccupied ground-state molecular orbital. In structures I–IV, the highest occupied MO very closely resembles the highest occupied MO in formaldehyde and we designate this as a nonbonding (n) MO, even though it has some in-plane π antibonding character between the carbonyl oxygen and the ring carbon atoms. In V–VII, the highest occupied MO is somewhat less localized on the carbonyl group (compared with formaldehyde and with I–IV), but we shall still refer to this orbital as an n MO in these structures. The lowest unoccupied ground-state MO is called π^* throughout our discussion in this section.

The largest atomic orbital (AO) coefficients (*i.e.*, those coefficients $>|0.100|$) calculated for the highest occupied (n) and the lowest unoccupied (π^*) molecular orbitals (MO) in the ground state are listed in Tables II and III, respectively. Note that the AO composition of the n MO is nearly constant throughout the series of structures studied except for V (2-methylcyclopentanone with a planar ring). In structures I–IV, VI, and VII, the n MO is localized primarily on the carbonyl oxygen atom with some additional amplitude on the carbonyl carbon atom and the two α ring carbons. Furthermore, the two α-carbons are nearly identical so far as the in MO is concerned. In structure V, the $2p_x$ AO on C_α' makes the principal contribution to the highest occupied MO while the $2p_x$ AO on the carbonyl oxygen makes a lesser contribution. In this case, the highest occupied MO is better described as an in-plane antibonding π orbital between the carbonyl oxygen and just one of the α-carbon atoms than as a "nonbonding" orbital. The anomalous electronic properties of structure V are further illustrated by the results given in Table IV for the electron densities calculated at selected atomic sites in structures I–VII.

Table II: Calculated Properties for $n \rightarrow \pi^*$ (Singlet) Transition

Compd	ΔE, eV	$f \times 10^{-4}$	$D \times 10^{-38}$ cgs	$[R]^a$	g, cgs
I	5.36	20	9.67	+23.99	0.099
II	5.39	7	3.45	+0.64	0.007
III	5.44	19	9.32	+21.60	0.093
IV	5.46	15	7.41	−22.04	0.119
V	5.35	285	141	+94.95	0.027
VI	5.69	68	31.8	+69.47	0.087
VII	5.64	117	54.9	+47.40	0.034

[a] $[R]$ = reduced rotatory strength $\cong 1.08 \times 10^{-40} R$(cgs).

The lowest unoccupied MO in structures I–IV is localized primarily on the carbonyl group and can be characterized as a π antibonding orbital between C and O. In structures V–VII, the lowest unoccupied MO retains its carbonyl π^* character, but it also has considerable contributions from the 2s and 2p AO's on the

Table III: MO Coefficients: "n" Orbital

Compd	O(z)	C(z)	C_α(s)	C_α(z)	C_α(z)	C_α'(s)	C_α'(z)	C_α'(z)
I	+0.788	−0.270	−0.165	+0.271	−0.210	+0.165	+0.271	+0.210
II	+0.788	−0.268	−0.166	+0.276	−0.211	+0.174	+0.277	+0.193
III	+0.783	−0.271	−0.150	+0.265	−0.233	+0.158	+0.263	+0.209
IV	+0.788	−0.270	−0.160	+0.269	−0.216	+0.164	+0.270	+0.209
V	+0.437	−0.261	−0.219	+0.310	−0.121	−0.227	+0.631	−0.127
VI	+0.772	−0.267	−0.150	+0.289	−0.218	+0.183	+0.249	+0.205
VII	+0.769	−0.263	−0.151	+0.270	−0.247	+0.169	+0.238	+0.205

[a] O, carbonyl oxygen; C, carbonyl carbon; C_α, α-carbon closest to alkyl ring substituent; C_α', α-carbon on side of ring opposite to substituent site; (s, x, y, z), 2s, $2p_x$, $2p_y$, and $2p_z$ atomic orbitals.

Table IV: MO Coefficients: "π^*" Orbital

Compd	O(y)	C(y)	C_α(s)	C_α(y)	C_α'(s)	C_α'(y)	C_s(z)	C_s(y)	H_α, $_\alpha H'$
I	−0.635	+0.682		+0.254		+0.254			0.3–0.4
II	−0.638	+0.684		+0.256		+0.258			0.3–0.4
III	−0.637	+0.684		+0.257		+0.253			0.3–0.4
IV	−0.638	+0.686		+0.250		+0.256			0.3–0.4
V	+0.497	−0.498		−0.110	−0.535	−0.409	+0.220	+0.982	0.1–0.2
VI	−0.618	+0.640	−0.139	+0.117	−0.287	+0.403	−0.214	+0.608	0.1–0.2
VII	−0.589	+0.581	−0.315	+0.225	−0.289	+0.355	−0.185	+0.572	0.1–0.2

[a] O, C, C_α, C_α': same as in Table III; C_s, carbon atom of methyl substituent located at ring site C_α (2-methyl group); H_α, hydrogen atoms attached to C_α; H_α', hydrogen atoms attached to C_α'.

Table V: Electron Densities on Atoms

Compd	O	C	C_α	C_α'	C_β	C_β'	C_s	H_s	H_s	H_s
I	6.31	3.69	4.02	4.02	3.95	3.95				
II	6.31	3.69	4.02	4.02	3.95	3.95	3.94	1.02	1.02	1.02
III	6.31	3.69	4.02	4.02	3.95	3.95	3.95	1.02	1.02	1.02
IV	6.31	3.69	4.02	4.02	3.94	3.95	3.95	1.02	1.02	1.02
V	6.31	3.65	4.13	4.26	3.96	3.76	3.35	1.20	1.20	1.20
VI	6.30	3.69	4.11	3.85	3.93	3.97	3.34	1.20	1.21	1.21
VII	6.27	3.70	3.97	3.96	3.79	3.88	2.64 (α)	1.09 (α)	1.09 (α)	1.09 (α)
							3.36 (β)	1.19 (β)	1.20 (β)	1.20 (β)

[a] O, C, C_α, C_α', C_s, see Table IV; C_β, β-carbon closest to alkyl substituent; C_β', β-carbon on side of ring opposite to substituent site; H_s, hydrogen atoms attached to C_s.

α-carbon atoms and from the 2p AO's on the methyl substituent carbon. In structure V, the lowest unoccupied MO is predominantly comprised of substituent AO's.

The first singlet transition in all structures except V essentially involves reorganization of electron density on the carbonyl group and to a lesser extent on the α carbons and α hydrogens. In structure V, this transition has considerable charge-transfer character. Electron density is shifted from the carbonyl group and C_α' to the substituent methyl group.

In Table V the transition energies, oscillator strengths, dipole strengths, rotatory strengths, and dissymmetry factors calculated for the n → π^* (singlet) transition in structures I–VII are listed. Experimentally,[6] the n → π^* absorption band of 3(+)-methylcyclopentanone in cyclohexane solvent has its origin at ≈328 nm (3.78 eV), its ϵ_{max} at 300 nm (4.13 eV), and it spans the spectral region 245–328 nm (5.06–3.78 eV). We calculated a transition energy of about 230 nm (5.40 eV) for the n → π^*(singlet) transition in 3-methylcyclopentanone. Chandler and Goodman[11] reported an oscillator strength of 4.8×10^{-4} for the n → π^* transition in unsubstituted cyclopentanone (in n-pentane solvent). Our calculated oscillator strength for twisted cyclopentanone (compound I) is 20×10^{-4}. The transition energy for the n → π^* transition in formaldehyde was calculated to be 4.54 eV on our INDO-CI model. This result is also high compared with the experimentally determined n → π^* band

origin at 3.51 eV,[52] and the transition energy of 3.80 eV calculated by Whitten[53] using an *ab initio* approach.

The calculated dipole strengths, rotatory strengths, and dissymmetry factors which are given in Table V for structures I–IV can be compared with the following experimental data: (1) 3(+)-methylcyclopentanone in water (ref 6), $D = 3 \times 10^{-38}$ cgs = 0.03 D², $R = +5.1 \times 10^{-40}$ cgs, $g = 0.017$ cgs, λ_{max} (CD) = 287 nm, λ_{max} (abs) = 280 nm; (2) 3(+)-methylcyclopentanone in EPA solvent (ref 14 and 15), $[R] = +6.02$, reduced rotatory strength at 25°; $[R] = +9.88$, reduced rotatory strength at −192°; λ_{max} (CD) = 300 nm; (3) 5α-androstan-16-one in EPA solvent (ref 14)

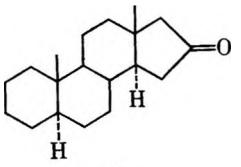

A

$[R]$ +1 =8.7 at 25°, $[R] = +18.1$ at −192°; (4) 3β-hydroxy-5α-androstan-16-one in methanol solvent (ref 54)

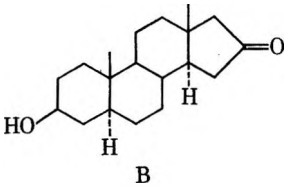

B

$D = 5.81 \times 10^{-38}$ cgs = 0.0581 D², $f = 9.1 \times 10^{-4}$ $R = 16.7 \times 10^{-40}$ cgs, $[R] = 18.0$, $g = 0.115$, λ_{max} (CD) = 300 nm, λ_{max} (abs) = 300 nm; (5) (+)-hydrindanone in isooctane solvent (ref 55)

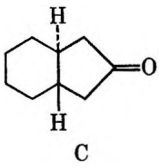

C

$D = 3.88 \times 10^{-38}$ cgs = 0.0388 D² = total dipole strength, $D^z = 1.84 \times 10^{-38}$ cgs = 0.0184 D² = Z component (along >C=O axis) of dipole strength, $R = +14.9 \times 10^{-40}$ cgs, $[R] = +16.1$ at 25°, $g = 4R/D = 0.154$, $g^z = 4R/D^z = 0.325$, λ_{max} (CD) = 300 nm, λ_{max} (abs) = 300 nm.

In compounds A, B, and C, shown above, the cyclopentanone ring is expected to be twisted into a rigid, nonplanar conformation with C_2 symmetry. The absolute configurations of these structures are known and the cyclopentanone ring is required to be twisted with a left-handed screw sense (about the C_2 (Z) axis). The chirality of the ring is identical with that of our structures I and III (see Figures 1a and 1c.) Since conformational mobility is forbidden (or, at least, highly unlikely) in these compounds, their rotatory strengths should not be temperature dependent. The CD data on compound A indicate this to be the case. Emeis[55] performed a detailed vibronic analysis on the isotropic absorption and CD spectra of compound C and was able to separate the z-polarized contributions to g and D from the x- and y-polarized contributions. His analysis was based on the assumption that in systems with C_2 symmetry vibronic coupling, to first order, cannot induce a net rotatory strength in an $A \rightarrow A$ (*e.g.*, n → π*) transition but can induce a net dipole strength of x, y-polarization. This assumption is rigorously correct to first order in the Herzberg–Teller vibronic coupling mechanism,[51] and so Emeis' analysis yields some very useful information concerning the static *vs.* vibronic contributions to the absorption intensity of the n → π* transition in compound C. The f, D, and g values given for compound B were obtained from the total integrated intensities of the absorption and CD spectra and so represent the total isotropic quantities.

Since vibronic effects are excluded from our computational model, the calculated f, D, and g values given in Table V for structure I have only z-polarized components. Our calculated dipole strengths for structures I and III are about five times as large as those reported for compounds B and C, and the calculated g factors are about one-third as large as the g^z value reported by Emeis for compound C. The calculated rotatory strength for III is about 20% larger than the experimentally determined ones for A and B, and is about 35% as large as the value reported for C. Optically active 3,4-dimethylcyclopentanone, in which both methyl substituents are in equatorial positions, provides a better basis for comparison with A, B, and C than does structure III. The substituent atoms directly attached to the cyclopentanone ring in A, B, and C are identical with those in the 3,4(*e*,*e*)-dimethylcyclopentanone structure and also have the same spatial orientations. If it can be assumed that the two methyl groups influence the n → π* optical rotatory properties independently, then one can deduce the rotatory strength of optically active 3,4-dimethylcyclopentanone from the calculated properties of I and III. The ring contribution to the rotatory strength of III is +23.99. Therefore the contribution of the equatorial 3-methyl group must be −2.39. An equatorial 4-methyl group should make a similar contribution to the rotatory strength of a twisted cyclopentanone ring of left-handed chirality. The reduced rotatory strength of optically active 3,4-dimethylcyclopentanone should, therefore, be given by: +23.99 − 2.39 − 2.39 =

(52) G. Herzberg, "Molecular Spectra and Molecular Structure: III. Electronic Spectra and Electronic Structure of Polyatomic Molecules," Van Nostrand, Princeton, N. J., 1967.

(53) J. L. Whitten and M. Hackmeyer, *J. Chem. Phys.*, 51, 5584 (1969).

(54) S. F. Mason, *Mol. Phys.*, 5, 343 (1962).

(55) C. A. Emeis, Ph.D. Dissertation, University of Leiden, The Netherlands, 1968.

+ 19.21. This value is within 20% of that observed for compound C and within 5% of those reported for A and B.

The five-membered ring in 3(+)-methylcyclopentanone is not expected to be conformationally rigid and at least two of the conformational structures which should be accessible to this compound are the structures III and IV shown in Figures 1c and 1d. The planar ring structure II is not expected to correspond to a stable or metastable conformational state. The conformational analysis performed by Ouannes and Jaques[12] on this compound indicates that structure III (in which the methyl substituent is equatorial to the ring and the ring is twisted into a half-chair conformation of C_2 symmetry) is the most stable form. Structure IV (in which the methyl substituent is axial to the ring and the ring is again in a half-chair conformation of C_2 symmetry) is also predicted by Ouannes and Jacques[12] to be very near to an energy minimum. However, IV is predicted to be less stable than III and to be nearly isoenergetic with two isomers in which the ring assumes an envelope (C_s) conformation. They predict that III is more stable than IV by about 0.25 kcal/mol. From Table I we see that the INDO-CI model used in the present study leads to the prediction that IV should be more stable than III by about 1.4 kcal/mol. As pointed out in section IV, the INDO model used here is not sufficiently reliable to allow us to attach much significance to such small energy differences. The conformational analysis performed by Ouannes and Jacques is also based on some rather crude assumptions about potential energy functions, but in view of the experimental CD data, it appears to predict correctly the dominant equilibrium conformation.

From the results given in Table V, we can deduce the the contributions made by the methyl substituent to the rotatory strength of 3-methylcyclopentanone in structures II, III, and IV. An equatorial methyl group contributes −2.39 to [R], an axial methyl group contributes +1.95, and a methyl group on the planar ring contributes +0.64. These results violate the octant rule as formulated by Moffitt, *et al.*,[56] for predicting the sign of the optical activity induced in a symmetric, cyclic ketone by dissymmetric substitution. If we partition the space occupied by the 3-methylcyclopentanone molecule into octants and define the three orthogonal planes which form the boundaries between octants in the same way as did Moffitt, we find that the methyl group (carbon and hydrogens) occupies the same octant in each of the structures II, III, and IV. If we define a coordinate system

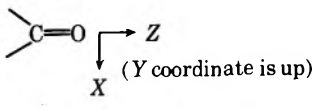

where the origin lies midway between C and O, the cartesian positional coordinates of the methyl carbon atoms in structures II, III, and IV are given by

	X, Å	Y, Å	Z, Å	XY, Å²	XYZ, Å³	r, Å
II	1.28	1.26	−3.68	1.61	−5.92	4.10
III	1.60	0.35	−3.97	0.56	−2.22	4.29
IV	0.65	1.83	−3.14	1.19	−3.74	3.69

According to both the octant (XYZ) rule and the quadrant (XY) rule,[57] the rotatory strengths induced in structures II, III, and IV by 3-methyl substitution should all have the same sign, and the simple one-electron model would further predict that the relative magnitudes of the induced rotatory strengths would follow the order: CH_3 (IV) > CH_3 (II) > CH_3 (III).

The 2-methylcyclopentanone structures, V and VI, were included in our study primarily to assess the importance of substituent proximity to the carbonyl group. Similarly to the 3-methylcyclopentanone structures the substituent group atoms in V and VI all lie in the same "octant" and "quadrant." For the substituent carbon atoms

	X, Å	Y, Å	Z, Å	XY, Å²	XYZ, Å³	r, Å
V	1.93	1.38	−1.45	2.66	−3.86	2.78
VI	2.07	1.26	−1.18	2.61	−3.08	2.70

In V and VI, the methyl substituent causes a significant distortion in both the highest occupied and lowest unoccupied ground-state MO's (*i.e.*, a distortion with respect to the composition of these same MO's in formaldehyde and in structures I–IV). In V, the lowest unoccupied orbital has a substantial amount of substituent character mixed into its C=O π^* character. The lowest singlet transition, therefore, involves considerable charge transfer between the carbonyl group and the substituent group, and is strongly z polarized.

In structure V the methyl group contributes +94.95 to [R], and in structure VI the methyl group (which is axial to the ring) contributes +45.48. With the methyl substituent adjacent to the carbonyl group, its contribution to the rotatory strength is nearly twice as large as that due to ring twist, 45.5 *vs.* 24.0. In the 3-methylcyclopentanone structures, ring twist accounts for the largest contributions to the rotatory strength.

The 2,3-dimethylcyclopentanone structure, VII, was considered primarily to determine if our MO model would predict an additivity rule for substituent contributions to the total rotatory strength. In other words if the 2-methyl and 3-methyl substituents exert independent influences on the n → π^* transition, then we should find that [R(VII)] = [R(III)] + [R(VI)] − [R(I)] = [R(3-methyl equatorial)] + [R(2-methyl axial)] + [R(twisted unsubstituted cyclopentanone)] = −2.39 + 45.48 + 23.99 = 67.08. The calculated re-

(56) W. Moffitt, R. B. Woodward, A. Moscowitz, W. Klyne, and C. Djerassi, *J. Amer. Chem. Soc.*, **83**, 4013 (1961).

(57) J. A. Schellman, *J. Chem. Phys.*, **44**, 55 (1966).

Table VI: Calculated Properties for Higher Energy (Singlet) Transitions

Compd		Transition A	B	C	D
I	ΔE =	11.97 eV	12.84	12.95	13.18
	f =	0.2150	0.0188	0.0834	0.0095
	$[R]$ =	+36.65	+139.95	−19.95	−43.87
II	ΔE =	11.98 eV	12.52	12.96	13.54
	f =	0.2683	0.0301	0.0316	0.0285
	$[R]$ =	+6.25	+15.33	+45.65	−14.07
III	ΔE =	11.96 eV	12.41	12.91	13.37
	f =	0.2478	0.0121	0.0319	0.0635
	$[R]$ =	+49.05	−10.57	−8.01	−55.18
IV	ΔE =	12.04 eV	12.63	12.99	13.44
	f =	0.2252	0.0150	0.0487	0.0521
	$[R]$ =	−52.07	−4.04	+27.30	+3.18
V	ΔE =	6.25 eV	8.39	10.08	10.80
	f =	0.7842	0.1205	0.1210	0.1452
	$[R]$ =	−103.76	−4.77	−21.68	+12.60
VI	ΔE =	11.54 eV	12.30	12.67	12.83
	f =	0.1225	0.0540	0.0162	0.0102
	$[R]$ =	+30.90	−2.73	−44.73	−3.68
VII	ΔE =	11.27 eV	11.86	12.11	12.70
	f =	0.0817	0.0590	0.0465	0.1653
	$[R]$ =	+22.44	−74.44	+52.59	−224.14

duced rotatory strength for VII is +47.40. The detailed AO and MO composition of the first excited singlet state of VII is similar to that of structure VI. One might expect, therefore, that the 3-methyl (equatorial) substituent would behave differently toward the "n → π^*" transition in VII than in III, and that additivity would not obtain in this case.

B. Higher Energy (Singlet) Transitions. The computed transition energies, oscillator strengths, and rotatory strengths are listed in Table VI for transitions to the next four excited states above the nπ^* state. For structures I–IV, the terminal states in transitions A–D can be characterized as

$$\text{n} \longrightarrow \sigma_{cc}^*(\text{s}) \quad \text{(A)}$$

$$\sigma_{co} \longrightarrow \pi^*; \quad \sigma_{cc} \longrightarrow \pi^* \quad \text{(B)}$$

$$\pi \longrightarrow \pi^* \quad \text{(C)}$$

$$\text{n} \longrightarrow \sigma_{co}^* \quad \text{(D)}$$

where σ_{cc}^*(s) represents a MO which is constructed primarily of 2s AO's centered on the ring carbon atoms and which has nodes between the α-ring carbons and the carbonyl carbon, and σ_{co} is mostly a σ-bonding MO between C and O. Transition A is strongly x-polarized and is calculated to have a relatively large oscillator strength in each of the structures I–IV. Transition C is strongly z-polarized. Transitions B and D have both x- and z-polarized components and there is significant configurational mixing in the excited states (as represented by virtual orbitals, of course, in our computational model) of these transitions.

In structures V–VII, transition C can again be identified with a localized $\pi \rightarrow \pi^*$ carbonyl transition. However, in these structures the excited states associated with transitions A, B, and D cannot be readily characterized in terms of any specific sets of calculated ground state occupied and unoccupied MO's. Transitions A and B appear to involve considerable charge transfer from the carbonyl group to the 2-methyl substituent as well as to the ring carbon skeleton.

The vapor-phase vacuum ultraviolet circular dichroism spectrum of (+)-3-methylcyclopentanone has recently been measured and reported by two different research groups. Feinleib and Bovey[16] reported three distinguishable absorption and CD bands in the 50,000–60,000-cm^{-1} region in addition to the n → π^* band centered at 33,000 cm^{-1}. The $\Delta\epsilon_{max}$ of the near-uv band (n → π^*) was reported to be ≈ 2. Their CD spectra for the far-uv region showed the bands: (a) $\bar{\nu}_{max} \cong$ 52,00 cm^{-1}, $\Delta\epsilon_{max} \cong -6$; (b) $\bar{\nu}_{max}$ = 56,000–58,000 cm^{-1}, $\Delta\epsilon_{max} \cong -13$; (c) $\bar{\nu}_{max} \cong$ 60,000 cm^{-1}, $\Delta\epsilon_{max} \cong$ +27. The first band exhibited two prominent vibronic components, and it was reported that the third band probably represented only the first vibronic component of a broad band centered further into the vacuum uv ($\bar{\nu} >$ 60,000 cm^{-1}). Schnepp, Pearson, and Sharman[17] also measured the CD of (+)-3-methylcyclopentanone in the vapor phase and suggested the presence of four distinct CD band systems in the 50,000–60,000-cm^{-1} spectral region. The lowest-energy band system in this region exhibits three vibronic components (with a spacing of ≈1150 cm^{-1}) and has a $\Delta\epsilon_{max} \approx -4$. The second CD band is located at about 54,600 cm^{-1} and shows a $\Delta\epsilon_{max} \approx -0.7$. The third CD band is at ≈56,800 cm^{-1} with $\Delta\epsilon_{max} \approx +0.7$; and the

fourth CD band (or the first vibronic peak of a broader band) is at $\approx 60{,}200\ cm^{-1}$ with $\Delta\epsilon_{max} \sim +3.5$.

The vapor of (+)-3-methylcyclopentanone can most likely be considered to consist of a equilibrium mixture of conformational isomers in which our structures III and IV are predominant. Furthermore, a comparison of our calculated rotatory strengths with those obtained experimentally for the n → π* transition, and the conformational analysis performed by Ouannes and Jacques,[12] indicate that structure III (in which the 3-methyl substituent is equatorial to ring) is the most important conformer in the mixture. Based on the results given in Table VI, the signs of the rotatory strengths predicted for the first four far-uv transitions of (+)-3-methylcyclopentanone are as follows: $R_A > 0$, $R_B < 0$, $R_C > 0$, $R_D < 0$. The sign predicted for transition A is opposite that found experimentally.[16,17] The signs predicted for transitions B and C are in agreement with the CD data reported by Feinleib and Bovey[16] but cannot explain the results given by Schnepp, *et al.*[17] The CD spectra reported by Schnepp were obtained with higher resolution than those reported by Feinleib and Bovey, and possibly provide the most accurate and detailed data available for $\bar{\nu} < 60{,}000\ cm^{-1}$.

VI. Conclusions

The rotatory strengths calculated on the INDO-CI molecular orbital model for the lowest energy singlet → singlet carbonyl transition (n → π*) appear to be in good agreement with the experimental CD data for chiral cyclopentanone systems. According to this direct computational model, the major contributor to the rotatory strength in the β-substituted systems is the inherent chirality of the twisted five-membered carbocyclic ring rather than the presence of an asymmetric center at the β ring carbon. For the optically active α-substituted systems (*e.g.*, structures V–VII), the calculated results indicate that the α-substituent has a larger direct influence on the optical properties of the n → π* transition than does ring deformation. The influence of the ring substituents on the n → π* rotatory strength were evaluated for each of the structures II–VII. In structures II–IV, the methyl substituent always lies in the same quadrant and octant. However, the sign of the substituent contribution to the rotatory strength of III differs from the signs of the substituent contributions in II and IV. This analysis was based on a selection of sectors as defined by Moffitt, *et al.*,[56] and not on sectors as defined by the nodal surfaces of the n and π* MO's in twisted cyclopentanone (structure I).

The rotatory strengths calculated for the second, third, fourth, and fifth singlet → singlet transitions of (+)-3-methylcyclopentanone appear not to be in good agreement with the available experimental data. It is possible that the rotatory strength calculated for the fourth transition (π → π*; transition C in Table VI) is in agreement with respect to sign, with the reported CD spectra.[16,17] However, neither the number nor the detailed nature of the bands observed in the experimental CD spectra has been unambiguously determined. Unfortunately, in this case assessment of the theory must await better experiments. The sign of the calculated rotatory strength for the second singlet → singlet transition (transition A in Table VI) is clearly opposite that of the second band in the experimental CD spectrum.

Acknowledgments. We thank Drs. B. Gilson and P. Dobosh for their contributions to the development of the INDO-CI molecular orbital program used in this study. Discussions with Professor W. Kauzmann were also of great benefit to us. One of us (D. D. S.) gratefully acknowledges the support of the Center of Advanced Studies, University of Virginia, in the form of a postdoctoral fellowship. This work was also supported in part by the Petroleum Research Fund (PRF No. 2022-G2) and the National Science Foundation (NSF Institutional Grant to the University of Virginia).

Bond Energy Terms for Methylsilanes and Methylchlorosilanes

by D. Quane

Chemistry Department, East Texas State University, Commerce, Texas 75428 *(Received February 18, 1971)*

Publication costs assisted by the Robert A. Welch Foundation

The difficulty of obtaining reliable thermochemical data for organometallic compounds has long been a problem. Two recent experimental studies have given heats of formation of methylsilanes based on electron impact appearance potentials, and of methylchlorosilanes based on calorimetric methods. Values for silicon bond energy terms based on these studies are widely divergent. It is shown that if a modified Allen bond-interaction scheme is used, both sets of data can be reproduced, to within ±3 kcal/mol, by the following bond energy and bond-interaction (Γ) terms: Si–C 64.9, Si–H 77.9, Si–Cl 102.0, Γ(CSiC) 1.5, Γ(CSiCl) 0.8, Γ(ClSiCl) −4.2 kcal/mol. The possible significance of the negative value of Γ(ClSiCl) in terms of (p → d)π bonding is discussed.

Introduction

The difficulty of obtaining reliable thermochemical data on organometallic compounds in general and organosilicon compounds in particular has often been noted.[1-3] A recent paper on bond energy terms for group IV organometallic compounds does not include any values for alkylsilanes. The lack of reliable data is cited as the reason for this omission.[4] This being the case, it is of some interest to determine if the reliable data which *do* exist can be used as a tool for predicting unknown heats of formation. Three recent papers[2,5,6] have proposed bond energy term schemes for organosilicon compounds. One[6] of these is based largely on older values for the heats of formation of the methylsilanes,[7] which have been repeatedly rejected by subsequent workers[1-4,8] as unreliable and internally inconsistent. The other two papers make use of new experimental data. Potzinger and Lampe[2] have analyzed electron impact mass spectrometric data to obtain bond energy terms which will best account for the heats of formation of organosilicon ions from alkylsilanes. Hajiev and Agarunov[5] have derived bond energy terms from their measured heats of combustion of methylchlorosilanes. The bond energy terms obtained in these two papers are presented in Table I. The lack of agreement is obvious.

Table I: Literature Values of Silicon Bond Energy Terms

	Electron impact,[a] kcal/mol	Thermochemical,[b] kcal/mol
B(Si–H) or E(Si–H)	76.77	81.8
B(Si–C) or E(Si–C)	60.3	74.8
D(Si–Cl) or E(Si–Cl)	123.9	98.0

[a] Reference 2. [b] Reference 5.

It is possible that the disagreement may be due to a lack of consistency between the two sets of data, either due to a fundamental difference between the two experimental methods, or to some systematic error in one or the other results. Closer analysis indicates that it is just as likely that the inconsistency lies, not in the experimental data, but in differences in the treatment of the raw data used by the two groups.

One important difference is in the definition of a bond energy term. Hajiev and Agarunov use a simple additivity postulate, by which the heat of atomization of the compound is considered to be the sum of the energies (E) of the individual bonds. Potzinger and Lampe use a modified version of the Allen bond interaction scheme,[9] in which the heat of atomization is considered as the sum of bond energy (B) and bond interaction (Γ) terms. The energy reported for the Si–Cl bond in the latter paper[2] is a bond dissociation energy (D) for a particular cleavage reaction

(1) H. A. Skinner, *Advan. Organometal. Chem.*, **2**, 49 (1964).

(2) P. Potzinger and F. W. Lampe, *J. Phys. Chem.*, **74**, 719 (1970).

(3) J. D. Cox and G. Pilcher, "Thermochemistry of Organic and Organometallic Compounds," Academic Press, London, 1970, pp 67–68, 468–471.

(4) A. S. Carson, P. G. Laye, J. A. Spencer, and W. V. Steele, *J. Chem. Thermodyn.*, **2**, 659 (1970).

(5) S. N. Hajiev and M. J. Agarunov, *J. Organometal. Chem.*, **22**, 305 (1970).

(6) M. J. Van Dalen and P. J. Van den Berg, *ibid.*, **16**, 381 (1969).

(7) S. Tannenbaum, *J. Amer. Chem. Soc.*, **76**, 1027 (1954).

(8) S. J. Band, I. M. T. Davidson, and C. A. Lambert, *J. Chem. Soc. A*, 2068 (1968).

(9) (a) A referee has pointed out that the "modified" Allen bond energy scheme used by Potzinger and Lampe,[2] and in this paper, by omitting Allen's trio interaction terms,[9b] is actually closer to Zahn's bond-interaction scheme,[9c] and might better be so called. Use of the complete Allen scheme for the compounds discussed in this paper would require four additional parameters—Δ^{Si}_{CCC}, Δ^{Si}_{CCCl}, Δ^{Si}_{CClCl}, and Δ^{Si}_{ClClCl}; a ten-parameter scheme would not be justified by the data available. Nevertheless, discussion of bond energy terms for organometallic compounds has been primarily in terms of the Allen scheme,[1,10,11] and it seems desirable, in order to facilitate comparison of the analysis in this paper with previous work, to emphasize the relationship of the bond energy terms used here to those derived from the Allen scheme. (b) T. L. Allen, *J. Chem. Phys.*, **31**, 1039 (1959); (c) C. T. Zahn, *ibid.*, **2**, 671 (1934).

$$(CH_3)_3SiCl(g) \longrightarrow (CH_3)_3Si(g) + Cl(g) \quad (1)$$

rather than a mean thermochemical bond energy.

A second difference lies in the auxillary thermochemical data used in the two papers. Of particular interest here is the heat of atomization of silicon, for which Potzinger and Lampe use 106 kcal/mol, Hajiev and Agarunov 110 kcal/mol.

In view of this, it appears worthwhile to determine whether the existing data, taken from both calorimetric and electron impact studies, could be used to generate a consistent bond-energy term scheme. The Allen bond-interaction scheme was employed, due to its previous record of success in correlating thermodynamic data on organometallic compounds.[1,10,11]

Calculation of Bond Energy Terms

The available thermodynamic data[5,12,13] on simple silanes along with the auxillary thermodynamic quantities used in these calculations are shown in Table II, the electron impact data in Table III. In the latter table the reactions are shown in pairs, each pair having a common ion as the product. Since the heat of formation of an ion is independent of the reaction forming it, the difference between the appearance potentials, after the heats of formation of the other molecules or radicals produced by these reactions have been taken into account, must be due to differences in the heat of formation of the reactant compounds.

Table II: Thermodynamic Data Used in Calculating Bond Energy Terms

Species	Enthalpy of formation, kcal/mol	Species	Enthalpy of formation, kcal/mol
H(g)	52.095[a]	CH_3(g)	33.2[a]
C(g)	171.29[a]	$SiCl_4$(g)	−158.3[b]
Si(g)	108.9[a]	$(CH_3)_3SiCl$(g)	−79.4[c]
Cl(g)	29.082[a]	$(CH_3)_2SiCl_2$(g)	−105.7[c]
CH_4(g)	−17.88[a]	$(CH_3)_2SiHCl$	−67.8[c]
SiH_4(g)	8.2[a]	CH_3SiCl_3(g)	−134.6[c]
$SiHCl_3$(g)	−122.6[a]	CH_3SiHCl_2(g)	−93.8[c]

[a] Reference 12. [b] Calculated using the enthalpy of formation of $SiCl_4$(l), −165.49 kcal/mol, from ref 13, and the enthalpy of vaporization, 7.2 kcal/mol, from ref 12. [c] Calculated from the values given in ref 5, using the more recent value of the enthalpy of formation of SiO_2(amorphous, hydrated in dilute HCl), −212.2 kcal/mol, from ref 13, rather than the value (−217.4 kcal/mol) assumed in ref 5.

In order to test the hypothesis that there is no fundamental inconsistency between data obtained using the two experimental methods, the available data were divided into two sets; "electron impact" and "calorimetric". The heat of formation of SiH_4 was included as a reference point for the electron impact data, as had been done by Potzinger and Lampe. Since the five heats of formation determined by Hajiev and Agarunov are not sufficient to determine the six parameters required by the Allen scheme, the heats of formation of $SiCl_4$ and $SiHCl_3$ are included with these data.

A least-squares procedure was used in fitting the two sets of data to the Allen bond interaction scheme using six variable parameters, three bond energy terms, B(Si–C), B(Si–H), and B(Si–Cl), and three bond interaction terms, Γ(CSiC), Γ(CSiCl), and Γ(ClSiCl). (Only three of these terms are needed to fit the electron impact data.) The C–H bond energy term in the methyl group was assumed to be the same as that in methane, 99.4 kcal/mol.

The results of these calculations are shown in Table IV, the second and third columns. The differences in bond energy terms generated by the two sets of data are reduced, to within the probable combined limits of experimental error.[14] This being the case, it seems justified to use the least-squares procedure to find a set of bond energy terms which will best reproduce the entire body of data, from both experimental methods. The resulting terms are shown in the last column of Table IV.

Discussion

In Table V are presented the heats of formation of the 15 compounds containing only CH_3, H, or Cl bonded to silicon, calculated using the bond energy terms from the last column of Table IV, along with experimental values of those eight compounds for which reliable data are available. The standard deviation of the calculated values from these experimental values is 2.1 kcal/mol.

With regard to the electron impact data, the differences in appearance potentials of Potzinger and Lampe have been calculated from the data of Table V, and the results are presented in Table VI. The values calculated in this way reproduce Potzinger and Lampe's data more closely than the bond energy terms calculated in that paper.[2] The improved agreement is most likely due to B(Si–H) being taken as a variable parameter in this paper, whereas in the earlier paper it had been assumed that the Si–H bond energy in the methylsilanes is the same as that in SiH_4. It may also be noted that the only large disagreement between the calculated and

(10) J. V. Davies, A. E. Pope, and H. A. Skinner, *Trans. Faraday Soc.*, **59**, 2233 (1963).

(11) D. J. Colman and H. A. Skinner, *ibid.*, **62**, 1721 (1966).

(12) *Nat. Bur. Stand. (U. S.) Tech. Note*, **270-3** (1968).

(13) P. Gross, C. Hayman, and S. Mwroka, *Trans. Faraday Soc.*, **65**, 2856 (1969).

(14) Potzinger and Lampe[2] have estimated an accuracy of ±5 kcal/mol for their calculated heats of formation; Hajiev and Agarunov[5] have estimated the uncertainty in their measured heats of combustion to be in the range 0.5–0.8 kcal/mol, which uncertainty is also quoted for the derived heats of formation. This does not take into account any uncertainty in the value assumed for the heat of formation of SiO_2 (amorphous, hydrated in dilute HCl). Cox and Pilcher have indicated (ref 3, pp 470–471) that this probably underestimates the actual uncertainty.

Table III: Electron Impact Appearance Potentials from Methylsilanes (all data from ref 2)

Ion	Reaction	Energy, eV
SiH_2^+	$SiH_4 + e^- \rightarrow SiH_2^+ + H_2 + 2e^-$	11.90
	$CH_3SiH_3 + e^- \rightarrow SiH_2^+ + CH_4 + 2e^-$	11.50
CH_3SiH^+	$CH_3SiH_3 + e^- \rightarrow CH_3SiH^+ + H_2 + 2e^-$	11.45
	$(CH_3)_2SiH_2 + e^- \rightarrow CH_3SiH^+ + CH_4 + 2e^-$	10.85
$CH_3SiH_2^+$	$CH_3SiH_3 + e^- \rightarrow CH_3SiH_2^+ + H + 2e^-$	11.80
	$(CH_3)_2SiH_2 + e^- \rightarrow CH_3SiH_2^+ + CH_3 + 2e^-$	11.51
$(CH_3)_2Si^+$	$(CH_3)_2SiH_2 + e^- \rightarrow (CH_3)_2Si^+ + H_2 + 2e^-$	10.71
	$(CH_3)_3SiH + e^- \rightarrow (CH_3)_2Si^+ + CH_4 + 2e^-$	10.50
$(CH_3)_2SiH^+$	$(CH_3)_2SiH_2 + e^- \rightarrow (CH_3)_2SiH^+ + H + 2e^-$	11.12
	$(CH_3)_3SiH + e^- \rightarrow (CH)_2SiH^+ + CH_3 + 2e^-$	10.91
$(CH_3)_3Si^+$	$(CH_3)_3SiH + e^- \rightarrow (CH_3)_3Si^+ + H + 2e^-$	10.52
	$(CH_3)_4Si + e^- \rightarrow (CH_3)_3Si^+ + CH_3 + 2e^-$	10.25

Table IV: Bond Energy Terms for Silicon Compounds Calculated Using the Allen Bond Interaction Scheme

	Electron impact	Thermochemical	All data
B(Si–C)	62.5	67.3	64.9
B(Si–H)	77.3	81.9	77.9
B(Si–Cl)		96.3	102.0
Γ(CSiC)	2.1	1.5	1.5
Γ(CSiCl)		1.0	0.8
Γ(ClSiCl)		−0.2	−4.2

Table V: Standard Heats of Formation of Silicon Derivatives (all values in kcal/mol)

Compd	Exptl[a]	Calcd[b]	Compd	Calcd[b]
SiH_4	8.2	5.7	CH_3SiH_3	−4.0
$SiCl_4$	−157.6	−158.3	$(CH_3)_2SiH_2$	−15.2
$SiHCl_3$	−122.6	−123.1	$(CH_3)_3SiH$	−28.0
CH_3SiCl_3	−134.6	−135.2	$(CH_3)_4Si$	−42.2
CH_3SiHCl_2	−93.8	−95.6	CH_3SiH_2Cl	−51.9
$(CH_3)_2SiCl_2$	−105.7	−108.4	SiH_2Cl_2	−84.3
$(CH_3)_2SiHCl$	−67.8	−63.9	SiH_3Cl	−41.4
$(CH_3)_3SiCl$	−79.4	−77.4		

[a] See Table II. [b] This work.

Table VI: Agreement of Calculated Heats of Formation with Electron Impact Data

Reaction	Difference between measured appearance potentials, kcal/mol: Exptl, ref 2	Calcd, ref 2	Calcd, this work
$SiH_4 \rightarrow$, $CH_3SiH_3 \rightarrow$ } SiH_2^+	9.2	11.6	8.2
$CH_3SiH_3 \rightarrow$, $(CH_3)_2SiH_2 \rightarrow$ } CH_3SiH^+	13.8	9.1	6.7
$CH_3SiH_3 \rightarrow$, $(CH_3)_2SiH_2 \rightarrow$ } $CH_3SiH_2^+$	6.7	10.1	7.7
$(CH_3)_2SiH_2 \rightarrow$, $(CH_3)_3SiH \rightarrow$ } $(CH_3)_2Si^+$	4.8	7.0	4.9
$(CH_3)_2SiH_2 \rightarrow$, $(CH_3)_3SiH \rightarrow$ } $(CH_3)_2SiH^+$	4.8	8.6	6.1
$(CH_3)_3SiH \rightarrow$, $(CH_3)_4Si \rightarrow$ } $(CH_3)_3Si^+$	6.2	4.0	4.7
Standard deviation		3.3	3.1

experimental values lies in a single value, the difference between the appearance potentials of the CH_3SiH^+ ion.

The silicon–carbon bond energy term obtained in this paper may be compared with the comparable bond energy terms obtained by Carson, Laye, Spencer, and Steele[4] for the methyl derivatives of the group IV elements: B(Si–C), 64.9; E(Ge–C), 63; E(Sn–C), 51.5; E(Pb–C), 36. However, the usefulness of this comparison is somewhat reduced by the difference in the definition of bond energy terms used in the two papers. The bond energy terms (E) for germanium, tin, and lead were calculated using a simple additivity postulate, rather than the Allen bond-interaction scheme used in this paper. In addition different values were assumed for the C–H bond energy term in the two papers. A more useful comparison, avoiding these difficulties, may be found in the bond dissociation energies, $\bar{D}$(M–CH_3), obtained from the calculated heats of formation of the tetramethyl compounds: $\bar{D}$(Si–Me), 71.0; $\bar{D}$(Ge–Me), 64.2; $\bar{D}$(Sn–Me), 52.4; $\bar{D}$(Pb–Me), 36.9 kcal/mol. The expected regular decrease from silicon to lead is seen.

Literature values for the appearance potential of $(CH_3)_3Si^+$ ion from the reaction

$$(CH_3)_3SiCl + e^- \longrightarrow (CH_3)_3Si^+ + Cl + 2e^- \quad (2)$$

show considerable lack of agreement, values of 10.9,[3]

11.5,[15] and 12.40 eV[16] having been reported in recent years. Ordinarily, all other things being equal, the lowest appearance potential reported is most likely to be correct, but Potzinger and Lampe[2] maintain that the experimental methods used to obtain the two lower values are more likely to detect the ion-pair reaction

$$(CH_3)_3SiCl + e^- \longrightarrow (CH_3)_3Si^+ + Cl^- + e^- \quad (3)$$

rather than the onset of reaction 2. When the values from Table V for the heats of formation of $(CH_3)_3SiH$(g) and $(CH_3)_4Si$(g) are combined with appearance potentials from Table III, a value of 162 kcal/mol is obtained for the heat of formation of $(CH_3)_3Si^+$. If this value is combined with the calculated value of the heat of formation of $(CH_3)_3SiCl$ (g) from Table V, the predicted appearance potential for reaction 2 would be 11.6 eV. This, in general, supports Potzinger and Lampe's argument that lower values may be due to the ion-pair process, but also leaves open the possibility that the low-sensitivity RPD method used by Hess, Lampe, and Sommer[16] gives too high a value for the onset of reaction 2.

The large negative value obtained for the interaction energy (Γ) between adjacent Si–Cl bonds is of some interest. If the principle interaction between bonds were due to the inductive effect, the value of Γ would be expected to be positive[17] and probably small.[18] Silicon–chlorine bonds are generally considered to have considerable double-bond character through $(p \rightarrow d)\pi$ interactions.[19] If conjugation occured, through silicon, between adjacent π bonds, then Γ would be both positive and large. Considerable doubt, however, has been cast on the possibility of such conjugation in tetrahedral systems both on theoretical[20] and experimental[21] grounds.

A negative interaction energy could be justified in terms of $(p \rightarrow d)\pi$ bonding in a number of ways. It has been proposed that only some of the 3d orbitals of silicon can participate in such bonding.[20] Thus, as the number of potential π-bonding substituents increases, the amount of π bonding per substituent would decrease. This "competitive interaction" has been used to explain the nonadditivity of nmr chemical shifts in the halosilanes[22] and vinylsilanes,[23] and would seem the most likely explanation of the negative value of Γ(ClSiCl) obtained in this paper. Cotton,[24] however, has shown, using symmetry arguments, that all five d orbitals are available for π bonding in tetrahedral compounds. If this conclusion is correct, any competitive interaction would be unlikely, unless the various d orbitals differ greatly in their ability to act as π acceptors.

If the amount of π bonding were sufficiently great, a reverse inductive effect might be possible in which successive π-donor groups, by increasing the electron density at silicon, would make the silicon d orbitals less available to act as π acceptors toward additional groups. Such a reverse inductive effect may *possibly* be true of the Si–F bond, where there is seen in the nmr spectrum a shift of the proton resonance to higher fields as successive fluorines are substituted for hydrogen in the series $H_{4-n}SiF_n$ (n = 1–3),[25] indicating an increase in the shielding of the protons. It is unlikely for the Si–Cl bond, where the nmr chemical shifts in the corresponding compounds[25] are all in the direction expected for an electronegative substituent.

It is also possible that the large negative value obtained for Γ may not be real, but an artifact of the method of treating the data. In this respect it may be significant that the value of Γ(ClSiCl) calculated from the calorimetric data alone, while still negative, is much smaller. Since the electron impact data do not include any compounds with Si–Cl bonds, it is suprising that this inclusion has such a large effect on the chlorine bond interaction term. Although the results presented in Table IV indicate that possible inconsistencies between the electron impact and the calorimetric data are smaller than had at first seemed likely, it is still possible that there is some inconsistency.

Acknowledgment. The author gratefully acknowledges support from the Robert A. Welch Foundation, and the help of Mr. Norman Roberts in adapting a least-squares program to the requirements of these calculations.

(15) J. A. Conner, G. Finney, G. J. Leigh, R. N. Haszeldine, P. J. Robinson, R. D. Sedgwick, and R. F. Simmons, *Chem. Commun.*, 178 (1966).

(16) G. G. Hess, F. W. Lampe, and L. H. Sommer, *J. Amer. Chem. Soc.*, **87**, 5327 (1965).

(17) H. A. Bent, *Can. J. Chem.*, **38**, 1235 (1960).

(18) For the corresponding carbon compounds, Γ(ClCCl) is −0.25 kcal/mol (ref 3, p 594). The negative value is presumably due, in this case, to steric factors being more important than the inductive effect. For the silicon halides the inductive effect would be expected to be greater, and the steric effect less important.

(19) For a review with extensive references see E. A. V. Ebsworth, "Organometallic Compounds of the Group IV Elements," Vol. 1, A. G. MacDiarmid, Ed., Marcel Dekker, New York, N. Y., 1968, Chapter 1.

(20) H. H. Jaffe, *J. Phys. Chem.*, **58**, 185 (1954).

(21) D. R. Eaton and W. R. McClellan, *Inorg. Chem.*, **6**, 2134 (1967).

(22) E. A. V. Ebsworth, "Volatile Silicon Compounds," Macmillan, New York, N. Y., 1963, p 56.

(23) J. Schraml and V. Chvalovsky, *Collect. Czech. Chem. Commun.*, **31**, 503 (1966).

(24) F. A. Cotton, *J. Chem. Soc.*, 5269 (1960).

(25) E. A. V. Ebsworth and J. J. Turner, *J. Phys. Chem.*, **67**, 805 (1963).

Ion-Exchange Kinetics in Vermiculite

by W. Lutze* and N. Miekeley

Nuclear Chemistry Division, Hahn-Meitner-Institut, Berlin, Germany *(Received December 1, 1970)*

Publication costs assisted by the Hahn-Meitner-Institut

Ion-exchange rates have been measured for the Sr–Ba ion exchange and its reversal in vermiculite. The mathematical treatment of the exchange process has shown that the experimentally obtained curves could not be interpreted by the simple theory of Helfferich. Isotopic exchange experiments with biionic Sr–Ba vermiculites have revealed that the self-diffusion coefficients of Sr^{2+} and Ba^{2+} depend strongly on the ionic composition of the exchanger phase. Extension of the theoretical treatment by introduction of concentration dependent self-diffusion coefficients into the computation of Helfferich's interdiffusion coefficients yielded much better, in one direction even almost exact, agreement between theory and experiment.

Introduction

After the theory of ion-exchange kinetics by Helfferich and Plesset[1] the interdiffusion coefficient D_{AB} has to be calculated from the corresponding self-diffusion coefficients D_A and D_B

$$\dot{C}_A = D_{AB}\nabla C_A \tag{1}$$

with

$$D_{AB} = \frac{D_A D_B(Z_A^2 C_A + Z_B^2 C_B)}{D_A Z_A^2 C_A + D_B Z_B^2 C_B} \tag{2}$$

where C_A, C_B are the cationic fractions in the exchanger phase, and Z_A, Z_B the corresponding ionic valencies.

D_A and D_B are obtained from isotopic exchange experiments with the pure A and B forms of the ion exchanger. As an approximation these values are usually assumed to be independent of the concentrations of A and B which change during the exchange processes A → B and B → A, respectively. Furthermore, gradients of the thermodynamic activity coefficients in the solid phase and a possible water transport between the two phases are neglected by the simple form of Helfferich's theory. Nevertheless many ion-exchange rates can be explained by the unrefined theory, mainly those obtained from experiments with organic resins.[2,3]

Hitherto, very few experiments with mineral ion exchangers have been published. Rees and Brooke[4,5] have investigated the system Ca–Sr chabazite. They have found experimental rates for Ca → Sr and Sr → Ca, respectively, which were in the reversed sequence, as has been predicted by the basic Helfferich treatment.

Their experimental studies of the Sr–Ba-exchange isotherm had revealed a strongly S-shaped curve. This indicated the existence of gradients of activity coefficients in the chabazite phase. The authors have therefore used an extended theoretical treatment by introducing an activity correction term for the solid phase concentrations, which is usually done for interdiffusion in ion-exchange membranes. This leads to the expression

$$D_{AB} = \frac{D_A D_B\left(Z_A^2 C_A \dfrac{\partial \ln a_B}{\partial \ln C_B} + Z_B^2 C_B \dfrac{\partial \ln a_A}{\partial \ln C_A}\right)}{D_A C_A Z_A^2 + D_B C_B Z_B^2} \tag{3}$$

The introduction of eq 3 into the computations revealed the required reversal of the theoretical curves.[4] Yet the quantitative agreement between experimental and theoretical curves remained relatively poor.

For the system Ba–Sr vermiculite[6] the exchange rates in the two directions show a sequence also different from that one to be expected from Helfferich's original theory (see Figure 6a), after which an ion-exchange process requires less time in that direction where the ion with the higher mobility (higher self-diffusion coefficient) is in the solid phase initially. In vermiculite, however, the Sr–Ba exchange is faster than its reversal, although $D_{Ba} = 2D_{Sr}$ (for convenience $\bar{A}$ means that A is initially in the solid phase).

Previous investigations[6,7] have indicated that the Sr^{2+} and Ba^{2+} self-diffusion coefficients depend upon the concentrations of the ionic species in the vermiculite phase. Therefore it seemed not to be appropriate to take the D values obtained for the pure Sr and Ca forms of the exchanger in order to calculate interdiffusion coefficients. Moreover, looking thoroughly into the matter one finds out that this is not at all justified because these values are irrelevant to ion exchange.

(1) F. Helfferich, M. S. Plesset, *et al.*, *J. Chem. Phys.*, **28**, 418 (1958).
(2) F. Helfferich, *J. Phys. Chem.*, **66**, 36 (1962).
(3) F. Helfferich, *ibid.*, **67**, 1157 (1963).
(4) L. V. C. Rees and N. M. Brooke, *Trans. Faraday Soc.*, **64**, 3383 (1968).
(5) N. M. Brooke and L. V. C. Rees, *ibid.*, **65**, 2728 (1969).
(6) N. Miekeley and H. W. Levi, International Conference on Ion-Exchange in the Process Industries, London, July 1969.
(7) N. Miekeley, Dissertation, Berlin, 1968.

At any stage of a binary ion-exchange process diffusion of the one ion takes place in the presence of the other one. Therefore, one has to consider diffusion coefficients for the single ions which have been measured under appropriate conditions. These values might be more or less different from those obtained for the pure ionic forms.

In this investigation the concentration dependence of D_{Sr} and D_{Ba}, respectively, as well as the exchange isotherm have been measured. From the results it was concluded that a further modification of eq 2 was necessary to yield a better agreement between theoretical and experimental curves.

Experimental Section

The measurements were performed with the same experimental methods and devices and with the same vermiculite as has been reported elsewhere.[6-8]

Exchange Equilibria. A single vermiculite disk (d = 0.270 cm) was equilibriated at 71.5° with Ba–Sr salt solutions of various compositions, one of the ions being labeled with ^{133}Ba and ^{85}Sr, respectively. The total concentration of the solution was 0.1 equiv/l. The equivalent fractions of the ions in the solid phase were determined by counting the γ-ray activity of the labeled ion in the vermiculite sample.

Isotopic exchange rates were measured to determine the self-diffusion coefficients for biionic vermiculite. The radioactively labeled $\overline{Ba}$–$\overline{Sr}$ vermiculite was contacted with solutions of corresponding equilibrium compositions. This procedure ensured that the ionic composition of the solid phase remained constant while the isotopic exchange took place. The decreasing activity of the solid phase has been measured as function of time.

The exchange isotherm at 71.5° for $\overline{Ba}$ vermiculite + $Sr^{2+} \rightleftharpoons \overline{Sr}$ vermiculite + Ba^{2+} is shown in Figure 1. The results of the isotopic exchange experiments are given in Figures 2 and 3. $D(t/r^2)$ has been plotted against t[8,9] for various compositions of the exchanger phase. (D = self-diffusion coefficient of the ionic species to be investigated, r = radius of the cylindrical sample, t = time of exchange.) Figure 4 shows the dependence of D_{Ba} and D_{Sr} upon the cationic fraction of Ba and Sr, respectively. The values were obtained from the slopes of the curves in Figures 2 and 3. It can be seen from Figure 4 that D_{Ba} changes with concentration by a factor of 4. D_{Ba} decreases from 2.96 $\times 10^{-7}$ cm²/sec (C_{Ba} = 1.0) to 0.67 $\times 10^{-7}$ cm²/sec at Ba trace concentration, while D_{Sr} increases from 1.47 $\times 10^{-7}$ cm²/sec (C_{Sr} = 1.0) to 2.96 $\times 10^{-7}$ cm^{-2}/sec at Sr trace concentration. It is obvious from Figures 2 and 3 that this is in fact due to concentration only. The straight lines clearly demonstrate that ideal solid-state diffusion governs the whole exchange process in each case. Any change of diffusion mechanism can be excluded.

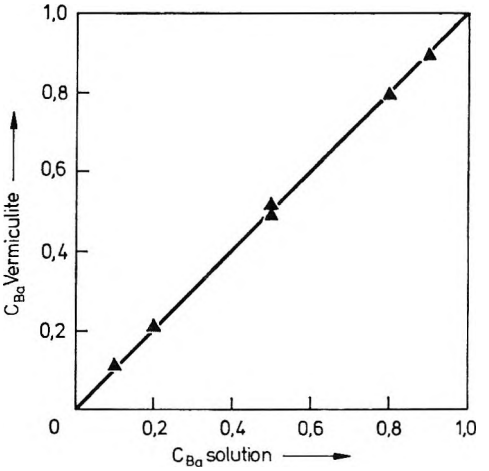

Figure 1. Ba–Sr exchange isotherm: temperature 71.5°; total concentration 0.1 equiv/l. C_{Ba} means cationic fraction of Ba.

Discussion

It can be seen from Figure 1 that the vermiculite has no measurable selectivity for Sr and Ba, respectively. Hence there are no activity coefficient gradients in the solid phase. Consequently the extended treatment with activity correction terms (eq 3) cannot yield any improvement for the theoretical curve. For the system under study eq 2 is still valid.

Because $C_A + C_B = 1$ and $Z_A = Z_B$ it reduces to

$$D_{AB} = \frac{D_A D_B}{(D_A - D_B)C_A + D_B} \tag{4}$$

On the other hand D_A and D_B depend strongly on the ionic fraction present in the solid phase. Therefore, we have introduced D_A and D_B as functions of ionic fractions. Equation 4 becomes then

$$D_{AB} = \frac{D_A(C_A)D_B(C_A)}{[D_A(C_A) - D_B(C_A)]C_A + D_B(C_A)} \tag{5}$$

D_{AB} values have been computed after eq 4 using the constant self-diffusion coefficients obtained for the pure Sr and Ba form, respectively, and after eq 5 using the data of Figure 4. The results are given in Figure 5. The D_{AB} curve calculated with variable self-diffusion coefficients is completely different from that obtained for constant self-diffusion coefficients.

It can be seen from Figure 4 that $D_{Sr} > D_{Ba}$ except for very high ionic fractions of Ba where $D_{Sr} \approx D_{Ba}$. This means that the experimental results—$\overline{Sr}$–Ba faster than $\overline{Ba}$–Sr—are now in qualitative agreement with Helfferich's rule which states that the ion-exchange process is faster when the ion with the higher mobility is in the solid phase initially.

(8) E. Hoinkis, H. W. Levi, W. Lutze, N. Miekeley, and T. Tamberg, *Z. Naturforsch. A*, 22, 220 (1967).

(9) K. E. Zimen and T. Lagerwall, EUR 1372.e (1964).

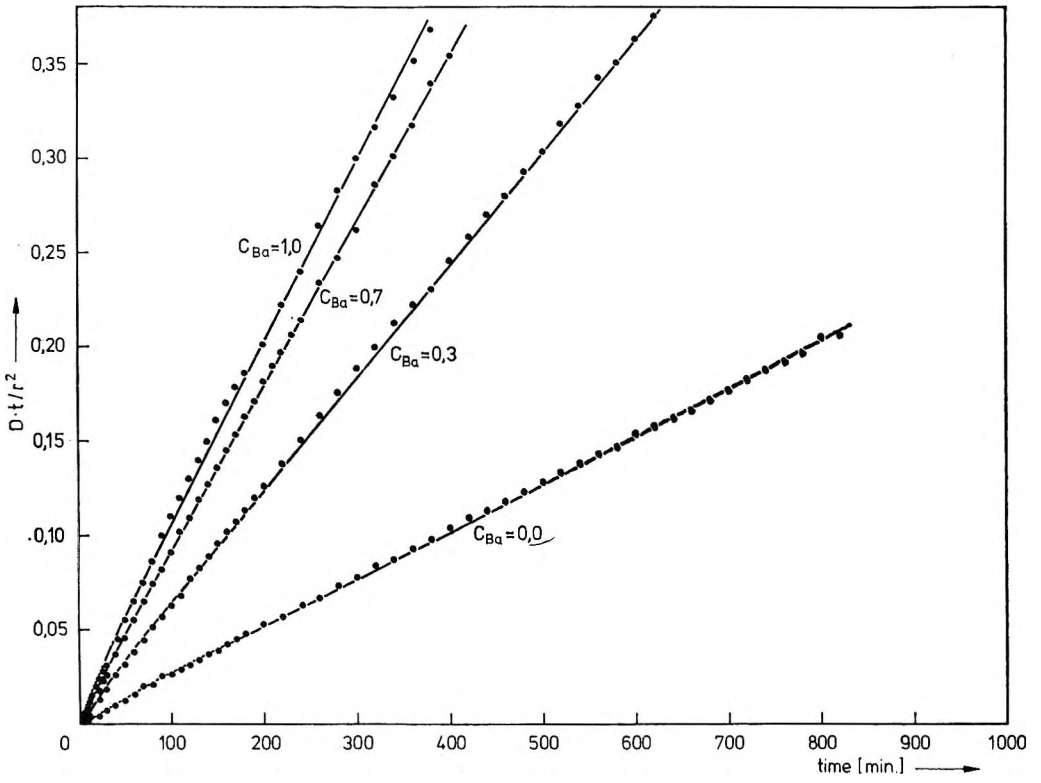

Figure 2. Self-diffusion of Ba^{2+} in Ba–Sr vermiculite (isotopic exchange).

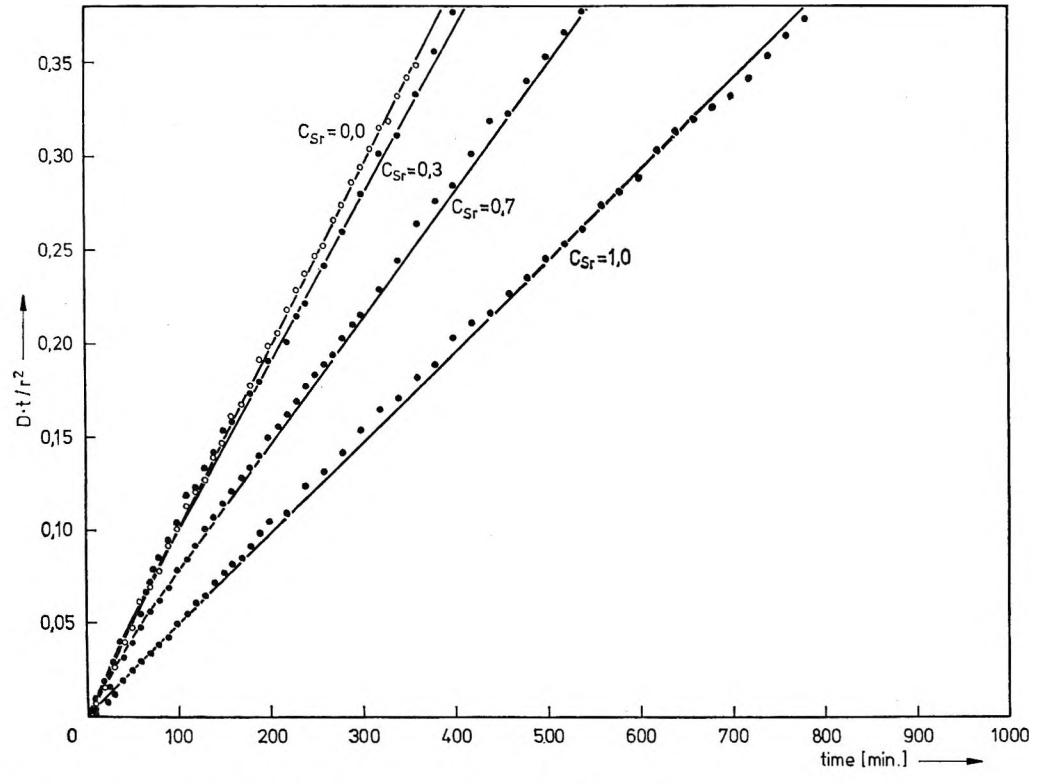

Figure 3. Self-diffusion of Sr^{2+} in Ba–Sr vermiculite (isotopic exchange).

Figure 5 shows that D_{AB} calculated from variable self-diffusion coefficients increases with increasing fraction of Ba in the vermiculite. That means increasing D_{AB} towards the periphery of the grain for the Sr–Ba exchange and *vice versa*. If the interdiffusion coefficient is highest at the periphery the process will be faster than in the opposite case, because sharper concentration profiles will be maintained throughout the process.

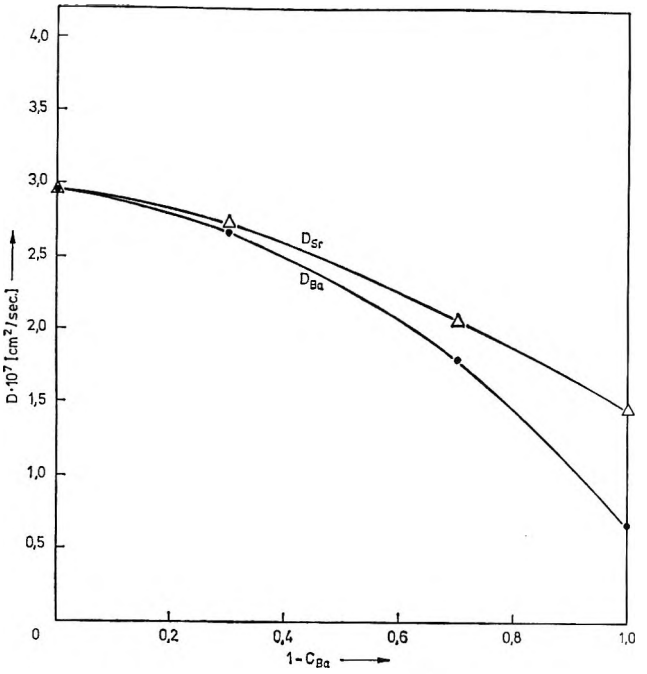

Figure 4. Sr^{2+} and Ba^{2+} self-diffusion coefficients *vs.* ionic fraction in the exchanger phase.

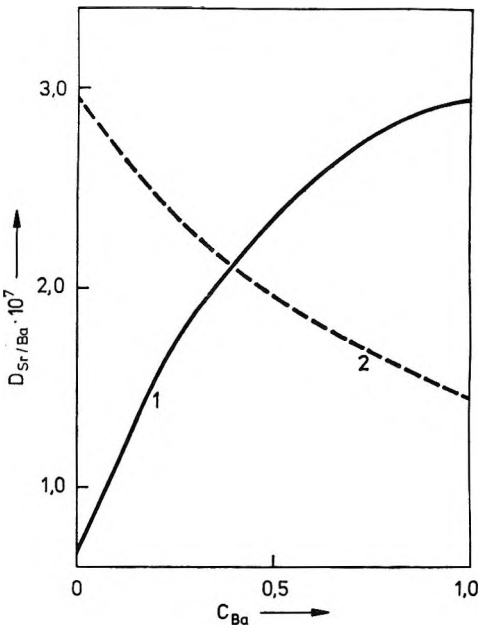

Figure 5. Interdiffusion coefficient *vs.* ionic fraction of Ba in the exchanger phase: 1, from concentration dependent self-diffusion coefficients; 2, from constant self-diffusion coefficients (after Helfferich).

The shape of the D_{AB} curve is reversed in case constant self-diffusion coefficients are used. Thus, it is quite clear that better agreement between experimental and calculated ion-exchange curves may be expected if variable self-diffusion coefficients are taken into consideration. These speculations were proved by calculating the ion-exchange process according to both models.

The theoretical curves for Sr vermiculite + Ba^{2+} and Ba vermiculite + Sr^{2+} are shown in Figure 6a and b, together with the experimental results. The theoretical curves of Figure 6a where self-diffusion coefficients were considered to be constant during ion-exchange are in the wrong sequence compared with the experimental ones. In contrast to this the introduction of concentration dependent self-diffusion coefficients into the theoretical treatment leads to the right sequence of

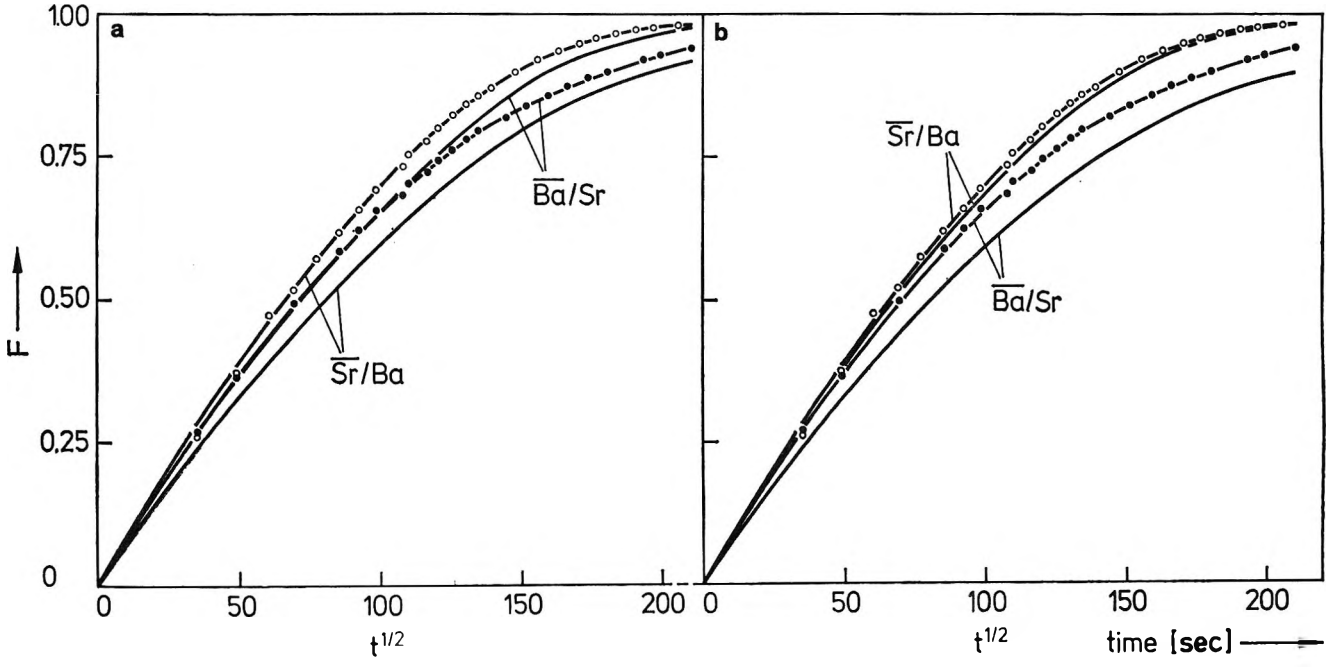

Figure 6. Comparison of experimental and theoretical ion-exchange curves: a, experimental curves and computed curves after Helfferich's theory with constant self-diffusion coefficients; b, experimental curves and computed curves with concentration dependent self-diffusion coefficients.

computed and measured curves (Figure 6b). Moreover, almost perfect agreement has been achieved for the Sr–Ba-exchange process. The remaining deviations between experimental and theoretical curves mainly for the Ba–Sr-exchange might possibly be explained by the fact that there is a slight water transport during ion exchange, which has been neglected in the theoretical treatment.

For the computation of the theoretical ion-exchange curve (fractional attainment of equilibrium as function of time) eq 1 was solved under the appropriate initial and boundary conditions. It has to be pointed out that no diffusion takes place perpendicular to the layers of the vermiculite crystal.[7] Thus, the mathematical problem reduces to the two-dimensional case. The standard forward-finite-difference technique used by Helfferich and Brooke was employed. The calculations have been performed using the Fortran IV computer program written by N. M. Brooke for the above mentioned Sr–Ca chabazite system. The program was adapted to the present case.

Finally the question shall be discussed of why the self-diffusion coefficients are concentration dependent.

According to Walker[10] Ba^{2+} is tetrahedrally surrounded by water molecules, whereas hydrated Sr^{2+} has an octahedral configuration in vermiculite. On the other hand we have found[6] that wet crystals of Sr vermiculite and Ba vermiculite have almost the same layer distance (15.2 and 14.7 Å, respectively). This seems to indicate that in Ba vermiculite, although the overall water content is the same as that in Sr vermiculite, a larger fraction of the water is unbound. Therefore, one has to assume that there is a higher degree of order in the water arrangement in Sr vermiculite than in Ba vermiculite. Consequently a higher mobility of whatever ion is being looked upon has to be expected with increasing Ba content of the vermiculite.

Acknowledgment. The authors are indebted to Dr. L. V. C. Rees and Dr. N. M. Brooke for helpful discussions and for the copy of the Fortran IV program. Furthermore, one of us thanks the "Fonds der Chemie" for financial support. Thanks are due the "Deutsche Forschumpgemeinschaft" for funding a study trip to London. The computations were performed at the department of mathematics, Hahn-Meitner-Institut, with a Siemens 4004/55.

(10) G. F. Walker, "X-ray Identification and Structure of the Clay Minerals," Mineralogical Society of Great Britain, Monograph, 1951.

Spectrophotometric Dissociation Field Effect Kinetics of Aqueous Acetic Acid and Bromocresol Green[1a]

by James J. Auborn,[1b] Percy Warrick, Jr., and Edward M. Eyring*

Department of Chemistry, University of Utah, Salt Lake City, Utah 84112 *(Received February 16, 1971)*

Publication costs assisted by the U. S. Air Force Office of Scientific Research

The acid–base dissociation kinetics of dilute aqueous acetic acid at 25° have been investigated using a square-wave dissociation field effect apparatus with spectrophotometric detection. The acetic acid equilibrium was coupled to that of a somewhat slower optical indicator, bromocresol green. Direct spectrophotometric observation of the indicator alone was used first to determine its dissociation kinetics. Relaxation times as fast as 60 nsec were measured using either the acid or basic absorption peaks of the indicator. Indicator rate constants were determined to be $5.4 \times 10^{10}\ M^{-1}\ \text{sec}^{-1}$ for ion recombination and $7.5 \times 10^{5}\ \text{sec}^{-1}$ for dissociation. The indicator was then coupled to the faster acetic acid system, and the kinetics of the coupled system followed by observation of the indicator dianion. The kinetic data were analyzed for the coupled system to yield an ion recombination rate constant for acetic acid of $7.2 \times 10^{10}\ M^{-1}\ \text{sec}^{-1}$ and a dissociation rate constant of $1.3 \times 10^{6}\ \text{sec}^{-1}$. This specific rate for the ion recombination of acetic acid is in closer agreement than previously reported values to that predicted by the Debye–Eigen–Smoluchowski relation.

Introduction

The ion recombination rate constant of acetic acid was measured 15 years ago by Eigen and Schoen by amplitude dispersion of the dissociation field effect (DFE) as $4.5 \times 10^{10}\ M^{-1}\ \text{sec}^{-1}$ at 25° and $10^{-4}\ M$ ionic strength.[2] A more recent investigation utilizing a square-wave DFE apparatus and conductometric de-

(1) (a) This work was supported by AFOSR(SRC)-OAR, USAF, Grant No. 69-1717-D. (b) NDEA Title IV Fellow.

(2) M. Eigen and J. Schoen, *Z. Elektrochem.*, 59, 483 (1955).

tection led to an ion recombination rate constant for acetic acid of $1.1 \times 10^{10}\ M^{-1}\ \text{sec}^{-1}$ under similar conditions.[3] Theories of diffusion controlled reactions in dilute aqueous solution predict an ion recombination rate constant about two times larger than Eigen's original value rather than four to five times lower.[4] The present study of acetic acid was undertaken in an attempt to resolve this discrepancy.

Our DFE apparatus produced a high-voltage square-wave pulse immediately following which the change in optical density of the reaction mixture was observed in zero field with a photomultiplier. Since acetic acid does not absorb at a visible wavelength, a colored acid–base indicator was used. Bromocresol green (3,3′,5,5′-tetrabromo-*m*-cresolsulfonphthalein) with a $pK_a = 4.90$[5] near that of acetic acid, $pK_a = 4.756$,[6] is ideally suited for this purpose. However, it was first necessary to determine the dissociation kinetics of the aqueous indicator alone.

The dianion form of aqueous bromocresol green has an intense absorption maximum at 615 nm, while the acid form absorbs at 410 nm. These maxima are well separated from each other, so it is possible to follow either the change in concentration of the indicator dianion or the anion in kinetic experiments. These properties make bromocresol green particularly useful for following rates of reactions associated with pH changes.

When an indicator is used in kinetic experiments, it is usually chosen so that the rate of the indicator reaction is much faster than the rates of the reactions being studied and can be ignored or approximated. A quantitative knowledge of the indicator rate constants makes it possible to couple the indicator reaction to other fast reactions involving pH changes and thereby determine their kinetics. This has been done for the acetic acid system which in this case is even faster than the indicator system.

Experimental Section

Acetic acid solutions were prepared by diluting Baker and Adamson ACS grade glacial acetic acid with redistilled demineralized water. This stock solution was titrated with certified primary standard THAM [tris(hydroxymethyl)aminomethane] from Fisher Scientific Co. and found to be $9.06 \times 10^{-3}\ M$. Quantitative dilution of this stock solution yielded the solutions used in these experiments.

Bromocresol green from Matheson Coleman and Bell was recrystallized from boiling glacial acetic acid and vacuum dried for several hours over refluxing benzene. It was stored over Drierite in a desiccator and dried for 1 hr at 90° in an oven before being weighed out on a Mettler H16 analytical balance.

All water used in these experiments was distilled, Deeminized, and redistilled in an all glass system. Immediately before use, this water was vigorously boiled for several minutes and ultrasonicated to remove dissolved gases. Dilute hydrochloric acid or sodium hydroxide solutions were used to adjust the pH of solutions as measured on a Beckman Model 1019 pH meter equipped with Beckman 39402 reference and 39301 glass electrodes. pH measurements were made in the cell used for kinetic experiments immediately before and after DFE experiments and were constant within ±0.02 pH unit.

The reaction cell was manufactured from a 2-in. diameter high-density polyethylene with 1.5-cm diameter polished stainless steel electrodes with flat faces located 4.1 mm apart. The upper electrode was hollow and was used for thermostating the cell to ±0.05° by circulating water inside the electrode with a Lauda K2 circulator. The cell windows were 3 mm × 12 mm cross-section Plexiglass strips with flat polished ends, mounted with a Varian Torr seal into horizontal slits in the cell located midway between the electrodes. The optical path length inside the cell was 15 mm. The cell was coaxially mounted in a copper can so that the electrical discharge path was from the lower to upper electrode and down around the outside of the cell to the ground. Rectangular slits were cut into this can for the light path.

A 30–52-kV square-wave pulse was generated by charging a low inductance 0.005-μf high-voltage plastic capacitor from a high-voltage power supply. One triggered EG & G, Inc. GP-15B spark gap was used to apply the voltage on the capacitor to the cell and an identical triggered spark gap was used to discharge the capacitor to ground 0–29 μsec later. These experiments utilized 45-kV pulses 0.3–3 μsec long. The pulse fall time was 22 nsec. The maximum field strength attainable in the cell described in the previous paragraph was 127 kV/cm.

The optical system consisted of a 150-W quartz–iodine tungsten lamp powered by a constant voltage power supply, a Bausch and Lomb 1200 line/mm grating monochromator, and lenses to focus the light passing through the cell to the end of an 8-ft long American Optical Corp. LGM-3 glass fiber optic. The fiber optic led to a Fairchild KM2433 photomultiplier tube located as far from the cell as possible to avoid electrical noise associated with the generation of the high-voltage pulse. The photomultiplier was operated with a 15-kilohm dynode string powered by a Model 412B Fluke HV power supply. Either a 3-kilohm or a 300-ohm termination resistor was used. The light intensity and high voltage applied to the photomultiplier were adjusted so that the photomultiplier anode current was 1 mA under

(3) B. R. Staples, D. J. Turner, and G. Atkinson, *Chem. Instrum.*, 2, 127 (1969).

(4) E. M. Eyring and B. C. Bennion, *Annu. Rev. Phys. Chem.*, 19, 129 (1968).

(5) I. M. Kolthoff, *J. Phys. Chem.*, 34, 1466 (1930).

(6) H. S. Harned and R. W. Ehlers, *J. Amer. Chem. Soc.*, 55, 652 (1933).

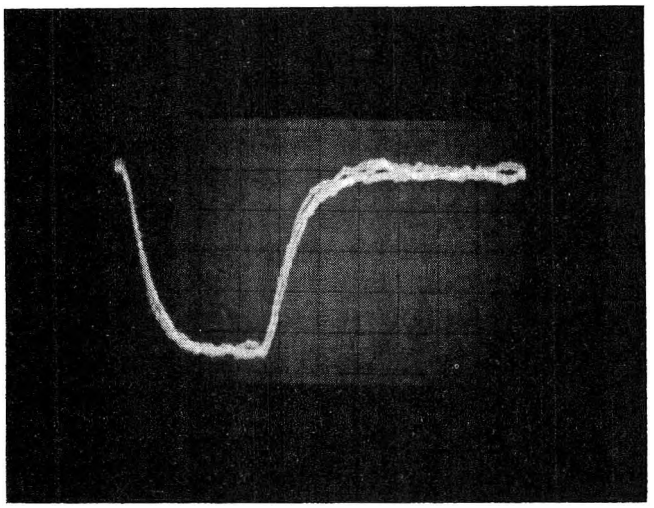

Figure 1. Dissociation field effect relaxation of 50 μM aqueous bromocresol green, at 25°: vertical axis, 100 mV/division; horizontal axis, 0.5 μsec/division. Direction of increasing light intensity is toward top of page. Steady-state light intensity is 3.0 V across 3 kilohm termination. Three traces of successive 45-kV pulses 1.8 μsec long spaced 60 sec apart are shown.

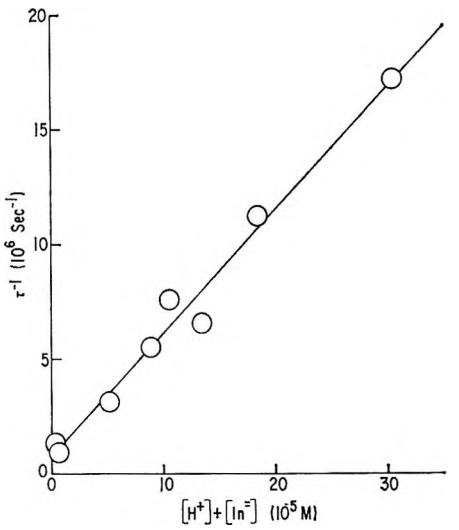

Figure 2. Plot of dissociation field effect reciprocal relaxation times, τ^{-1}, *vs.* ([H$^+$] + [In^{2-}]) where the latter are equilibrium concentrations of hydronium ion and bromocresol green dianion, respectively, at 25°.

steady-state conditions. The photomultiplier output was fed directly into a Hewlett-Packard 183A oscilloscope with an 1801 vertical amplifier and an 1840A time base. The 3-kilohm terminating resistance was used for the slower relaxations, while the 300-ohm terminator was used for relaxations shorter than 0.3 μsec. The light to dark photomultiplier voltage was 100 times as great as the high-frequency noise, while the amplitude change attributable to the relaxation was usually 10 times as great as the high-frequency noise.

Oscilloscope traces were photographed with a Hewlett-Packard 195A oscilloscope camera on Type 47 Polaroid film. The pictures were analyzed for a single relaxation by determining the slope of a log amplitude *vs.* time graph hand plotted on semilog paper. A typical oscilloscope photograph is shown in Figure 1. The relaxation analyzed was that observed after the high-voltage pulse was turned off. Errors of a factor of 2 or more are possible if the relaxation within the field is analyzed. These errors result from a decrease in the high-voltage pulse due to conductance of the solution within the cell and the accompanying temperature rise. This temperature jump within the pulse combined with the pulse degradation can either increase or decrease the observed relaxation time depending on the reaction studied but will have no effect on the relaxation outside the pulse other than to shift the equilibrium temperature at which the reaction is observed. In our experiments, the pulse was shortened so that no more than 10% pulse degradation occurred resulting in less than 0.1° temperature rise per experiment.

The ionic strength μ of our aqueous bromocresol green solutions was variable but never exceeded 3×10^{-4} M. At this ionic strength the Debye–Hückel activity coefficient for HCl at 25° is 0.98. In the case of our aqueous mixtures of acetic acid and bromocresol green the ionic strengths were even smaller. Therefore, activity corrections in our calculations of rate constants would be much smaller than the inaccuracies introduced by experimental errors in the relaxation times and thus activity coefficients were not used in our calculations.

Data and Results

The bromocresol green indicator reaction may be written

$$H^+ + In^{2-} \underset{k_{21}}{\overset{k_{12}}{\rightleftharpoons}} HIn^- \qquad (1)$$

where In^{2-} represents the indicator dianion and HIn^- represents the indicator anion. The relaxation time τ is given by

$$\tau^{-1} = ([H^+] + [In^{2-}])k_{12} + k_{21} \qquad (2)$$

Our data for the bromocresol green dissociation are given in Table I. A graph of τ^{-1} *vs.* ([H$^+$] + [In^{2-}]) is plotted in Figure 2. The least-squares straight line has a slope $k_{12} = 5.4 \times 10^{10}\ M^{-1}$ sec $^{-1}$ and an intercept $k_{21} = 7.5 \times 10^5$ sec^{-1} corresponding to the ion recombination and dissociation rate constants, respectively. The equilibrium constant $K_i = k_{21}/k_{12}$ from these data is 1.4×10^{-5} M. This equilibrium constant yields an indicator $pK_a = 4.86$ in excellent agreement with Kolthoff's[5] titrimetric $pK_a = 4.90$ at 25° and zero ionic strength.

In the case of the coupled acetic acid–bromocresol green system we must consider the indicator ion recombination–dissociation, the ion recombination–dissociation for acetic acid, and the possibility of proton ex-

Table I: Dissociation Field Effect Relaxation Data for Aqueous Bromocresol Green at 25°

c_i,[a] 10^{-5} M	pH[b]	τ, μsec[c]	$\{[H^+] + [In^{2-}]\}$, 10^{-5} M[d]
0.202	5.53	0.86	0.46
0.202	5.25	0.99	0.70
5.06	4.40	0.32	5.12
5.06	4.08	0.18	8.97
10.11	4.02	0.127	10.64
10.11	3.90	0.151	13.52
10.11	3.75	0.089	18.45
10.11	3.52	0.058	30.6

[a] Total molar concentration of bromocresol green. [b] Average of pH measured in the sample cell before and after DFE experiments. [c] Experimental relaxation time. [d] Sum of equilibrium concentrations calculated from c_i, pH, and pK_a = 4.90.

change between acetic acid and indicator. The complete coupled mechanism may be written

$$\begin{array}{ccc} In^{2-} + H^+ + A^- & & \\ {\scriptstyle k_{12}}\,\rightleftharpoons\,{\scriptstyle k_{21}} & & {\scriptstyle k_{13}}\,\rightleftharpoons\,{\scriptstyle k_{31}} \\ HIn^- + A^- & \underset{k_{32}}{\overset{k_{23}}{\rightleftharpoons}} & In^{2-} + HA \end{array} \quad (3)$$

where HA represents acetic acid, A^- represents acetate anion, and the other symbols are defined as above. Standard kinetic analysis yields two simultaneous differential equations from which the two relaxation times may be calculated by evaluating the determinant[7]

$$\begin{vmatrix} (\alpha_{11} + \epsilon_a) - \tau^{-1} & (\alpha_{12} - \epsilon_i) \\ (\alpha_{21} - \epsilon_a) & (\alpha_{22} + \epsilon_i) - \tau^{-1} \end{vmatrix} = 0 \quad (4)$$

where

$$\alpha_{11} = ([H^+] + [In^{2-}])k_{12} + k_{21} = ([H^+] + [In^{2-}] + K_i)k_{12} \quad (5)$$

$$\alpha_{12} = [In^{2-}]k_{12} \quad (6)$$

$$\alpha_{21} = [A^-]k_{13} = c_{21}k_{13} \quad (7)$$

$$\alpha_{22} = ([H^+] + [A^-])k_{13} + k_{31} = ([H^+] + [A^-] + K_a)k_{13} = c_{22}k_{13} \quad (8)$$

$$\epsilon_i = [HIn^-]k_{23} + [In^{2-}]k_{32} \quad (9)$$

$$\epsilon_a = [A^-]k_{23} + [HA]k_{32} \quad (10)$$

The α_{11} and α_{12} terms are determined from the bromocresol green data. Given the equilibrium constant for acetic acid, the α_{21} and α_{22} terms are determined except for k_{13}. The exchange terms ϵ_i and ϵ_a are small corrections and can be estimated from the difference in pK_a between acetic acid and the indicator from Eigen's data on proton exchange between acetic acid and various proton acceptors.[7] Eigen's data show $k_{23} \approx k_{32} \approx 3 \times 10^8$ M^{-1} sec $^{-1}$ so the exchange terms (9) and (10) may be approxmated as $\epsilon_a \approx k_{23}c_a$ and $\epsilon_i \approx k_{23}c_i$, where c_a is the total concentration of acetic acid in all forms and c_i is the total concentration of indicator in all forms. In the worst case (line four of Table II) the assumption

Table II: Dissociation Field Effect Relaxation Data for a Coupled Aqueous Acetic Acid–Bromocresol Green System at 25°

c_a,[a] 10^{-6} M	c_i,[b] 10^{-6} M	pH[c]	τ,[d] μsec	k_{13},[e] 10^{10} M^{-1} sec^{-1}
4.52	50.6	4.30	0.195	7.38
4.52	50.6	4.38	0.170	9.62
4.52	50.6	4.52	0.204	9.70
4.52	50.6	4.64	0.285	7.69
45.2	5.06	4.62	0.272	5.96
45.2	5.06	4.77	0.304	5.56
45.2	5.06	5.06	0.312	5.44
18.12	20.22	4.28	0.229	5.75
18.12	20.22	4.57	0.258	7.26
18.12	20.22	4.70	0.290	7.06

[a] Total molar concentration of acetic acid. [b] Total molar concentration of bromocresol green. [c] Average of pH measured in the sample cell before and after DFE experiments. [d] Faster of two experimental relaxation times. [e] Specific rate of reaction $H^+ + A^- \xrightarrow{k_{13}} HA$ calculated from eq 11 and these data.

that $k_{23} \approx k_{32} \approx 3 \times 10^3$ M^{-1} sec^{-1} rather than 3×10^8 M^{-1} sec^{-1} leads to a $k_{13} \approx 7.5 \times 10^{10}$ M^{-1} sec^{-1} which differs by less than 3% from the value of k_{13} shown in the table. Thus the value of k_{13} that we report is quite insensitive to possible error in our estimate of k_{23} and k_{32}. Substituting (5)–(10) into (4) and solving for k_{13} results in the following expression used to evaluate the acetic acid ion recombination rate constant

$$k_{13} = \frac{\tau^{-1}[\tau^{-1} - (\alpha_{11} + \epsilon_a + \epsilon_i)] + \alpha_{11}\epsilon_i + \alpha_{12}\epsilon_a}{c_{22}[\tau^{-1} - (\alpha_{11} + \epsilon_a)] + c_{21}(\alpha_{12} - \epsilon_i)} \quad (11)$$

where τ^{-1} is the reciprocal of either of the two observed relaxations. The faster of these relaxations was most accurately measured and was used in our analysis. The long relaxation, greater than 1 μsec, could be seen in several of our experiments but was more uncertain.

The acetic acid data are tabulated in Table II. The average ion recombination rate constant is $k_{13} = 7.2 \pm 1.6 \times 10^{10}$ M^{-1} sec^{-1}. When taken with the titrimetric equilibrium constant for this system, this yields an acetic acid dissociation rate constant of 1.3×10^6 sec^{-1}. It is interesting to note that the acetic acid is faster than bromocresol green for both recombination and dissociation.

Discussion

The accuracy of the bromocresol green data is not open to serious doubt. The kinetic pK_a agrees to within 0.04 pK unit of the equilibrium pK_a of 4.90.[5] The $k_{12} = 5.4 \times 10^{10}$ M^{-1} sec^{-1} also agrees with the ion re-

(7) M. Eigen, *Angew. Chem., Int. Ed. Engl.*, **3**, 1 (1964).

combination rate constants determined for other sulfonphthaleins listed in Table III, and is consistent with the upper limiting value calculated from the Debye equation for diffusion controlled reaction between a proton and a spherical dianion in water at 25° and zero ionic strength.[8]

Table III: Rate Constants for Several Aqueous Sulfonphthalein Indicators

	k_{12}, 10^{10} M^{-1} sec^{-1}	k_{21}, sec^{-1}	Conditions	Method
Bromocresol purple[a]	8.0	2.4×10^4	15°	DFE
Phenol red[a]	7.2	4.9×10^2	15°	DFE
Chlorophenol red[b]	2.3	1.9×10^2	15° 0.1 M KNO_3	T-jump
Bromocresol green	5.4	8.5×10^5	25°	This work

[a] G. Ilgenfritz, Doctoral Dissertation, Georg-August University, Gottingen, 1966. [b] M. Eigen and G. G. Hammes, *J. Amer. Chem. Soc.*, **82**, 5951 (1960).

Our recombination rate constant for acetic acid is significantly faster than that reported most recently using conductometric detection[3] and slightly faster than that determined by Eigen and Schoen.[2] Our apparatus has been shown to be sufficiently fast for this system. The fastest relaxation time observed for bromocresol green alone was 0.058 μsec, more than three times as fast as the shortest relaxation observed for the coupled system. Our electrodes were fairly large and over 4 mm apart so we have minimized polarization effects that might have led to errors in the conductometric result. Our $k_{13} = 7.2 \times 10^{10}$ M^{-1} sec^{-1} agrees well with the acetic acid ion recombination rate constant estimated by the Debye–Eigen–Smoluchowski relation in aqueous solution at 25°,[8] when this theoretical result is corrected to 10^{-4} M ionic strength and the hydrodynamic interaction between reacting solute species described by Friedman[9] are taken into account: k_{13} (theor) $= 7.6 \times 10^{10}$ M^{-1} sec^{-1}. A further correction for the nonsphericity of the acetate ion would result in a still smaller theoretical k_{13}, but whether this factor decreases the rate constant by as much as $^1/_2{}^7$ is open to question.

Acknowledgment. The design and construction of the high-voltage pulse generator and control circuitry by Steven L. Olsen, Ronald L. Silver, and Lloyd P. Holmes is gratefully acknowledged. This work was sponsored by AFOSR(SRC)-OAR, USAF, Grant No. 69-1717-D.

(8) H. Eyring and E. M. Eyring, "Modern Chemical Kinetics," Reinhold, New York, N. Y., 1963.
(9) H. L. Friedman, *J. Phys. Chem.*, **70**, 3931 (1966).

The Ionization of Trichloroacetic Acid in Aqueous Solutions

by O. D. Bonner,* H. B. Flora, and H. W. Aitken

Department of Chemistry, University of South Carolina, Columbia, South Carolina 29208 *(Received January 28, 1971)*

Publication costs borne completely by The Journal of Physical Chemistry

The degree of ionization of trichloroacetic acid in aqueous solutions has been calculated at several concentrations from Raman measurements in which the intensity of the carboxylate band is compared with that of the C–Cl vibrational band. These values have been compared with literature values determined by Raman and nmr measurements and found to be in satisfactory agreement in dilute solutions. A larger degree of ionization was found in more concentrated solutions. Activity and osmotic coefficients are reported for sodium trichloroacetate and these are used to calculate an ionization constant of 3.2 ± 0.1 for trichloroacetic acid.

Introduction

There have been at least four studies of the ionization of trichloroacetic acid in aqueous solutions, the most recent of which is that of Covington and coworkers.[1] They summarize the previous work in which ionization constants ranging from 0.232 to 1.0 have been found and report a new value of 2 to 5 based upon Raman and nmr measurements. The large uncertainty in the value of the constants is caused primarily by the uncertainty in the values of the activity coefficient corrections at various concentrations. One of the present authors

(1) A. K. Covington, J. G. Freeman, and T. H. Lilley, *J. Phys. Chem.*, **74**, 3773 (1970).

had overcome this difficulty[2] in determining the ionization constant of iodic acid and it was the initial intent of this work to merely make the necessary activity coefficient corrections and perform the extrapolation to infinite dilution in order to evaluate the thermodynamic constant. It became necessary, however, as will be indicated in the subsequent discussion to redetermine some of the values of α, the degree of ionization, and new Raman data are also reported.

Experimental Section

Osmotic and Activity Coefficients. The osmotic and activity coefficients of the sodium salt of trichloroacetic acid were determined by the usual isopiestic technique with sodium chloride solutions being used as references. Sodium trichloroacetate was prepared by the careful neutralization of vacuum distilled trichloroacetic acid. It was then dried in a vacuum oven at 65°.

Raman Measurements. The Raman spectra were recorded using a Spex Ramalog spectrophotometer with a Spectra Physics Model 125 helium–neon gas laser. The frequencies recorded for all sharp lines are expected to be accurate to ± 3 cm^{-1}. Band intensities were reproducible to 1–1.5%.

Results

The Raman spectrum of a 1.01 *M* solution of sodium trichloroacetate is shown in Figures 1 and 2. The intensities of the ν_1 band (C–O stretch) at 1344 cm^{-1} and the band at 434 cm^{-1} (C–Cl stretch) are used for the calculations in this work. It may be noted that a relatively flat base line was obtained even when considerable amplification was used. The spectrum of a solution of sodium perchlorate over the range 1200–1500 cm^{-1}, in which no band occurs, has the same near zero slope as the base upon which the carboxylate band is resting. This is in sharp contrast to the statement by Covington that it is situated on a sloping base line and that intensities could be estimated to only 4–5%. The differences in the observed spectra are undoubtedly caused in part by a difference in exciting sources. Solutions of organic compounds fluoresce much more when a blue source (Toronto arc) is used than when a red source is used. The degree of ionization of the acid in the various solutions was calculated from a comparison of the ratio of the intensities of the 1344- and 434-cm^{-1} bands with the ratio in a solution of the sodium salt for which the ionization is complete. This ratio was confirmed to be independent of solution concentration for the sodium salt and no difference was found between ratios of band maxima and ratios of integrated areas. Values of α for acid solutions at six concentrations are given in Table I.

Osmotic and activity coefficients of sodium trichloroacetate as determined from isopiestic comparison with sodium chloride standards are presented in Table II. These coefficients are found to be larger than those of

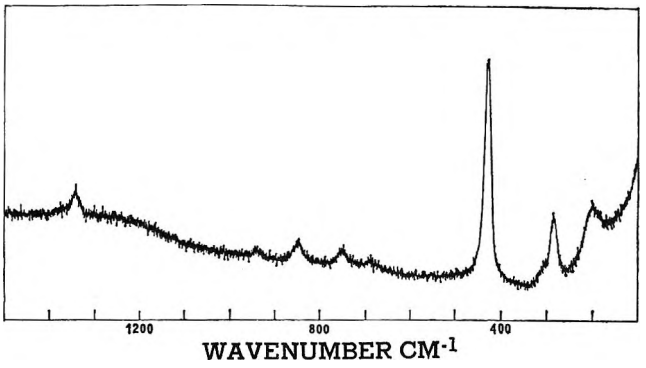

Figure 1. Raman spectrum of 1.01 *M* sodium trichloroacetate: full scale sensitivity 0.1 × 10^{-6} A; rise time, 0.3 sec; slit width 12 cm^{-1}; slit height 5 min; dynode voltage, 1800 V.

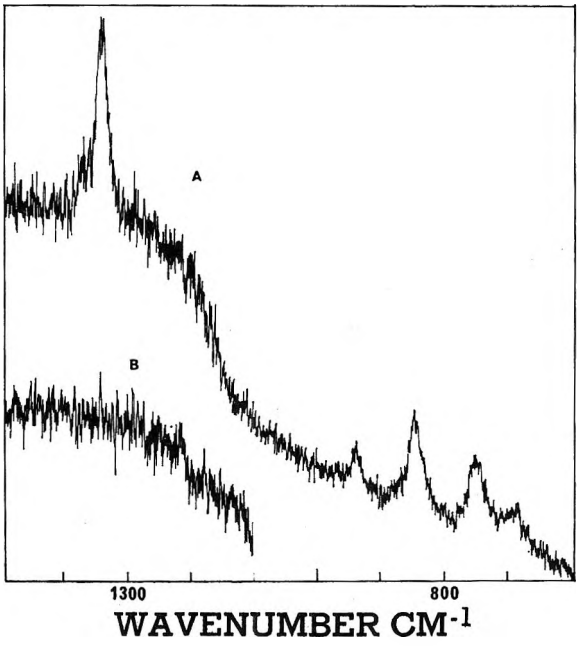

Figure 2. Raman spectrum of 1.01 *M* sodium trichloroacetate: (A) full scale sensitivity 0.03 × 10^{-6} A; rise time, 1 sec; slit width 12 cm^{-1}; slit height 5 min; dynode voltage, 1800 V; (B) base line.

Table I: Degree of Ionization of Trichloroacetic Acid as Determined from Raman Measurements

Concentration, mol/l.	Degree of ionization
0.31	0.93
0.63	0.88
0.94	0.82
1.25	0.76
1.57	0.66
2.27	0.57
3.35	0.42

(2) J. R. Durig, O. D. Bonner, and W. H. Breazeale, *J. Phys. Chem.*, 69, 3886 (1965).

sodium chloride and slightly larger than those of sodium acetate.

Table II: Osmotic and Activity Coefficients of Sodium Trichloroacetate at 25°

M	ϕ	γ
0.1	0.944	0.797
0.2	0.947	0.768
0.3	0.955	0.758
0.4	0.962	0.757
0.5	0.972	0.759
0.6	0.983	0.765
0.7	0.994	0.770
0.8	1.005	0.778
0.9	1.015	0.788
1.0	1.025	0.797
1.2	1.045	0.818
1.4	1.058	0.839
1.6	1.074	0.857
1.8	1.085	0.877
2.0	1.096	0.894
2.5	1.123	0.941
2.7	1.130	0.958

Discussion

It has been adequately emphasized[1,2] that ionic rather than stoichiometric activity coefficients are necessary for the correction of the quotient

$$k = \frac{\alpha^2 C}{1 - \alpha}$$

in order to determine the thermodynamic ionization constant. The former may not be determined directly for a weak acid and the latter are also not possible by isopiestic methods for trichloroacetic acid because of its volatility. Emf measurements would be difficult because of the lack of a reversible trichloroacetate electrode. Ionic activity coefficients may be estimated, however, for many acids by a technique which was presented previously. Activity coefficient data[3] are available for five strong acids[4] and their sodium salts. It may be noted that for acids and salts containing anions as large or larger than iodide there is a constant ratio of acid to salt activity coefficient values at any concentration up to 1.4 M. The ratio varies slightly for the bromides and somewhat more for the chlorides. With this knowledge and the values of the sodium trichloroacetate activity coefficients one may now estimate the *ionic* activity coefficients of the trichloroacetic acid. The product $K\beta$ may now be calculated from the relationship

$$K\beta = \frac{\alpha^2 C}{1 - \alpha} f_{\pm}^2$$

where $f_{\pm}$ is the ionic activity coefficient of the acid and β is the activity coefficient of the un-ionized acid. An extrapolation of $K\beta$ to infinite dilution yields the thermodynamic ionization constant.

A plot of the degree of ionization, α, as a function of concentration (Figure 3) reveals that there is substantial agreement among the three sets of data up to concentrations of about 2 M. Values of α taken from the smoothed curve (Figure 3) of the three sets of data at even concentrations were used to calculate the values of $K\beta$ (Table III). The value of $K = 3.2 \pm 0.1$ which is obtained (Figure 3) falls nearly in the center of the range $5 > K > 2$ reported by Covington.[1] This is true, however, in spite of the fact that the activity coefficient corrections are larger than those which were used for his estimate. The behavior of $K\beta$ is quite reasonable in that one would expect the activity coefficient of the un-ionized acid to remain relatively close to unity. The approximate values of β are 0.97 at 1 M and 0.93 at 1.5 M.

Table III: Calculation of the Ionization Constant of Trichloroacetic Acid

C	α	αC	$k = \frac{\alpha^2 C}{1 - \alpha}$	$\gamma_{\pm}$ salt	$f_{\pm}$ acid	$K\beta$
0.50	0.901	0.450	4.09	0.758	0.869	3.09
0.75	0.855	0.641	3.78	0.767	0.923	3.22
1.00	0.805	0.805	3.32	0.778	0.976	3.16
1.25	0.756	0.945	2.93	0.792	1.028	3.10
1.50	0.708	1.062	2.58	0.803	1.071	2.96
1.75	0.660	1.155	2.24	0.813	1.109	2.76
2.00	0.612	1.224	1.93	0.820	1.137	2.50
2.25	0.569	1.280	1.69	0.826	1.163	2.29
2.50	0.532	1.330	1.51	0.832	1.191	2.14

It should be noted that the values of α obtained in this work for solutions more concentrated than 2.0 M are substantially larger than those reported by Covington. It is felt that the present data are more accurate for three reasons. (1) The use of the C–Cl band as an internal reference is inherently more accurate since it eliminates errors in sample positioning and there is less error due to instrumental drift as comparisons are made in a short time interval. (2) The use of the helium–neon laser as an exciting source reduces appreciably the fluorescence which is present in concentrated solutions of organic compounds and this requires less zero suppression and yields a flatter base line. (3) A calculation of the concentration of ionized acid, αC, shows that a maximum value is reached in about 2.3 M solutions using the nmr data and about 3.0 M solutions using the Raman data of ref 1. It seems unreasonable that the concentration of ionized acid should *decrease* with increasing stoichiometric concentration in solu-

(3) R. A. Robinson and R. H. Stokes, "Electrolytic Solutions," Butterworths, London, 1959.

(4) Nitric acid is essentially completely ionized in the concentration range of interest.

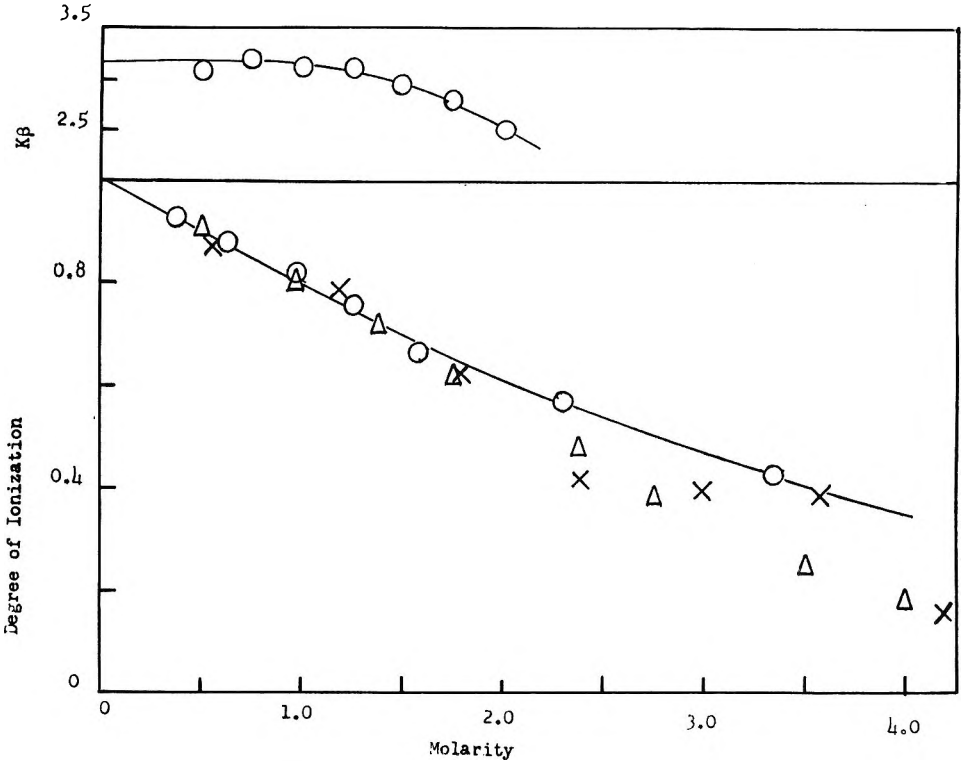

Figure 3. The degree of ionization and ionization constant of trichloroacetic acid: (×) ref 1, Raman; (△) ref 1, nmr; (○) this work.

tions of 0.95 mol fraction solvent. The redetermined values indicate that αC slowly approaches a limiting value of about 1.4 M at a stoichiometric concentration of 3.5 to 4 M.

Acknowledgment. The authors wish to thank the Savannah River Laboratory for the use of the Raman instrument and Dr. A. L. Marston for his assistance in the measurements.

Dissociation and Homoconjugation Constants of Some Acids in Methyl Isobutyl Ketone

by J. Juillard and I. M. Kolthoff*[1]

School of Chemistry, University of Minnesota, Minneapolis, Minnesota 55455 *(Received January 28, 1971)*

Publication costs borne completely by The Journal of Physical Chemistry

The dissociation constant of perchloric acid in methyl isobutyl ketone (MIBK) has been determined conductometrically, $pK^d_{HClO_4} = 4.5$. The glass electrode was found to be a reliable indicator electrode for pa_H; it was calibrated in solutions of perchloric acid and mixtures of the acid and s, its tetrabutylammonium salt ($pK^d_s = 3.6$, determined conductometrically). Equations have been derived for the calculation of K^d_{HA} and of $K^f_{HA_2^-}$ from pa_H of mixtures of an acid and its tetraalkylammonium salt, K^d_s being determined conductometrically. The following data for acids are reported: $pK^d_{2,4,6\text{-trinitrobenzenesulfonic acid}} = 5.5$; $pK^d_{\text{picric acid}} = 11.0$, $K^f_{HA_2^-} \sim 1$, $pK^d_{2,6\text{-dinitrophenol}} = 17.6$; $pK^d_{3,5\text{-dinitrobenzoic acid}} = 18.8$, $K^f_{HA_2^-} = 2 \times 10^4$. For three cationic acids, anilinium, diphenylguanidinium, and tetramethylguanidinium, the following values of $pK^d_{BH^+}$ were found: 9.6, 15.9, and 20.3, respectively. The $pK^d_{BH^+}$ of the *o*-nitroanilinium ion was estimated to be 3.3. Owing to incomplete dissociation of all salts in the low dielectric constant solvent MIBK, $pa_{H_{1/2}}$ (at HNP) at a salt concentration of 0.001 was found of the order of 0.5 to 0.6 unit smaller than pK^d_{HA} for uncharged acids, and 0.5 to 1 unit greater than $pK^d_{BH^+}$ for the cationic acids. The differences become greater with increasing salt concentrations. It has been concluded that MIBK is a stronger base than acetonitrile even though two hydration constants of the proton, $K^f_{H^+_{3w}}$ and $K^f_{H^+_{4w}}$, are found to be almost the same in both solvents.

Methyl isobutyl ketone (MIBK) is a dipolar aprotic solvent with a dielectric constant $\epsilon = 12.92$.[2a] Bruss and Wyld[2b] were the first to report titration curves of acids and mixtures of acids with tetraalkylammonium hydroxide in this solvent and to have observed good resolution of acid strength as compared with that in water. Because of the leveling effect of water, titration curves of dilute solutions of perchloric, hydrochloric, nitric, and sulfuric acids are identical in water, but in MIBK, like in other protophobic solvents, resolution of strength of some of these acids is obtained. Pietrzyk and Beslisle[3] made use of the resolution of acid strength in the titration of benzenesulfonic acids in MIBK. From the values of the half-neutralization potential (HNP) of a series of benzoic acids Miron and Hercules[4] concluded that the resolution is of the same order of magnitude as in acetonitrile and some other aprotic solvents. Like acetone[5,6] ($\epsilon = 20$) MIBK is expected to be a slightly stronger base than AN[7] and other nitriles are.[6] No quantitative data on acid–base strength in MIBK are reported in the literature; a preliminary study from this laboratory was reported in 1961.[8] Because of the low dielectric constant and weak basic character of MIBK, perchloric acid was found[8] to be a weak acid with a dissociation constant of the order of 10^{-5}. Owing to incomplete dissociation of tetraalkylammonium—and other salts in MIBK—the $pa_{H_{1/2}}$(pa_H at HNP) is no longer equal to the dissociation constant of an acid.

In the present work the glass electrode was calibrated in perchloric acid and in mixtures of this acid with its tetrabutylammonium salt after conductometrically determining the dissociation constants of the acid K^d_{HA} and the salt (K^d_{BA}). In the potentiometric determination of K^d_{HA} of a few selected acids and their homoconjugation constants $K^f_{HA_2^-}$ the pa_H was measured in mixtures of the acid with its tetraalkylammonium salt BA. By widely varying the ratio of picric acid in mixtures with its tetrabutylammonium salt, good agreement was obtained between experimental and calculated values of pa_H, substantiating the reliability of the glass electrode as a pa_H electrode. Other tests described in the experimental part supported this conclusion. Because of its small dielectric constant, calculations of K^d_{HA} and $K^f_{HA_2^-}$ are much more involved in MIBK than in aprotic solvents with a dielectric constant of the order of 40. The pK values reported in this paper may be no more accurate than ± 0.15.

(1) This work was supported by Grant GP 5732 from the National Science Foundation. One of us (J. J.) wishes to express his sincere thanks to the Centre National de la Recherche Scientifique, France, for a 1-year leave of absence and to NATO for a travel grant. We are grateful to Dr. M. K. Chantooni, Jr., for helpful discussions.

(2) (a) H. C. Eckstrom, J. E. Berger, and L. R. Dawson, *J. Phys. Chem.*, **64**, 1458 (1960); (b) D. B. Bruss and G. E. A. Wyld, *Anal. Chem.*, **29**, 232 (1957).

(3) D. J. Pietrzyk and J. Beslisle, *ibid.*, **38**, 999 (1966).

(4) R. R. Miron and D. M. Hercules, *ibid.*, **33**, 1770 (1961).

(5) F. Aufauvre, Thèse Doc. Sc., Clermont, France, 1969.

(6) J. F. Coetzee and D. K. McGuire, *J. Phys. Chem.*, **67**, 1810 (1963).

(7) I. M. Kolthoff, S. Bruckenstein, and M. K. Chantooni, Jr., *J. Amer. Chem. Soc.*, **83**, 3927 (1961).

(8) C. E. Gracias, Ph.D. Thesis, University of Minnesota, Minneapolis, Minn., 1961.

Calculation of Dissociation Constants of Acids, K^d_{HA}, from pa_H. The following four equations are fundamental in the calculation of K^d_{HA} from the experimentally determined values of pa_H in mixtures of an acid HA and its salt BA.

$$K^d_{HA} = \frac{[H^+][A^-]f_\pm^2}{[HA]} \quad (1)$$

$$K^f_{HA_2^-} = \frac{[HA_2^-]}{[HA][A^-]} \qquad f_{HA_2^-} = f_{A^-} \quad (2)$$

Formation of higher conjugates $HA_2^- + nHA \rightleftarrows (HA)_{n+1}A^-$ has not been considered because the calculation of the overall equilibria becomes very involved and also because the concentration of HA in the mixtures was usually small enough to make $[(HA)_{n+1}A^-]$ negligible.

$$K^d_{BA} = \frac{[B^+][A^-]f_\pm^2}{[BA]} \quad (3)$$

$$K^d_{BHA_2} = \frac{[B^+][HA_2^-]f_\pm^2}{[BHA_2]} \quad (4)$$

Denoting c_a and c_s as the analytical concentrations of the acid and salt

$$c_a = [HA] + [HA_2^-] + [BHA_2] + [H^+] \quad (5)$$

$$c_s = [BA] + [BHA_2] + [A^-] + [HA_2^-] \quad (6)$$

Introducing into eq 1 yields

$$pK^d_{HA} = pa_H - \log \frac{c_s - [BA] - [HA_2^-] - [BHA_2]}{c_a - [HA_2^-] - [BHA_2]} - \log f_\pm \quad (7)$$

$[H^+]$ being generally negligible in the mixtures with respect to the concentration of the other species. If [BA] and $[BHA_2]$ were also negligibly small in equimolar mixtures of acid and salt, eq 7 would become

$$pK^d_{HA} = pa_{H_{1/2}} - \log f_\pm \quad (8)$$

However, this simple equation does not hold in MIBK because of incomplete dissociation of salts in this low dielectric constant solvent. If the dissociation of BHA_2 is complete, but that of BA is not, $[A^-] \approx \alpha c_s - [HA_2^-]$ where α is the degree of dissociation of the salt

$$pK^d_{HA} = pa_H - \log \frac{\alpha c_s - [HA_2^-]}{c_a - [HA_2^-]} - \log f_\pm \quad (9)$$

In case of negligible homoconjugation as in mixtures of picric acid and its salt we get, when $c_a = c_s$

$$pK^d_{HA} = pa_{H_{1/2}} - \log \alpha_s - \log f_\pm \quad (10)$$

A similar equation can be derived for mixtures of salts (s) of cationic acids and free base when $c_b = c_s$

$$pK^d_{BH^+} = pa_{H_{1/2}} + \log \alpha_s + \log f_\pm \quad (10')$$

assuming negligible formation of B_2 and B_2H^+.

If homoconjugation is not negligible, we use a convenient method to find K^1_{HA} by carrying out a series of pa_H measurements at large dilutions ($c_a = c_s$) and graphically extrapolating the data to zero concentration where $\alpha = 1$, $\log f = 0$, and $pK^d_{HA} = (pa_{H_0})_{1/2}$. When $[H^+]$ is not negligible with respect to [HA] and $[A^-]$, but when homoconjugation is negligible, the following relations hold: $[HA] = c_a - [H^+]$ and $[A^-] = \alpha c_s + [H^+]$, and eq 9 can be written

$$pa_H = pK + \log \frac{\alpha c_s + [H^+]}{\alpha c_s - [H^+]} + \log f_\pm \quad (11)$$

This equation is used in calculating pa_H in perchloric acid and its buffers. The ionic strength in such mixtures is $\alpha c_s + [H^+]$ and, using the limiting Debye–Hückel equation: $\log f_\pm = -A\sqrt{\alpha c_s + [H^+]}$, A being 7.36. The value of pa_H is then found using a series of successive approximations.

Calculation of Homoconjugation Constants $K^f_{HA_2^-}$. Previously, equations were derived for systems in which BA and BHA_2 are completely dissociated and in those in which BHA_2 is completely, but BA incompletely, dissociated.[9] If both salts in MIBK are incompletely dissociated, the homoconjugation constant was found graphically, making use of eq 1–8 and the electroneutrality rule

$$[H^+] + [B^+] = [A^-] + [HA_2^-] \quad (12)$$

Under our experimental conditions $[H^+]$ is negligible in eq 5 and 12 and does not contribute to the ionic strength in the calculation of $f_\pm$; thus we have 8 equations with 9 unknowns. The constants K^d_{BA} and K^d_{BHA}, have been determined conductometrically. In each mixture of acid and its salt, c_a and c_s are known and pa_H has been measured. Using an estimated value of $[B^+]$, the value of $\log f = -7.36\sqrt{[B^+]}$. Values of $[A^-]/[BA]$ and $[HA_2^-]/[BHA_2]$ are calculated from eq 3 and 4, while $[A^-] + [HA_2^-]$ is found from eq 12. Combination of eq 3, 4, and 12 with eq 5 yields $[A^-]$, $[BHA_2]$, and $[HA_2^-]$, while [HA] is now found from eq 5. Thus K^d_{HA} and $K^f_{HA_2^-}$ can now be calculated from eq 1 and 2. These calculations are repeated at given c_s but varying c_a using different values of $[B^+]$, and the values of pK^d_{HA} are plotted *vs.* $pK^f_{HA_2^-}$. Thus for each value of c_a a different plot is obtained, the point of intersection of the curves yielding the true values of pK^d_{HA} and $pK^f_{HA_2^-}$. Small errors in the determination of pa_H cause relatively large variations in the pK values. Only those data of pa_H are useful which yield strongly curved plots. In the experimental part an example is given of the calculation of the "constants" from pa_H in 0.001 M tetraethylammonium 3,5-dinitrobenzoate.

(9) I. M. Kolthoff, M. K. Chantooni, Jr., and S. Bhowmik, *J. Amer. Chem. Soc.*, **88**, 5430 (1966).

Experimental Section

Solvent Purification. An Eastman product was shaken with dry calcium chloride for about 10 hr. This operation was repeated three times. After decantation the solvent was passed through a column of chromatographic alumina and then distilled at least three times over phosphorus pentoxide in a dry and carbon dioxide free stream of nitrogen. The distillation column was packed with steel wool. A red coloration appeared upon addition of the anhydride. During the third distillation this coloration was very weak and developed very slowly. A final distillation was carried out without phosphoric anhydride and the solvent stored in bottles equipped with a siphon allowing the solvent to be drawn out without contact with the atmosphere. The water content was determined by the Karl Fischer method, using a biamperometric titration method. In two different batches a water content of 1.3 and 2.2 $\times$ 10^{-5} M, respectively, was found. The average conductivity of different freshly distilled batches was 1.2 $\pm$ 0.2 $\times$ 10^{-7} ohm^{-1} cm^{-1}, the conductivity remaining the same after 2 months of storage. The concentration of basic impurities was estimated spectrophotometrically by addition of picric acid; it was found to be less than 8 $\times$ 10^{-5} M.

Chemicals. Tetrabutylammonium 2,4,6-trinitrobenzenesulfonate was prepared by neutralization of the acid with a freshly prepared aqueous tetrabutylammonium hydroxide solution. After evaporation the salt was recrystallized twice from water and dried in a vacuum oven. The potassium 2,4,6-trinitrobenzenesulfonate was prepared by neutralizing the acid with potassium hydroxide. After evaporation the salt was recrystallized from a mixture 90% in ethanol and 10% in water. The acid was an Eastman product. From titration with standard sodium hydroxide it was concluded that the acid contained 2 molecules of water. After heating for 3 days in a vacuum oven the water content corresponded to 1.2 mol per mol of acid. Other chemicals had been used previously in this laboratory.

Solution of Perchloric Acid. A 0.92 M solution of perchloric acid was prepared in anhydrous acetic acid following Coetzee's directions,[10] and diluted with MIBK immediately before making conductometric or potentiometric measurements.

Potentiometry. The same apparatus was used as described in a previous paper.[9] A Beckman 1190-72 type glass electrode was used. The reference electrode consisted of a silver wire immersed in a saturated solution of silver nitrate in MIBK. A 10^{-1} M tetrabutylammonium perchlorate solution in MIBK served as a salt bridge. The glass electrode attained equilibrium within 5 min in relatively acidic solutions and in 30 min in solutions with a pH of 12 or greater. The constant of the electrode was checked daily in picric acid–picrate buffers. Conductometric,[11] differential vapor pressure (osmometer), and spectrophotometric measurements were carried out using the same apparatus as described previously.[12] All measurements were carried out at 25 $\pm$ 0.1°.

Results

Calibration of the Glass Electrode. The dissociation constants of perchloric acid and its tetrabutylammonium salt were determined conductometrically. For the salt the following values were found: $K^d_{BClO_4}$ = 2.3 $\times$ 10^{-4}, Λ_0 = 102. The value of $\lambda_0(NBu_4^+)$ = 37 was calculated by applying Walden's rule to the values in acetone, acetonitrile, propionitrile,[6] and methyl ethyl ketone[13] (viscosity of MIBK, 0.548 cP). This yields $\lambda_0(ClO_4^-)$ = 65. Conductance data of perchloric acid are given elsewhere.[14] The acid is quite weak in MIBK and the successive approximation method of Fuoss and Kraus[15] yielded highly uncertain values. Although Walden's rule does not hold for the solvated proton, the value of 49 found by this method, using values of $\lambda_0(H^+)$ reported in acetone, acetonitrile, and propionitrile,[8] is certainly reliable within 20%. With $\lambda_0(H^+)$ = 49 and $\lambda_0(ClO_4^-)$ = 65 we find from Kohlrausch's rule $\Lambda_0(HClO_4)$ = 114. $K^d_{HClO_4}$ is calculated from the relation $K^d_{HA} = (\alpha^2 cf^2)/(1 - \alpha)$ and $\alpha = (\Lambda)/[\Lambda_0 F(z)]$ where $F(z)$ is the function tabulated by Fuoss.[15]

The glass electrode was calibrated in mixtures of perchloric acid and tetrabutylammonium perchlorate. In such solutions with a pH of less than about 4, the glass electrode did not attain a constant potential. Such solutions became red, indicating reaction with the solvent. In Table I are listed the composition of the buffers used (pH >4.0), the calculated pa_H from eq 11, and the potentials measured which were corrected for liquid junction potential E_j calculated from the Henderson equation. Also, a correction was made for the change of the medium due to presence of acetic acid. The assumption was made that this correction is the same as the determined change in pa_H upon addition of glacial acetic acid to a buffer mixture of picric acid and its tetrabutylammonium salt. The values of E_{cor} in Table I incorporate the sum of corrections for E_j and acetic acid. From a comparison of $E_{exptl} - E_j$ and E_{cor} in Table I it is evident that the correction for acetic acid is very small and equal to 4 mV when c_a = 5 $\times$ 10^{-4} M (and [HAc] = 9 $\times$ 10^{-3} M), 6 mV when

(10) J. F. Coetzee, Ph.D. Thesis, University of Minnesota, Minneapolis, Minn., 1967.

(11) I. M. Kolthoff and M. K. Chantooni, Jr., *J. Amer. Chem. Soc.*, **85**, 426 (1963).

(12) M. K. Chantooni, Jr., and I. M. Kolthoff, *ibid.*, **90**, 3005 (1968).

(13) S. R. C. Hughes and D. H. Price, *J. Chem. Soc. A*, 1093 (1967).

(14) Experimental data will appear immediately following this article in the microfilm edition of this volume of the journal. Single copies may be obtained from the Reprint Department, ACS Publications, 1155 Sixteenth Street, N.W., Washington, D. C. 20036. Remit $3.00 for photocopy or $2.00 for microfiche.

(15) R. M. Fuoss, *J. Amer. Chem. Soc.*, **57**, 488 (1935).

$c_a = 10^{-3}$ M, and 8 mV when $c_a = 2 \times 10^{-3}$ M. Figure 1 presents a plot of pa_H *vs.* $E_{cor.}$, the numbers referring to the numbers in Table I. The data fit a straight line with a slope of 59 mV. Even though some of the data deviate as much as ±8 mV, the fact that the best line drawn through the points has the theoretical slope gives confidence in the reliabil ity of the glass electrode as a pa_H indicator and in the correctness of the involved equations and the assumptions made.

Table I: Potential and pa_H in $HClO_4$–Bu_4NClO_4 Mixtures (Molar Scale)

No.	c_a, M	c_s, M	E_{exptl} mV	$E_{exptl} - E_j$, mV	E_{cor} mV	pa_H
1	10^{-3}	10^{-3}	303	280	274	4.16
2	5×10^{-4}	5×10^{-4}	260	244	240	4.70
3	10^{-3}	10^{-2}	277	265	259	4.52
4	2×10^{-3}	2×10^{-2}	297	289	281	4.37
5	5×10^{-4}	10^{-1}	231	231	227	5.13
6	10^{-3}	10^{-1}	253	253	247	4.83
7	2×10^{-3}	10^{-1}	275	275	267	4.53

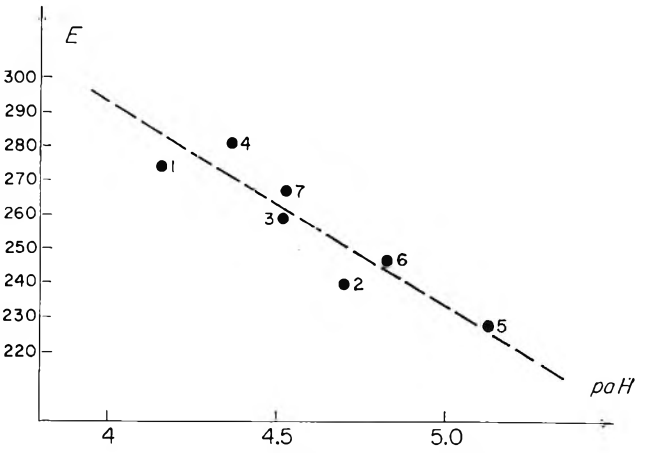

Figure 1. Plot of calculated pa_H and corrected potentials in perchloric acid–tetrabutylammonium perchlorate buffers (numbers are the same as those in Table I).

2,4,6-Trinitrobenzenesulfonic Acid Dihydrate. From conductance data values of $\Lambda_0 = 81$ and $K^d_s = 1.8 \times 10^{-4}$ for the tetrabutylammonium salt were obtained. Using $\lambda_0(Bu_4N^+) = 37$ and $\lambda_0(H^+) = 49$, we obtain $\Lambda_0 = 93$ for the acid. From the conductance[14] of solutions of the acid an "apparent" constant pK^d_{app} was calculated, pK^d_{app} decreasing with increasing concentration of the acid. The reason is that water greatly increases the dissociation of the acid. Graphical extrapolation to an acid and water concentration of zero of a plot of $\sqrt{c}$ *vs.* pK^d_{app} yielded a value of $pK^d_{HA} = 5.5$. Table II lists $pa_{H_{1/2}}$ values of equimolar mixtures of the acid and its tetrabutylammonium salt. The plot of $\sqrt{c}$ *vs.* pa_H yielded a straight line with a values of $pa_H = pK^d_{HA} = 5.6$ at zero concentration of the constituents. Considering the uncertainties involved, the agreement between the extrapolated values of 5.5 (conductometrically) and 5.6 (Table II) is satisfactory. It is fair to conclude that the true values of $pK^d_{HA} = 5.5_5 \pm 0.15$.

Table II: pa_H of Equimolar HTNBS–Bu_4NTNBS Mixtures[a]

$c_a \approx c_s$, $M \times 10^3$	c_w, M	E_{exptl}, mV	$E_{exptl} - E_j$, mV	pa_H
5	1.1×10^{-2}	−258	−240	4.90
2	4.4×10^{-3}	−249	−223	5.19
1	2.2×10^{-3}	−244	−217	5.29
0.5	1.1×10^{-3}	−238	−209	5.42

[a] Extrapolated value $pK^d = 5.6$.

Picric Acid and Its Homoconjugation Constant. The molecular weight of picric acid in MIBK was measured by the differential vapor pressure method and found to correspond to that of a monomer. Picric acid solutions were titrated spectrophotometrically and conductometrically with tetramethylguanidine. Spectrophotometric titrations of 0.8×10^{-4} M picric acid solutions were carried out at wavelengths of 428, 438, and 448 mμ, where the absorption of the acid was found negligible. The absorption increased linearly with concentration of base added, and remained unchanged after the end point. The results, which were accurate and precise within 0.5 %, indicated that at the small concentrations used tetramethylguanidine (TMG) gives quantitative salt formation with picric acid and that solutions of the picrate obey Beer's law. The conductometric titration curve of 0.01 M picric acid with TMG is presented in Figure 2. From the experimental data (dots on curve in Figure 2) values of $K^d_{BA} = 1.8 \times 10^{-4}$ and $\Lambda_0 = 97$ were found. Homoconjugation of picric acid was found to be negligible (see below) as was evident from the change in glass electrode potential in mixtures of 0.01 M tetrabutylammonium picrate with varying concentrations of picric acid. A plot of log c_a/c_s *vs.* E in Figure 3 yielded a straight line with the theoretical slope of 59 mV. The same slope was found in a similar plot for mixtures of 0.001 M diphenylguanidinium picrate with varying concentrations of diphenylguanidine, indicating negligible B_2H^+ formation at the concentrations used. The plots in Figure 3 substantiate the conclusion that the glass electrode potential in MIBK is a good indicator of pa_H, considering that the change in pa_H of the various mixtures amounted to as much as about 2 units. The homoconjugation constant of picric acid in acetonitrile was found to be of the order of 2[16] and it was expected to find a constant

(16) (a) I. M. Kolthoff and M. K. Chantooni, Jr., *J. Phys. Chem.*, **73**, 4029 (1969); (b) *J. Amer. Chem. Soc.*, **87**, 4428 (1965).

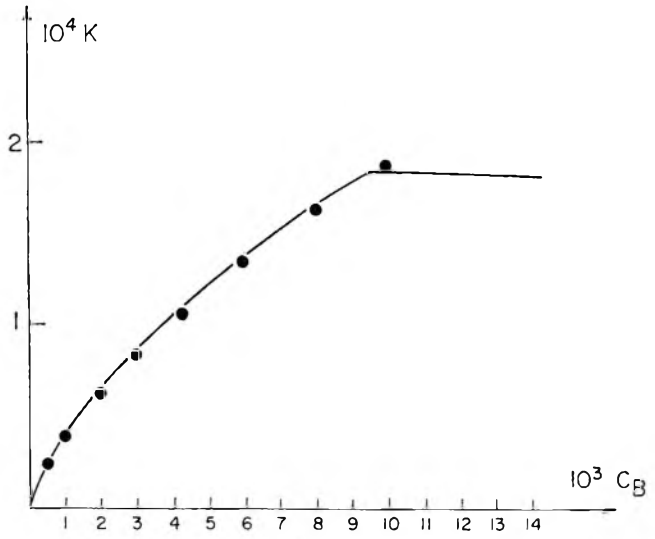

Figure 2. Conductometric titration of 1.03×10^{-2} M picric acid with 0.99 M tetramethylguanidine (B). The abscissa gives the concentration of B added.

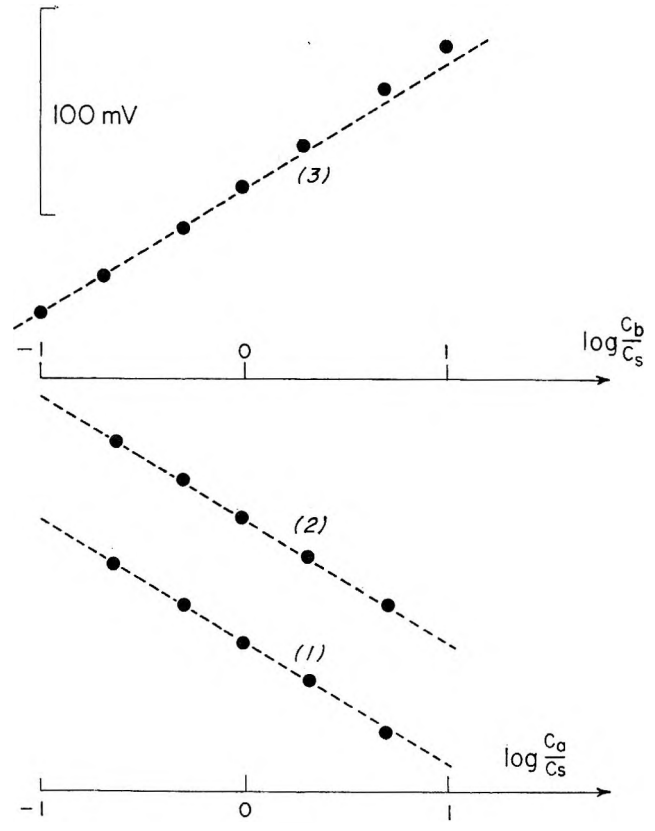

Figure 3. Glass electrode potentials in picrate and in diphenylguanidinium buffers at constant salt concentration: (1) and (2) picric acid–butylammonium picrate, $c_s = 10^{-2}$ M; (3) diphenylguanidine–diphenylguanidinium picrate, $c_s = 10^{-3}$ M. Lines drawn with slope of 59 mV.

of similar magnitude in MIBK. The constant was calculated from the values of the solubility of potassium picrate in solutions of picric acid.[16b] The saturated solutions were titrated potentiometrically with freshly prepared solutions of 2,4,6-trinitrobenzenesulfonic acid, using the glass electrode as indicator electrode. The solubility of the salt increases only very slightly in the presence of picric acid[14] and homoconjugation could be neglected in the interpretation of the results in Figure 3. In order to find the order of magnitude of $K^f_{HA_2^-}$, the value of $K^d_{KPi} = 7 \times 10^{-5}$ was determined conductometrically [Λ_0 (KPi) = 90]. From the total solubility of 1.90×10^{-3} M of potassium picrate and its K^d we find K_{sp}(KPi) = 9.2×10^{-8}. In estimating $K^f_{HPi_2^-}$ we assume complete dissociation of $KHPi_2$ and thus find a value for the homoconjugation constant of the order of 1.

K^d_{HA} of Picric Acid, 2,6-Dinitrophenol, and Three Cationic Acids. In acetonitrile $K^f_{HA_2^-}$ of 2,6-dinitrophenol (HDNP)[16b] is negligibly small. Since $K^f_{HA_2^-}$ for picric acid is of the same order of magnitude in acetonitrile[16a] as in MIBK, homoconjugation of this acid could be neglected in the calculation of pK^d_{HA}. Undoubtedly the same is true for HDNP. Analogous to the situation in acetonitrile[17] and acetone,[5] negligible homoconjugation of the three cationic acids anilinium, diphenylguanidinium ($DPGH^+$) (see Figure 3), and tetramethylguanidinium ($TMGH^+$) could be assumed under our experimental conditions. The pK^d_{HA} of the various acids in Table III was calculated from the pa_H of equimolar solutions being 10^{-3} M both in acid and its conjugate salt or base and its salt respectively by means of eq 10 or 10′. The values of pa_H were obtained from the measured potentials, corrected for liquid junction potentials. Conductometrically determined values of K^d_s of the salts and the corresponding values of α and f are also listed in Table III.

3,5-Dinitrobenzoic Acid (HDNB). The pa_H was determined in mixtures which were 0.001 M in tetraethylammonium dinitrobenzoate and 0.25 to 19×10^{-3} M in acid. From the large variation in Table IV of pa_H with the ratio c_a/c_s it is evident that $K^f_{HA_2^-}$ must be large. From conductance data of the tetraethylammonium salt values of $K^d_{BA} = 7 \times 10^{-5}$ and $\Lambda_0 = 129$ were obtained. From conductance data of the salt in 0.1 M HDNB the corresponding values of the homoconjugate salt were $K^d_{BHA_2} = 1.3 \times 10^{-3}$ and $\Lambda_0 = 79$. From the graphical method described earlier in the section on calculations, values of $pK^d_{HA} = 18.75 \pm 0.2$ and $K^f_{HA_2^-} = 2 \pm 0.5 \times 10^4$ were obtained. An example of the results of the involved calculations is given in Table V. Similar sets of calculations were made at $c_a = 2.5 \times 10^{-4}$, 1.14×10^{-3}, 2.13×10^{-3}, 4.9×10^{-3}, 7.10×10^{-3}, and 1.9×10^{-2} M. Plots of pK^d_{HA} *vs.* $pK^f_{HA_2^-}$ were strongly curved at values of c_a less than 4.9×10^{-3} M. From their points of intersection (isosbestic point) the above values of pK^d_{HA} of 18.75 ± 0.2 and $K^f_{HA_2^-} = 2 \pm 1 \times 10^4$ were found.

(17) J. F. Coetzee, G. R. Padmanabhan, and G. P. Cunningham, *Talanta*, 11, 93 (1964).

Table III: Dissociation Constants of Two Phenols and Three Cationic Acids (c_s = 0.001 M)

Acid	Salt	K^d_{salt}	Λ_0(salt)	α	f	$pa_{H1/2}$	pK^d_{acid}
HPi	Bu_4N^+	5.4×10^{-4}	93	0.68	0.68	10.63	11.0
HDNP	Et_4N^+	1×10^{-4}	104	0.35	0.73	16.97	17.6
$TMGH^+$	Pi^-	1.8×10^{-4}	97	0.41	0.71	21.02	20.5
$DPGH^+$	Pi^-	1.1×10^{-5}	97	0.11	0.84	16.97	15.9
Anilinium	ClO_4^-	2.6×10^{-5}	122	0.20	0.76	10.43	9.6

At values of c_a greater than 5×10^{-3} M, small differences in an assumed $[B^+]$ value gave rise to extremely large variations in pK^d_{HA} and $pK^f_{HA_2^-}$ and the results of the graphical procedure became unreliable. For example, at $c_a = 7.10 \times 10^{-3}$ M, pK^d_{HA} and $-pK^f_{HA_2}$ were 18.4 and 3.9 at $[B^+] = 7.6 \times 10^{-4}$ M, and 19.4 and 4.8, respectively, at $[B^+] = 8 \times 10^{-4}$ M. A solution with the aid of a computer of the various equations given earlier in this paper is contemplated.

Table IV: pa_H in Mixtures of 3,5-Dinitrobenzoic Acid and Its Tetraethylammonium Salt, $c_s = 1.0 \times 10^{-3}$ M

c_a, $M \times 10^3$	log c_a/c_s	pa_H
0.25	−0.60	19.31
0.64	−0.19	18.53
1.14	0.06	17.83
2.13	0.33	17.00
4.90	0.69	16.05
7.10	0.85	15.66
9.78	0.89	15.34
18.8	1.27	14.58

Effect of Water on Dissociation of Picric Acid. These experiments were carried out for a twofold reason: (1) the results yield quantitative information on the hydration of the proton in MIBK; (2) the extrapolated value to a water content of zero yields an independent check of K^d_{HPi}, and thus of the reliability of the glass electrode as pa_H indicator electrode. The effect of water was determined both spectrophotometrically by measuring the total picrate concentration, and potentiometrically by measuring pa_H in the solutions which were 0.001 M in tetraethylammonium perchlorate. The results are reported in Table VI. The techniques used and the method of calculation of pK^d_{HPi} (at zero water concentration) are identical with those presented for a similar study in acetonitrile.[18] The (approximate) values of the hydration constants of the proton with 1, 2, 3, and 4 molecules of water, respectively, are $K^f_{1w} = 3 \times 10^4$, $K^f_{2w} = 5 \times 10^4$, $K^f_{3w} = 5 \times 10^4$, and $K^f_{4w} = 3.5 \times 10^5$, K^f_{3w} and K^f_{4w} being almost the same as in AN. It is gratifying that the extrapolated value of pK^d_{HPi} of 11.0 is in exact agreement with the value derived from pa_H measurements with the glass electrode.

Table V: Example of the Results of the Calculation of the Concentrations of Various Species and of pK^d_{HA} and $K^f_{HA_2^-}$ ($c_s = 10^{-3}$ M, $c_a = 6.4 \times 10^{-4}$ M, pa_H = 18.53)

Assumed $[B^+]$, $M \times 10^4$	f	$[A^-]/[BA]$, $M \times 10$	$[HA_2^-]/[BHA_2]$	$[A^-]$, $M \times 10^4$	$[HA_2^-]$, $M \times 10^5$	$[BA]$, $M \times 10^4$	$[BHA_2]$, $M \times 10^4$	pK^d_{HA}	$K^f_{HA_2^-} \times 10^4$
4	0.71	3.4	6.4	1.9	2.1	5.7	0.33	19.1	0.3
5	0.69	3.0	5.5	1.3	3.7	4.3	0.67	18.9	1.4
6	0.66	2.7	4.5	0.8	5.2	2.9	1.0	17.9	48

Table VI: Proton Hydration and Picric Acid Dissociation ($c_{HPi} = 10^{-2}$, $c_{BH^+} = 7.8 \times 10^{-6}$)

H_2O, M	$[Pi_t]^a$	$pa_{Pi_s^-}$ [b]	pa_{H_s} [c]	pK^d_{HPi} [c]
0.05	(2.11×10^{-5})	(4.73)	(8.23)	(11.0)
0.10	3.27×10^{-5}	4.56	8.26	10.8
0.20	5.25×10^{-5}	4.38	8.60	11.0
0.40	1.50×10^{-4}	3.99	9.08	11.0
0.60	3.87×10^{-4}	3.66	9.42	11.1
0.80	8.20×10^{-4}	3.42	9.52	10.9

[a] Spectrophotometric measurements λ 480 mμ. [b] From $[Pi_t^-] = [Pi_s^-][v + K^f_{HPi_2^-}[HPi]]$ where v 1 + $K_{Pi_w^-}[H_2O]$ (eq 6, ref 18). [c] $pK^d = pa_{H_s} + pa_{Pi_s^-} + \log [HPi]$.

Solubility Products of Some Salts and the Medium Effect between Acetonitrile (AN) and MIBK. These data are essential in connection with a discussion of the medium effect between AN and MIBK, denoted by $_{AN}\gamma^{MIBK}_{ion}$. Molar solubilities (s_t), ionic solubilities (s_i), and solubility products of potassium perchlorate, picrate, and 3,5-dinitrobenzoate are presented in Table VII. The total solubility of potassium perchlorate was obtained by evaporating the saturated solution to dryness, dissolving the residue in water, and

(18) I. M. Kolthoff and M. K. Chantooni, Jr., *J. Amer. Chem. Soc.*, 92, 2236 (1970).

Table VII: Ionic (s_i) and Total (s_t) Solubilities and Solubility Products (K^{sp}) of Some Potassium Salts

	κ^a	Λ_0	s_i	s_t	K^{sp}
Perchlorate	7.0×10^{-6}	104	6.9×10^{-5}	3.9×10^{-4}	4.5×10^{-9}
Picrate	3.8×10^{-5}	96	4.3×10^{-4}	1.9×10^{-3}	7.6×10^{-8}
3,5-Dinitrobenzoate	3.3×10^{-7}	116	3.0×10^{-6}		1×10^{-11}

[a] Conductivity of saturated solution corrected for conductance of solvent.

determining the perchlorate by the procedure of Fritz.[19] The molar solubility of the picrate was found from the spectrophotometrically determined picrate concentration, assuming the spectrum of the ion pair to be the same as that of the free picrate ion. The solubility of potassium 3,5-dinitrobenzoate was too small to be determined analytically. The ionic solubility was estimated from the conductance of the saturated solution (corrected for the conductance of the solvent). Values of Λ_0 in Table VII were obtained by using Kohlrausch's rule. The value of pK^{sp}_{KDNB} of 11.0 in Table VII may be 0.2 unit in error. The ionic solubilities of the perchlorate and picrate were found from the conductance of the saturated solutions. The conductance of various dilutions of saturated solutions yielded $K^d_{KClO_4} = 1.4\ 10^{-5}$ and $K^d_{KPi} = 5 \times 10^{-5}$. The solubility in MIBK of 3,5-dinitrobenzoic acid was determined gravimetrically and found equal to 0.37 M, as compared with a value of 0.23 M in AN,[20] yielding a value of $\log {}^{AN}\gamma^{MIBK}_{HA} = (\log {}^{A}\gamma^{M}_{HA}) = -0.2$, the negative sign indicating greater solubility in MIBK than in AN. The solubility of picric acid in MIBK was determined titrimetrically and found equal to 0.93 M[20] as compared with a value of 3.0 M in AN. Although a solution at such a high concentration cannot be considered as ideal, it is fair to estimate $\log {}^{A}\gamma^{M}_{HPi}$ to be of the order of +0.5.[21] Solubility products in AN of the salts in Table VII have been determined previously.[22] From the well known expressions[23]

$$(\Delta pK^d_{HPi})^{AN}_{MIBK} = 0 = -\log {}^{A}\gamma^{M}_{H^+} - \log {}^{A}\gamma^{M}_{Pi^-} + \log {}^{A}\gamma^{M}_{HPi} \quad (13)$$

and

$$(\Delta pK^{sp}_{KPi})^{AN}_{MIBK} = -2.5 = -\log {}^{A}\gamma^{M}_{K^+} - \log {}^{A}\gamma^{M}_{Pi^-} \quad (14)$$

we calculate

$$\log {}^{A}\gamma^{M}_{H^+} + \log {}^{A}\gamma^{M}_{Pi^-} = +0.5$$

Using the above data we find $\log {}^{A}\gamma^{M}_{H^+} - \log {}^{A}\gamma^{M}_{K^+} = -2.0$. From similar data for 3,5-dinitrobenzoic acid and its potassium salt we find $\log {}^{A}\gamma^{M}_{H^+} - \log {}^{A}\gamma^{M}_{K^+} = -1.7$. Using the average value of −1.8 we calculate from the data in Table VIII for perchloric acid $\log {}^{A}\gamma^{M}_{HClO_4} = 2.4 + 1.8 - 4.3 = -0.1$. This would indicate that undissociated perchloric acid has about the same solubility in AN as in MIBK. Values italicized in Table VIII are obtained from experimental data and do not involve any assumption.

Table VIII: Medium Effect $\log {}^{A}\gamma^{M}$ for Some Acids and Their Ions (A = Acetonitrile, M = Methyl Isobutyl Ketone)

	$(\Delta pK^d_{HA})^{AN}_{MIBK}$	$\log {}^{A}\gamma^{M}_{HA}$	$\log {}^{A}\gamma^{M}_{K^+} + \log {}^{A}\gamma^{M}_{A^-}$	$\log {}^{A}\gamma^{M}_{H^+} + \log {}^{A}\gamma^{M}_{A^-}$
$HClO_4$	*2.4*[a]	−0.1	*4.3*	*+2.5*
HPi	*0.0*	*+0.5*	*2.5*	*+0.5*
HDNB	*1.9*	*−0.2*	*3.7*	*+2.1*

[a] From $pK^d_{HClO_4}$ in AN = 2.1; J. F. Coetzee and G. R. Padmanabhan, *J. Phys. Chem.*, **66**, 1708 (1962), corrected for calibration of glass electrode, see ref 6.

Discussion

Even though the salt concentration in Tables III and IV was only 0.001 M, the pK^d_{HA} of uncharged acids was found to be of the order of 0.5 to 0.6 unit greater than $pa_{H_{1/2}}$ and the $pK^d_{BH^+}$ of cation acids 0.5 to 1 unit smaller than $pa_{H_{1/2}}$, the difference being due to incomplete dissociation of the salts. If salt concentrations of the order of 0.01 M would have been used the differences would be much greater. Quite generally, relatively large differences between pK^d_{HA} or $pK^d_{BH^+}$, and $pa_{H_{1/2}}$ can be expected in solvents of low dielectric constant, the difference increasing with decreasing dissociation constants of the salts. From the difference in pK^d_{HA} of a few uncharged acids in MIBK and AN and MIBK and water, respectively (third and fifth column in Table IX) it is seen that the resolution of acid strength with reference to water is of the same order of magnitude in both aprotic protophobic solvents. For example, for 3,5-dinitrobenzoic acid $K^f_{HA_2^-}$ is 2×10^4 as compared with 1×10^4 in AN.[11] Since homoconjugation and also the effect of water and alcohols on pa_H of mixtures of salts with their conjugate acids with large $K^f_{HA_2^-}$ are small in aprotic protophilic solvents,

(19) J. S. Fritz, J. E. Abbnik, and P. A. Campbell, *Anal. Chem.*, **36**, 2123 (1964).

(20) M. K. Chantooni, Jr., unpublished results.

(21) I. M. Kolthoff, M. K. Chantooni, Jr., and S. Bhowmik, *J. Amer. Chem. Soc.*, **90**, 23 (1968).

(22) M. K. Chantooni, Jr., and I. M. Kolthoff, *ibid.*, **89**, 1582 (1967).

(23) See, *e.g.*, I. M. Kolthoff, J. J. Lingane, and W. D. Larson, *ibid.*, **60**, 2512 (1938).

Table IX: pK^d_{HA} and $pK^d_{BH^+}$ in MIBK and Comparison with Data in Water, AN, and Acetone

Acid	pK^d_{MIBK}	$(\Delta pK^d)^{AN}_{MIBK}$	$(\Delta pK^d)^{acetone}_{MIBK}$	$(\Delta pK^d)^{water}_{MIBK}$
Perchloric	4.5	2.4	2.1	
Picric	11.0	0.0	2.2	10.7
2,6-Dinitrophenol	17.6	1.2	3.8 (?)	12.8
3,5-Dinitrobenzoic	18.8	1.9		14.1
Anilinium	9.6	−1.0		5.0
Diphenylguanidinium	15.9	−2.0	+0.5	5.8
Tetramethylguanidinium	20.3	−3.0	+1.7	6.6

Table X: Calculation of $pK^d_{IH^+}$ and $K^f_{IHClO_4}$ from Spectrophotometric Data Determined by Gracias[8] (I = *o*-Nitroaniline; $c_I = 8 \times 10^{-5}$ *M*)

c_{HClO_4}, $M \times 10^4$	R^a	$[H^+]$, $M \times 10^5$	[I], $M \times 10^5$	$[IH^+]$, $M \times 10^6$	$[IHClO_4]$, $M \times 10^5$	$[HClO_4]$, $M \times 10^4$	$pK^d_{IH^+}$	$K^f_{IHClO_4} \times 10^{-3}$
0.88	0.170	5.1	6.8	3.9	0.8	0.4	3.5	3.3
1.75	0.441	7.4	5.5	6.5	1.5	1.0	3.2	2.7
3.00	2.710	9.5	4.7	6.9	2.6	2.0	3.2	2.8
4.00	0.984	11	3.9	7.7	3.3	2.6	3.3	3.3
5.00	1.204	12.5	3.2	8.3	4.0	3.4	3.3	3.7
6.00	1.493	13.4	3.2	8.8	3.9	4.3	3.3	2.8
7.00	1.708	14.5	3.0	7.6	4.3	5.1	3.3	2.8
8.00	1.967	15.5	2.7	7.7	4.5	6.0	3.3	2.8
9.00	2.050	16.4	2.7	7.4	4.5	6.9	3.2	2.3
							Av 3.3	3×10^3

[a] $R = ([IH^+] + [IHClO_4])/[I]$.

like DMSO and to a lesser extent DMF, the latter type of solvent is much preferred over the protophobic solvents in the titration of mixtures of weak acids. On the other hand, in protophilic solvents there is no resolution of acid strength of acids which are very strong in water ($HClO_4$, HCl, HNO_3, H_2SO_4), while there is in protophobic solvents.[2]

From the data in Table IX it is seen that picric acid has the same dissociation constant in acetonitrile as in MIBK. The picrate ion is a relatively large ion with a delocalized charge, and the medium effect for this ion between two aprotic solvents should not be much affected by the dielectric constant (Born effect). Considering also that picric acid is some 4 times more soluble in AN than in MIBK ($\log {}^{AN}\gamma^{MIBK}_{HPi} = +0.5$), $\log {}^{AN}\gamma^{MIBK}_{Pi^-} = +0.5$ (Table VIII). The dielectric (Born) effect on γ_{H^+} is expected to be considerable, probably of the order of that of the potassium ion, which is roughly estimated to be of the order of 2. Assuming that $\log {}^{AN}\gamma^{MIBK}_{Pi^-}$ is of the order of 0.5, we would expect that $\log \gamma_{H^+} + \log \gamma_{Pi^-}$ would be of the order of 2.5, as compared with the experimental value of +0.5. The difference indicates that the ketone is a considerably stronger base than the nitrile and that $\log {}^{AN}\gamma^{MIBK}_{H^+}$ is of the order of zero. This is substantiated by some of the data in acetone (dielectric constant 20) reported by Aufauvre.[5] He finds in this solvent a p*K* of picric acid of 7.8[24] and Coetzee[6] a p*K* of perchloric acid of 2.4, as compared with 11.0 and 2.1, respectively, in AN. The relatively large values of $\log {}^{A}\gamma^{M}_{H^+} + \log {}^{A}\gamma^{M}_{A^-}$ (Table VIII) of 2.5 for perchloric and of 2.1 for 3,5-dinitrobenzoic acids indicate that the dielectric effect on their anions, which have a localized charge, is large, the nonelectric effect (third column in Table VIII) being about the same for both acids, The conclusion that the ketones are stronger bases than the nitriles is substantiated by the considerably smaller $pK^d_{BH^+}$ values of anilinium, diphenylguanidinium, and tetramethylguanidinium ions in MIBK (and also in acetone) as compared with those in AN. No comparison is made here with pK^d_{HA} values reported by Izmailov[25] in acetone, by Estranova[26] and also by Norberg[27] in methyl ethyl ketone, and by Dulova[28] in acetophenone and cyclohexanone. Norberg applied French and Roe's[29] treatment to solutions of picric acid in the various solvents in which the acid is so slightly dissociated that no reliable value for the constant can be found by the method used. Another indication that MIBK is a stronger base than AN is obtained from the value of $K^d_{BH^+}$ of the *o*-nitroanilinium perchlorate $IHClO_4$.[7] The ratio $R = ([IH^+] + [IHClO_4])/[I]$ of this Hammett indicator in solutions of

(24) F. Aufauvre, *Bull. Soc. Chim., Fr.*, 2802 (1967).

(25) A. N. Izmailov and V. N. Izmailova, *Zh. Fiz. Khim.*, **29**, 1053 (1955); Izmailov and Mazarava, *Russ. J. Phys. Chem.*, **34**, 737 (1960).

(26) K. J. Estranova, H. A. Raddat, and M. A. Kyruma, *Zh. Fiz. Khim.*, **63**, 2850 (1969).

(27) K. Norberg, *Acta Chem. Scand.*, **20**, 264 (1966).

(28) V. I. Dulova and I. A. Popova, *Tr. Sagu Novaya Serya*, **84**, 63 (1958).

(29) C. M. French and I. G. Roe, *Trans. Faraday Soc.*, **49**, 314 (1953).

perchloric acid in MIBK has been determined by Gracias.[8] Knowing $K^d_{HClO_4}$ and taking $K^d_{IHClO_4}$ = 2.6 × 10^{-5} (equal to $K^d_{anilinium\ perchlorate}$ determined in the present work) an average value of $K^f_{IHClO_4}$ = $[IHClO_4]/[I][HClO_4]$ = 3 × 10^3 and $pK^d_{IH^+}$ = 3.3 was calculated from the data in Table X. This compares with a value of 4.8 in AN[7] and 3.0 in acetone.[5] On the basis of the above discussion it is fair to conclude that the basic strength of MIBK is of the same order of magnitude as that of acetone and that both ketones are stronger bases than acetonitrile. On the basis of this conclusion it would be expected that the hydration constants of the proton would be some 10 to 50 times smaller in MIBK than in AN. The values of $K^f_{H^+3w}$ and $K^f_{H^+4w}$ reported in herein are virtually equal to those in AN.[18] Acetonitrile is miscible with water in all proportions, indicating strong solvation in this solvent, while the solubility of water in MIBK is only of the order of 1 *M*. This means that log $^{AN}\gamma^{MIBK}_{H_2O}$ is small and probably of the order of +1 to +2.

Molecular Complexes of Iodine with Some Mono *N*-Oxide Heterocyclic Diazines

by N. Kulevsky* and R. G. Severson, Jr.

Department of Chemistry, The University of North Dakota, Grand Forks, North Dakota 58201 *(Received February 24, 1971)*

Publication costs borne completely by The Journal of Physical Chemistry

The complexes of iodine with the mono *N*-oxides of pyridine, pyridazine, pyrimidine, and pyrazine were studied with the object in mind of determining whether the basic site in the diazine *N*-oxides was the lone pair on oxygen or nitrogen. Equilibrium constants for the association of the complexes as a function of temperature were determined from absorbance measurements at the maxima of the blue-shifted iodine peak. The values of $\Delta G°_{25}$ and $\Delta H°_{25}$ obtained from these measurements indicate that the order of donor ability is pyridine *N*-oxide > pyrimidine *N*-oxide > pyrazine *N*-oxide > pyridazine *N*-oxide. Arguments based upon considerations of the substituent effects of the nitrogen and *N*-oxide groups lead to the conclusion that this trend of donor strength is consistent only with oxygen acting as the donor site.

Introduction

The mono *N*-oxides of heterocyclic diazines are species whose interactions with electron acceptors may involve electron donation from either the π electron system of the ring or the nonbonded electrons on either the oxygen or the second ring nitrogen. Since previous studies with pyridine,[1] diazines,[2] and pyridine *N*-oxides[3-5] indicate that toward iodine these molecules are n-donors, it is likely that the mono *N*-oxides of the diazines also would behave as n-donors towards iodine. However, which of the two available lone pairs would be the primary donor site is open to question. Comparison of the existing data regarding the association in iodine complexes of pyridine[1] and pyridine *N*-oxide[3] (association constants at 25° in CCl_4 are 105 and 76 l. mol^{-1}, respectively) implies that when the two lone pairs are isolated from one another the aromatic nitrogen is a stronger donor than the oxygen of the NO group and thus would be the most likely donor site. Since, however, the two groups are not isolated from each other in the *N*-oxides of the three isomeric diazines the electronic effects of each group on the other must be considered. One quantitative measure of these effects, the Hammett σ constants obtained for ⟍N⫽ and ⟍N⁺–O⁻⫽ as substituents for ⟍CH⫽ in benzene,[6,7] indicates that

(1) W. McKinney and A. I. Popov, *J. Amer. Chem. Soc.*, **91**, 5215 (1969), and references therein.

(2) V. G. Krishna and M. Chowdhury, *J. Phys. Chem.*, **67**, 1067 (1963).

(3) T. Kubota, *J. Amer. Chem. Soc.*, **87**, 458 (1965).

(4) T. Kubota, K. Ezumi, M. Yamakawa, and Y. Matsui, *J. Mol. Spectrosc.*, **24** (1967).

(5) R. C. Gardner and R. O. Ragsdale, *Inorg. Chim. Acta*, **2**, 139 (1968).

(6) H. H. Jaffe and H. L. Jones, *Advan. Heterocycl. Chem.*, **3**, 209 (1964).

(7) A. R. Katritzky and F. J. Swinbourne, *J. Chem. Soc.*, 6707 (1965).

both are base weakening substituents. However, these data are not sufficient to establish which group would be the donor site towards iodine, as it is not clear how large these differences in substituent effects must be in order for the aromatic nitrogen to be a weaker donor than the oxygen of the NO group.

In a previous note concerning the infrared spectra of the iodine complexes of the several diazine *N*-oxides it was suggested that oxygen is the donor site.[8] This conclusion was based on the observation that the NO stretching frequency for each of the donors decreased when the complex formed. Since infrared data are not completely convincing evidence for this conclusion, we shall in this paper discuss the relationship between the thermodynamics of complex formation and the position of the donor site.

Experimental Section

Materials. Fisher-analyzed iodine was sublimed under vacuum three times and stored in a desiccator. Spectral grade CH_2Cl_2 which had been stored over a molecular sieve to eliminate water was used without any further treatment. Eastman practical grade pyridine *N*-oxide was distilled three times under vacuum. The diazine *N*-oxides were produced from the diazines and 30% hydrogen peroxide in glacial acetic acid by the methods developed by Ochiai.[9] They were then purified by recrystallization and sublimation or distillation. As all of the oxides appear to be more or less hygroscopic, they were stored in a desiccator over P_2O_5. The melting points and ir spectra obtained for the compounds were in agreement with literature data on them.

Apparatus. All of the spectra were recorded in the visible region using a Cary 14 spectrophotometer. The cell compartment was thermostated to ±0.1°. Cells of 1-cm path length were used for recording all spectra.

Preparation of Solutions. Stock solutions of donor and iodine were prepared by weighing out both the solvent and solute. Since all the donors are hygroscopic, stock solutions of the donors were prepared in a drybox under nitrogen. The solutions to be used in the measurements were prepared by mixing weighed quantities of stock donor, stock iodine, and pure solvent. By using these weights and assuming that the final dilute solutions had the same density as the pure solvent, the initial molar concentrations could be calculated.

The range of concentrations for the donors was 0.03–0.3 *M* for pyrazine *N*-oxide, 0.5–0.4 *M* for pyridazine *N*-oxide, 0.02–0.16 *M* for pyrimidine *N*-oxide, and 0.01–0.1 *M* for pyridine *N*-oxide. In all cases, the iodine concentrations ranged from 3×10^{-4} to 18×10^{-4} *M*. The absorbance values were measured in the range 0.1 to 1, although attempts were made to pick most of the concentrations so that absorbance readings would be around 0.5.

Absorbance measurements were made on the solutions immediately after mixing. All measurements were made using an iodine blank.

Results and Discussion

It was found that the mono *N*-oxides of the three isomeric diazines as well as pyridine *N*-oxide on being mixed with iodine produce a blue-shifted iodine peak. Also each of the donors in solution with iodine had fine isosbestic points over the range of concentrations used. The absorption data were treated using an equation derived by Tamres.[10] This equation (1) is valid for the association of 1:1 complexes if the complexes are weak and/or if the solutions are both dilute. In eq 1, a_c is the absorption coefficient of the complex, a_i is the absorption coefficient of free iodine, A is the absorbance of the solution measured with a reference solution containing the same concentration of iodine used in the solution of the complex, and K_c is the association constant. A plot of $(C_AC_D)/A$ *vs.* $(C_A + C_D)$ for several solutions is a straight line whose slope is $1/(a_c - a_i)$ and intercept is $1/K_c(a_c - a_i)$.

$$C_AC_D/(A) = (C_A + C_D)/(a_c - a_i) + 1/K_c(a_c - a_i) \quad (1)$$

The values of K_c and $(a_c - a_i)$ shown in Table I for the *N*-oxides studied were obtained using eq 1. The slopes and intercepts were calculated using the method of least squares. The values of $\Delta H°$ presented in Table II were calculated from a plot of ln K_c *vs.* $1/T$. The values of $\Delta G°_{298}$ given in Table II were calculated from the value of K_{298} given by the line obtained in the least-squares calculation of the data in Table I. All of the error limits presented in the tables are the standard deviations obtained from the least-squares treatment.

The values of $\Delta G°$ and $\Delta H°$ in Table II indicate that the order of stability for the complexes and thus the order of donor ability is pyridine *N*-oxide > pyrimidine *N*-oxide > pyrazine *N*-oxide > pyridazine *N*-oxide. This trend is the same as the trend of the frequency shifts between the NO stretch in the free and complexed donors.[8] Since the effect of complex formation on the infrared spectra of all the donors is to decrease the NO stretching frequency and the size of the frequency shifts parallels the thermodynamic stability of the complexes, it appears likely that all of the oxides studied are utilizing the same donor site.

Whether nitrogen or oxygen is the donor site, it is not unexpected that the *N*-oxides of the diazines are weaker donors than both pyridine *N*-oxide and pyridine, since as mentioned previously both the aromatic nitrogens and NO are base weakening substituents.[6,7] However,

(8) N. Kulevsky and R. G. Severson, Jr., *Spectrochim. Acta, Part A*, **26**, 2227 (1970).

(9) E. Ochiai, *J. Org. Chem.*, **18**, 534 (1953).

(10) M. Tamres, *J. Phys. Chem.*, **65**, 654 (1961).

Table I: Equilibrium Constants and Absorption Coefficients as a Function of Temperature for Iodine Complexes of Azine *N*-Oxides in CH_2Cl_2

	T, °C	$a_c - a_i$, l. mol^{-1} cm^{-1}	K_c, l./mol	λ_{max},[a] nm
Pyridine *N*-oxide	7.2	1755 ± 10	76.4 ± 2.0	
	14.4	1793 ± 21	54.7 ± 2.5	422
	25.3	1796 ± 24	37.5 ± 1.4	
Pyrazine *N*-oxide	10.0	1310 ± 10	5.22 ± 0.02	428
	16.4	1300 ± 10	4.40 ± 0.06	
	24.6	1290 ± 10	3.58 ± 0.03	
Pyrimidine *N*-oxide	7.5	1685 ± 10	10.4 ± 0.1	431
	15.1	1685 ± 10	8.4 ± 0.1	
	24.7	1770 ± 16	6.0 ± 0.1	
Pyridazine *N*-oxide	10.3	1430 ± 15	2.11 ± 0.03	
	17.5	1460 ± 35	1.79 ± 0.06	438
	24.3	1480 ± 40	1.55 ± 0.05	

[a] The maxima given here are those observed in the experimental curves of A *vs.* λ.

Table II: Thermodynamic Data for Association of Iodine–*N*-Oxide Complexes in CH_2Cl_2

	$-\Delta G°_{25}$, kcal/mol	$-\Delta H°$, kcal/mol	$-\Delta S°_{25}$, eu
Pyridine *N*-oxide	2.11 ± 0.02	6.82 ± 0.2	15.8
Pyrazine *N*-oxide	0.75 ± 0.01	4.33 ± 0.01	12.0
Pyrimidine *N*-oxide	1.04 ± 0.01	5.33 ± 0.24	14.1
Pyridazine *N*-oxide	0.25 ± 0.02	3.73 ± 0.08	11.7

the trend of donor strength found within the series of diazine *N*-oxides does not agree with the trend predicted on the basis of the NO group affecting an aromatic nitrogen acting as the basic site. On the other hand, if oxygen is the basic site the observed trend in basic strength can be rationalized by considering the resonance and inductive effects of the nitrogen on the N–O group. The primary reason for this is that the NO group, while overall an electron withdrawing group, is electron releasing by the resonance effect, whereas nitrogen is electron withdrawing by both the resonance and inductive effects. Thus if nitrogen is the donor site, the overall effect of NO must be electron withdrawing in all positions, and therefore the inductive effect of the group must outweigh the resonance effect. It would then appear that pyrimidine *N*-oxide, in which there is little resonance interaction between the groups, should be a weaker donor than pyrazine *N*-oxide where there is a weaker inductive effect and a stronger resonance effect.

The above arguments are at best qualitative, and they may be supported on a quantitative basis by using the Hammett equation. It has been shown that linear free-energy relationships are applicable to iodine complexes formed with some series of similar donors.[11] Therefore, an attempt was made to find a correlation between the association constants at 25° for the iodine complexes and two different sets of σ values. For the first set, nitrogen was assumed to be the donor site and σ_{NO} values were used with pyridine as the reference base, while for the second set, oxygen was assumed to be the donor site and σ_N values were used with pyridine *N*-oxide as the reference base. The σ values used in the correlations are those obtained for all three substituent positions by Katritzky and Swinbourne.[7] Although only three data points and the reference compound were available, there is an excellent correlation of the data with σ_N (correlation coefficient = 0.992, standard deviation = 0.13), while the correlation with σ_{NO} is very poor (correlation coefficient = 0.817).

Further support for the conclusion that oxygen is the donor site in the diazine *N*-oxides comes from a consideration of molecular orbital calculations performed on these molecules.[12] The results of these calculations indicate that the π-electron density at the oxygen and the donor ability decrease in the same order, while the π-electron density at nitrogen varies inversely with the donor ability.

One anomaly which may be observed on examination of the σ values used in the free energy correlation deserves mention. For substituents at both the α and β positions σ_{NO} is larger than σ_N, while the reverse is true for the γ position. Therefore it might be expected that in pyrazine *N*-oxide, nitrogen might be the donor site. The reason why it is not may be that steric as well as electronic factors govern the choice of the donor site. Steric repulsions between the hydrogens α to nitrogen and the large iodine molecule could cause oxygen to be the donor site even if the electronic factors are not completely favorable for it to do so. Gardner and Ragsdale suggested that such steric repulsions were important in order to explain why the association constants of pyridine and pyridine *N*-oxide iodine complexes were so close, while their pK_a values differed by 4.5 pK_a units.[5]

Acknowledgment. R. G. S. wishes to thank the National Science Foundation for support through the undergraduate research participation program, Grant No. GY-5765 and GY-7415. N. K. wishes to thank the University of North Dakota for the award of a summer research professorship.

(11) R. L. Carlson and R. S. Drago, *J. Amer. Chem. Soc.*, **85**, 505 (1963).

(12) T. Kubota and H. Watanabe, *Bull. Chem. Soc. Jap.*, **36**, 1093 (1963).

Mathematical Formulations of the Effects of Cell Distortion and Liquid Column Height Compression in Analytical Ultracentrifugation

by James A. Lewis*

Department of Physics and Engineering, Massey University, Palmerston North, New Zealand

and Norman F. Barber

Department of Physics, Victoria University of Wellington, Wellington, New Zealand *(Received December 4, 1970)*

Publication costs borne completely by The Journal of Physical Chemistry

The increase in demands for precision in current analytical ultracentrifuge techniques has necessitated the inclusion of correction terms previously neglected. The effect of cell distortion as distinct from rotor stretch is considered in this paper, where use is made of a theoretical model. The equations for the deformation of the model cell body under a centrifugal gravitational field are derived and the results are applied to cells used in current practice. The numerical calculations indicate that the correction terms are significant at the higher rotor speeds for high-precision Rayleigh interference work, and are particularly relevant in view of the increasing popularity of short-column high-speed methods. The experimental observables specific to cell distortion are shown to be a differential displacement of the liquid cell base, this being relevant to Yphantis-type cells, coupled with a decrease in the liquid column height. The latter observable could be confused with finite liquid compressibility and an analysis of this separate effect is included in an appendix to the paper. It is expected that the correction procedures indicated for the model can be extended to all practical cases where appropriate.

Introduction

The advent of high-speed analytical ultracentrifugation methods such as those of Yphantis,[1] together with the enhanced accuracy in the optical analysis as shown by LaBar[2] and others,[3-5] has led to an increasing demand for precision in techniques involving the analytical ultracentrifuge, and this has made it necessary to take into account effects heretofore neglected. Furthermore, improvements in rotor speed mechanisms such as that of Smiriga and Hearst[6] and elsewhere[7,8] have reduced the instantaneous deviations of rotor speed to less than 0.01% in the Beckman Model E instrument. In addition the instrument is equipped with a standard RTIC (Rotor Temperature Indicator and Control) unit[9] which maintains the rotor temperature constant to within 0.1° during operation. Thus the rotor and cell are effectively isothermal during operation and the centrifugal field terms $\omega^2 r$, where ω is the angular velocity and r the radius, can be calculated to 0.02%. This implies that for the true precision to be realized, account has to be taken of rotor stretch, and cell deformation in the centrifugal field. The former has been investigated experimentally by Kegeles and Gutter,[10] Schachman,[11] and Baghurst and Stanley,[12] from whose work data are available for both aluminum and titanium rotors. In addition, mathematical analyses of rotor stretch for variable geometry rotors have been formulated by Timoshenko[13] and by Biezeno and Grammel.[14] For the Beckman Model "E" ultracentrifuge it has been shown experimentally by Schachman[11] that the radial coordinates r can increase by 0.5% at 59,780 rpm for an aluminum rotor, and Baghurst and Stanley[12] have shown that r increases by as much as 0.75% at 67,770 rpm for an An-H titanium rotor. Hence as the above authors have intimated it is essential to correct for the effects of rotor stretch for precise work. However, owing to body forces in the centrifugal field the cell itself undergoes distortion (compression), and experimentally in the past this effect has been masked partially by the rotor stretch. It is the purpose

(1) D. A. Yphantis, *Biochemistry*, **3**, 297 (1964).

(2) F. E. LaBar, "Ultracentrifugation Using Rayleigh Interference Optics," Thesis in Biochemistry, Stanford University, 1963.

(3) J. W. Beams, N. Snidown, A. Robeson, and H. M. Dixon, *Rev. Sci. Instrum.*, **25**, 295 (1954).

(4) E. Richards and H. K. Schachman, *J. Phys. Chem.*, **63**, 1578 (1959).

(5) H. K. Schachman, *Biochemistry*, **2**, 887 (1963).

(6) S. R. Smiriga and J. E. Hearst, *Rev. Sci. Instrum.*, **40**, 233 (1969).

(7) Beckman Instruments, Inc., Technical Bulletin E-TB-013, Feb 1965.

(8) A. A. Windsor, T. H. Rich, R. E. Doyle, and F. T. Lindgren, *Rev. Sci. Instrum.*, **38**, 949 (1968).

(9) Beckman Instruments Inc., Technical Bulletin No. TB60003B, 1957.

(10) G. Kegeles and F. J. Gutter, *J. Amer. Chem. Soc.*, **73**, 3770 (1951).

(11) H. K. Schachman, "Ultracentrifugation in Biochemistry," Academic Press, New York, N. Y., and London, 1959, p 19.

(12) P. A. Baghurst and P. E. Stanley, *Anal. Biochem.*, **33**, 168 (1970).

(13) S. Timoshenko, "Strength of Materials," 3rd ed, Van Nostrand, Princeton, N. J., 1956, p 223, Part II.

(14) C. B. Biezeno and R. Grammel, "Technishe Dynamic," 2nd ed, Vol. II, Berlin-Gottingen-Heidelberg, 1953, p 25.

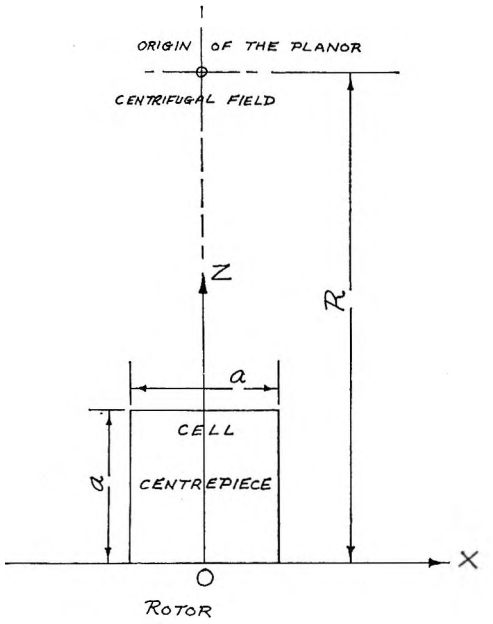

Figure 1. Diagram of the rectangular cell centerpiece within its coordinate axis system. The y axis is perpendicular to the plane of the paper.

of this paper to investigate cell distortion theoretically as distinct from rotor stretch, so that these effects may be assessed and their significance appreciated.

The Model and Theory

The model we have developed is the result of various attempts to simulate the conditions of the cell centerpiece in the rotor. We have analyzed this model according to the theory and notation of Landau and Lifshitz,[15] and for simplicity we have assumed rectangular symmetry for the cell and centrifugal field as indicated in the diagram of our cell centerpiece in Figure 1. To separate the effects of rotor stretch from those of cell distortion we have selected a symmetrical position, distance R from the axis of rotation, as the origin of our coordinate system. Naturally, R will vary with rotor speed owing to rotor stretch. The cell is located in the xy plane and the positive z axis of our system is in the negative radial direction of the rotor. The undeformed cell centerpiece considered is a rectangular block of square cross section a^2 in the xz plane and of length b in the y direction (the direction of the optical axis in the ultracentrifuge). Physically the field is that which applies for $R \gg a$. Hence the problem was to determine the deformation of the centerpiece resting in the rotor at z = zero subjected to a gravitational field $g_z = -\omega^2(R - z)$; $g_y = g_x = 0$, since the earth's field in the y direction is neglected. Furthermore, one boundary condition imposed was that the displacement vector u_z was zero when $z = 0$, since the centerpiece was assumed to be supported by the rotor in this plane.

It is shown by Landau and Lifshitz[15] that if a body is in equilibrium and is located in a gravitational field, then the internal stresses and the force of gravity per unit volume must vanish, and this result is expressed in their eq 2–7, *i.e.*

$$\frac{\partial \sigma_{ik}}{\partial x_k} + \rho g_i = 0 \tag{1}$$

where σ_{ik} is a general stress tensor element, x_k is a generalized coordinate, ρ is the density of the centerpiece material, and g_i is the component of the gravitational field in the ith direction.

From (1) the equations of equilibrium for our body become

$$\frac{\partial \sigma_{yk}}{\partial x_k} = \frac{\partial \sigma_{xk}}{\partial x_k} = 0 \tag{2}$$

and

$$\frac{\partial \sigma_{zk}}{\partial x_k} = \rho\omega^2(R - z) \tag{3}$$

Now, the boundary conditions that must be satisfied for our model are as follows: (a) on the sides of the centerpiece all components σ_{ik} vanish except σ_{zz}; (b) when $z = a$, $\sigma_{xy} = \sigma_{yz} = \sigma_{zz} = 0$. The solution of the equilibrium equations satisfying the boundary condition is

$$\sigma_{zz} = -\rho\omega^2[R(a - z) - \frac{1}{2}(a^2 - z^2)] \tag{4}$$

with all other

$$\sigma_{ik} = 0 \tag{5}$$

Knowing the stress tensor elements σ_{ik} we can find the strain tensor elements u_{ik} by use of Landau and Lifshitz's[15] eq 5-12, *i.e.*

$$u_{ik} = [(1 + \sigma)\sigma_{ik} - \sigma_{ll}\delta_{ik}]/E \tag{6}$$

Where σ is Poisson's ratio and E is Young's modulus for the centerpiece material, δ_{ik} is a unit matrix, and the double subscript for the stress tensor indicates summation in accordance with standard tensor notation. Whence

$$u_{xx} = \frac{\rho\omega^2}{E}\sigma[R(a - z) - \frac{1}{2}(a^2 - z^2)] \tag{7}$$

$$u_{yy} = \frac{\rho\omega^2}{E}\sigma[R(a - z) - \frac{1}{2}(a^2 - z^2)] \tag{8}$$

$$u_{zz} = -\frac{\rho\omega^2}{E}[R(a - z) - \frac{1}{2}(a^2 - z^2)] \tag{9}$$

and

$$u_{xy} = u_{xz} = u_{zy} = 0 \tag{10}$$

the strain tensor being symmetrical of course as shown by Landau and Lifshitz's[15] eq 1-4. The object of

(15) L. D. Landau and E. M. Lifshitz, "Theory of Elasticity of Course of Theoretical Physics," Vol. 7, Pergamon Press, London, New York, Paris, and Los Angeles, 1959.

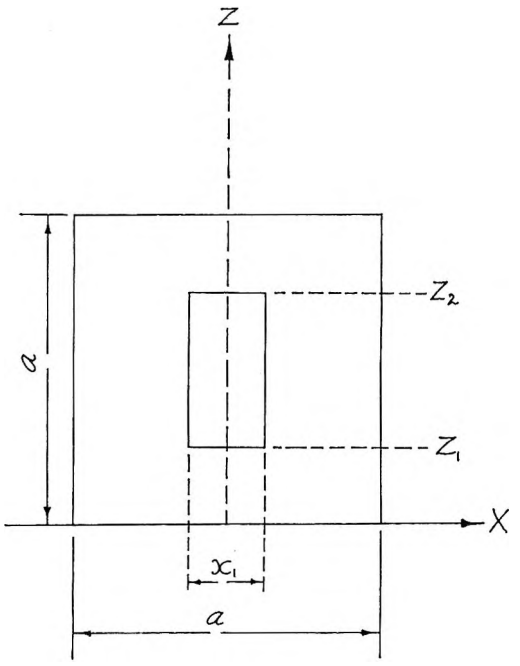

Figure 2. Diagram of the symmetrical rectangular cavity within the model centerpiece. The cavity has dimension y_1 perpendicular to the plane of the paper.

our analysis is to determine the displacement vector $\bar{u}$ at any point in the centerpiece, since this is the quantitative measure of deformation. This is found from the relationship between the strain tensor elements and the displacement vector formulated in Landau and Lifshitz's[15] eq 1-5

$$u_{ik} = \frac{1}{2}\left(\frac{\partial u_i}{\partial x_k} + \frac{\partial u_k}{\partial x_i}\right) \tag{11}$$

Where the double subscript indicates strain tensor elements, and the single subscript the relevant displacement vector component. Thus by integration we obtain the components of the displacement vector

$$u_x = \frac{\rho\omega^2}{E}\sigma[R(a - z) - \frac{1}{2}(a^2 - z^2)]x \tag{12}$$

$$u_y = \frac{\rho\omega^2}{E}\sigma[R(a - z) - \frac{1}{2}(a^2 - z^2)]y \tag{13}$$

$$u_z = -\frac{\rho\omega^2}{2E}\left[Rz(2a - z) - z\left(a^2 - \frac{z^2}{3}\right) + \sigma(R - z)(x^2 + y^2)\right] \tag{14}$$

It should be noted at this stage that the expression for u_z satisfies the boundary condition $u_z = 0$ only at the point of origin of our coordinate system, and hence the solution is not valid near this plane. However, the solution near this latter plane is not required in the subsequent analysis.

A cell cavity in our model has rectangular geometry and initially we shall assume that it is positioned symmetrically as shown in Figure 2. In practice the liquid under investigation is placed in the cavity in the cell centerpiece, and it is of interest to determine the cavity deformation in the centrifugal field. In stress analysis this problem frequently introduces complexity owing to new boundary conditions, but in the present model the problem is relatively simple, since we note from eq 4 and 5 that only σ_{zz} is finite and all other σ_{ik} are zero. Physically, this means that a cavity and body material in our cell centerpiece behave identically.

It can be shown by the use of eq 14 that the fractional change in the overall length of side z_2z_1 owing to cell deformation is given by

$$p_z = \frac{\rho\omega^2}{2E}\left[2Ra - R(z_2 + z_1) - a^2 + \frac{z_2^2 + z_2z_1 + z_1^2}{3} - \sigma(x^2 + y^2)\right] \tag{15}$$

whereas by use of eq 12 and 13 the fractional changes in the overall lengths of the sides parallel to the x and y axes located at z_1 and z_2, respectively, are given by

$$p_{x1} = p_{y1} = \frac{\rho\omega^2\sigma}{2E}(a - z_1)(2R - a - z_1) \tag{16}$$

$$p_{x2} = p_{y2} = \frac{\rho\omega^2\sigma}{2E}(a - z_2)(2R - a - z_2) \tag{17}$$

where p_{x1} is the overall fractional change in the side parallel to the x axis located at z_1, etc.

Thus from eq 15, 16, and 17, and a knowledge of the undeformed cavity dimensions, the deformation of the cavity may be calculated.

By inspection of eq 16 and 17 we note that the right-hand sides are always positive and hence the dimensions in the xy plane are always increased owing to cell deformation, whereas the right-hand side of eq 15 could be positive, negative, or zero. A diagrammatic picture of the deformed rectangular cavity is shown in Figure 3.

Consider a rectangular cavity of initial volume

$$V = (z_2 - z_1)x_1y_1 \tag{18}$$

where $(z_2 - z_1)$, x_1, and y_1 are the undeformed lengths of the sides. It can be shown that the volume V' of the deformed cell depicted in Figure 3 is given to a close approximation by

$$V' = \frac{(z_2 - z_1)'_0}{2}[y'_{12}(x'_{11} + x'_{12}) + x'_{11}(y'_{11} - y'_{12})] \tag{19}$$

where $(z_2 - z_1)'_0$[16] is the deformed length of the side $(z_2 - z_1)$ evaluated at $x = 0$, $y = 0$; and y'_{12} is the deformed length of the side y_1 evaluated at z_2, etc.

(16) Note the variation in $(z_2 - z_1)'$ over the range of values of x and y used for the cavities within our model is negligible.

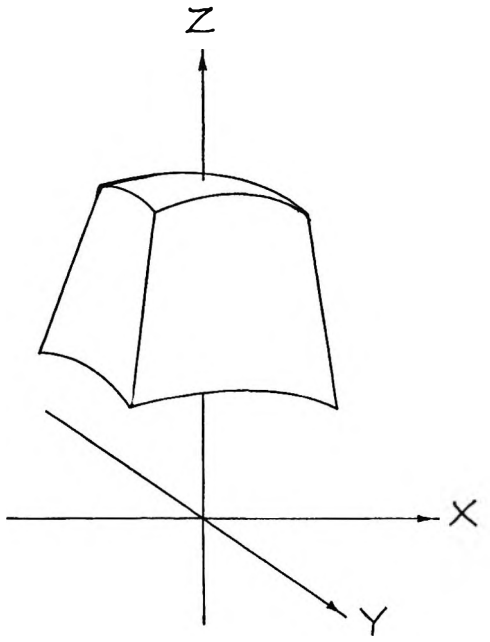

Figure 3. Diagrammatic representation of the cavity shown in Figure 2 after deformation owing to the centrifugal body forces.

Using eq 18 and 19 it can be shown that fractional volume change (δ) of the cavity is

$$\delta = \frac{\rho\omega^2}{2E}\left[(2\sigma + 1)\{a(2R - a) - R(z_2 + z_1)\} + \frac{z_2 z_1}{3} + \frac{1}{3}(3\sigma + 1)(z_2^2 + z_1^2)\right] \quad (20)$$

The practical significance of eq 20 insofar as the ultracentrifuge is concerned is that the height of the liquid column in the cell varies with the rotor speed, and this effect if observed may be misinterpreted as additional liquid compression. A separate analysis of this latter effect together with an appropriate discussion of the effects and magnitudes to be expected from this source are included in an Appendix to this paper. However, assuming that a liquid in the cell under investigation is incompressible we can determine the change in liquid column height in terms of the known parameters using eq 20. Doing this we find that in the deformed cell the liquid column height h' is given by

$$h' = h(1 - q) \quad (21)$$

where

$$q = \frac{\rho\omega^2}{2E}\sigma[2a(2R - a) - 2R(z_b + z_m) + z_b^2 + z_m^2] \quad (22)$$

and in which z_b and z_m are the locations of the liquid base and meniscus, respectively. From eq 22 we note that q can be positive, negative, or zero, and that the sign depends only on the rotor and cell coordinates, and is independent of materials and rotor speed. Thus it should be possible (theoretically) to design a centrifuge system partially to eliminate this effect.

We also see from eq 22 that the fractional change in liquid column height q is itself a function of the column height $h = (z_m - z_b)$ and of its location z_b in the cell. Rewriting eq 22 in terms of these latter two observable parameters we obtain

$$q = \frac{\rho\omega^2}{2E}\sigma[2a(2R - a) - 2R(2z_b + h) + z_b^2 + (z_b + h)^2] \quad (23)$$

Application of Theory and Discussion

Having derived equations relevant to a cell in an ultracentrifuge it is important to determine an estimate of the order of magnitude of the aforementioned effects. To this end, data relevant to the Beckman Model "E" instruments were inserted into the equations, under the assumption that the cell was constructed of duralumin, but the results may be applied readily to centerpieces constructed from other materials. The data used are as follows, assuming the symmetrical cavity of Figure 2: $R = 7.5$ cm; $a = 2.2$ cm; $z_1 = 0.6$ cm; $z_2 = 1.6$ cm; $x_1 = 0.25$; $y_1 = 1.2$ cm. From Kaye and Laby[17] for duralumin: $\rho = 2.8$ g/ml; $\sigma = 0.33$; $E = 7.3 \times 10^{11}$ dyn cm^{-2}; and the rotor speed varies in the range zero–75,000 rpm. The above data are applicable to a typical cell used for long column experiments.

Since z_b is fixed by the above data to about 0.6 cm (*i.e.*, $r_b \cong 6.9$ cm from axis of rotation), it was of interest to use eq 23 to find the column height for which q, the fractional change in column height, was zero. The resulting calculation gave column heights $h = 4.0$ cm and 9.8 cm which are physically impossible with the cells used. For a typical cell $0 \leq h \leq 1.0$ cm and therefore a change in liquid column height should be present in practice. Furthermore, by differentiating eq 23 with respect to h and inserting values of h in the range $0 \leq h \leq 1.0$ cm, we find that dq/dh is always negative, indicating that the shorter the column the greater the effect. The latter result is important owing to recent emphasis on high-speed, short-column methods,[1] and contrasts with the effect associated with finite liquid compressibilities (see Appendix). Again from eq 23 for h in our experimental range, we find that q is always positive, and hence from eq 21 we see that liquid column heights should always contract owing to cell distortion under the applied experimental conditions. Figures 4 and 5 show graphically the percentage contraction for liquid column heights in the range of interest for the duralumin cell model under consideration. Data are plotted over the typical rotor speed range 0–75,000 rpm of the Beckman Model "E"

(17) G. W. C. Kaye and T. H. Laby, "Tables of Physical and Chemical Constants," 11th ed, Longmans, Green and Co., London, New York, and Toronto, 1957.

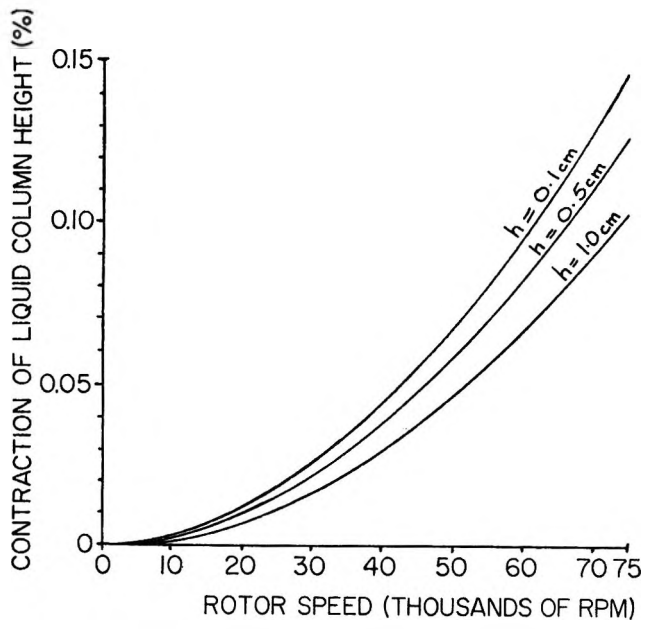

Figure 4. Graph showing the percentage contraction of liquid height with rotor speed for three different column heights in the duralumin model.

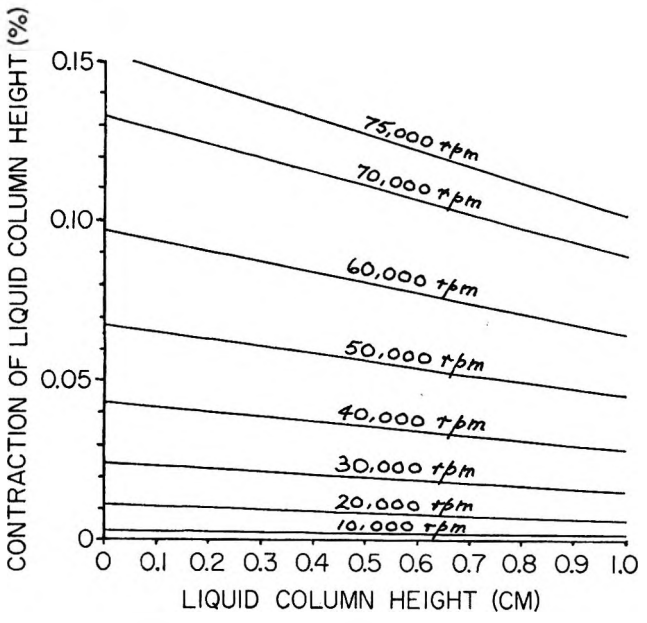

Figure 5. Graph showing the percentage contraction of liquid column height with liquid column height at constant rotor speeds for the duralumin model.

instrument. From graphs we note that at 70,000 rpm for a short-column experiment of 3 mm the percentage contraction is in the region of 0.12%. This gives an actual change in column height of about 0.0004 cm. Since the interference–schlieren optical system of the ultracentrifuge magnifies the radial dimensions by about 2 times this would result in a change of about 0.001 cm on the photographic plate. This should be observable since the microcomparators employed in plate analysis for interference work have a least count of 0.0001 cm. In practice cell distortion is coupled with window distortion, since the above stress analysis could apply equally to isotropic cell windows, and such a simple extrapolation is not really relevant at these speeds owing to uncertainties associated with locating the exact positions of the meniscus and base on the photographic plates. However, with the introduction of laser sources[18,19] coupled with improved window holder design[20] the menisci will be more clearly defined and it should be possible to measure the above effect in practice and make any necessary corrections when precise work (particularly interference) is being undertaken. Obviously for cells with an improved density to strength ratio (ρ/E) this effect will be diminished as expected, and this is indicated in the theoretical equations.

For an interference cell model in which there are two cavities symmetrically located about the z axis we find the results for each cavity similar to those for the single cavity described above.

A cell that is becoming increasingly popular in experimental work and to which cell distortion could be of major importance is the high-speed Yphantis-type cell—of which a recently improved side-access version has been described by Ansevin, Roark, and Yphantis.[20] This latter cell is specifically designed for rotor speeds in excess of 40,000 rpm. Now this cell is fabricated to improve among other things its density to strength ratio, and to consider a duralumin version as an example of the effects of cell distortion is unduly pessimistic. However the results obtained by the analysis of a duralumin cell will emphasize the effects cell distortion could have in such a cell, and indicate relevant correction procedures should these be found necessary. A diagram of a three channel Yphantis cell applicable to our model is shown in Figure 6. Cell distortion could be of primary importance in a cell of this type owing to its discriminatory effects among the channels. This is in contrast to rotor stretch which affects all channels equally. Fundamentally, the cell distortion effects are twofold: (a) the displacement of the cell base position (u_{zb}) will be different for each channel, and (b) the variation in liquid column height (q) for similar levels (h) in the channels will be different.

An estimate of the effect of cell base position displacement can be found from eq 14 where z is replaced by the appropriate z_b and the other parameters have the same numerical values as defined previously However, the last term in the brackets indicating the effect of the cell position in the xy plane is small and hence eq 14 may be rewritten as

$$u_{zb} = -\frac{\rho\omega^2}{2E}\left[Rz_b(2a - z_b) - z_b\left(a^2 - \frac{z_b}{3}\right)^2\right] \quad (24)$$

(18) Beckman Instruments Inc., "Future Product Information, 1969".

(19) J. A. Lewis and J. W. Lyttleton, unpublished work.

(20) A. T. Ansevin, D. E. Roark, and D. A. Yphantis, *Anal. Biochem.*, **34**, 237 (1970).

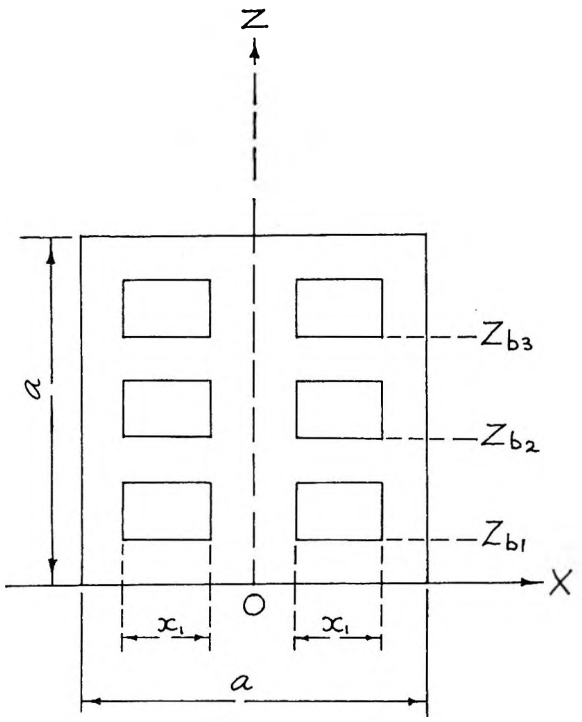

Figure 6. Diagram of the three channel Yphantis-type cell centerpiece applicable to our model.

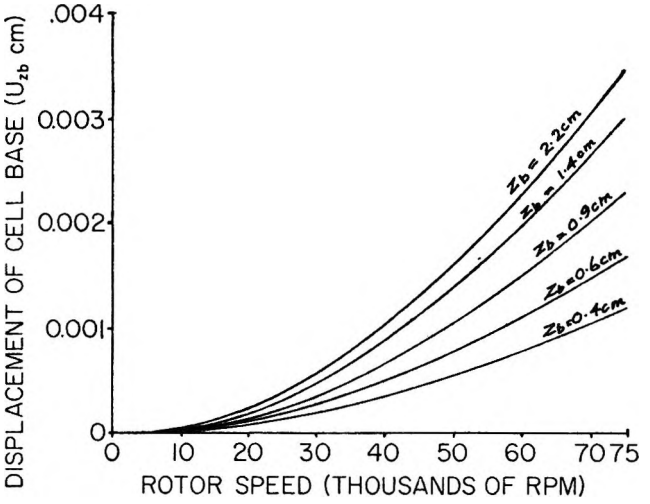

Figure 7. Graph showing cell base displacement *vs.* rotor speed for various initially fixed positions of the cell base within the duralumin model.

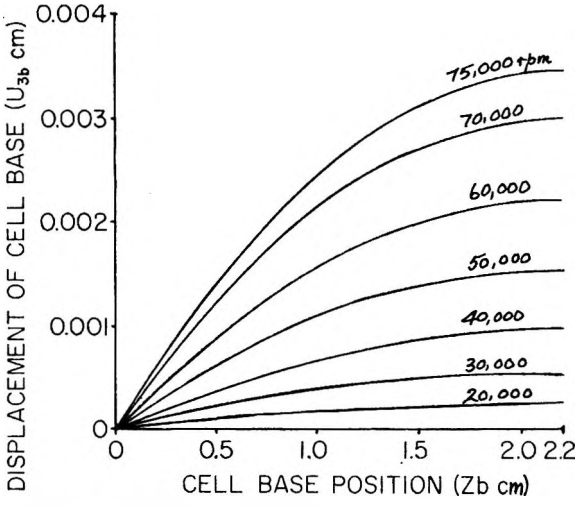

Figure 8. Graph showing the variation of cell base displacement *vs.* cell base position at constant rotor speeds for duralumin model.

Note the negative sign indicates that the displacement is in the negative z direction, *i.e.*, in the radial direction of the rotor as expected. We see that the displacement is proportional to (i) the square of the rotor speed, (ii) the density to strength ratio of the cell material, and (iii) the location of the base in the cell centerpiece (assuming that the cell centerpiece dimensions and positions within the rotor are fixed). The base positions selected for our model Yphantis cell were $z_{b1} = 0.4$ cm, $z_{b2} = 0.9$ cm, and $z_{b3} = 1.4$ cm, where the subscripts 1, 2, and 3 indicate the three channels numbered from bottom to top of the cell. The cell base displacement (u_{zb}) is plotted against rotor speed in Figure 7 for the position of the three channels above as well as for the top of the centerpiece $z_b = 2.2$ cm and for $z_b = 0.6$ cm, the latter being typical for the cells used for long-column experiments and schlieren work. Figure 8 depicts the variation in base displacement (u_{zb}) as a function of the position within the centerpiece, while rotor speed is maintained constant. It should be appreciated that the origin relative to the axis of rotation of the rotor will itself vary with rotor speed owing to rotor stretch and moreover the displacement at the top of the centerpiece gives rise to a widening of the gap between the rotor and cell already present owing to rotor stretch. By extrapolation one can determine the relative base displacements for any base position with respect to a reference position (channel) since these depend on their relative positions. Thus at 70,000 rpm we note that the base position in channel 2 has a radial displacement of about 2 times that of channel 1, whereas the base position in channel 3 has a radial displacement of just over 2.5 times that of channel 1. Naturally as noted previously from eq 24 the order of magnitude depends on ω^2 and ρ/E, but for our duralumin model the radial displacement of channel 1 at 70,000 rpm is about 0.001 cm which would be measurable in such a cell. However the radial displacement of a single channel base position is masked by rotor stretch in practice owing to the practical origin of coordinates being the axis of rotation and not the centerpiece base. In contrast, the relative displacements indicative of cell distortion are not masked and experimental evidence of this as regards the inner and outer reference positions of a cell counterbalance is intimated by Baghurst and Stanley.[12]

The channel discrimation exhibited by change in liquid column heights is depicted in Figure 9. Here the percentage decrease in liquid column height for a fixed

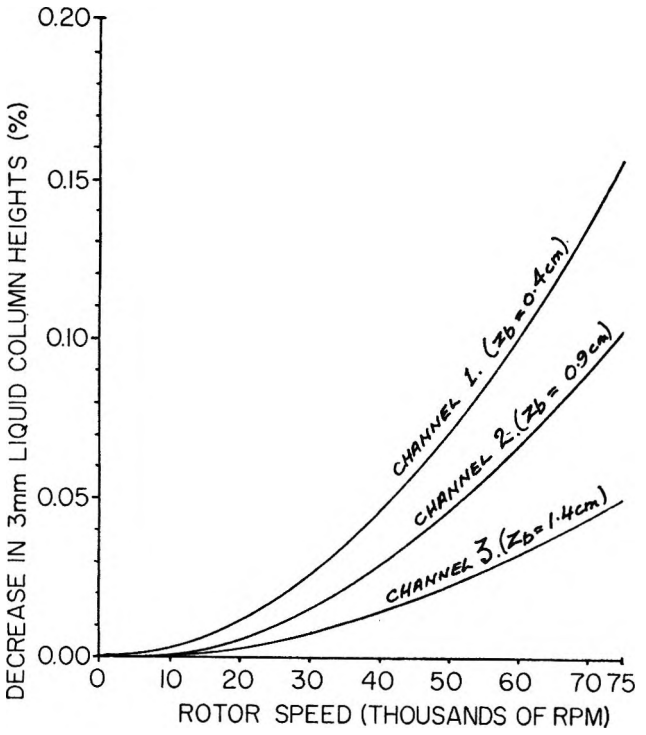

Figure 9. Graph showing the percentage contraction of 3-mm liquid column heights in the channels of the Yphantis type model of Figure 6 *vs.* rotor speed.

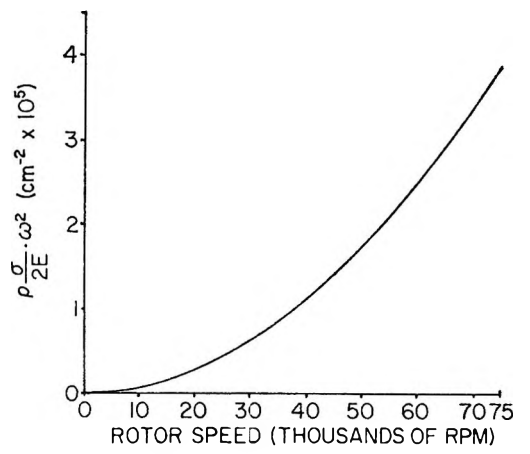

Figure 10. Graph of $(\rho\sigma/2E)\omega^2$ *vs.* rotor speed for a duralumin cell model.

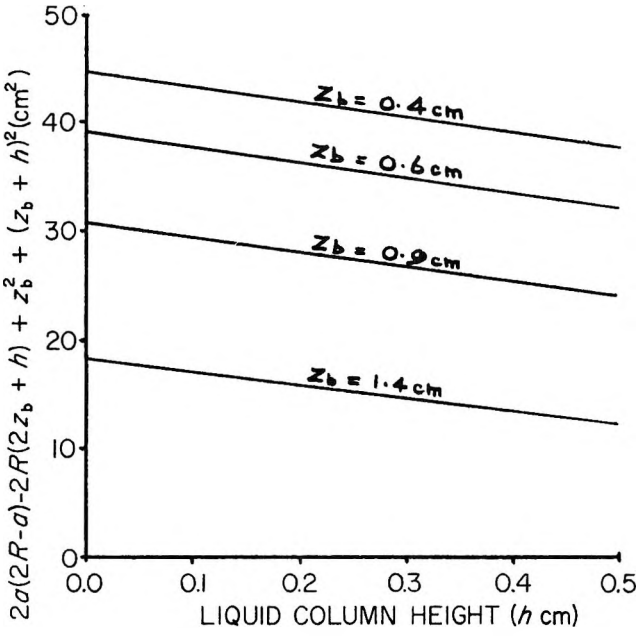

Figure 11. Graph of $2a(2R - a) - 2R(2z_b + h) + z_b^2 + (z_b + h)^2$ *vs.* liquid column height (h) for various base positions within a model cell centerpiece.

initial column height of $h = 0.3$ cm in each channel is plotted against rotor speed (rpm). The data for this graph were obtained from eq 23. From eq 23 we make a general observation that the magnitude of the fractional decrease in liquid column height (q) is the product of two distinct functions, this observation applying equally to the radial displacement u_z in eq 15. Firstly as expected it depends on the centrifugal field and the cell material $[(\rho\omega^2\sigma)/(2E)]$, and secondly on relevant cell dimensions and positions $[2a(2R - a) - 2R(2z_b + h) + z_b^2 + (z_b + h)^2]$. If the first is plotted against rotor speed and the second is plotted against liquid column height (h) over the range of interest for various relevant positions (z_b) in a centerpiece, it is possible by normal extrapolation procedures to determine the effective value of "q" for any rotor speed, column height, and base position of interest, and in theory for a practical case such plots could form the basis for experimental correction procedures. The plots applicable to our model duralumin cell are shown in Figures 10 and 11 for illustration—from which Figure 9 could be derived. Obviously, a similar procedure could be used to evaluate the radial displacement—u_z from eq 15. Finally, it is appropriate to mention the experimental work of Schachman[21] and Cheng and Schachman,[22] who investigated the compressibility of liquids from ultracentrifuge measurements. This is because the observable decrease in liquid column heights arising from finite liquid compressions, that is discussed in the Appendix to this paper, could be exaggerated by cell centerpiece deformation if precautions are not taken. Furthermore, as indicated by Schachman[21] the experimental conditions are complicated by window bulging and distortion owing to liquid pressure effects. In practice the effects of cell distortion as regards decrease in liquid column height with increase of the rotor speed are accentuated by the above effects. However, our model indicates that the effects of cell distortion may be evaluated devoid of the complications of window bulging and finite liquid compressibility. This is acheived experimentally by using a Yphantis-

(21) H. K. Schachman, "Ultracentrifugation in Biochemistry," Academic Press, New York, N. Y., and London, 1959, pp 32, 177–180.

(22) P. Y. Cheng and H. K. Schachman, *J. Amer. Chem. Soc.*, **77**, 1498 (1955).

type cell centerpiece and making simultaneous measurements of liquid column height contraction, together with relative base position displacements, the latter being independent of the aforementioned complications.

Conclusion

We have introduced a model of a cell in an analytical ultracentrifuge and have formulated mathematical expressions specific for the effects of cell centerpiece deformation under the centrifugal body forces. Data relevant to standard cells used with the Beckman Model "E" instrument have been evaluated and have indicated effects to be of an order of magnitude relevant for correction in present day high-precision methods. The orders of magnitude established are similar to those intimated by experimentally derived raw data results of Baghurst and Stanley[12] applicable to the inner and outer reference holes in a counterbalance cell. However, these authors stressed that an analysis of covariance failed to confirm the effect at the 5% probability level, but a suggestion of cell compression was made. The model has highlighted the specific effects of cell distortion, as distinct from rotor stretch, and has indicated correction procedures that could be relevant for high-precision sedimentation equilibrium Rayleigh interference work. The analysis of experimental data for the latter sometimes assumes the conservation of mass to evaluate a constant of integration, when use is made of the initial concentration of solute in the cell. The variation in liquid column height owing to cell distortion and finite liquid compressibility could influence the result of this calculation if precautions are not taken. Furthermore the radial displacement of the base region owing to cell distortion should be considered along with the corrections for rotor stretch. For the less precise schlieren work the effects will be relatively minor, although theoretically they would exaggerate effects of radial dilution. In particular the model has warned of possible complications associated with the use of Yphantis-type cells and has indicated appropriate correction procedures for precise work.

Finally, it must be emphasized that the theory is based on a model, and that the exact results evaluated are really only applicable to this model. However the model does approximate the experimental conditions experienced; the results it predicts are intuitively correct, and these are of the orders of magnitude expected from experimental evidence to date. Therefore we feel within the limitations imposed that the model is useful and applicable to the task in hand.

Appendix

A Mathematical Formulation of Liquid Column Height Compression Owing to Finite Liquid Compressibility in the Analytical Ultracentrifuge. At the higher rotor speeds (about 60,000 rpm) a large pressure difference exists between the air–liquid meniscus (where the pressure is 1 atm) and the bottom of a centrifuge cell. Svedberg and Pedersen,[23] Fujita,[24] and Schachman[21] have discussed the effects of this pressure variation and give appropriate references to both experimental and theoretical work undertaken in this area. However, the analysis above has indicated that one of the observable effects of cell deformation in these large centrifugal fields is an effective compression of the liquid column, and hence in the context of this paper it is appropriate to determine the relative contributions that these two independent sources make to the experimentally observable compression.

Using the notation of Fujita[24] the pressure distribution in a sector-shaped centrifuge cell may be determined from

$$\frac{\partial p}{\partial r} = \rho\omega r^2 \tag{A1}$$

where ρ = density of the solution at the radical position r, ω is the rotors' angular velocity, and p is the pressure.

For dilute solutions ρ may be replaced by the density of the solvent ρ_0 at the same point. Denoting the compressibility by β we obtain

$$\rho_0 = \frac{\rho_0^0}{1 - \beta p} \cong \rho_0^0(1 + \beta p) \tag{A2}$$

i.e.

$$\rho_0 = \rho_0^0 + \lambda p \tag{A3}$$

where $\lambda = \rho_0^0\beta$ with ρ_0^0 being the value of ρ_0 at $p = 0$, and this approximates the value at the meniscus (r_m).

Whence by substitution and integration the solvent density is given by

$$\rho_0(r) = \rho_0^0 \exp[{}^1/_2\beta\rho_0^0\omega^2(r^2 - r_m^2)] \tag{A4}$$

Defining

$$x = \left(\frac{r}{r_m}\right)^2 \tag{A5}$$

and

$$\nu = ({}^1/_2)\beta\rho_0^0\omega^2 r_m^2 \tag{A6}$$

We get

$$\rho_0(x) = \rho_0^0 \exp[\nu(x - 1)] \tag{A7}$$

The fractional decrease in liquid column height (q) is defined by

$$h' = h(1 - q) \tag{A8}$$

where h' is the liquid column height at rotor frequency ω and h its value when $\omega = 0$. It is easy to show that

(23) T. Svedberg and K. O. Pedersen, "The Ultracentrifuge," Clarendon Press, Oxford, 1940, pp 37, 267, 447.

(24) H. Fujita, "Mathematical Theory of Sedimentation Analysis," Academic Press, New York, N. Y., and London, 1962, pp 130–139.

$$\frac{\bar{\rho}_0(x)}{\rho_0^0} = \frac{1}{1-q}\left(1 - \frac{hq}{2r_b}\right) \qquad \text{(A9)}$$

where r_b is the radial position of the liquid column base and $\bar{\rho}(x)$ is the average density of the liquid at angular frequency ω.

In practice $hq/2r_b \ll 1$ and hence from eq A9 the fractional liquid column height compression (q) is given by

$$q = \frac{\bar{\rho}_0(x)}{\rho_0^0} - 1 \qquad \text{(A10)}$$

Defining a function $f(x)$ by

$$f(x) = \frac{\rho_0(x)}{\rho_0^0} - 1 \qquad \text{(A11)}$$

we see from eq A10 that the mean value of $f(x)$ is q. Substituting $\rho_0(x)$ from eq A7 into eq A11 we obtain

$$f(x) = \exp[\nu(x-1)] - 1 \qquad \text{(A12)}$$

and since in practice $\nu(x-1) \ll 1$ eq A12 becomes to a close approximation

$$f(x) = \nu(x-1) \qquad \text{(A13)}$$

Thus the required fractional liquid column height compression is given by

$$q = \nu(\bar{x} - 1) \qquad \text{(A14)}$$

where $\bar{x}$ is the mean value of x for the centrifuge cell. Writing x_b as the value for x at the cell base we find that

$$q = \frac{\nu}{2}(x_b - 1) \qquad \text{(A15)}$$

By the reinsertion of previously defined terms we can rewrite eq A15 as

$$q = \frac{\rho_0^0\omega^2\beta}{4}[h(2r_b - h)] \qquad \text{(A16)}$$

Differentiating eq A16 with respect to h we note that (dq/dh) is positive for all values of h used experimentally, and hence the larger the column (h) the greater q, this latter effect contrasting with the effective compression produced by cell centerpiece deformation. Figure 12 shows the variation in q and h at constant rotor speeds, calculated from eq 16 with: $r_b = 7.1$ cm; $\rho_0^0 = 0.998$ g cm^{-3}; and $\beta = 40 \times 10^{-6}$ atm^{-1}. These data are applicable to water at 20° in a typical ultracentrifuge cell. By comparison of Figures 12 and 5 the relative effects of cell distortion and finite compressibility may be estimated.

As with cell distortion it is of interest to determine the discrimatory effects of finite liquid compressibility among the channels of a high speed Yphantis-type centrifuge cell.

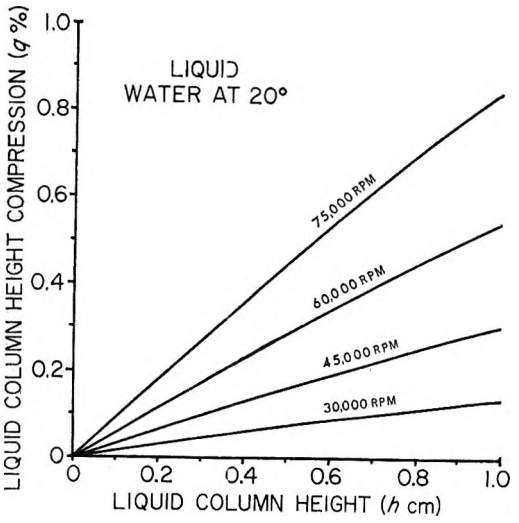

Figure 12. The variation in liquid column height compression (q) *vs.* liquid column height (h) in a centrifuge cell at constant rotor speeds, owing to finite liquid compressibility.

The percentage compression (q) of a fixed water column height of 0.3 cm at 20° in each of the three channels was determined using the following pertinent data: $\omega^2 = 4 \times 10^7$ (rad sec^{-1})^2; $r_{b1} = 7.1$ cm; $r_{b2} = 6.6$ cm; and $r_{b3} = 6.1$ cm.

The numerical subscript indicates the channel numbered from bottom to top of the cell. The calculations gave: $q_1 = 0.35\%$; $q_2 = 0.32\%$; and $q_3 = 0.30\%$. These imply that the overall radial movement of the menisci for the above conditions as recorded photographically in the ultracentrifuge would be in the region of 0.002 cm, account being taken of the $\times 2$ magnification of the radial cell coordinates by the interference–schlieren optical system of the ultracentrifuge. The variations among the channels is shown to be small, but they do lie within the precision of the instrument. Naturally, should the liquid employed have a larger compressibility and/or density then the observable effect from this source will be increased accordingly, as indicated by eq A16. Again, as for cell deformation, it is anticipated that appropriate precautions for the aforementioned physical effects should be made in accurate sedimentation equilibrium studies employing Rayleigh interference optics.

Acknowledgments. This work was supported in part by a grant (code reference 68337) from the University Grants Committee of New Zealand. In addition we thank Dr. J. W. Lyttleton of the Applied Biochemistry Division, Department of Scientific and Industrial Research, Palmerston North, for his helpful advice and assistance. Furthermore, the encouragement given by Professor G. N. Malcolm of the Chemistry and Biochemistry Department, and that of the members of the Physics and Engineering Department, Massey University is acknowledged.

Kinetics and Mechanism of the Reduction of Iodate to Iodite by Bromide in the Presence of Phenol

by Devendra Nath Sharma and Yugul Kishore Gupta*

Department of Chemistry, University of Rajasthan, Jaipur, India *(Received February 19, 1971)*

Publication costs borne completely by The Journal of Physical Chemistry

Iodate reacts with bromide in the presence of phenol according to the equation

$$IO_3^- + 2Br^- + 2H^+ = IO_2^- + Br_2 + H_2O$$

Phenol is not oxidized by the iodate under the acid conditions employed, but it reacts with the products, iodite and bromine. Kinetic behavior becomes complicated if phenol in less than optimum concentration is employed. The following rate law holds

$$\frac{-d[IO_3^-]}{dt} = \frac{[IO_3^-][Br^-]^2[H^+]^2(k_1 + k_2[H^+]^2)}{1 + K_5[H^+]}$$

k_1 and k_2 were found to be 22 $l.^4/(mol^4\ sec)$ and 152 $l.^6/(mol^6\ sec)$ at 35° and $\mu = 1.0\ M$ and K_5 is the association constant for IO_3^- and H^+. Almost identical results were obtained by employing hydrobromic acid instead of sodium or potassium bromide. The rate decreases by increasing the dielectric constant of the medium. Salt effect on the rate of the reaction appears to be explained by the equation $\log k_3 = \log k_0 - 2[(\sqrt{\mu}/(1 + \sqrt{\mu})) - 0.2\mu]$ where k_3 is the rate constant at constant hydrogen ion concentration. Attempts to isolate and identify the products of the side reaction by the conventional methods met with no success. There appear to be at least four products, all having iodine and bromine. The chromatographic analysis in conjunction with the sharp peaks of their spectrum of the crude product strongly suggests the latter to be a mixture of isomers.

Reduction of iodate[1] is one of the most extensively studied reactions. Depending on the pH and the concentrations of the reactants, the end products are hypoiodite, iodine, or iodide. However, most of the workers have indicated that the reduction occurs in stages through the intermediate formation of highly reactive iodite. Landolt[2] suspected the formation of iodite in the reduction of iodate. Abel[3] assumed its formation in the oxidation of oxalate. A mechanism involving the same species has been given by Masson and Race[4] in the oxidation of hydrocarbons. In the conversion of hypoiodite to iodate, Lievin[5] and Guiseppe[6] indicated the formation of iodite. By an analytical procedure Gupta and Bhargava[7] have shown the formation of iodite in the oxidation of iodide by permanganate and the reduction of iodate by some carboxylic acids. Recently, Harmelin and Duval[8] have given ir spectroscopic and thermogravimetric analytical evidence in favor of iodite when a mixture of lead and sodium iodate is heated. In view of the analogous species bromite and chlorite which are more stable, attempts have been made in the past to prove the existence of iodite and possibly isolate it, but without any success.

The reactions of halates with halides in general have been discussed by Hirade.[9] Schwicker and Schaw[10] have assumed an equilibrium for the reaction of iodate and bromide with an equilibrium constant of 1.6×10^{-22} at 14°.

$$2IO_3^- + 10Br^- + 12H^+ \rightleftharpoons I_2 + 5Br_2 + 6H_2O \quad (1)$$

Any kinetic study of this equilibrium or reaction with iodine and bromine together in the system along with iodate would be difficult. It has been shown by Hirade[9] that the slow rate-determining step does not give the end products and that intermediate species are formed which finally give iodine and bromine. In order to have a better insight into the mechanism it was considered desirable that the reduction of iodate be restricted to the slow step or in other words the first reduction product, iodite, not be allowed to react with

(1) I. M. Kolthoff and R. Belcher, "Volumetric Analysis," Vol. 3, Interscience, New York, N. Y., 1957, p 449.

(2) H. Landolt, *Sitzbar Akad. Bodin*, 249 (1885).

(3) E. Abel, *Z. Phys. Chem., Abt. A*, **154**, 167 (1931).

(4) I. Masson and E. Race, *J. Chem. Soc.*, 1718 (1937).

(5) O. Lievin, "Memoires et Travaux des Facultes Catholiques de Lille," 1923.

(6) D. Guiseppe, *Boll. Chim. Farm.*, **78**, 117 (1939).

(7) Y. K. Gupta and A. P. Bhargava, *Bull. Chem. Soc. Jap.*, **38**, 12 (1965).

(8) M. Harmelin and C. Duval, *C. R. Acad. Sci.*, **260** (9), 2461 (1965).

(9) J. Hirade, *Bull. Chem. Soc., Jap.*, **10**, 97 (1939).

(10) A. Schwicker and G. Schaw, *Z. Phys. Chem.*, **122**, 482 (1926).

bromide or bromine. It was with this aim in view that we employed phenol which removed bromine and iodite as soon as they formed. The slow step can broadly be represented as

$$IO_3^- + 2Br^- + 2H^+ \longrightarrow IO_2^- + Br_2 + H_2O \quad (2)$$

There is stoichiometric, kinetic, and circumstantial evidence to show that iodite and bromide do not react among themselves and that they immediately react with phenol forming such products which do not interfere with the iodometric determination of iodate. It is well established that hypohalites and halites rapidly react[11-13] with phenol and the fact has been utilized in analytical procedures. It is, therefore, expected that iodite, if formed as an intermediate product, would also react rapidly or rather more rapidly than other halites and hypohalites. Pollak[14] has used phenol in the reaction of bromate and bromide with the same aim in view. The reaction of phenol and bromine is also well known.[15] It is the hypobromous acid which formed *via* the equilibrium, $Br_2 + H_2O = HOBr + HBr$, reacts with phenol.[16,17]

Experimental Section

Materials and Solutions. Potassium iodate and potassium bromide were of BDH AnalaR quality and other chemicals were also of the same quality or E Merck GR quality. Stock solutions of sodium perchlorate were prepared by neutralizing perchloric acid with BDH AnalaR sodium carbonate and boiling off the carbon dioxide. Ethanol for solvent-effect study was obtained from the commercial grade sample after purification by the method of Smith.[18] All stock solutions were prepared in redistilled water, the second distillation being done with the permanganate.

Kinetic Procedure. Reactions were carried out in a thermostatic bath at 35° unless otherwise mentioned. The reaction was initiated by adding a temperature-equilibrated solution of potassium iodate to the reaction vessel containing the desired amounts of potassium bromide, sulfuric or perchloric acid, phenol, and water. The kinetics were followed by removing 10- or 5-ml aliquot portions after suitable intervals and quenching the reaction by the addition of a solution of potassium iodide. The liberated iodine was titrated against a standard solution of sodium thiosulfate. In most cases duplicate rate measurements were reproducible to ±5%. The maximum error in the analysis of the aliquot portions was ±0.02 ml of thiosulfate. This introduced an error of ±1–6% in the rate constants depending on the volume of the titrant.

A preliminary investigation indicated that a slow reaction between iodate and phenol occurs if the hydrogen ion concentration is large, but it is insignificant in less than 1.0 *M* $[H^+]$. All kinetic studies were therefore made in less than 1.0 *M* $[H^+]$.

Bromide Determination. For the estimation of bromide in the reaction mixtures in connection with the stoichiometry, a slightly modified method[19] was employed. The acid of the reaction mixture was first exactly neutralized by adding a calculated amount of caustic soda and then acetic acid was added so that the pH was 2.5–2.8. Under these conditions the titration of bromide solutions with silver nitrate using eosin as an absorption indicator[19] yielded a sharp end point.

Side Products. A white gelatinous precipitate was obtained from concentrated solutions. It was filtered and recrystallized from petroleum ether. Ir spectra (with a Perkin-Elmer grating Model 257) of the crude product, characteristic of phenyl groups, aromatic substitution, and C-halogen bonding, showed sharp peaks suggesting a pure compound. Fractional precipitation from alcoholic solution by the addition of water yielded white impure products with a melting point varying from 133 to 87°. All of them contained iodine and bromine. Thin layer chromatography of all these products with petroleum ether and ethyl acetate (1:1 v/v) as solvent gave one spot at equal distances suggesting a pure compound. The gas chromatography (Perkin-Elmer F, 71 HF gas chromatograph with 415B, 2.01 polyester column at 220°) done on these impure products showed two, three, or four peaks. The crude white product therefore appears to be a mixture of a number of isomers all containing iodine and bromine. Attempts to separate these by employing different solvents met with no success. The original crude product was subjected to sublimation under reduced pressure and the sublimed product melting at 94–96° gave two peaks in gas chromatography, one of which was 94%. These two portions could not be separated. These side products do not seem to have a bearing on the kinetics of the reaction and hence further study of the products was abandoned.

Results

Stoichiometry. Stoichiometry of the reaction was determined in the usual way by varying the concentrations of the reactants, phenol and sulfuric acid. Excess bromide was determined by the method described earlier. It was found that 2 moles of bromide are used up for each mole of iodate. Stoichiometry with excess iodate was not determined due to the phenol–iodate reaction.

(11) R. M. Chapin, *J. Amer. Chem. Soc.*, **56**, 2211 (1934).
(12) L. Farkas and M. Levin, *Anal. Chem.*, **19**, 662 (1947).
(13) E. Schulek, *Z. Anal. Chem.*, **67**, 142 (1925).
(14) F. Pollak, *Monatsh.*, **53**, 914 (1929).
(15) R. P. Bell and D. J. Rawlinson, *J. Chem. Soc.*, 63 (1961).
(16) E. A. Shilov, *J. Gen. Chem. USSR*, 519 (1938).
(17) H. Baines, *J. Chem. Soc.*, **121**, 2810 (1922).
(18) E. L. Smith, *ibid.*, 1288 (1927).
(19) I. M. Kolthoff and V. A. Stengar, "Volumetric Analysis," Vol. II, Interscience, New York, N. Y., 1964, p 271.

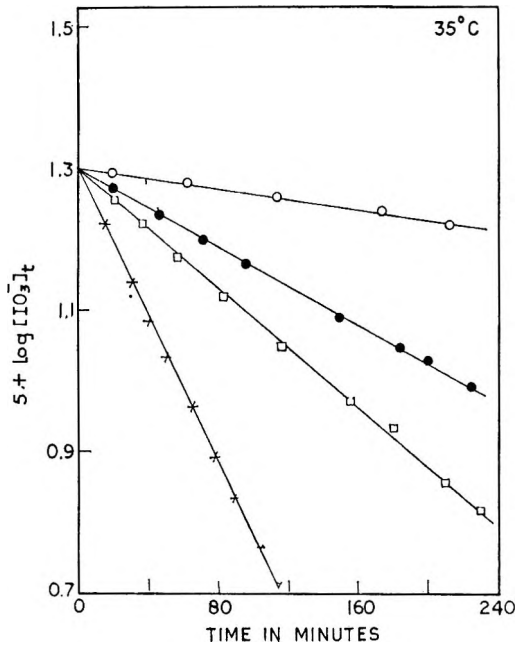

Figure 1. Pseudo-first-order plots of the reaction between iodate and bromide in the presence of phenol: $[KIO_3] = 2 \times 10^{-4}\ M$; $[C_6H_5OH] = 5 \times 10^{-3}\ M$; $[H_2SO_4] = 0.5\ M$; [KBr] = ○, $2 \times 10^{-3}\ M$; ●, $4 \times 10^{-3}\ M$; □, $5 \times 10^{-3}\ M$; ×, $7.5 \times 10^{-3}\ M$.

Order and Rate Constants. The reaction is first order in iodate and second order in bromide. Some of the pseudo-first-order plots are shown in Figure 1 and the derived third-order rate constants are shown in Table I. The simplified rate expression is

$$-d[IO_3^-]/dt = k_3[IO_3^-][Br^-]^2 \qquad (3)$$

A more complicated rate expression is given later when the hydrogen-ion concentration is also considered. When bromide concentration is large, (3) will reduce to (4) with k' as the pseudo-first-order rate constant.

$$-d[IO_3^-]/dt = k'[IO_3^-] \qquad (4)$$

The bromide concentration used in column 5 for the calculation was the average of the initial and final concentrations. In some of the experiments, bromide is not in large excess and only first few points were considered for the calculation of the pseudo-first-order rate constants. For experiments 8, 17, 21, and 22 with somewhat larger concentrations of bromide, the results with $5 \times 10^{-3}\ M$ phenol were irregular and the rate constants were larger. On employing a higher concentration of the phenol as indicated in Table I, expected results were obtained. Second-order nature with respect to bromide is quite obvious from Table I. A log–log plot of the rate and the bromide concentration yielded a straight line with a slope of 1.98. A plot of rate and bromide concentration passes through the origin and hence there is no term independent of bromide in the rate expression. This removes any doubt about a significant possibility of iodate–phenol reaction or the reduction of iodate in any other way.

Table I: Pseudo-First-Order and Third-Order Rate Constants

$[H_2SO_4] = 0.5\ M$; [phenol] $= 5 \times 10^{-3}\ M$; $t = 35°$

Expt no.	$10^4[IO_3^-]$, M	$10^3[Br^-]$, M	$10^4k'$, sec^{-1}	$k_3 = k'/[Br^-]^2$, $l.^2\ mol^{-2}\ sec^{-1}$
1	1.00	5.00	8.87	3.69
2	2.00	5.00	8.25	3.58
3	2.00	6.00	11.9	3.54
4	2.00	7.50	19.2	3.60
5	3.00	5.00	8.36	3.78
6	3.00	6.00	12.2	3.75
7	3.00	7.50	19.2	3.70
8[a]	3.00	9.00	28.0	3.70
9	4.00	5.00	8.38	3.62
10	4.00	6.00	11.5	3.67
11	4.00	7.50	18.7	3.71
12	5.00	5.00	8.05	3.98
13	5.00	6.00	12.0	3.97
14	5.00	7.50	18.9	3.86
15	6.00	6.00	11.9	3.97
16	6.00	7.50	18.9	3.97
17[a]	6.00	9.00	26.8	3.80
18[b]	7.00	7.50	18.7	4.04
19[b]	8.00	6.00	11.8	4.36
20[b]	8.00	7.50	19.0	4.23
21[a]	4.00	9.00	29.2	3.95
22[a]	5.00	9.00	27.1	3.75
23	2.50	7.50	19.6	3.74

[a] Phenol was $2 \times 10^{-2}\ M$. [b] Phenol was $1 \times 10^{-2}\ M$.

Some more results with stoichiometric concentrations of iodate and bromide are shown in Figure 2. The third-order rate constants calculated from the slopes of the straight lines of this figure are similar to those of Table I. Some of these experiments were carried out in the presence of $2 \times 10^{-2}\ M$ phenol. With 0.005 M phenol in these experiments, few initial points were not on the straight line and the reaction was faster in the beginning as is obvious from Figure 3. Incidently these are the cases of higher concentrations of iodate. All these reaction mixtures turned slightly yellow and had the odor of bromine. Normal behavior of the reaction, however, was found by increasing the concentration of phenol. Figure 3 shows how by increasing phenol, deviation from the third-order plots yielding straight line decreases. Further, it is also seen from Figure 3 and from other plots (not shown) that in the later stages of the reaction almost parallel straight lines are obtained, indicating the same rate in all the cases. The reason for initial deviation from the third-order straight-line plots is not obvious.

Reaction Between HBr and KIO_3. In a few experiments HBr was employed instead of potassium bromide and the results of Table II fairly agree with those of Table I. The third-order rate constants are slightly

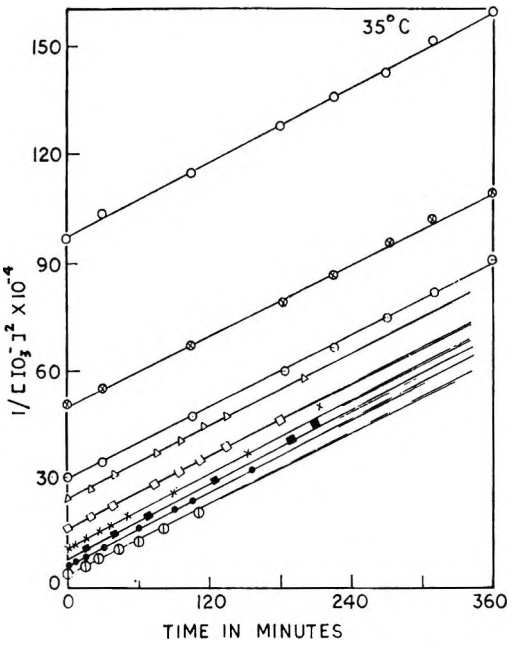

Figure 2. Third-order plots of the reaction between iodate and bromide in the presence of phenol: $[H_2SO_4] = 0.5\ M$; ○, ⊗, ⊖, △, □—$[C_6H_5OH] = 5 \times 10^{-3}\ M$; ×, ■, ●,—$[C_6H_5OH] = 2 \times 10^{-2}\ M$; ⊕, $[C_6H_5OH] = 3 \times 10^{-2}\ M$. In the reaction, $2[IO_3^-] = [Br^-]$: ○, $2.0 \times 10^{-3}\ M$; ⊗, $2.8 \times 10^{-3}\ M$; ⊖, $3.6 \times 10^{-3}\ M$; △, $4.0 \times 10^{-3}\ M$; □, $5 \times 10^{-3}\ M$; ×, $6 \times 10^{-3}\ M$; ■, $7 \times 10^{-3}\ M$; ●, $8 \times 10^{-3}\ M$; ⊕, $10 \times 10^{-3}\ M$.

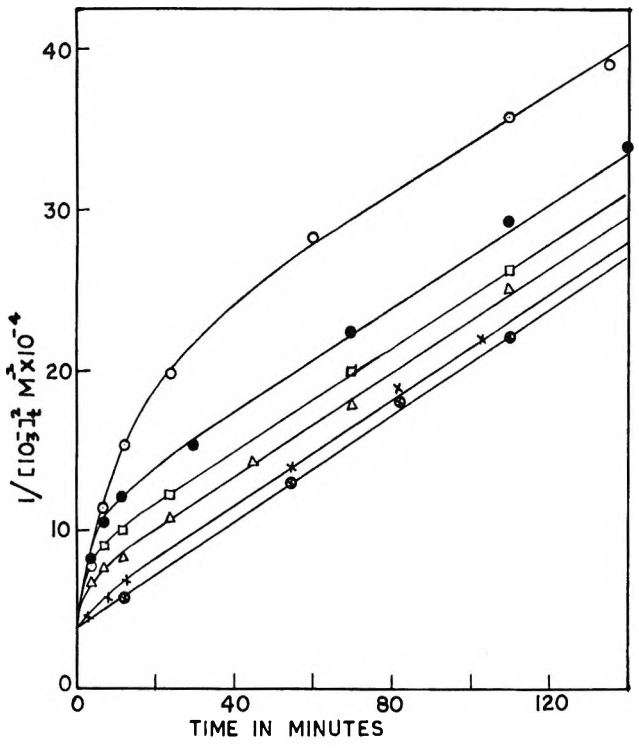

Figure 3. Effect of phenol on the reaction between iodate and bromide and deviation from the third-order plots for the reaction, $2[IO_3^-] = [Br^-] = 1 \times 10^{-2}\ M$: $[H_2SO_4] = 0.5\ M$; $[C_6H_5OH]$ = ○, $8 \times 10^{-3}\ M$; ●, $1 \times 10^{-2}\ M$; □, $1.2 \times 10^{-2}\ M$; △, $1.4 \times 10^{-2}\ M$; ×, $1.7 \times 10^{-2}\ M$; ⊗, $2 \times 10^{-2}\ M$.

higher in the case of higher concentrations of HBr than those of KBr.

Table II: Third-Order Rate Constants for HBr–KIO_3 Reaction

$[H_2SO_4] = 0.5\ M$; $[IO_3^-] = 5.0 \times 10^{-4}\ M$; [phenol] = $5 \times 10^{-3}\ M$, $t = 35°$

Expt no.	10^3[HBr], M	$10^4k'$, sec^{-1}	k_3, $l.^2\ mol^{-2}\ sec^{-1}$
24	4.00	5.01	4.09
25	5.00	8.06	3.98
26	6.00	11.5	3.80
27	7.00	15.3	3.62
28	7.50	19.4	3.96
29	8.00	22.9	4.07
30	9.00	30.9	4.28

Hydrogen-Ion Dependence. Hydrogen-ion concentration was varied with perchloric acid at different ionic strengths and temperatures. The rate increases significantly with the increase of hydrogen-ion concentration. Plots of first-order constants *vs.* $[HClO_4]$ yield curves passing through the origin and hence the rate has no term independent of hydrogen ions. A log–log plot of the rate and hydrogen-ion concentration yielded a straight line with a slope of 2.6.

Effect of Ionic Strength and Salts. Ionic strength was changed with the help of sodium perchlorate, and perchloric acid was used instead of sulfuric acid. The results at different hydrogen-ion concentrations are shown in Table III. The minimum in the rate is observed at the ionic strength of 0.6 M with the three concentrations of perchloric acid employed for the investigation.

A few more salts like sodium chloride, sodium nitrate, sodium sulfate, barium nitrate, and aluminum nitrate, etc., were also employed for the investigation. The change in k_3 was small and negative.

Tervalent aluminum salt contributes more to the ionic strength and hence the decrease in the rate was large. The rate in the presence of nitrate was lower than that expected. A similar effect was observed by Amis and coworkers[20] in the oxidation of iodide by bromate ion. It appears that the nitric acid formed increases the iodometric value in the determination of iodate. In the presence of chloride the rate was slightly higher. Skrabal and Weberitsch[21] reported that chloride ion accelerates the analogous reaction between bromate and bromide.

Effect of Varying the Dielectric Constant. A few reactions were carried out in mixtures of water and ethyl alcohol. The rate increased with the lowering

(20) Indelli, G. Nolan, and E. S. Amis, *J. Amer. Chem. Soc.*, **82**, 3233 (1960).

(21) A. Skrabal and S. R. Weberitsch, *Monatsh.*, **36**, 211 (1915).

Table III: Third-Order Rate Constants at Different Ionic Strengths

$[IO_3^-] = 5 \times 10^{-4}\ M$; $[Br^-] = 1.5 \times 10^{-2}\ M$; [phenol] $= 1 \times 10^{-2}\ M$; $t = 35°$

μ, M	0.1	0.2	0.3	0.4	0.5	0.6	0.7	0.8	1.0	1.1	1.2	1.5	2.2
10^2k_3, l.^{2} mol^{-2} sec^{-1} [H$^+$] = 0.1	8.0	6.1		5.5	5.2	5.0	5.4			6.2		7.2	
10^2k_3, l.^{2} mol^{-2} sec^{-1} [H$^+$] = 0.2		38	33	31		30		31	34		39	46	87
10^2k_3, l.^{2} mol^{-2} sec^{-1} [H$^+$] = 0.3			98			80		100				125	

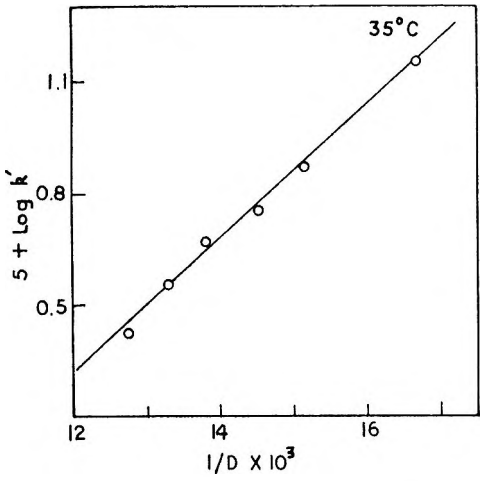

Figure 4. Variation of rate constant with dielectric constant of the medium (different mixtures of water and alcohol): $[KIO_3] = 5 \times 10^{-4}\ M$; $[KBr] = 6.4 \times 10^{-3}\ M$; $[H_2SO_4] = 0.35\ M$; $[C_6H_5OH] = 0.015\ M$.

in the dielectric constant. A plot of log k' against $1/D$ (Figure 4) yields a straight line.

Energy and Entropy of Activation. The reaction was studied at five other temperatures within the range 30–45°. The third-order rate constants were found to be 2.55, 3.23, 3.68, 4.61, 5.51, and 7.35 l.^{2} mol^{-2} sec^{-1} at 30, 33, 35, 38, 40, and 45°, respectively. The energy of activation for the overall reaction was 14.0 ± 0.5 kcal mol^{-1} and the entropy of activation was −12.3 cal deg^{-1} mol^{-1}.

Discussion

In general the rate laws for the iodate oxidations and in fact most halate–halide reactions[22] exhibit second-order hydrogen-ion dependence, although one[23] and three[24] orders have also been reported in the iodate–iodide reaction. Proton catalysis can be considered to be due to the labilization of the oxide ion separating from the iodine(V) atom of the iodate.[25] The order with respect to the hydrogen ion may apparently suggest a two-term rate law, one involving $[H^+]^2$ and the other involving $[H^+]^3$. However, one has to consider equilibrium 5 also before giving the exact form of the rate law.

$$H^+ + IO_3^- \underset{}{\overset{K_5}{\rightleftharpoons}} HIO_3 \qquad (5)$$

Recent studies on conductance,[26–29] pH, absorption spectra, and other properties have shown that acid solutions of iodate largely have IO_3^- and HIO_3 together with small proportions of more protonated species and polymerized forms.[30,31] The rate law showing complete hydrogen-ion dependence and in conformity with the observed results would be of the form

$$-d[IO_3^-]/dt = \frac{[IO_3^-][Br^-]^2[H^+]^2(k_1 + k_2[H^+]^2)}{1 + K_5[H^+]} \qquad (6)$$

where k_1 and k_2 are complex rate constants for the two steps. From this it follows that at constant iodate and bromide

$$k_3 = \frac{[H^+]^2(k_1 + k_2[H^+]^2)}{1 + K_5[H^+]} \qquad (7)$$

Thus a plot of $k_3\ (1 + K_5\ [H^+])/[H^+]^2$ against $[H^+]^2$ would yield a straight line from the slope and intercept of which k_2 and k_1 can be calculated. The values of K_5 at different temperatures were obtained from the work of Li and Lo.[32] Figure 5 shows such plots at different ionic strengths and Figure 6 shows them at different temperatures. Table IV shows the values of k_1 and k_2 and energy and entropy of activation corresponding to the two steps. The rate laws (6) or (7) might appear

(22) J. O. Edwards, *Chem. Rev.*, **50**, 455 (1952).
(23) H. Kubina, *Montash.*, **43**, 439 (1923).
(24) M. Wronska and B. Banas, *Bull. Acad. Pol., Sci., Ser. Sci., Chim.*, **13** (1), 5 (1965).
(25) J. O. Edwards, "Inorganic Reaction Mechanism," W. A. Benjamin, New York, N. Y., 1964, p 137.
(26) J. F. Harvey, J. P. Redfern, and J. E. Salmon, *J. Inorg. Nucl. Chem.*, **26**, 1326 (1964).
(27) A. D. Pethybridge and J. E. Prue, *Trans. Faraday Soc.*, **63**, 2019 (1967).
(28) G. C. Hood, A. C. Jones, and C. A. Reilly, *J. Phys. Chem.*, **63** 101 (1959).
(29) J. R. Durig, O. D. Bonner, and W. H. Breazeale, *ibid.*, **69**, 3886 (1965).
(30) R. M. Fuoss and C. A. Kraus, *J. Amer. Chem. Soc.*, **55**, 476 (1933).
(31) M. R. Mayer, *Curr. Sci.*, **8**, 73 (1939).
(32) N. C. C. Li and Y.-T. Lo, *J. Amer. Chem. Soc.*, **63**, 394, 397 (1941).

Table IV: Separate Rate Constants k_1 and k_2 at Different Ionic Strengths and Temperatures

$[IO_3^-] = 5 \times 10^{-4}\ M$; $[Br^-] = 6 \times 10^{-3}\ M$; [phenol] $= 1 \times 10^{-2}\ M$

	Temp, °C						E_a, kcal mol^{-1}	$\Delta S^{\pm}$, cal deg^{-1} mol^{-1}
	30	35				40		
Ionic strength, M	0.84	0.8	1.0	1.5	2.0	0.8		
k_1, l.^{4} mol^{-4} sec^{-1}	9.0	15	22	25	33	24	18.5 ± 0.7	4.93
k_2, l.^{6} mol^{-6} sec^{-1}	92	146	152	220	372	242	18.3 ± 0.9	9.07

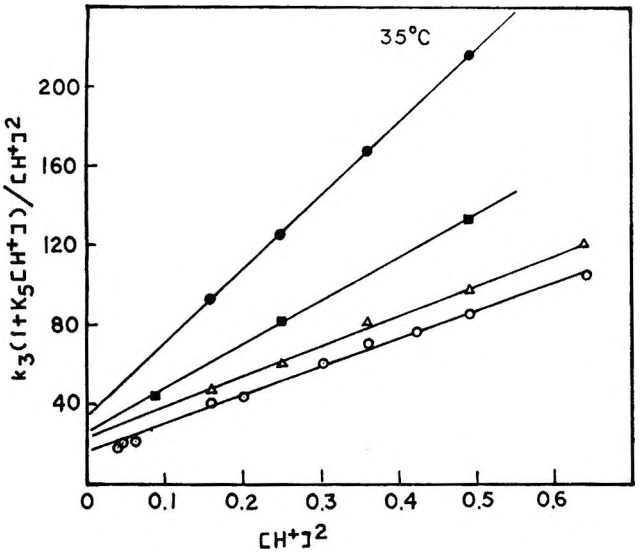

Figure 5. k_1 and k_2 at different ionic strengths adjusted by $NaClO_4$; $K_5 = 6.94$ (35°): $[KIO_3] = 5 \times 10^{-4}\ M$; [KBr] $= 6 \times 10^{-3}\ M$; $[C_6H_5OH] = 1 \times 10^{-2}\ M$; ●, $\mu = 2\ M$; ■, $\mu = 1.5\ M$; △, $\mu = 1\ M$; ○, $\mu = 0.8\ M$.

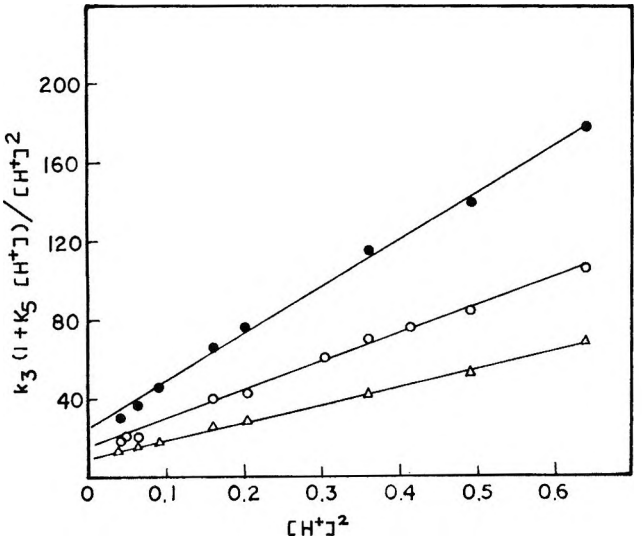

Figure 6. k_1 and k_2 at different temperatures at ionic strengths adjusted by $NaClO_4 = 0.8\ M$: $[KIO_3] = 5 \times 10^{-4}\ M$; [KBr] $= 6 \times 10^{-3}\ M$; $[C_6H_5OH] = 1 \times 10^{-2}\ M$; ●, 40°; ○, 35°; △, 30°; $K_5 = 7.4$ (40°); 6.94 (35°); 6.54 (30°).

unusual but probably no other rate law can explain the variation of order in hydrogen ion between two and three, and also the fact that iodate exists mainly as IO_3^- and HIO_3 in the acid solutions employed. In fact, the range of hydrogen ion investigated is very limited on account of the iodate–phenol reaction becoming significant above 1.0 M $HClO_4$ and the main reaction becoming too slow in solutions less acidic than 0.2 M ($HClO_4$). The reliability of the rate law insofar as hydrogen ion dependence is concerned, is therefore limited.

In spite of many common features in the halate–halide reactions, no one mechanism[22] conforms to the observed results and this is more true for the iodate reactions. Also no unique mechanism for a particular iodate reaction can be given and the possibility of alternatives always exists. The hydrogen-ion effect has been interpreted[33,34] in terms of the formation of cationic species IO_2^+ in the iodate–iodide reaction. Bray and Liebhasky[35] assume the formation of $H_2I_2O_3$ in the same reaction. It is, therefore, quite probable that the hydrogen-ion involvement occurs in the formation of cationic species as in reactions 8 and 9.

$$IO_3^- + 2H^+ \rightleftharpoons IO_2^+ + H_2O \quad (8)$$

$$HIO_3 + 2H^+ \rightleftharpoons HIO_2^{2+} + H_2O \quad (9)$$

Although iodyl cation has not been produced in solution as free ion, it does appear in complex[36] form as $IO_2HSO_4 \cdot H_2SO_4$ in sulfuric acid solutions. However, whether it is iodyl cation or its complex form is not known. Further support to the existence of this species is lent by the postulation of BrO_2^+ by several workers[20,37] in the bromate oxidations and the formation of the molecule,[38] bromyl fluoride BrO_2F. It is, therefore, quite probable that species such as shown in (8) and (9) can form in the present system. Barton and Wright,[39,40] however, do not favor this postulate in the bromate–iodide and iodate–iodide reaction catalyzed by

(33) M. G. Peard and C. F. Cullis, *Trans. Faraday Soc.*, **47**, 616 (1951).

(34) K. J. Morgan, *Quart. Rev. Chem. Soc.*, **8**, 123 (1954).

(35) W. C. Bray and H. A. Liebhasky, *J. Amer. Chem. Soc.*, **52**, 3580 (1930).

(36) R. J. Gillespie and J. B. Senior, *Inorg. Chem.*, **3**, 440 (1964).

(37) E. Abel, *Helv. Chim. Acta*, **33**, 785 (1950).

(38) M. Schmeisser and E. Pammer, *Angew. Chem. Int. Ed. Engl.*, **69**, 781 (1957).

(39) A. F. M. Barton and G. A. Wright, *J. Chem. Soc. A*, 1747 (1968).

(40) A. F. M. Barton and G. A. Wright, *ibid.*, 2096 (1968).

acetate and other carboxylate ions. The probability is that the iodyl cation would interact as soon as formed with iodide or bromide (in low acid medium) forming iodyl iodide or iodyl bromide. The central iodine atom can still hold atoms increasing its coordination number, and thus attack by nucleophiles I^-, Br^-, and carboxylate ions can be explained.

Three mechanisms can explain the hydrogen-ion dependence observed and it is not possible to distinguish them kinetically.

(A) IO_2^+ reacts with Br^- and also HBr

$$IO_2^+ + 2Br^- \xrightarrow{k_{10}} IO_2^- + Br_2 \quad (10)$$

$$H^+ + Br^- \overset{K_{11}}{\rightleftharpoons} HBr \quad (11)$$

$$IO_2^+ + 2HBr \xrightarrow{k_{12}} HIO_2 + Br_2 + H^+ \quad (12)$$

Reactions 10 and 12 might be more complicated, each one of them occurring in two steps; *e.g.*, reaction 10 could be a combination of reactions 13 and 14.

$$IO_2^+ + Br^- \overset{k_{13}}{\rightleftharpoons} IO_2 \cdot Br \quad (13)$$

$$IO_2 \cdot Br + Br^- \xrightarrow{k_{14}} IO_2^- + Br_2 \quad (14)$$

The concentration of HBr, however, is very small and only a small fraction of the reaction is likely to occur *via* the second part of this path (with a term square in HBr). This is likely to be of some importance in high acid media.[41]

(B) IO_2^+ reacts with Br^- (step 10) and HIO_2^{2+} reacts with both Br^- and HBr.

$$HIO_2^{2+} + Br^- \overset{K_{15}}{\rightleftharpoons} HIO_2 \cdot Br^+ \quad (15)$$

and

$$HIO_2 \cdot Br^+ + HBr \xrightarrow{k_{16}} HIO_2 + Br_2 + H^+ \quad (16)$$

or

$$HIO_2^{2+} + HBr \overset{K_{17}}{\rightleftharpoons} HIO_2 \cdot HBr^{2+} \quad (17)$$

and

$$HIO_2 \cdot HBr^{2+} + Br^- \xrightarrow{k_{18}} HIO_2 + Br_2 + H^+ \quad (18)$$

This appears to be more probable than the second part of (A) but it is difficult to explain the fact that HBr rather than Br^- reacts in step 16 or 17.

(C) If one assumes that IO_2^+ reacts with Br^- and also with HBr, and HIO_2^{2+} reacts only with Br^-, a rate law similar to (19) involving three terms in hydrogen ion would be obtained

$$-d[IO_3^-]/dt = \frac{[IO_3^-][Br^-]^2[H^+]^2(k' + k''[H^+] + k'''[H^+]^2)}{1 + K_6[H^+]} \quad (19)$$

Although this rate law is slightly different than (6), its possibility is not ruled out because this also can explain the varying order in hydrogen ion between two and three. However, its verification is not possible with the data available for the limited range of hydrogen ion.

Table III shows a minimum in the rate at ionic strength *ca.* 0.6 *M*. Similar minima of rate with increasing ionic strength have been reported in the Cr^{VI}–iodide[42] and $Fe(CN)_6^{3-}$–iodide[43] reactions. This is, however, expected from the Davies[44] equation (20) with a suitable value for *B*.

$$-\log f_f = AZ_+Z_-[(\sqrt{\mu}/(1 + \sqrt{\mu})) - B\mu] \quad (20)$$

Scatchard's[45] development of the kinetic rate law leads to expression 21 where **e** is the electronic charge, **k** is the Boltzmann constant, r is the radius of the activated complex, and f_1 is a typical activity coefficient for a univalent ion. Since the rate of reaction is proportional to f_1^4, Figure 4 gives the value of r as 1.2×10^{-8} which is not very different from the ionic radii of univalent ions.

$$\log f_1^4 = \mathbf{e}^2/2.3D\mathbf{k}Tr \quad (21)$$

(41) C. N. Hinshelwood, *J. Chem. Soc.*, 694 (1947).

(42) K. E. Howlett and S. Sarsfield, *J. Chem. Soc. A*, 683 (1968).

(43) Y. A. Majid and K. E. Howlett, *ibid.*, 679 (1968).

(44) C. W. Davies, "Ion Association," Butterworths, London, 1962.

(45) G. Scatchard, *Chem. Rev.*, **10**, 229 (1932).

Ion Exchange in Molten Salts. V. Potassium Zeolite A as an Ion Exchanger in Nitrate Melts

by M. Liquornik*[1] and Y. Marcus

Israel Atomic Energy Commission, Soreq Nuclear Research Center, Yavneh, Israel *(Received November 30, 1970)*

Publication costs borne completely by The Journal of Physical Chemistry

The exchange of sodium and potassium ions between nitrate melts and zeolite at 350° shows that the potassium zeolite A, $K_{12}(AlSiO_4)_{12}$, behaves differently from the occluded sodium zeolite $Na_{22}[(AlSiO_4)_{12}(NO_3)_{10}]$; only after exchanging $7K^+$ with Na^+ does partial occlusion of $Na^+NO_3^-$ ion pairs occur. Small amounts of K^+ in the zeolite are sufficient to block the channels of the zeolite and interfere with the absorption of more nitrate ions. At 450° occlusion starts at much lower sodium concentration than at 350°. The order of selectivity is Ag > Li > Na > K for potassium zeolite and dilute solutions in a potassium nitrate melt.

Introduction

In a previous paper in this series,[2] dealing with the formation of occlusion compounds of zeolites and molten nitrates, it was reported that potassium zeolite A does not occlude molten potassium nitrate at 350°. It was therefore felt that it would be interesting to look into the ion-exchange properties of this zeolite and compare them with those of sodium zeolite A which gives occlusion compounds, and the ion-exchange properties of which have already been investigated.[3,4] This paper reports on exchange reactions of the potassium zeolite A in melts containing potassium nitrate and sodium, lithium, or silver nitrates.

Experimental Section

The nitrate salts used were of reagent grade, and were oven dried at 110° for at least 1 hr. The Linde Molecular Sieve A exchanger was obtained in powder form from Linde Air Products Ltd. The exchanger was first sieved through a 200 mesh sieve and then sedimented in water in a 100-cm column. The main fraction was collected and analyzed. The ratios SiO_2–Al_2O_3 = 1.94 and Na_2O–Al_2O_3 = 0.965 were found to be in good agreement with the composition expected from the formula of the unit cell. The potassium form was prepared by ion exchange with aqueous solutions of KNO_3 and was contaminated by less than 0.1% sodium. Attempts to prepare potassium zeolite by ion exchange with pure molten KNO_3 at 350° failed. Indeed after a single treatment with molten KNO_3 only 6.6 Na^+ ions from a total of 12 available could be exchanged with potassium. Repeating this treatment four times with fresh potassium nitrate melts, not more than 9 Na^+ ions have been exchanged.

The experimental and analytical procedures have been described in the first part of this series;[3] both the exchanger and the liquid phase were analyzed. Previously it was shown that equilibrium was reached in a matter of hours, but for technical reasons the experiments were maintained for 16–24 hr at the desired temperature.

The unit cell of potassium zeolite, $K_{12}(AlSiO_4)_{12}$, taken as 1 mol of zeolite, will henceforth be called $K_{12}A$ where A stands for the group $(AlSiO_4)_{12}$; $\bar{n}_K$, etc., are the number of moles of potassium, etc., ions per mole of zeolite. The concentrations in the liquid phase are expressed as mole fractions N, according to Temkin's model.

Results

The exchange reaction with sodium was investigated at 350 and 450° and for the other ions at 350°. At the lower temperature the concentration of the sodium ions in the solution varied from a dilute solution of Na^+ in KNO_3 (N_{NaNO_3} = 0.009) to a solution of K^+ in $NaNO_3$ (N_{NaNO_3} = 0.76). The results are shown in Figure 1.

From the exchange isotherm given in Figure 1, it is evident that up to an exchange of seven K^+ by Na^+, the reaction is stoichiometric, therefore for every Na^+ which enters the zeolite, 1 K^+ joins the solution, and indeed the alkali:silica ratio in the zeolite for the first nine points is 0.983 ± 0.052 as compared with 1.000, the ideal ratio. Beyond this point, the ratio increases and reaches 1.39 for the last point (N_{NaNO_3} = 0.76), and the reaction changes its nature from an exchange reaction to one of occlusion of $Na^+NO_3^-$ ion pairs

$$Na_7K_5(AlSiO_4)_{12} \xrightarrow[4.7NaNO_3]{1Na^+} Na_{12.7}K_{4.0}[(AlSiO_4)_{12}(NO_3)_{4.7}] + K^+ \quad (1)$$

In view of the above results, the question arises whether it is possible to obtain $Na_{22}[(AlSiO_4)_{12}(NO_3)_{10}]$

(1) Physical Chemistry Laboratory, Imperial College of Science and Technology, London S.W. 7.

(2) M. Liquornik and Y. Marcus, *Isr. J. Chem.*, 6, 115 (1968).

(3) M. Liquornik and Y. Marcus, *J. Phys. Chem.*, 72, 2885 (1968).

(4) M. Liquornik and Y. Marcus, *ibid.*, 72, 4704 (1968).

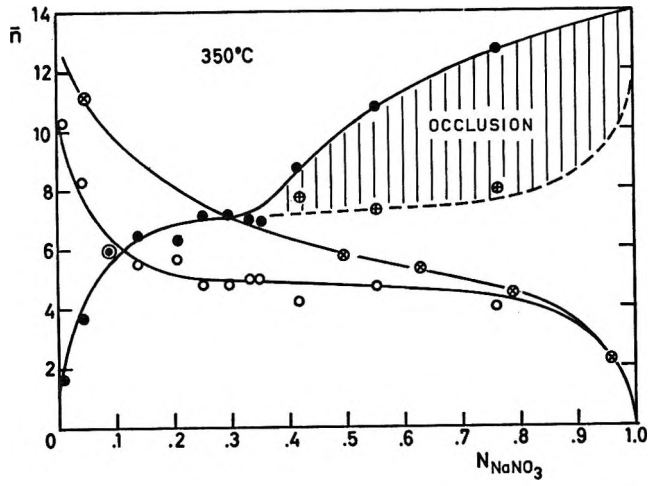

Figure 1. Exchange isotherm at 350°: ●, $\bar{n}_{Na}$; ○, $\bar{n}_K$; ⊕, 12-$\bar{n}_K$ all starting with $K_{12}A$; ⊗, $\bar{n}_K$ starting with $Na_{12}A \cdot 10NaNO_3$. The occlusion of nitrate ($\bar{n}_{NO_3} = \bar{n}_{Na} + \bar{n}_K - 12$) is shown.

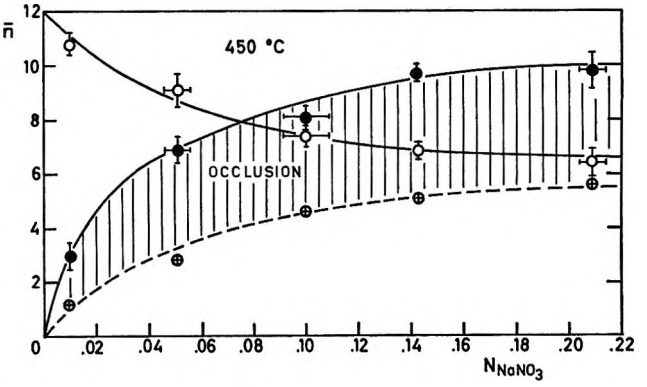

Figure 2. Exchange isotherm at 450°; the symbols are the same as in Figure 1.

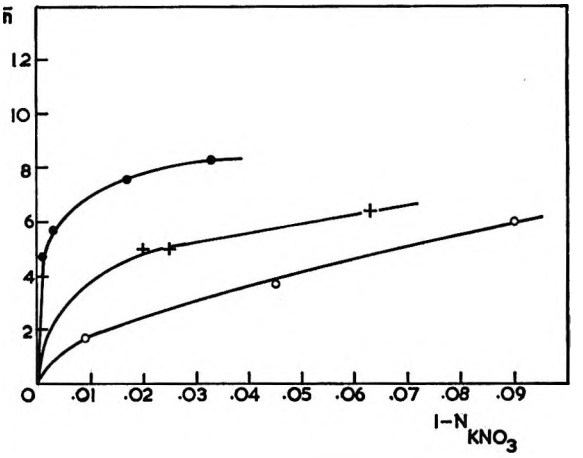

Figure 3. Exchange isotherm at 350°: ●, $\bar{n}_{Ag}$; +, $\bar{n}_{Li}$; and ○, $\bar{n}_{Na}$ (from Figure 1) for the dilute region, starting with $K_{12}A$.

from $K_{12}(AlSiO_4)$ at all. In order to answer this question and to test whether the above exchange reactions are reversible, a sample of potassium zeolite was kept on a shaker for 1 week at 350° with molten sodium nitrate. After filtering the liquid phase, the zeolite was cooled, the excess salt washed off, a sample of the zeolite was taken for analysis, while the rest was added to pure potassium nitrate, and the whole again heated on a shaker for 1 week at 350°. The results of these experiments can be written as follows

$$K_{12}(AlSiO_4)_{12} + NaNO_3 \text{ (large excess)} \longrightarrow Na_{12.2}K_{2.2}[(AlSiO_4)_{12}(NO_3)_{2.4}] + KNO_3(N_{NaNO_3} = 0.96) \quad (2)$$

$$Na_{12.2}K_{2.2}[(AlSiO_4)_{12}(NO_3)_{2.4}] + KNO_3 \text{ (large excess)} \longrightarrow Na_{3.0}K_{9.0}[(AlSiO_4)_{12}(NO_3)_{2.7}] + NaNO_3(N_{NaNO_3} = 0.037) \quad (3)$$

Further results were obtained at the higher temperature of 450°. The concentration range of the solution was more restricted and varied from $N_{NaNO_3} = 0.01$ to 0.21, and every experiment was performed in duplicate, so that a better appreciation of the experimental and analytical error could be obtained. In Figure 2, where the exchange isotherm is given, every point shows the spread in values obtained by averaging the results.

In order to compare the selectivity series of KA and NaA, the distribution of Li^+ and Ag^+ ions from diluted molten potassium nitrate solutions was determined and the results are shown in Figure 3. Only the minor constituent of the solution was determined analytically and the distribution calculated by the difference between this concentration and the initial one.

Discussion

The exchange reactions involving $K_{12}A$ are expected to be quite different from those with $Na_{12}A$ because of the ability of the latter to occlude $Na^+NO_3^-$ ion pairs and the absence of occlusion by the former.[2] Indeed, exchanging the K^+ in the $K_{12}A$ with Na^+, one would expect that the reaction would proceed

$$K_{12}(AlSiO_4)_{12} + 22Na^+ + 10NO_3^- \longrightarrow Na_{22}[(AlSiO_4)_{12}(NO_3)_{10}] + 12K^+ \quad (4)$$

It is obvious that such a reaction cannot be stoichiometric; we proceed from a zeolite which has 12 cations (K^+) and finish with a zeolite containing 22 cations (Na^+). Furthermore, the question of the reversibility of such a reaction also arises; in other words, if proceeding from the occluded sodium zeolite (the only stable form in a molten sodium nitrate solution) will the occlusion be driven out?

$$Na_{22}[(AlSiO_4)_{12}(NO_3)_{10}] + 12K^+ \longrightarrow K_{12}(AlSiO_4)_{12} + 12Na^+ + 10NaNO_3 \quad (5)$$

It is evident that small amounts of potassium ions in the zeolite are sufficient to block the channels of the zeolite and therefore interfere with the absorption of more nitrate ions. The zeolite can be considered as

an interconnected tridimensional network of undulating channels, with cations located at the entrance to these channels. Apparently, the presence of one potassium ion in one of those channels is sufficient to block it for the big NO_3^- ions and therefore only partial occlusion occurs. It is conceivable that only with the last K^+ removed does the total occlusion of the zeolite occur, but the last K^+ ions are difficult to exchange. It should be further pointed out that the same is true in the aqueous system.[5] Indeed $Na_{12}A$ and water at room temperature (and therefore 20–25° above the melting point of the liquid phase) will give the hydrated zeolite $Na_{12}A \cdot 27H_2O$ and the reaction is strongly exothermic. Barrer,[6] from thermodynamic considerations, proved that the free energy of the zeolite is lowered by the occlusion of foreign molecules, and that on reversing the reaction, there is no energetic reason for the zeolite to eliminate the occluded molecules.

At 450° the occlusion of NO_3^- ions begins at a much lower sodium concentration, at $N_{NaNO_3} = 0.01$ (Figure 2). Indeed, already at this concentration the alkali–silica ratio is significantly different from unity (1.15 ± 0.04), which corresponds to an occlusion of 1.8 mol of NO_3^-/mol of $K_{12}A$. It is remarkable that the occlusion rapidly reaches the maximum value for this range of concentration, of 4.1 ± 0.5 mol of NO_3^-/mol of $K_{12}A$, and which is about the same occlusion as that reached at the lower temperature. So far, there is no direct evidence, which may explain why at higher temperatures there is an occlusion at such a low sodium concentration.

It may be recalled that Barrer and Walker[7] found analogous behavior in an aqueous system and $Na_{12}A$. They report that at room temperature there is no absorption of sodium chloride from the aqueous solution into the zeolite, but at 90° the zeolite occludes 1 mol of sodium chloride.

Breck[8] pointed out that at −196° oxygen is freely absorbed by the zeolite, while nitrogen is essentially excluded, whereas at −100° both gases are equally well absorbed. Although the nitrogen molecule is only 0.2 Å larger than the oxygen molecule, this difference is sufficient at −196° to effect the separation. "Over a temperature interval of 30–300° a variation in vibration amplitude of 0.1–0.2 Å is very reasonable and a variation of 0.3 Å in the aperture diameter could result from this thermal effect alone. Thus the aperture may be effectively smaller at low temperature.[8]" Additionally, at the higher temperatures, the K^+ ion may change its position, by being drawn closer to the oxygen ions of the interior of the α-cage opening. All these factors together act to allow the occlusion of NO_3^- ions. Furthermore, it is also possible that at 450° the occlusion is made from $K^+NO_3^-$ ion pairs. Supporting this suggestion is the fact that the occlusion is essentially constant (4.1 mol of NO_3^-/mol of $K_{12}A$) over most of the range examined (except the first point) and is not a function of the sodium concentration in the melt, unlike at 350°.

Figure 3 shows the order of selectivity Ag > Li > Na > K for exchange from very dilute solutions of nitrate of the foreign ions in potassium nitrate with potassium zeolite A. The order for these three ions is the same as that for the corresponding sodium nitrate–sodium zeolite A system.[3] The transposition of potassium to the least preferred position in the selectivity series when the space in the α cage is used up by large ions has been noted and discussed previously.[3]

(5) R. M. Barrer, L. V. C. Rees, and D. J. Ward, *Proc. Roy. Soc., Ser. A*, **273**, 180 (1963).

(6) R. M. Barrer, *J. Phys. Chem. Solids*, **16**, 84 (1960).

(7) R. M. Barrer and A. J. Walker, *Trans. Faraday Soc.*, **60**, 171 (1964).

(8) D. W. Breck, *J. Chem. Educ.*, **41**, 678 (1964).

Shock Tube Isomerization of Cyclopropane

by E. A. Dorko,* D. B. McGhee, C. E. Painter, A. J. Caponecchi, and R. W. Crossley

Department of Aero-Mechanical Engineering, Air Force Institute of Technology, Wright-Patterson Air Force Base, Ohio 45433 *(Received June 22, 1970)*

Publication costs assisted by the Air Force Institute of Technology

The shock tube isomerization of cyclopropane to propylene has been studied as a possible model system for shock tube isomerizations of small-ring compounds. At low (0.1–1%) concentrations of cyclopropane in helium–argon matrix the reaction is unimolecular with a high-pressure first-order rate $k_\infty = 10^{14.50\pm0.14} e^{-65100\pm800/RT}$ sec^{-1} in the temperature range 935–1397°K. The rate constants are smaller than the extrapolated low-temperature results. This difference is expressed in a smaller value for the frequency factor. A discussion of reasons for this difference is given. When the substrate concentration was increased to 5% it was found that the Arrhenius parameters are no longer in agreement with the values obtained at low substrate concentration. At this concentration the exothermicity of the reaction and other effects so seriously affect the ideality of the shock wave that the model cannot be relied upon for kinetic analysis.

Introduction

The single pulse shock tube[1] isomerization of cyclopropane to propylene has been studied as a possible model system for shock tube isomerizations of small-ring compounds. We wish to report that a kinetic analysis of this reaction in the shock tube gave values for the Arrhenius parameters for infinite pressure which allow the extension of the kinetic analysis[2] to a higher temperature regime. The Arrhenius parameters obtained from a least squares fit of the data for the temperature range 935–1397°K are given in eq 1.

$$k_\infty = 10^{14.50\pm0.14} e^{-65,100\pm800/RT} \quad (1)$$

These parameters were obtained at a substrate concentration of 0.1–1% in a helium–argon matrix. When the substrate concentration was increased to 5% it was found that the Arrhenius parameters were no longer in agreement with the values obtained at low substrate concentration. The parameters are given in eq 2.

$$k_\infty = 10^{7.66\pm0.15} e^{-30,200\pm400/RT} \quad (2)$$

Graphs of data to support eq 1 and 2 are shown in Figures 1 and 2, respectively.

Experimental Section

Procedure. The shock tube was fabricated in the school machine shop and was of the double diaphragm type described by Glick, Squire, and Hertzberg.[3] It was fabricated of 2.5-in. stainless steel with a 5-ft driver and 10-ft driven section. The dump tank was 10 ft^3 in volume. The test section, comprising the last 4 ft of the driven section, was honed with a J-7 finished stone to a microfinish of 14 to 16 to ensure a smooth inner surface.

The driven section of the shock tube was evacuated to 1 μ pressure by means of an oil diffusion pump. The leak rate at this pressure was 1–2 μ/hr. The dump tank and driver section were evacuated to 400 μ pressure.

Diaphragm material was 0.020-in. aluminum (5052-H32) scored to 0.010 in.

Velocity measurements were made by means of $^1/_{16}$ in. wide thin-film platinum heat gauges which were placed 12.000 in. apart. The signal from the heat gauges was fed into an electronic counter (Hewlett–Packard Universal Counter, 5325A) which counted to 0.1 μsec.

Pressure in the driven section was measured with a Wallace and Tiernan gauge (Model No. FA145) accurate to ±0.1 psia. Initial driven pressures varied from 2.0 to 5.0 psia.

Dwell time was obtained either from the appropriate wave diagram for ideal flow based on the Mach number of the shock wave and on the gas properties[4] or according to the method described by Lifshitz, Bauer, and Resler.[5] The pressure trace necessary for the second method was obtained with a Kistler pressure transducer (Model No. 603A) imbedded in the end plate of the shock tube. A slight modification of the latter method was necessary since the isolation valve was in the end plate rather than upstream of the test section. When the isolation valve was opened immediately after the

(1) S. H. Bauer, *Science*, **141**, 867 (1963).

(2) (a) B. R. Davis and D. S. Scott, *Ind. Eng. Chem., Fundam.*, **3**, 20 (1964); (b) B. S. Rabinovitch, E. W. Schlag, and K. B. Wiberg, *J. Chem. Phys.*, **28**, 504 (1958); (c) H. O. Pritchard, R. G. Sowden, and A. F. Trotman-Dickenson, *Proc. Roy. Soc., Ser. A*, **217**, 563 (1953); (d) E. S. Corner and R. N. Pease, *J. Amer. Chem. Soc.*, **67**, 2067 (1945); (e) T. S. Chambers and G. B. Kistiakowsky, *ibid.*, **56**, 399 (1934).

(3) H. S. Glick, W. Squire, and A. Hertzberg, "A New Shock Tube Technique for the Study of Higher Temperature Gas Phase Reactions," in "Fifth Symposium (International) on Combustion," Reinhold, New York, N. Y., 1955.

(4) See A. J. Caponecchi, M.S. Thesis, Air Force Institute of Technology, Wright–Patterson Air Force Base, Ohio, June 1967, for a development of the theory and for the necessary computer program.

(5) A. Lifshitz, S. H. Bauer, and E. L. Resler, Jr., *J. Chem. Phys.*, **38**, 2056 (1963).

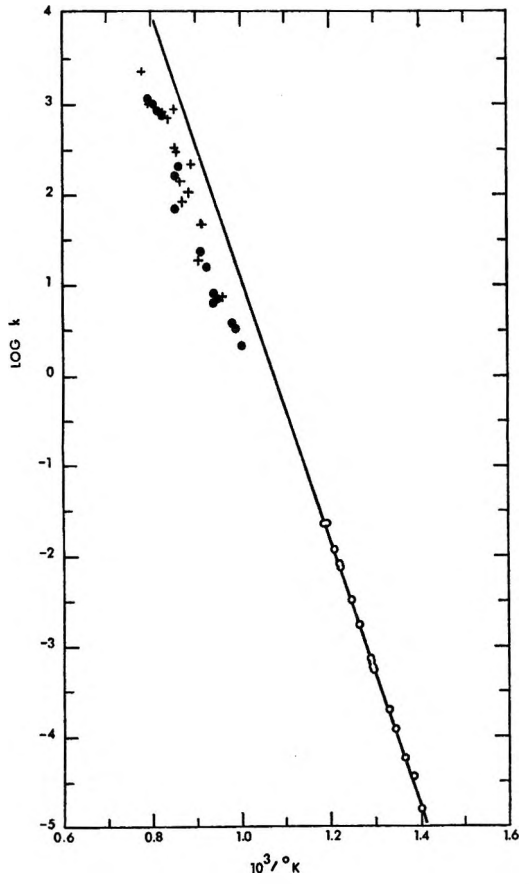

Figure 1. Arrhenius plot of the first-order rate constants for the unimolecular isomerization of cyclopropane: O, low-temperature work;[2] ●, 0.1% cyclopropane; +, 1.0% cyclopropane.

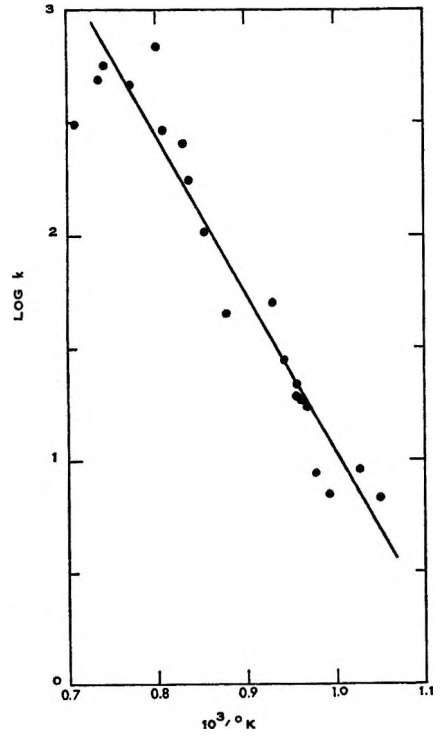

Figure 2. Arrhenius plot of the first-order rate constants for unimolecular isomerization of cyclopropane (5% C_3H_6).

gas mixture had been shocked, a sample of the shocked gas was withdrawn into an evacuated sample chamber of known volume. The assumption was made that the volume of gas that flows from the shock tube exactly equals the volume of the sample chamber. The appropriate expressions for the calculation of the space-averaged dwell time are given in eq 3 and 4.

$$t_{av} = t_{meas} + (1 + 1/M_R)b/a_5 \quad (3)$$

$$b = -V/2A \quad (4)$$

M_R is the Mach number of the reflected shock wave, a_5 is the sonic velocity behind the reflected shock wave, V is the volume of the sample chamber, and A is the cross-sectional area of the shock tube. Both methods gave identical results for dwell time.

In order to maximize dwell time, the shocks were "tailored." Impedance matching was achieved for the various pressure ratios by varying the ratio of helium and argon in the driven section from a He/Ar ratio of 3.5 to a ratio of 1.5.[4] With this technique, dwell times of the order of 2.1 msec were achieved.

Analysis of the gas in the sample chamber was done by gas chromatography. Immediate isolation of a gas sample after the shock prevented diffusion of cold gas mixture from the upstream section of the driven section.[6] This procedure ensured that the gas sample used for analysis came from the test section of the shock tube. The gas mixture was analyzed on a 20 ft × 1/8 in. column packed with 15% triacetin on 60–80 mesh Chromosorb P which was operated at room temperature. For the higher gas concentrations thermister detectors were used. For 0.1% substrate concentration flame ionization detection was used. Retention times were 8.0 min for cyclopropane and 6.0 min for propylene. Extent of reaction was based on the amount of propylene formed. Side products were detected only in the 5% samples shocked at high temperatures (1300–1400°K). The major side product was separated with a 10 ft × 1/4 in. 5A molecular sieve column and was identified as methane. The amount of methane accounted for no more than 2% of the final gas mixture. Other side products were present in much lesser amounts and no attempt was made to identify them.

The shock temperature calculated from the initial shock velocity[4] was corrected for the temperature increase due to the heat of reaction according to eq 5.

$$T = T_{SHOCK} + \frac{2}{3}\frac{\Delta H_{reaction}}{C_{p\ gas\ mixture}} \times (\%\ substrate)(\%\ reaction) \quad (5)$$

Heat capacity values for argon and helium were obtained from the JANAF Tables and the values for cyclopropane were calculated from spectroscopic data.[7]

(6) A. Bar-Nun and A. Lifshitz, *J. Chem. Phys.*, **47**, 2878 (1967).

(7) H. P. Nielsen, M.S. Thesis, Air Force Institute of Technology, Wright-Patterson Air Force Base, Ohio, June 1969.

The temperature correction is necessary since release of the heat of reaction will cause a temperature increase during the course of the reaction. The factor of $^2/_3$ is used instead of the more obvious factor of $^1/_2$ to take into account the nonlinearity of the temperature–rate relationship. For small temperature changes which do not affect the ideality of the shock wave, the correction serves as a refinement to the temperature determination. However, as the temperature increase becomes large the correction can only be taken as approximate (see below).

In order to test the shock tube and the shock procedure, *tert*-butyl alcohol was converted into isobutylene in the shock tube. The analysis procedure followed was that described by Tsang.[8] The Arrhenius parameters obtained are given in eq 6.

$$k = 10^{13.35\pm0.20}e^{-60{,}500\pm100/RT} \quad (6)$$

The parameters are comparable, within experimental error, to those obtained by Tsang.[8]

Error Estimate. The Arrhenius parameters, A and E, were calculated using program ACTEN,[9] a program which calculates least squares with both the logarithmic (linear) and the exponential (nonlinear) forms of the Arrhenius equation. The values reported are those which yield the minimum sum of squares for the conventional linear form.

The tolerances reported for the parameters also were obtained from the results of program ACTEN. The program displays sums of squares corresponding to selected confidence levels[10] as well as sums of squares over any desired range of (A,E). Thus, loci of the selected confidence levels can be plotted on the A,E plane. The tolerance reported for each parameter was determined from the intersection of the reported value of the other parameter with the 99% confidence level.

The deviations from ideality of the shock wave and the various other sources of random error present in a kinetic analysis by a single-pulse shock tube technique have been discussed at length by Lifshitz, Bauer, and Resler[5] and by Tsang[8] among others. The procedure employed by the present authors was checked out using the *tert*-butyl alcohol system studied by Tsang.[8] To preclude the possibility of invalid results due to systematic errors, the low concentration analysis was performed at 0.1% and 1.0% substrate concentration. The plot of Figure 1 shows that the kinetic analysis is independent of concentration in this range.

Discussion

Figures 1 and 2 are Arrhenius plots of the shock data for the concentrations listed. In addition, Figure 1 shows the Arrhenius curve extrapolated from low-temperature results. The data on which the plots are based are listed in Tables I and II.

A first-order mechanism was assumed and the data were reduced according to eq 7 where C_0 and C_f are the initial and final concentrations of cyclopropane and t_{av} is the dwell time of the extracted gas sample. The rate constants were corrected for infinite pressure in the following manner. The total pressure in the reflected shock (P_5) was split into the partial pressures of the component gases. The inert portion of the gas mixture was assumed to be 30% argon and 70% helium. The pressure efficiencies of argon and helium were taken to be 0.06 and 0.053, respectively, that of cyclopropane.[2c]

$$k_1 = \ln (C_0/C_f)/t_{av} \quad (7)$$

Table I: Summary of Data for the Unimolecular Isomerization of Cyclopropane at Low (0.1–1%) Concentrations

Temp, °K	P_5,[a] mm	P_1,[b] mm	Dwell time, msec	Extent of reaction	k_{uni}, sec^{-1}	k_∞, sec^{-1}
			1% Cyclopropane			
1042.3	1767	103	2.005	0.010	4.8	7.6
1055.3	2698	155	2.055	0.008	4.5	6.7
1096.1	2875	155	2.216	0.062	28.8	44.6
1103.6	2892	155	1.756	0.021	11.9	18.9
1125.9	2996	155	2.197	0.266	140.7	222.8
1127.8	2024	103	2.007	0.116	61.3	106.4
1146.2	3128	155	2.167	0.105	51.2	83.0
1158.6	2621	129	2.058	0.147	77.3	134.3
1168.0	2123	103	2.408	0.333	168.4	306.2
1169.6	3297	160	2.188	0.345	193.5	321.4
1172.8	2123	103	2.158	0.644	478.3	891.3
1191.7	3274	155	2.228	0.603	414.4	687.1
1214.2	3380	155	2.209	0.634	455.7	792.5
1264.5	3638	155	2.210	0.707	556.3	988.6
1281.6	2479	103	2.210	0.916	1121.9	2239.0
			0.1% Cyclopropane			
998.7	2362	155	1.254	0.002	1.5	2.1
1003.8	3187	207	1.304	0.003	2.4	3.3
1017.5	3255	207	1.404	0.004	2.6	3.6
1057.4	3481	207	1.555	0.008	4.9	7.1
1060.3	1729	103	1.955	0.007	3.8	6.6
1062.9	3524	207	1.355	0.006	4.4	8.0
1081.0	4535	259	1.456	0.016	11.1	15.7
1095.4	2792	155	1.266	0.019	14.9	23.6
1156.6	3070	155	2.108	0.229	123.4	208.9
1166.4	3105	155	2.258	0.191	94.0	163.3
1170.2	3113	155	2.208	0.083	39.4	68.6
1215.6	3352	155	2.109	0.559	387.9	706.3
1231.2	2250	103	2.259	0.606	412.3	841.4
1233.7	2257	103	2.259	0.658	474.8	993.1
1250.9	3482	155	2.259	0.815	747.5	1107.0

[a] Reflected shock pressure. [b] Initial driven section pressure.

(8) W. Tsang, *J. Chem. Phys.*, **40**, 1498 (1964).

(9) R. W. Crossley and E. A. Dorko, Program ACTEN, available from the Quantum Chemistry Program Exchange, Indiana University, Bloomington, Ind., No. QCPE 179.

(10) R. S. Burington and D. C. May, "Handbook of Probability and Statistics," Handbook Publishers, Sandusky, Ohio, 1958, p 158.

Table II: Summary of Data for the Unimolecular Isomerization of Cyclopropane at High (5%) Concentrations

Temp, °K	P_b,[a] mm	P_1,[b] mm	Dwell time, msec	Extent of reaction	k_∞, sec^{-1}
955.7	2404	155	2.231	0.015	6.7
974.1	2741	168	2.435	0.022	8.9
1006.2	2641	155	2.397	0.017	7.0
1021.6	2744	155	2.258	0.020	8.8
1031.8	2763	155	2.083	0.036	17.4
1040.4	3405	181	1.880	0.035	18.8
1044.0	2836	155	2.208	0.048	22.1
1048.5	2861	155	2.108	0.039	19.1
1060.7	3224	169	2.141	0.057	27.7
1074.2	3028	156	1.992	0.095	50.1
1140.0	2809	130	1.407	0.061	44.8
1169.9	2813	129	2.351	0.240	116.8
1192.6	3448	155	2.411	0.348	177.4
1203.9	3467	155	2.412	0.470	263.1
1240.7	3556	146	2.069	0.448	287.3
1249.9	3654	155	1.409	0.609	667.2
1296.8	3614	142	1.785	0.563	463.2
1350.0	2733	103	2.554	0.765	567.4
1361.2	3542	130	2.311	0.688	503.6
1412.1	3412	116	2.352	0.513	305.6

[a] Reflected shock pressure. [b] Initial driven section pressure.

The rate constant was corrected for this effective pressure by utilizing the falloff curve determined at 491°.[11] In addition, the effect of temperature on the position of the plot of log (k/k_∞) against log p was taken into account by utilization of eq 8.[11] The factor n was

$$\Delta \log p = {}^1/_2 n \log (T_2/T_1) \tag{8}$$

taken to be 14, the number of independent vibrations in cyclopropane.[12]

For comparison with present results the commonly accepted low-temperature rate equation for infinite pressure is shown.

$$k_\infty = 10^{15.17} e^{-65{,}500/RT} \tag{9}$$

It can be seen that the activation energies agree but the frequency factors differ by a power of 0.67. The question must immediately be asked if the high-temperature shock tube results represent a direct extension of the low-temperature results. It is obvious from Figure 1 and from a comparison of eq 1 and 9 that this is not the case. The rate constants appear to be smaller than the extrapolated low-temperature results. This difference is expressed in a smaller value for the frequency factor.

Tsang[8] and others[5] have discussed some of the reasons why the rate constants determined in a single pulse shock tube tend to be smaller than expected from low-temperature extrapolation. However, one effect which has not been considered in previous discussions is the large difference in residence time between shock tube experiments and conventional heating techniques. Residence or dwell times in a single pulse shock tube are of the order of several hundreds of microseconds. In comparison, residence times for the low-temperature experiments are much longer than this. In order to understand the significance of this difference, let us consider the mechanism postulated for cyclopropane isomerization. The process is usually represented as an initial second-order activation followed by a first-order decomposition[13] as shown in eq 10 and 11.

$$\nabla + M \underset{k_{-1}}{\overset{k_1}{\rightleftharpoons}} \nabla^* + M \tag{10}$$

$$\nabla^* \xrightarrow{k_2} \text{ 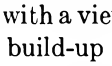 } \tag{11}$$

The rate expressions are given as eq 12 and 13.

$$-\frac{d[\nabla]}{dt} = \frac{k_2 k_1 [\nabla][M]}{k_{-1}[M] + k_2} \tag{12}$$

$$-\frac{d[\nabla]}{dt} = \frac{k_2 k_1 [\nabla]}{k_{-1}} \text{ where } k_{-1}[M] \gg k_2 \tag{13}$$

Equation 12 represents the general rate expression and eq 13 represents the rate expression for high pressure. These two equations can only be developed if it is assumed that after a relatively short initial period the concentration of reactive intermediate reaches its steady-state concentration (the steady-state assumption).[14] The assumption maintains that this induction time is negligibly small compared to the total time of the kinetic determination. As the total residence time decreases this assumption becomes more and more tenuous. Currently, research is being conducted with a view toward determining the time required for the build-up of the concentration of reactive intermediate. Preliminary experiments indicate that this induction time can be as high as 10% of the total dwell time.[15] A subsequent report will deal with this effect in detail.

The activation parameters obtained for the high (5%) substrate concentration vary significantly from the corresponding values obtained for the low-concentration reactions. The activation energy drops and the frequency factor value is no longer of the expected order of magnitude for a first-order reaction. It is quite likely that the deviation at the high concentration is caused by the substantial change from ideality in the shock tube due to the exothermicity of the isomerization. The average temperature change, as calculated by eq 5, for the 5% concentration can be as high as 60–70°K. A

(11) N. B. Slater, *Phil. Trans.*, **A246**, 57 (1953).

(12) W. E. Falconer, T. F. Hunter, and A. F. Trotman-Dickenson, *J. Chem. Soc.*, 609 (1961).

(13) S. W. Benson and H. E. O'Neal, "Kinetic Data on Gas Phase Unimolecular Reactions," NSRDS-NBS-21, U. S. Government Printing Office, Washington, D. C. 20402, 1970, p 15.

(14) W. S. Benson, *J. Chem. Phys.*, **20**, 1605 (1952).

(15) E. A. Dorko, U. Grimm, G. Mueller, and R. W. Crossley, work in progress.

temperature change of this magnitude should have a significant effect on the shock wave, and most likely a simple analysis based on an ideal, one-dimensional wave is no longer adequate. At the high concentration the reacting mixture may be exothermic enough to cause the velocity to approach the Chapman–Jouget or detonation velocity.[16] This effect would make the simple shock wave model invalid. In addition to the heat effects there may be a series of systematic errors such as boundary layer effects which become appreciable at the high concentration.[17] In addition there may be a significant change in kinetic mechanism.

A discrepancy exists between the present high-concentration results and the results of a previous high-concentration isomerization performed by Miyama and Takeyama.[17] Their work utilized 5 and 10% cyclopropane concentrations. Their analysis as a first-order reaction shows a bend in the curve at 1200°K. This bend was not observed in the present work, whether an Arrhenius plot was made assuming either a first- or second-order mechanism. However, a first-order plot of the present data and a plot of the previous work indicate that the present rate constants are lower by almost two orders of magnitude than the constants determined by the previous researchers. An Arrhenius plot of both sets of data leads to two parallel lines for the region below 1200°K. We feel that the temperature determination by Miyama and Takeyama is too low. Apparently no correction was made for the heat given off by the reaction. At the 5% concentration this could lead to as much as a 60–70°K temperature difference and at the 10% concentration the difference could be as great as 120–140°. Another discrepancy could arise due to difference in shock velocity determination.

Clearly additional work remains to be performed with the higher cyclopropane concentrations. The important consideration at this point is that only the low-concentration data can be reasonably compared with the low-temperature work.

Acknowledgments. We wish to thank Dr. Ulrich Grimm and Dr. Gerhard Mueller for advice and assistance given during the fabrication of the shock tube. The technical assistance of Mr. John Parks and Mr. Ernest Pinti is gratefully acknowledged. The work was supported in part by the Air Force Office of Aerospace Research through the OAR/AFIT Research Support Fund.

(16) R. L. Belford and R. A. Strehlow, *Ann. Rev. Phys. Chem.*, **20**, 247 (1969).

(17) H. Miyama and T. Takeyama, *Bull. Chem. Soc. Jap.*, **38**, 2189 (1965).

NOTES

Entropies of Vaporization for Fluorocarbons and Hydrocarbons from the Hildebrand Rule

by E. W. Funk and J. M. Prausnitz*

Department of Chemical Engineering, University of California, Berkeley, California 94720 *(Received October 5, 1970)*

Publication costs borne completely by The Journal of Physical Chemistry

The anomalous behavior of solutions containing saturated hydrocarbons and fluorocarbons, first noted by Hildebrand and Scott,[1] continues to be incompletely understood. In an effort to contribute toward a better understanding of such solutions we have calculated the entropies of vaporization of 12 saturated hydrocarbons and of the corresponding 12 fluorocarbons. For reasons given by Hildebrand many years ago,[2] we have calculated these entropies not at the same temperature nor at the same reduced temperature but at the same saturated vapor volume, arbitrarily chosen to be 49.5 l. per mol.

Data Reduction

The molar entropy of vaporization Δs is given by the Clapeyron equation

$$\Delta s = \Delta v\left(\frac{dP}{dT}\right) \tag{1}$$

where P is the saturation (vapor) pressure at temperature T and Δv is 49.5 l. minus the molar volume of the saturated liquid. The pressure and temperature corresponding to the selected saturated-vapor volume are found from simultaneous solution of two equations

$$49.5 = \frac{RT}{P} + B(T) \tag{2}$$

$$P = f(T) \tag{3}$$

(1) J. H. Hildebrand and R. L. Scott, "Solubility of Nonelectrolytes," Reinhold, New York, N. Y., 1950.

(2) J. H. Hildebrand, *J. Chem. Phys.*, **7**, 233 (1939).

where $B(T)$ is the second virial coefficient at temperature T and where $f(T)$ is an empirical function (*e.g.*, the Antoine equation) representing the saturation pressure data.

For the hydrocarbons, saturation pressure and volumetric data were taken from Rossini, *et al.*[3] Data for fluorocarbons were taken from several sources as shown in Table I. Second virial coefficients were calculated using the correlation of Pitzer and Curl[4] with critical data taken from Zwolinski.[5]

Results

Entropies of vaporization are shown in Table I; some of the results for hydrocarbons were presented earlier by Hermsen.[6] For each hydrocarbon and its corresponding fluorocarbon we find that the latter has a larger entropy of vaporization by about 1 eu; this result had been anticipated by Hildebrand and Rotariu.[7] If we make the reasonable assumption that the configurational entropy of a hydrocarbon at 49.5 l. per mol is equal to that of its corresponding fluorocarbon at the same volume, we conclude that the saturated fluorocarbon liquid has a lower configurational entropy (more order) than that of the corresponding hydrocarbon. We note that the consistently higher entropy of vaporization for fluorocarbons is maintained despite temperature differences. For example, for methane the equilibrium temperature is 92.6°K, whereas for perfluoromethane it is higher, 126.0°K. On the other hand, for cyclopentane the equilibrium temperature is 302.3°K, whereas for perfluorocyclopentane it is lower, 275.6°K. Nevertheless, in both cases the entropy of vaporization of the fluorocarbon is larger than that of the corresponding hydrocarbon by 1.4 eu.

Table I: Entropies of Vaporization at a Saturated Vapor Volume of 49.5 l./mol

Hydrocarbon[a]	T, °K	Δs, cal mol^{-1} °K^{-1}
Methane	92.6	22.5
Ethane	163.2	22.7
Propane	209.3	22.6
Butane	251.2	22.3
Pentane	288.6	22.3
Isopentane	279.8	22.1
Hexane	323.1	22.2
2-Methylpentane	313.6	22.1
3-Methylpentane	316.1	22.1
2,3-Dimethylbutane	311.6	21.7
Heptane	353.3	22.4
Cpclopentane	302.3	22.4
Corresponding fluorocarbon		
Tetrafluoromethane[c]	126.0	23.9
Hexafluoroethane[d]	174.2	23.5
Perfluoropropane[e]	215.2	23.0
Perfluorobutane[f]	250.4	23.2
Perfluoropentane[g]	282.5	23.7
Perfluoro-2-methylbutane[g]	283.3	23.4
Perfluorohexane[g]	311.0	23.3
Perfluoro-2-methylpentane[g]	311.2	23.1
Perfluoro-3-methylpentane[g]	311.7	22.8
Perfluoro-2,3-dimethylbutane[g]	313.7	23.1
Perfluoroheptane[h]	337.3	23.6
Perfluorocyclopentane[b,g]	275.6	23.8

[a] For saturation pressure, see ref 3. [b] Saturation pressure of liquid perfluorocyclopentane was extrapolated to lower temperatures by plotting the logarithm of saturation pressure *vs.* $1/T$. [c] M. Simon, C. M. Knobler, and A. G. Duncan, *Cryogenics*, 138 (1967). [d] E. L. Pace and J. G. Aston, *J. Amer. Chem. Soc.*, **70**, 566 (1948). [e] J. A. Brown, *J. Chem. Eng. Data*, **8**, 106 (1963). [f] J. A. Brown and W. H. Mears, *J. Phys. Chem.*, **62**, 960 (1958). [g] G. A. Crowder, Z. L. Taylor, T. M. Reed, and J. A. Young, *J. Chem. Eng. Data*, **12**, 481 (1967). [h] G. D. Oliver and J. W. Grisard, *J. Amer. Chem. Soc.*, **73**, 1688 (1951).

The difference between hydrocarbon liquids and fluorocarbon liquids may have an appreciable effect on the excess functions of their mixtures, as pointed out by Patterson;[8] the Prigogine theory of mixtures of large molecules shows that excess functions depend not only on differences in molecular size and intermolecular energy, but also on differences in the degrees of freedom affected by the environment, as measured by Prigogine's parameter c.

For a fluid whose molecules are perfectly spherical, evaporation at constant temperature affects only translational degrees of freedom but for polyatomic molecules, rotational and vibrational degrees of freedom may be affected also. The higher order in the larger fluorocarbon liquids may be due to hindered rotation and vibration; while such motions are no doubt hindered in hydrocarbon liquids also, it is possible that hindrance is more pronounced in the larger fluorocarbons. This

However, differences in rotation and vibration cannot explain why the entropy of vaporization of tetrafluoromethane is larger than that of methane; for these molecules it is likely that rotational and vibrational degrees of freedom are not at all hindered in the liquid phase. The difference in entropy of vaporization, therefore, cannot be explained by hindered rotation and vibration but may be ascribed to free volumes in the fluorocarbons which are smaller than those of the corresponding hydrocarbons. This conclusion follows directly from the definition of free volume as given by Hildebrand and Scott (reference 1, Chapter 5, eq 32); in this definition the free volume is a function of density but not

(3) F. D. Rossini, K. S. Pitzer, R. L. Arnett, R. M. Braun, and G. C. Pimentel, "Selected Values of the Physical and Thermodynamic Properties of Hydrocarbons and Related Compounds," Carnegie Press, Pittsburgh, Pa., 1953.

(4) K. S. Pitzer and R. F. Curl, *J. Amer. Chem. Soc.*, **79**, 2369 (1957).

(5) A. P. Kudchadker, G. H. Alani, and B. J. Zwolinski, *Chem. Rev.*, **68**, 659 (1968).

(6) R. W. Hermsen and J. M. Prausnitz, *J. Chem. Phys.*, **34**, 1081 (1961).

(7) J. H. Hildebrand and G. J. Rotariu, *J. Amer. Chem. Soc.*, **74**, 4455 (1952).

(8) D. Patterson, *Macromolecules*, **2**, 672 (1969).

of temperature. Further, it is consistent with Sherwood's analysis of second-virial coefficient data[9] which shows that when experimental data are reduced with the square-well potential, the reduced well width for methane is 1.60, whereas that for tetrafluoromethane is 1.48.

Acknowledgment. The authors are grateful to the National Science Foundation for financial support and to J. H. Hildebrand and R. L. Scott for helpful discussions.

(9) A. E. Sherwood and J. M. Prausnitz, *J. Chem. Phys.*, **41**, 429 (1964).

Some Observations on the Viscosity Coefficients of Ions in Various Solvents

by Cecil M. Criss* and Martin J. Mastroianni

Department of Chemistry, University of Miami, Coral Gables, Florida 33124 *(Received November 13, 1970)*

Publication costs assisted by the National Science Foundation

Much has been written concerning the effect of the simple alkali metal, halide, and tetraalkylammonium ions on the thermal and transport properties of aqueous solutions.[1-8] The effects are generally ascribed to the ability of the various ions to increase or decrease the structure of water over that of the pure solvent. The general argument is that small simple ions such as lithium are structure makers while large simple ions such as cesium are structure breakers. On the other hand the tetraalkylammonium salts follow the reverse pattern from the simple ions, and this is usually explained in terms of the special hydrophobic interactions of the hydrocarbon groups with water to increase its "ice-like" structure.[3] Presumably these effects will be observed only in solvents having a high degree of initial structure and capable of being structured still further through hydrophobic interactions. Because of this water has been considered anomalous in this respect. The effect should not be observed for solvents exhibiting only a small amount of structure.

Wu and Friedman[5] and Friedman[6] have examined the heats of transfer of several ions between water and propylene carbonate as a function of ionic radius and observed that ΔH_t° decreases as r increases for the simple ions, but the trend reverses for the tetraalkylammonium ions. Since it is expected that propylene carbonate is nonstructured and is therefore an ideal solvent, this reversal in trend is ascribed entirely to the specific interactions with water. On the other hand, Bhatnagar and Criss[9] examined ΔH_t° for several alkali metal and tetraalkylammonium iodides in various solvents and in some cases observed interruptions in regularity for ΔH_t° of ions between the various nonaqueous solvents. Unfortunately the scarcity of data precluded a definite conclusion. Similar trend reversals for apparent molal heat contents of ions in aqueous solution have been observed by Lindenbaum.[7] For both cations and anions the interruption occurs between the largest simple ion and the smallest complex ion. The results are explained in terms of water structure promotion by the large complex ions.

Viscosities of electrolytic solutions have long been used as an indication of the amount of structure within a solution.[2,10-12] The relative viscosity of an electrolytic solution is given by the well-known Jones–Dole equation[13] in which η and η_0 are the viscosities of the

$$\frac{\eta}{\eta_0} = 1 + A_\eta\sqrt{c} + B_\eta c \qquad (1)$$

solution and pure solvent respectively, A_η and B_η are empirical constants, and c is the concentration. A_η can be calculated theoretically[14,15] and is associated with ion–ion interactions, while B_η, the ion–solvent parameter, cannot presently be calculated satisfactorily on an *a priori* basis. However, this parameter can be evaluated experimentally, and when it is divided into its ionic components to obtain B_η (ion) it provides a very useful tool for indicating the degree of structure in solution.

A survey of the literature has produced B_η coefficients for a number of electrolytes containing both simple and complex ions, in the solvents water, methanol, and acetonitrile.[8,10,16-18] The validity of eq 1 for the nonaqueous solutions indicates that, for the

(1) H. S. Frank and W. Wen, *Discuss. Faraday Soc.*, **24**, 133 (1957).

(2) M. Kaminsky, *ibid.*, **24**, 171 (1957).

(3) Th. Ackerman, *ibid.*, **24**, 180 (1957).

(4) H. Rüterjans, F. Schreiner, U. Sage, and Th. Ackerman, *J. Phys. Chem.*, **73**, 986 (1969).

(5) Y. C. Wu and H. L. Friedman, *ibid.*, **70**, 501 (1966).

(6) H. L. Friedman, *ibid.*, **71**, 1723 (1967).

(7) S. Lindenbaum, *ibid.*, **74**, 3027 (1970).

(8) R. L. Kay, T. Vituccio, C. Zawoyski, and D. F. Evans, *ibid.*, **70**, 2336 (1966).

(9) O. N. Bhatnagar and C. M. Criss, *ibid.*, **73**, 174 (1969).

(10) R. W. Gurney, "Ionic Processes in Solution," McGraw-Hill, New York, N. Y., 1953.

(11) R. H. Stokes and R. Mills, "Viscosity of Electrolytes and Related Properties," in "The International Encyclopedia of Physical Chemistry and Chemical Physics," E. A. Guggenheim, J. E. Mayer, and F. C. Tompkins, Ed., Pergamon Press, New York, N. Y., 1965.

(12) E. R. Nightingale, Jr., "Chemical Physics of Ionic Solutions," B. E. Conway and R. G. Barradas, Ed., Wiley, New York, N. Y., 1966, Chapter 7.

(13) G. Jones and M. Dole, *J. Amer. Chem. Soc.*, **51**, 2950 (1929).

(14) H Falkenhagen and M. Dole, *Z. Phys. Chem., Abt. B*, **6**, 159 (1929).

(15) H. Falkenhagen and E. L. Vernon, *Phys. Z.*, **30**, 140 (1932).

(16) G. Jones and H. J. Fornwalt, *J. Amer. Chem. Soc.*, **57**, 2041 (1935)

(17) D. F. Tuan and R. M. Fuoss, *J. Phys. Chem.*, **67**, 1343 (1963).

(18) R. P. T. Tomkins, E. Andalaft, and G. J. Janz, *Trans. Faraday Soc.*, **65**, 1906 (1969).

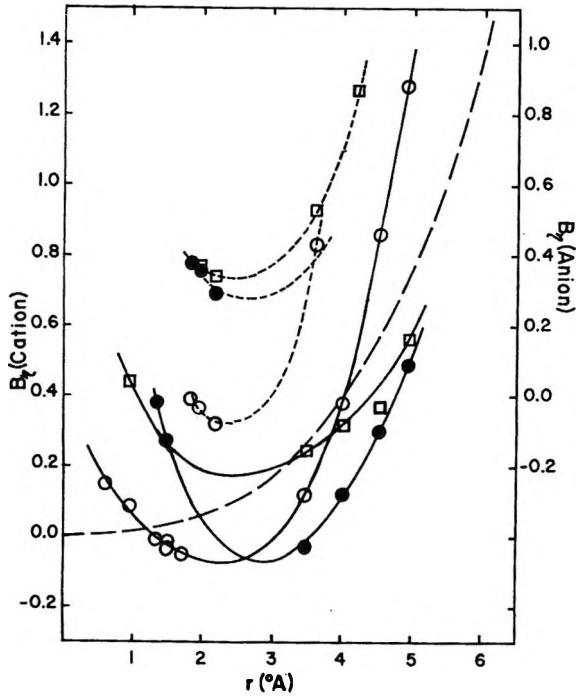

Figure 1. Variation of B_η (ion) coefficients with radius of ion: cations, solid curves; anions, dashed curves; theoretical value, broken curve; open circles, aqueous solutions; solid circles, methanolic solutions; squares, acetonitrile solutions.

concentrations over which B_η was evaluated, no dissociation was occurring and therefore ion-pair formation is probably not significant. Furthermore, for acetonitrile B_η (ion) has been shown to be approximately additive.[17] The B_η (ion) data along with the radii of the various ions are summarized in Table I. For the solvents, water and methanol, the division of B_η into its ionic components is on the basis that B_η (K^+) = B_η (Cl^-); in acetonitrile, B_η (Me_4N^+) is assigned a value of 0.25. However, for the present discussion the choice of division of B_η is unimportant. Values of B_η (ion) as a function of radius are plotted in Figure 1.

As expected and observed by others, B_η (ion) for aqueous solutions of cations decreases with radius for the simple ions and increases for the tetraalkylammonium ions. Not unexpectedly, the few data that are available for anions appear to follow the same trend. If B_η (ion) were governed by the Einstein effect,[19] as suggested by some authors, then one would have

$$B_\eta \text{ (ion)} = 2.5\bar{V}_i \qquad (2)$$

where $\bar{V}_i$ is the partial molal volume of the solute ion. Accordingly, one would expect a continual increase in B_η (ion) with the radius of the ion. One must keep in mind that the Einstein relationship is derived for noncharged spherical particles and that its application to ions, even large ions with low charge densities, may not be valid. Nevertheless, it is instructive to compare

Table I: B_η (ion) Coefficients in Various Solvents at 25°

Ion	Radius, Å[a]	B_η (ion) Water[b]	Methanol[c]	Acetonitrile[d]
Li^+	0.60	0.15		
Na^+	0.95	0.09		0.44
K^+	1.33	−0.007	0.382	
Rb^+	1.48	−0.03		
Cs^+	1.69	−0.05		
NH_4^+	1.48	−0.01	0.279	
Me_4N^+	3.47	0.12	−0.03	0.25
Et_4N^+	4.00	0.38	0.12	0.32
Pr_4N^+	4.52	0.86	0.30	0.37
Bu_4N^+	4.94	1.28	0.49	0.56
Cl^-	1.81	−0.007	0.382	
Br^-	1.95	−0.03	0.358	0.37
I^-	2.16	−0.08	0.293	0.34
Pic^-	3.71	0.43[e]		0.53
BPh_4^-	4.2			0.87

[a] Radii of simple ions and NH_4^+ are from L. Pauling, "The Nature of the Chemical Bond," Cornell University Press, Ithaca, N. Y., 1960. Radii of the tetraalkylammonium ions are from R. A. Robinson and R. H. Stokes, "Electrolyte Solutions," Academic Press, New York, N. Y., 1959. The radius of the picrate ion is from ref 18 and the radius of the tetraphenylboride ion is from E. Grunwald, G. Baughman, and G. Kohnstam, *J. Amer. Chem. Soc.*, **82**, 5801 (1960). [b] Data are from ref 11, except for the picrate ion which is from ref 12. [c] Data are from ref 9 and 17. [d] Data are from ref 18 except Na^+ which was evaluated from viscosity data from ref 19. [e] 18°.

this relationship with the available data, and therefore B_η (ion), calculated by eq 2, is included in Figure 1. The partial molal volume term is assumed to be the volume occupied by 1 mol of hard spheres of radius r. The fact that aqueous solutions of simple ions do not even qualitatively follow this equation can be partly explained in terms of the structure-breaking effect of the simple ions on water as the radius increases, which in some cases leads to negative B_η (ion) values. However, if the decrease were entirely dependent upon structure breaking by the larger simple ions, then in principle it would not be observed in "structureless" solvents.

A similar trend is observed for cations in methanol, and the few data for the simple anions in this solvent indicate that they too will exhibit a similar curve. This is somewhat unexpected in view of the fact that methanol is generally considered to be much less structured than water. One must conclude that the smaller simple ions either have much less effect in destructuring methanol, if one assumes the solvent to be initially structured, or conversely the smaller ions have a much better ability of structuring the solvent, presumably through electrostriction, if one assumes the solvent to be structureless. On the basis of partial molal volumes of electrolytes in this solvent,

(19) A. Einstein, *Ann. Phys.*, 19, 289 (1906); *ibid.*, 34, 591 (1911).

Millero[20] has suggested that electrostriction is much greater than for aqueous solutions. Similarly, the tetramethylammonium ion is either most capable of destructuring the solvent, or conversely least capable of structuring the solvent.

Even more surprising is the similar trend exhibited by ions in acetonitrile. In this presumably "structureless" solvent the larger simple ions of both valence types apparently exhibit smaller B_η (ion) values than the smaller ions. This can only be explained in terms of structuring of the solvent by the smaller cations, again presumably through electrostriction. In addition, if the division of B_η is even approximately correct, the complex anions appear to have an ability to structure acetonitrile even more than that exhibited by the tetraalkylammonium ions on the structure of water. As one would expect, the Einstein effect is not even qualitatively in agreement with the pattern observed for B_η (ion).

Considering that the curves for B_η (ion) in all three solvents are qualitatively similar in spite of the fact that the natures of the solvents are widely different, and different explanations must be invoked, leads one to conclude that all these interactions exist to a more or less degree in every solvent, and that one should be careful in attempting to explain results solely on the basis of unique specific interactions of certain ions with water structure.

Acknowledgment. We are grateful to the National Science Foundation for their financial support through Grant GP-14537.

(20) F. J. Millero, *J. Phys. Chem.*, **73**, 2417 (1969).

Negative Ion–Molecule Reactions in Perfluoropropane

by Timothy Su, Larry Kevan,*[1]

Department of Chemistry, Wayne State University, Detroit, Michigan 48202

and Thomas O. Tiernan

Aerospace Research Laboratories, Chemistry Research Laboratory, Wright-Patterson Air Force Base, Ohio 45433

(Received March 29, 1971)

Publication costs assisted by the Aerospace Research Laboratories

A variety of negative ions have been observed by electron impact on perfluorocarbons.[2-4] The F^- ion is generally much more abundant than the carbon-containing negative ions. Reactions of these negative ions may be of importance in the radiation chemistry of fluorocarbons[5] and are of intrinsic interest in general ion–molecule reaction chemistry. Since there is no information available on such reactions, we present here a quantitative study of the negative ion–molecule reactions in C_3F_8. Reactions have been identified and their kinetic energy dependence deduced in a tandem mass spectrometer. Studies at higher pressure were performed with a single-source, time-of-flight mass spectrometer. F^- is unreactive with C_3F_8, but the carbon-containing negative ions undergo collision-induced dissociation (CID) reactions.

Experimental Section

Perfluoropropane was obtained from Air Products and Chemicals, Inc., and was purified by trapping the middle portion of the C_3F_8 peak from a 4.6 × 0.63 cm diameter silica gel gas chromatographic column operated at 120°. The C_3F_8 was further degassed before use. Unpurified C_3F_8 contained an unidentified trace impurity which led to 86% F_2^- formation at 200 μ pressure. The purified C_3F_8 gave less than 0.5% F_2^- formation at 200 μ pressure.

The ARL in-line tandem mass spectrometer was used for studying the individual ion–molecule reactions. This instrument has been described previously.[6,7] Reactant ions are produced by electron impact in a specially designed negative ion source.[8] The mass-analyzed reactant ion beam is decelerated to any desired kinetic energy over the range of ~0.3–100 eV before entering the collision chamber. The pressure of a desired target gas can be varied in the collision chamber. Product ions are mass-analyzed in a second mass spectrometer and detected with an electron multiplier using pulse counting techniques. The collision chamber and the reactant ion source were at room temperature for these experiments.

Rate constants were calculated by comparing the observed secondary ion to primary ion ratios with the NO_2^- to O^- ratio from reaction 1 under similar experimental conditions.

$$O^- + NO_2 \longrightarrow NO_2^- + O \qquad (1)$$

The rate constant for reaction 1 was taken as 1.3×10^{-9} cm^3 molecule^{-1} sec^{-1} for thermal energy ions.[9] The accuracy of this procedure with regard to collec-

(1) John Simon Guggenheim Fellow, 1970–1971.

(2) M. M. Bibby and G. Carter, *Trans. Faraday Soc.*, **59**, 2455 (1963).

(3) K. A. G. MacNeil and J. C. J. Thynne, *Int. J. Mass Spectrom. Ion Phys.*, **2**, 1 (1969).

(4) C. Lifshitz and R. Grajower, *ibid.*, **3**, 211 (1969).

(5) L. Kevan and P. Hamlet, *J. Chem. Phys.*, **42**, 2255 (1965).

(6) J. H. Futrell and C. D. Miller, *Rev. Sci. Instrum.*, **37**, 1521 (1966).

(7) C. D. Miller, F. P. Abramson, and J. H. Futrell, *ibid.*, **37**, 1618 (1966).

(8) T. O. Tiernan, "Development of a High-Efficiency Negative Ion Source for Mass Spectrometers," OAR Progress 1969, Office of Aerospace Research, U. S. Air Force Report OAR-69-0017, 1969, p 49. Available as AD 699300 from Clearinghouse, U. S. Dept. of Commerce, Springfield, Va. 22151.

(9) J. F. Paulson, *Advan. Chem. Ser.*, **No. 58**, 28 (1966).

tion efficiency for the product ions has been discussed.[10] The reaction dependencies on kinetic energy are most conveniently plotted in terms of cross sections. The cross section scale is established for the lowest kinetic energy by dividing the rate constant by the appropriate ion velocity at 0.3 eV.

A modified Bendix Model 12-101 time-of-flight (TOF) mass spectrometer which permits operation at source pressures up to 1 Torr[11] was used for high-pressure studies. The electron current was maintained at about 5×10^{-9} A and the electron energy at 100 eV in these experiments. The ion source was operated at room temperature.

Results and Discussion

Two CID reactions are the only ones observed. The reaction energetics and rate constants are given in Table I. The values of the heats of formation of $C_2F_5^-$, CF_3^-, and F^- used to calculate the heats of reaction are -267.9, -58.7, and -63.2 kcal/mol, respectively. These values are based on thermochemical data for fluorocarbon species tabulated previously[12] and the following electron affinities: $E(C_2F_5) = 2.3$ eV,[4] $E(CF_3) = 2.0$ eV,[4] and $E(F) = 3.45$ eV.[13]

Table I: Negative Ion–Molecule Reactions (CID Reactions) in Perfluoropropane

Reaction	$\Delta H°_{rxn}$, kcal/mol	Rate constant, cm³ molecule⁻¹ sec⁻¹
(1) $CF_3^- + M \rightarrow F^- + CF_2 + M$	59.1 ± 3^a	3×10^{-12}
(2) $C_2F_5^- + M \rightarrow F^- + C_2F_4 + M$	52.3 ± 3	8×10^{-12}

[a] Estimated uncertainties.

When either CF_3^- and $C_2F_5^-$ are impacted on xenon in the collision chamber of the tandem mass spectrometer, only F^- is observed as a product. The F^- increases linearly as a function of xenon pressure and extrapolates to zero xenon pressure. This linear increase in F^- demonstrates that these reactions indeed proceed by collision-induced dissociation. Similar results are observed with C_3F_8 in the collision chamber.

Figure 1 shows the reaction cross section dependence on the center-of-mass kinetic energy for collision of CF_3^- and $C_2F_5^-$ with xenon. The increase in cross section with kinetic energy is consistent with the endothermic nature of CID reactions and has also been observed for positive fluorocarbon ion CID reactions.[12,14] Table I shows that the CID reactions are endothermic by 2.45 and 2.15 eV, respectively, for ground state CF_3^- and $C_2F_5^-$. Since the observed apparent thresholds are considerably lower than these values, as shown in Figure 1, the reactant fluorocarbon ions must be internally excited by several electron volts. Although most of the negative ions are formed by low-energy electrons in the negative ion source used,[8] it is certainly possible that the ions are produced with internal excitation.

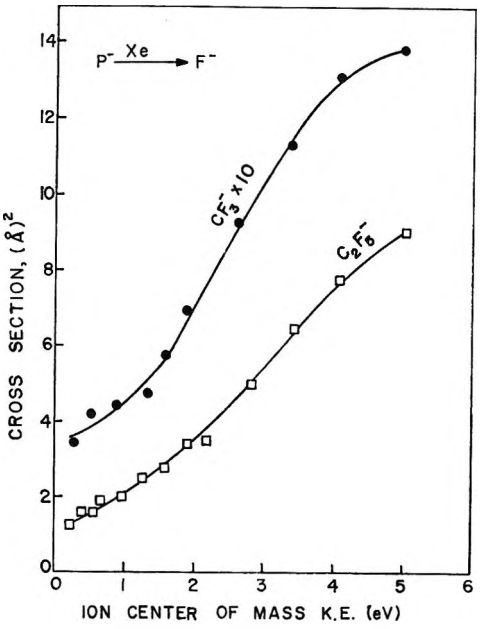

Figure 1. Cross section for collision-induced dissociations of CF_3^- and $C_2F_5^-$ with xenon as a function of center-of-mass kinetic energy.

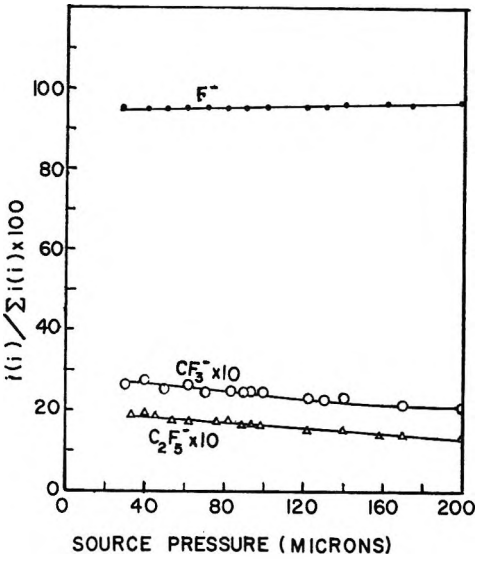

Figure 2. Effect of pressure on the negative ion mass spectrum of perfluoropropane in a Bendix TOF mass spectrometer with -6-V repeller potential.

(10) T. O. Tiernan and R. E. Marcotte, *J. Chem. Phys.*, **53**, 2107 (1970).

(11) J. H. Futrell, T. O. Tiernan, F. P. Abramson, and C. D. Miller, *Rev. Sci. Instrum.*, **39**, 340 (1968).

(12) T. Su, L. Kevan, and T. O. Tiernan, *J. Chem. Phys.*, **54**, 4871 (1971).

(13) R. S. Berry and C. W. Reimann, *ibid.*, **38**, 1540 (1963).

(14) R. Marcotte and T. O. Tiernan, *ibid.*, **54**, 3385 (1971).

The effect of pressure on the negative ion abundances in pure C_3F_8, as observed in the TOF mass spectrometer, is illustrated in Figure 2. It can be seen that CF_3^- and $C_2F_5^-$ decrease in relative intensity as the pressure is increased, while F^- increases. That is, of course, compatible with the tandem mass spectrometer results. The log of the ordinate in Figure 2 *vs.* pressure gives a good straight line, the slope of which allows us to calculate the total disappearance cross sections for CF_3^- and $C_2F_5^-$ given in Table II.

Table II: Total Reaction Cross Sections for Negative Ions in Perfluoropropane

Ion	*m/e*	Cross section
CF_3^-	69	1×10^{-16} cm^2
$C_2F_5^-$	119	2×10^{-16}

The qualitative kinetic energy dependence of the CID reactions in pure C_3F_8 can also be demonstrated by varying the repeller potential in the TOF mass spectrometer. The results are shown in Table III. The kinetic energy of the ions is increased at higher repeller fields. The abundance of CF_3^- and $C_2F_5^-$ decreases at higher repeller fields which indicates a greater reaction cross section with increasing kinetic energy. Thus, these results are consistent with Figure 1.

Table III: Effect of Repeller Potential on the Perfluoropropane Negative Ion Spectrum

Source pressure, μ	Repeller potential, V	% abundance		
		F^-	CF_3^-	$C_2F_5^-$
70	3	95.5	2.6	1.9
	6	95.8	2.5	1.7
	9	96.6	2.3	1.1
94	3	95.2	2.8	2.0
	6	95.9	2.4	1.7
	9	96.2	2.3	1.5
130	3	96.0	2.4	1.6
	6	96.2	2.3	1.5

Acknowledgment. L. K. thanks the Department of Chemistry, University of Utah for their hospitality and services.

COMMUNICATIONS TO THE EDITOR

Methylene Reactions in Photolytic Systems Involving Methyl Iodide

Publication costs assisted by Division of Research, U. S. Atomic Energy Commission

Sir: The gas phase photolysis of methyl iodide in the first absorption continuum provides more energy than necessary for the simple C–I bond rupture of (1),[1-3] and results in the formation of "hot" methyl radicals

$$CH_3I + h\nu \longrightarrow CH_3 + I \qquad (1)$$

excited with some of this excess energy (*e.g.* $\geq$ 42 kcal/mol in 2288-Å photolysis). Such hot methyl radicals show enhanced chemical reactivity, especially through the formation of methane by abstraction of hydrogen despite the presence of free radical scavengers.[4-9] Two recent reports have suggested that these hot methyl radicals are also capable of forming higher alkanes by the substitution of methyl for H in O_2-scavenged alkanes.[10,11] These interesting products, as well as some others not readily accounted for by hot methyl reactions,[12-17] have prompted a study of some

(1) D. Porrett and C. F. Goodeve, *Proc. Roy. Soc., Ser A.*, **165**, 31 (1938).

(2) J. R. Majer and J. P. Simons, *Advan. Photochem.*, **2**, 137 (1964).

(3) J. G. Calvert and J. N. Pitts, Jr., "Photochemistry," Wiley New York, N. Y., 1966.

(4) R. D. Schultz and H. A. Taylor, *J. Chem. Phys.*, **18**, 194 (1950).

(5) F. P. Hudson, R. R. Williams, Jr., and W. H. Hamill, *ibid.*, **21**, 1894 (1953).

(6) G. M. Harris and J. E. Willard, *J. Amer. Chem. Soc.*, **76**, 4678 (1954).

(7) R. D. Souffie, R. R. Williams, Jr., and W. H. Hamill, *ibid.*, **78**, 917 (1956).

(8) R. D. Doepker and P. Ausloos, *J. Chem. Phys.*, **41**, 1865 (1964).

(9) (a) B. G. Dzantiev and A. P. Shvedchikov, *High Energy Chem. (USSR)*, **3**, 28 (1969); (b) B. G. Dzantiev, S. T. Kozlov, A. N. Mushkaev, and A. P. Shvedchidov, *ibid.*, **3**, 32 (1969).

(10) J. Saunders and D. Urch, *Chem. Phys. Lett.*, **8**, 277 (1971).

(11) J. W. Root and G. W. Mutch, Abstracts, 160th National Meeting of the American Chemical Society, Chicago, Ill., Sept 1970.

Table I: Selected Products from Cadmium Resonance Photolysis of Radioactive Methyl Iodide

Reactants, Torr[a]			Relative product yield						
						Hydrocarbons			
$^{14}CH_3I$	O_2	Other	$^{14}CH_4$	^{14}CO	$^{14}CO_2$		ΣC_2	Other	
2.0	7	150 n-C_4H_{10}	100	20	36		2	<0.1 C_5	
2.5	10	100 C_3H_8	100	165	142		1	0.3 C_4	
CH_2TI	O_2	Other	CH_3T	HT	C_2H_5T	C_2H_3T	n-$C_5H_{11}T$	2-$C_5H_{11}T$	
2.0	0	150 n-C_4H_{10}	100	5	4.4	0.07	0.38	0.37	
1.0	14	150 n-C_4H_{10}	100	135	<0.1	<0.1	0.49	0.47	
$^{14}CH_3I$	O_2	Other	$^{14}CH_4$	^{14}CO	$^{14}CO_2$	ΣC_2	C_3H_8	C_3H_6	c-C_3H_6
4.0	0	230 C_2H_4	100	2.8	d	4.7	6.8	74	5.3
4.4	20	200 C_2H_4	100	430	1120	14	<1	200	≤2
4.0	0	230 C_2D_4	100	2.8	d	6.2	6.3	26[b]	4.7
4.0	20	200 C_2D_4	100	430	760	15	<1	92	≤2
CH_2TI	O_2	Other	CH_3T	HT	C_2H_5T	C_2H_3T	C_3H_8	C_3H_6	c-C_3H_6
1.1	0	218 C_2H_4	100		2.3	6.0	0.5	73[c]	6.8

[a] Ratio $^{14}CH_3I/CH_3I = 0.07$; $CH_2TI/CH_3I \sim 4 \times 10^{-3}$. [b] Isotopic analysis: $CD_2H^{14}CH{=}CD_2$, 3.2; $CD_3CD{=}{}^{14}CH_2$, 2.8; ($^{14}CH_3$-$CD{=}CD_2$ + $^{14}CH_2DCD{=}CD_2$), 20.4. [c] Isotopic analysis: tritium in olefinic position of propylene 5.6 ± 1.0% of total propylene-t. [d] Not determined.

of the lower yield reaction paths in the photolysis of CH_3I–alkane systems. We report here chemical evidence for the presence of both singlet and triplet methylene during the photolysis of methyl iodide. The known reactions of these two species provide an alternate, albeit more prosaic, explanation for the formation in such systems of alkanes with one carbon atom more than the substrate molecule.

Radioactively labeled methyl iodide ($^{14}CH_3I$ or CH_2TI) has been photolyzed in mixtures with n-butane, propane, or ethylene, both with and without O_2, in cells equipped with Suprasil quartz windows and greaseless stopcocks and joints, using either a cadmium[18] or mercury resonance lamp. Products were analyzed by radio gas chromatography.[19,20] Typical experimental data are summarized in Table I.

Triplet methylene has recently been shown to react with O_2 to form HT (from CHT), ^{14}CO, and $^{14}CO_2$ (both from $^{14}CH_2$).[21] The data of Table I indicate that these along with methane are the only important products observed during the photolysis of CH_2TI or $^{14}CH_3I$ in the presence of O_2. When the photolysis is carried out in the absence of O_2 and with metallic Ag present to remove molecular iodine, a very much larger total yield of products is observed, consistent with the absence of the usual back-reaction (2).

$$CH_3 + I_2 \longrightarrow CH_3I + I \qquad (2)$$

Both singlet and triplet methylene react with ethylene to form cyclopropane and propylene,[22-24] and these products are both found in the ethylene systems. While most of the labeled propylene is formed by the reactions of hot methyl radicals with ethylene, these reactions should lead only to the formation of CH_2T-$CH{=}CH_2$ from $CH_2TI + C_2H_4$ and $^{14}CH_3CD{=}CD_2$ from $^{14}CH_3I + C_2D_4$. The presence of other isotopic forms of propylene in both cases (see footnotes) can only readily be attributed to the reactions of methylene with ethylene, followed by the isomerization of the resulting cyclopropane. These yields are substantially reduced by O_2 scavenger, indicating that most of the methylene is triplet methylene, scavengeable by O_2. With O_2 present, the yield of labeled cyclopropane drops to a very low yield;[25] but the isotopic propylene products from its isomerization are still present,[26]

(12) N. R. Davidson and T. Carrington, *J. Amer. Chem. Soc.*, **74**, 6277 (1952).

(13) R. T. Meyer, *J. Phys. Chem.*, **72**, 1583 (1968).

(14) G. J. Mains and D. Lewis, *ibid.*, **74**, 1694 (1970).

(15) C. D. Bass and G. C. Pimentel, *J. Amer. Chem. Soc.*, **83**, 3754 (1961).

(16) R. E. Rebbert and P. Ausloos, *J. Chem. Phys.*, **48**, 306 (1968).

(17) P. G. Barker, J. H. Purnell, and B. C. Young, *Trans. Faraday Soc.*, **66**, 2244 (1970).

(18) The cadmium lamp produces radiation with the wavelengths 2288, 2265, and 2144 Å in the approximate ratio of 15:3:1.

(19) J. K. Lee, E. K. C. Lee, B. Musgrave, Y.-N. Tang, J. W. Root, and F. S. Rowland, *Anal. Chem.*, **34**, 741 (1962).

(20) Since self-radiolysis of radioactive methyl iodide creates labeled hydrocarbon impurities very rapidly, the methyl iodide was routinely purified by degassing at −100° with added hydrocarbon carriers approximately 1 hr before the actual photolysis.

(21) R. L. Russell and F. S. Rowland, *J. Amer. Chem. Soc.*, **90**, 1671 (1968).

(22) D. Setser and B. S. Rabinovitch, *Can. J. Chem.*, **40**, 1425 (1962).

(23) C. McKnight, E. K. C. Lee, and F. S. Rowland, *J. Amer. Chem. Soc.*, **89**, 469 (1967).

(24) F. S. Rowland, C. McKnight, and E. K. C. Lee, *Ber. Bunsenges. Phys. Chem.*, **72**, 236 (1968).

(25) The half-pressure for stabilization of excited c-C_3H_5T has been reported at 170 Torr for ^{3}CHT and about 1700 Torr for ^{1}CHT from the 3130-Å photolysis of CHTCO.[24]

(26) The apparent absence of cyclopropane and propylene as products in CH_2TI–C_2H_4 photolysis was the basis for the conclusion that singlet methylene was *not* present in methyl iodide photolysis systems, and therefore could not be responsible for the butane products in CH_2TI–C_3H_8 mixtures.[10]

confirming the presence of singlet methylene in these systems.

The yields of C_5 products from n-C_4H_{10} and C_4 products from C_3H_8 are quite low in O_2-scavenged systems at 2288 Å. However, these yields are considerably higher with an 1849-Å, 2537-Å Hg resonance lamp, and occur with the ratios n-C_5H_{12}/i-C_5H_{12} = 1.2 for both CH_2TI and $^{14}CH_3I$ with O_2-scavenged n-C_4H_{10}, and n-C_4H_{10}/i-C_4H_{10} = 2.3 for the $^{14}CH_3I$-C_3H_8-O_2 system. The insertion reactions of singlet methylene can readily account for the formation of these higher alkanes, and the ratios of n-C_4H_{10}/i-C_4H_{10}[10] and n-C_5H_{12}/i-C_5H_{12},[27] respectively, are quite similar to those obtained for the reactions of singlet methylene from the photolysis of diazomethane and ketene.[28-30]

The presence of methylene in the reaction system also suggests it as a possible precursor[31] for all or part of the yields for several products found in earlier methyl iodide studies, *e.g.*, ethylene ($^3CH_2 + CH_3$) and acetylene ($^3CH_2 + {}^3CH_2$) in flash photolytic systems;[13,14] and, from $CD_3I + C_2H_4$,[16] $CH_2CH_2CD_2$ ($^3CD_2 + C_2H_4$). Finally, the reaction of ^3CHT with O_2 leads to the formation of hot T atoms,[21] and small yields of products characteristic of energetic tritium atom reactions can be expected in O_2-scavenged systems.

The mechanistic source of methylene species has not been unequivocally identified, although sufficient energy exists for the formation of CH_2 + HI as a minor direct photolysis route. In any event, the major photolytic route (>95%) is certainly the split into CH_3 and I at these wavelengths.

(27) The very much higher n-pentane/isopentane ratios reported in CH_2TI-n-C_4H_{10} mixtures apparently had substantial contributions from Hg-photosensitization reactions: ref 11 and private communication from J. W. Root.

(28) R. L. Johnson, W. L. Hase, and J. W. Simons, *J. Chem. Phys.*, **52**, 3911 (1970).

(29) J. W. Simons, C. J. Magee, and G. W. Taylor, *J. Phys. Chem.*, **72**, 769 (1968).

(30) R. L. Russell and F. S. Rowland, unpublished results.

(31) P. S.-T. Lee, R. L. Russell, and F. S. Rowland, *Chem. Commun.*, 18 (1970).

(32) This research has been supported by A.E.C. Contract No. AT-(04-3)-34, Agreement No. 126.

DEPARTMENT OF CHEMISTRY[32] C. C. CHOU
UNIVERSITY OF CALIFORNIA P. ANGELBERGER
IRVINE, CALIFORNIA 92664 F. S. ROWLAND*

RECEIVED FEBRUARY 1, 1971

The Dominance of Intramolecular Dipole–Dipole Mechanisms upon Carbon-13 Relaxation in Benzene and Cyclohexane

Publication costs assisted by the National Science Foundation

Sir: Publications[1-4] from this laboratory have emphasized the dipole–dipole mechanism of carbon-13 nuclear spin relaxation and have suggested that these dipolar mechanisms are dominated by intramolecular processes.[1-4] However, heretofore only indirect evidence has been presented to support this suggestion,[1-4] and this work contains data on a dilution study which will now substantiate the validity of this conclusion for two very representative hydrocarbons.

Table I contains carbon-13 nuclear Overhauser effect, NOE, and proton-decoupled relaxation time, T_1,[3-5] measurements obtained on Varian AFS-60 and XL-100-15 spectrometers. The adiabatic rapid passage technique[3] was used at two different frequencies and at 36 ± 2° for benzene, cyclohexane, and a 50:50 (v:v) mixture of the two liquids. From the NOE and T_1 data, the dipolar relaxation contribution, T_{1D}^C, was determined[2-3] ($T_{1D}^C \cong 2T_1/\eta$). Observe that the relaxation processes are dominated by dipole–dipole mechanisms (η = 2.00 and η_{av} = 1.80 for the cyclohexane and benzene, respectively). The carbon-13 relaxation times, T_1, of benzene and cyclohexane at 62.5 MHz agree[6] reasonably well with the data at 15 and 25 MHz indicating that chemical shift anisotropic effects are minimal in these compounds. Also, temperature studies from 35 to 60° disclose no spin-rotation effects.[7] The slight reduction in the benzene Overhauser effect from maximum to η_{av} = 1.80 is not statistically significant for the experimental errors which were obtained in this study.

Table I: Carbon-13 NOE and Spin-Lattice Relaxation Data for Benzene and Cyclohexane at 36°

Compound	Frequency, MHz	η = NOE − 1	T_1, sec	T_{1D}^C, sec	T_{1O}^C, sec
Cyclohexane	15.1	2.00 ± 0.10	17.5 ± 2	18 ± 3	>100
	25.1	2.00 ± 0.10	17.0 ± 2	17 ± 3	>100
Benzene	15.1	1.85 ± 0.15	22.0 ± 2	24 ± 5	>100
	25.1	1.80 ± 0.15	23.0 ± 2	25 ± 5	>100
50:50	25.1	2.00 ± 0.10	17.8 ± 2	18 ± 3	>100
mixture C_6H_{12}–C_6H_6	25.1	1.75 ± 0.15	24.0 ± 2	27 ± 5	>100

In order to determine if the dipolar relaxation contribution is dominanted by intramolecular effects, a 50:50 (v:v) solution of benzene–cyclohexane was studied. Intermolecular carbon–hydrogen terms would be expected to change for both cyclohexane and benzene in the mixture as a result of the twofold differences in proton populations for these two compounds. Since there are no significant differences in the values

(1) K. F. Kuhlman and D. M. Grant, *J. Amer. Chem. Soc.*, **90**, 7355 (1968).

(2) K. F. Kuhlman, D. M. Grant, and R. K. Harris, *J. Chem. Phys.*, **52**, 3439 (1970).

(3) T. D. Alger, S. C. Collins, and D. M. Grant, *ibid.*, **54**, 2820 (1971).

(4) J. Lyerla Jr., D. M. Grant, and R. K. Harris, *J. Phys. Chem.*, **75**, 585 (1971).

(5) R. A. Hoffman and S. Forsen, *J. Chem. Phys.*, **45**, 2049 (1966).

(6) H. Spiess, *et al.*, Max Planck Institute, private communication.

(7) D. K. Green and J. G. Powles *Proc. Phys. Soc., London*, **85**, 87 (1965), observed a similar lack of spin-rotation effects in the proton relaxation of benzene up to the critical temperature.

of T_1 and T_{1D}^C, for either compound in the neat liquid or in the 50–50 mixture (Table I), it is evident that intramolecular dipolar effects dominate the carbon-13 spin-lattice relaxation when protons are directly attached, and that neither spin-rotation coupling nor anisotropic chemical screening mechanisms are important in these two different characteristic hydrocarbons.

Since the T_{1D}^C values are dominated by intramolecular dipole effects, an effective rotational correlation time, τ_c, may be calculated from the data in Table I for both benzene and cyclohexane by assuming isotropic tumbling[8] [$1/T_{1D}^C$ (intra) = $n_H\gamma_C^2\gamma_H^2\tau_c/r_{CH}^6$, where n_H is the number of directly attached hydrogens]. The results of this calculation yield 1.7×10^{-12} sec for τ_c (benzene) and 1.3×10^{-12} sec for τ_c (cyclohexane). These results correlate well with the value of 1.5×10^{-12} sec obtained by Green and Powles[7] for the intramolecular relaxation of hydrogen in benzene. Note that the differences in T_{1D}^C for benzene and cyclohexane (T_{1D}^C = 25 sec and T_{1D}^C = 17 sec, respectively) are roughly explained by the twofold differences in the number of protons attached directly to carbons in the two compounds. The slightly longer correlation time observed for benzene does modify this twofold population factor as might be expected from the geometry of benzene and the greater molecular association anticipated from increased intermolecular π-electron interactions. The greater planarity of benzene may also suggest that some anisotropy in molecular rotation is giving rise to the longer effective correlation time or slower rotational diffusion rates.

Acknowledgments. This work was supported by grants from the National Institutes of Health (GM-0852-10) and the National Science Foundation (GP-18436).

(8) J. A. Pople, W. G. Schneider, and H. J. Bernstein, "High-resolution Nuclear Magnetic Resonance," McGraw-Hill, New York, N. Y., 1959, p 202.

DEPARTMENT OF CHEMISTRY
UTAH STATE UNIVERSITY
LOGAN, UTAH 84321
TERRY D. ALGER*

DEPARTMENT OF CHEMISTRY
UNIVERSITY OF UTAH
SALT LAKE CITY, UTAH 84112
DAVID M. GRANT

RECEIVED APRIL 27, 1971

The Effect of Molecular Association on C–H Nuclear Dipolar Relaxation Rates

Publication costs assisted by the National Science Foundation

Sir: It has long been recognized that nuclear spin-lattice relaxation times (T_1) can provide significant information relative to liquid dynamics.[1,2] However, the interpretation of T_1 data with respect to molecular motion for spin $^1/_2$ systems has often been hampered by the difficulties encountered in separating the various contributing relaxation mechanisms. For protons,[3] evaluation of the individual relaxation processes usually requires detailed dilution and temperature studies. However, it has been recently illustrated that such complex analysis can often be avoided in the consideration of carbon-13 relaxation times. In particular, it has been demonstrated that determination of the $^{13}C\{^1H\}$ nuclear Overhauser effect (NOE) and ^{13}C spin-lattice relaxation times under proton-decoupled conditions allows determination of the C–H intramolecular, dipolar relaxation time provided intermolecular C–H processes are negligible.[4–7] Knowledge of the C–H dipolar contribution, T_{1D}^C, to the spin-lattice relaxation time permits calculation of molecular reorientation rates with resultant insight into the dynamics of the systems.[6,7]

Herein are reported in Table I the proton-decoupled carbon-13 spin-lattice relaxation times and the incremental increase in signal (η) due to the NOE values ($1 + \eta$) for formic and acetic acids and their respective methyl esters. All relaxation measurements were made by adiabatic rapid passage[4,5] (ARP) techniques on degassed samples at 35 ± 2°. Experiments were performed at 14.1 kG on a Varian AFS-60 spectrometer and at 23.5 kG on a Varian XL-100-15 spectrometer. The $^{13}C\{^1H\}$ NOE enhancement factors were determined from the ratio of the integrated intensities of the ^{13}C decoupled and coupled spectra.[6,8] The carboxyl data were obtained from formic and acetic acid samples enriched[9] in the ^{13}C isotope to approximately 23% at the carboxyl position. At this level of enrichment only a single scan was required to acquire the necessary information on both instruments. The T_1 values of the two esters and the methyl carbon of acetic acid were obtained from nonenriched samples and thus required accumulation techniques using a Varian C-1024 time-averaging device.[4,5]

Listed also in Table I are the C–H dipolar relaxation times (T_{1D}^C) and the total relaxation time due to all other mechanisms (T_{1O}^C) obtained from the T_1 and NOE data *via* the formulations[4–7]

$$T_{1O}^C = \frac{\gamma_H}{2\gamma_C}\frac{T_1}{\eta} \qquad (1)$$

(1) J. S. Waugh in "Molecular Relaxation Processes," Academic Press, London, 1966.

(2) A. Abragam, "Principles of Nuclear Magnetism," Oxford University Press, New York and London, 1961, Chapter VIII.

(3) D. K. Green and J. G. Powles, *Proc. Phys. Soc., London*, **85**, 87 (1965).

(4) K. F. Kuhlman, D. M. Grant, and R. K. Harris, *J. Chem. Phys.*, **52**, 3439 (1970).

(5) T. D. Alger, S. C. Collins, and D. M. Grant, *ibid.*, **54**, 2820 (1971).

(6) J. Lyerla, Jr., D. M. Grant, and R. K. Harris, *J. Phys. Chem.*, **75**, 585 (1971).

(7) T. D. Alger and D. M. Grant, *ibid.*, **75**, 2538 (1971).

(8) K. F. Kuhlman and D. M. Grant, *J. Amer. Chem. Soc.*, **90**, 7355 (1968).

(9) These compounds were synthesized by Professor Edward G. Paul of Brigham Young University.

Table I: ^{13}C-NOE and Spin-lattice Relaxation Results for Formic and Acetic Acids and Their Methyl Esters

Compd	Carbon	T_1, sec (15 MHz)	T_1, sec (25 MHz)	$\eta_{^{13}C\{^1H\}}$[a]	T_{1D}^C	T_{1e}^C
Formic acid	Formyl	10.3 ± 1.0	10.1 ± 1.0	2.0 ± 0.15	10.0 ± 3.0	>100
Methyl formate	Formyl	15.1 ± 2.0	14.5 ± 1.5	1.55 ± 0.15	19.0 ± 5.0	83.0 ± 20
	Methyl	16.8 ± 2.0	18.0 ± 2.0	0.80 ± 0.10	43.0 ± 10	29.0 ± 10
Acetic acid	Acetyl	29.1 ± 2.2	30.0 ± 3.5	1.08 ± 0.04	53.6 ± 4.2	63.7 ± 5.0
	Methyl	10.5 ± 0.5	9.8 ± 0.6	1.40 ± 0.13	14.9 ± 1.5	35.5 ± 3.7
Methyl acetate	Acetyl[b]	35.0 ± 5.0	29.0 ± 5.0	0.25 ± 0.08	278 ± 84	40.0 ± 13
	Methyl	16.3 ± 1.3	17.4 ± 1.5	0.63 ± 0.08	53.0 ± 8.0	24.6 ± 3.7
	Methoxy	17.0 ± 1.5	18.3 ± 2.1	0.93 ± 0.04	37.6 ± 4.2	33.1 ± 3.7

[a] The values are from the AFS-60. [b] The carboxyl carbon of methyl acetate was not enriched and, therefore, the errors are large in the T_1 measurement of this peak due to the reduced signal intensity of this carbon.

and

$$\frac{1}{T_{1e}^C} = \frac{1}{T_1} - \frac{1}{T_{1D}^C} \tag{2}$$

Discussion of the various results requires consideration of the C–H dipolar relaxation rate in formalistic terms

$$\frac{1}{T_{1D}^C} = \sum_i \frac{\gamma_H^2 \gamma_C^2 \hbar^2}{r_{CHi}} \tau_{eff} \tag{3}$$

where the summation is over all protons in the sample, r_{CH} is the nuclear separation, and τ_{eff} is an effective correlation time for molecular reorientation.

The T_{1D}^C and T_{1e}^C results for the respective acids and esters illustrate the effects of dimerization upon the molecular reorientation times. In particular, the C–H dipolar process for the carboxyl of acetic acid is quite efficient for a quaternary carbon in view of the $1/r_{CH}^6$ dependence of T_{1D}^C. Furthermore, the methyl carbon has a rather short T_{1D}^C considering that very low barriers to internal rotation (476 cal[10]) usually give rise to substantial reductions in the dipolar process.[4,6,11] Both these results are consistent, however, since the effect of association is to slow down appreciably the molecule's reorientation rate, especially perpendicular to the dimer's long axis. As τ_{eff} of eq 3 is intimately related to the diffusion rates about the various axes of the molecular system,[12] the result of dimerization is to increase the effective correlation time. The increased value of τ_{eff} then gives rise to a much more efficient dipolar process for the carbons of acetic acid than that normally observed for corresponding type carbons in nonassociated liquids.

The results for the C–H dipolar rates in methyl acetate, where the association effects are precluded, reinforce the above discussion. The T_{1D}^C value for the methyl (53 sec) is consistent with the T_{1D}^C value for the methyl of acetonitrile (49 sec)[6] which is also a free rotor at room temperature. The methoxy T_{1D}^C value represents a somewhat more efficient process than for the methyl as might be expected in view of the higher barrier to rotation (~1200 cal[10]) about the C–O axis relative to that of the methyl C–C rotational barrier. Finally, the carboxyl now has a much longer dipolar relaxation time and is more in line with other quaternary carbons.[13] Hence the T_{1D}^C values in methyl acetate reflect the reduced τ_{eff} value for the molecular reorientation process when association effects are absent.

The results for formic acid and methyl formate are analogous with those of the acetic acid case. However, as the carboxyl is attached to a proton in methyl formate, it is possible for τ_{eff} to be estimated from eq 3 and the value for T_{1D}^C which is now dominated by the directly bonded proton. The τ_{eff} for the acid is 4.9×10^{-12} sec, while a value of 2.6×10^{-12} sec is obtained for the ester. Thus, dimerization has significantly affected the overall rate of molecular diffusion.

A few comments should be made regarding the origin of the T_{1e}^C processes in these systems. The field-dependent studies illustrate no appreciable effect within experimental error on the relaxation times of all the carbons. It is concluded, therefore, that the T_{1e}^C processes are due to the spin-rotation mechanism. The relatively short times observed for the methyl carbons are in accord with the facility of internal rotation.

In conclusion, these relaxation results for the formic and acetic acids and their methyl esters illustrate the high degree to which the dynamics of liquid systems are faithfully reflected in the C–H dipolar relaxation rate. In this regard, the study also indicates the potential importance of T_1 and Overhauser data as a technique to separate relaxation mechanisms.

Acknowledgments. This research was supported by grants from the National Institutes of Health (GM-08521) and the National Science Foundation (GP-18436).

(10) W. Gordy and R. L. Cook in "Technique of Organic Chemistry," Vol. 9, A. Weissberger, Ed., Interscience, New York, N. Y., 1970.

(11) K. T. Gillem, M. Schwartz, and J. H. Noggle, private communication.

(12) D. E. Woessner, *J. Chem. Phys.*, **37**, 647 (1962).

(13) T. D. Alger, D. M. Grant, and R. K. Harris, submitted for publication in *J. Phys. Chem.*

DEPARTMENT OF CHEMISTRY
UTAH STATE UNIVERSITY
LOGAN, UTAH 84321
TERRY D. ALGER*

DEPARTMENT OF CHEMISTRY
UNIVERSITY OF UTAH
SALT LAKE CITY, UTAH 84112
DAVID M. GRANT
JAMES R. LYERLA, JR.

RECEIVED APRIL 27, 1971

RADIATION CHEMISTRY

ADVANCES IN CHEMISTRY SERIES NOS. 81 AND 82

Seventy-seven papers and 34 abstracts from the International Conference on Radiation Chemistry at Argonne National Laboratories, chaired by Edwin J. Hart. Includes review and research papers from 12 countries besides U.S., Canada, and England, including 8 from U.S.S.R. and two other East European countries.

Volume I groups papers on radiation in aqueous media, radiation of biological systems, dosimetry, and one plenary lecture.

Volume II has papers on radiation of gases, of solids, and of organic liquids, plus three plenary lectures.

No. 81 Radiation Chemistry—I — 616 pages with index
No. 82 Radiation Chemistry—II — 558 pages with index
Each $16.00
Cloth (1968) Ordered together $30.00

Set of L.C. cards free with library orders.

Other books in the ADVANCES IN CHEMISTRY SERIES in physical and colloid chemistry include:

No. 68 Mössbauer Effect and its Application in Chemistry. Ten papers that will familiarize chemists with Mössbauer spectroscopy as an analytical tool, for studying chemical bonding, crystal structure, electron density, magnetism, and other properties. 178 pages
Cloth (1967) $8.00

No. 67 Equilibrium Concepts in Natural Water Systems. Sixteen papers represent the collaboration of aquatic chemists, analytical chemists, geologists, oceanographers, limnologists, and sanitary engineers, working with simplified models to produce fruitful generalizations and valuable insights into the factors that control the chemistry of natural systems. 344 pages
Cloth (1967) $11.00

No. 64 Regenerative EMF Cells. Seventeen papers survey current progress and research on regenerative systems for converting and storing electrical energy. Principal emphasis is on thermally regenerative systems, but chemical and photochemical systems are considered. 309 pages
Cloth (1967) $11.00

No. 63 Ordered Fluids and Liquid Crystals. Twenty-two studies on characterization, properties, and occurance of these phenomena in many substances such as tristearin, p-azoxyanisole, mono-and di-hydric alcohols, phospholipids and polypeptides. 332 pages
Cloth (1967) $11.50

No. 58 Ion-Molecule Reactions in the Gas Phase. Eighteen papers survey spectrometric and other methods for producing and studying ion-molecule reactions, such as pulsed sources for studing thermal ions, reactions in flames and electrical discharges. 336 pages
Cloth (1966) $10.50

No. 54 Advanced Propellant Chemistry. Primarily directed to the search for new oxidizers; 26 papers survey oxygen-containing oxidizers, fuels and binders, fluorine systems including oxygen difluoride and difluoramines and liquid systems. 290 pages
Cloth (1966) $10.50

No. 47 Fuel Cell Systems. Developments in theory, performance, construction, and new systems for the energy converter that is proving itself in military and space uses. 360 pages
Cloth (1965) $10.50

No. 43 Contact Angle, Wettability, and Adhesion. Twenty-six papers on theoretical and practical approaches to wettability and adhesion; with summary of the surface chemical studies of W. A. Zisman, the 1963 Kendall Award winner. 389 pages
Cloth (1964) $10.50

No. 40 Mass Spectral Correlations. By Fred W. McLafferty. Over 4000 spectral listed by mass/charge ratios of fragment ions with the most probable original structures for each. 117 pages
Paper (1963) $6.00

No. 33 Solid Surfaces and the Gas-Solid Interface. Thirty-seven papers from the Kendall Award Symposium honoring Stephen Brunauer. Theory and techniques for studying surface phenomena.
Cloth (1961) $12.00

No. 31 Critical Solution Temperatures. By Alfred W. Francis. CST answers the question, "Do two liquids mix?" and is widely used for screening solvents. Over 6000 systems are included, 70% with a hydrocarbon as one component; nearly 1100 non-hydrocarbon solvents are listed. 246 pages
Cloth (1961) $8.00

No. 29 Physical Properties of Chemical Compounds—III. By Robert R. Dreisbach. Supplements earlier volumes with properties of 434 aliphatic compounds and 22 miscellaneous compounds and elements. Index to volumes I, II, and III. 489 pages
Cloth (1961) $10.00

No. 25 Physical Functions of Hydrocolloids. Papers on natural gums, gelatin pectins and related polysaccharides, and theoretical and functional aspects of hydrocolloids, emulsions, foams, and dispersions. Strong food industry emphasis. 103 pages
Paper (1960) $5.00

No. 22 Physical Properties of Chemical Compounds—II. By Robert R. Dreisbach. Properties of 476 alkanes, haloalkanes, alkenes, haloalkenes, diolefins, and alkynes. 491 pages
Cloth (1959) $10.00

No. 18 Thermodynamic Properties of the Elements. By D. R. Stull and G. C. Sinke. Tabulated values of heat capacity, heat content, entropy, and free energy function of solid, liquid, and gas states of first 92 elements in range of 298° to 3000°K. Some auxiliary data frequently included.
Cloth (1956) $8.00

No. 15 Physical Properties of Chemical Compounds. By Robert R. Dreisbach. Tables of parameters for calculating physical properties of 511 organic cyclic compounds. 536 pages
Cloth (1955) $10.00

All books postpaid in U.S. and Canada; plus 30 cents in PUAS and elsewhere.

Order from: SPECIAL ISSUES SALES,
AMERICAN CHEMICAL SOCIETY
1155 SIXTEENTH ST., N.W.
WASHINGTON, D.C. 20036

Cleaning Our Environment
The Chemical Basis For Action

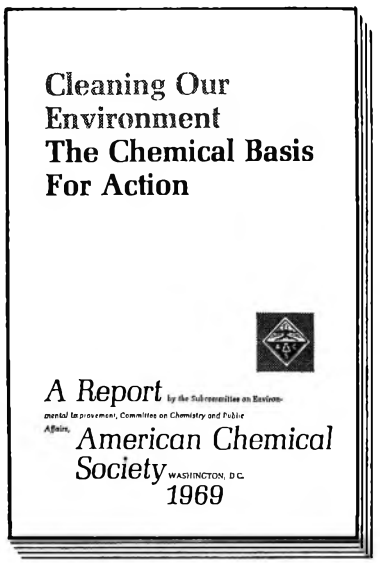

Cleaning Our Environment—The Chemical Basis for Action is the highly acclaimed 249-page report based on a three-year study by the Subcommittee on Environmental Improvement of the ACS Committee on Chemistry and Public Affairs. Leading experts from the fields of chemistry, biochemistry, chemical engineering, biology, entomology, and other disciplines comprised the Task Force on Environmental Improvement which conducted the study, one of the most comprehensive of its kind.

The report divides the problem of environmental improvement into four parts: air environment, water environment, solid wastes, and pesticides. It clearly shows where extensive fundamental research is required to provide a better working understanding of the environmental system. Focusing strongly on chemistry, chemical engineering, and related disciplines, the report concludes that the U.S. possesses enough technical know-how to take enormous strides now toward a cleaner environment.

Included in the report are 73 recommendations for action on such topics as:

- *flow, dispersion, and degradation of water and air pollutants*
- *short- and long-range effects of water and air pollutants*
- *municipal and industrial waste water treatment*
- *advanced treatment processes*
- *eutrophication*
- *air quality criteria*
- *air monitoring systems*
- *emission control on motor vehicles*
- *abatement of pollutants from power plants*
- *municipal and industrial solid wastes*
- *mining and processing wastes*
- *pesticides and human health*
- *pesticides and wildlife*
- *methods of pest control*

Although the ACS report is directed primarily at technical and nontechnical administrators in the environmental field, research managers, legislators and others working in this area, the nature of the subject makes it required reading for all scientists interested in environmental problems and their solutions.

The report is available from the ACS Special Issues Sales. Price: $2.75.

American Chemical Society
Special Issues Sales
1155 Sixteenth Street, N.W.
Washington, D.C. 20036

Please send me the ACS Report "Cleaning Our Environment—The Chemical Basis for Action."

Name_____

Address_____

City_____ State_____ Zip_____

Number of copies _____

I enclose _____. *(Payable to the American Chemical Society.)*

Please bill me _____. *$2.75 a copy.*